Investigating neuroinflammatory disease through retinal imaging and biomarkers

Candidate	Iris Kleerekooper
Supervisors	S Anand Trip Axel Petzold Gordon T Plant
Examiners	Nicholas G Strouthidis Moorfields Eye Hospital, London
	Nynke F Kalkers OLVG & AUMC location VUmc, Amsterdam

Thesis submitted for the Degree of Doctor of Philosophy

University College London

Department of Neuroinflammation

September 2021

Declaration

I, Iris Kleerekooper, confirm that the work presented in this thesis is my own. Where information has been derived from other sources, I confirm that this has been indicated in the thesis.

Abstract

Neuroinflammatory diseases, in particular multiple sclerosis (MS) and neuromyelitis optica spectrum disorder, often affect the anterior visual pathways. This can occur through direct inflammatory insult in the form of optic neuritis or through retrograde degeneration, but progressive neurodegenerative processes related to axonal loss and atrophy also play a role. Energy failure has been postulated as an important factor mediating factor in these neurodegenerative processes, but its exact role is poorly understood. The advent of optical coherence tomography (OCT) enables high resolution imaging of the retina with relative ease. In neurology research, OCT has mostly been used to quantify retinal layer thicknesses. This thesis focuses on the largely unexplored potential of OCT as a functional biomarker. The primary aim is to develop indirect non-invasive in-vivo biomarkers informing on metabolic function, taking into account the high energy demand of the retina, particularly during dark-adaptation. First, two novel functional OCT measures are presented; the dynamic dark-adaptation related thickening of the outer retinal layers and the relative reflectivity of the ellipsoid zone (EZ), which comprises the majority of retinal mitochondria. Both measures appeared to be reduced in acute optic neuritis, and also in chronic neuroinflammatory disease in the case of EZ reflectivity. Furthermore, pilot OCT-angiography (OCTA) data indicated that vascular density was reduced in acute optic neuritis. As reduced EZ reflectivity and lower vascular density were present to a similar degree in both eyes of acute optic neuritis patients suggest that a background level of mitochondrial dysfunction and hypoperfusion may occur in neuroinflammatory disease, independent from acute inflammatory activity. The work presented in this thesis illustrates that OCT has the potential to provide valuable information on retinal function in neuroinflammatory disease. In the future, artificial intelligence and big data analysis may enable the development of a holistic analysis method for raw OCT data, providing a summary report on both qualitative, such as presence of microcystic macular oedema (MMO), and quantitative scan features, such as layer thickness, vascular density and reflectivity. Comprehensive analysis of both functional and structural OCT data may facilitate diagnosis, inform on prognosis and provide important insight into the role of metabolic failure in the pathophysiology of neuroinflammatory disease.

Impact statement

This thesis describes the development and the performance of two novel optical coherence tomography (OCT) analysis methods, being the calculation of dynamic outer retinal layer thickness changes during dark-adaptation and the extraction of relative ellipsoid zone (EZ) reflectivity from OCT scans. These represent some of the first efforts to use OCT as a functional in addition to a structural measure. Preliminary data in this thesis indicate that both these metrics show reductions in neuroinflammatory disease, both during its acute and chronic stages, and in mitochondrial disorders. Given the known high retinal energy demands associated with dark-adaptation and the accumulation of mitochondria in the EZ, these novel OCT analysis metrics may provide in-vivo non-invasive measures of mitochondrial health. Future studies are needed to confirm this association with metabolic function, but these analysis methods could have an important impact in research disentangling the role of metabolic function in the pathophysiology of neuroinflammatory disease. This is important clinically, as there is currently a lack of non-invasive measurement techniques for metabolic function which hampers research in this subject. A better understanding of the role of metabolic failure in neuroinflammatory disease may lead to the development of novel treatment methods focused on improving mitochondrial function, which may be particularly relevant in the progressive forms of multiple sclerosis where effective drugs are currently lacking. The novel OCT analysis methods presented in this thesis may also provide outcome measures in current or future clinical trials of treatments aiming to improving metabolic function in multiple sclerosis. Furthermore, the description of the rare phenotype of primary progressive optic neuropathy in multiple sclerosis may improve timely diagnosis in these patients, the descried associations of smoking and alcohol consumption with neurodegeneration in multiple sclerosis could help guide clinical counselling regarding safe health behaviours in neuroinflammatory disease and, finally, the study identifying evidence for astrocytopathy in seronegative neuromyelitis optica spectrum disease helps to improve understanding of the pathophysiology in these patients.

Table of contents

List of abbreviations

AUC	-	Area Under the Curve
AQP4	-	Aquaporin-4
BCVA	-	Best Corrected Visual Acuity
CF	-	Count Fingers
cGMP	-	Cyclic Guanine Monophosphate
CIS	-	Clinically Isolated Syndrome
CNS	-	Central Nervous System
CRION	-	Chronic Relapsing Inflammatory Optic Neuropathy
CSF	-	Cerebrospinal Fluid
COX	-	Cytochrome-C-Oxidase
CPEO	-	Chronic Progressive External Ophthalmoplegia
DOA	-	Dominant Optic Atrophy
DMT	-	Disease Modifying Treatment
DNA	-	Deoxyribonucleic Acid
DVP	-	Deep Vascular Plexus
EAE	-	Experimental Autoimmune Encephalomyelitis
EDSS	-	Expended Disability Status Scale
ETDRS	-	Early Treatment Diabetic Retinopathy Study
EZ	-	Ellipsoid Zone
GCL	-	Ganglion Cell Layer
GFAP	-	Glial Fibrillary Acidic Protein
GS	-	Glutamine Synthetase
HM	-	Hand Motions
INL	-	Inner Nuclear Layer
IPL	-	Inner Plexiform Layer
IVMP	-	Intravenuos methylprednisolone
LHON	-	Leber Hereditary Optic Neuropathy
mGCIPL	-	Macular Ganglion Cell and Inner Plexiform Layer
MOG	-	Myelin Oligodendrocyte Glycoprotein
MOGAD	-	Myelin Oligodendrocyte Glycoprotein associated Disease
MOG-ON	-	Myelin Oligodendrocyte Glycoprotein associated Optic Neuritis
MMO	-	Microcystic Macular Oedema
MS	-	Multiple Sclerosis
MS-ON	-	Multiple Sclerosis associated Optic Neuritis
NMO-ON	-	Neuromyelitis Optica associated Optic Neuritis
NMOSD	-	Neuromyelitis Optica Spectrum Disorder
MRI	-	Magnetic Resonance Imaging
mtDNA	-	Mitochondrial Deoxyribonucleic Acid
NMDA	-	N-methyl-D-aspartate

NPL	-	No Perception of Light
OCBs	-	Oligoclonal bands
OCT	-	Optical Coherence Tomography
OCTA	-	Optical Coherence Tomography Angiography
ON	-	Optic Neuritis
ONL	-	Outer Nuclear Layer
OPL	-	Outer Plexiform Layer
OPR	-	Outer Segment Photoreceptor and Subretinal Potential Space
OS	-	Outer Segments
OSEL	-	Outer Segments Equivalent Layer
PDE	-	Phosphodiesterase
PERG	-	Pattern Electroretinography
PL	-	Photoreceptor Layer
PPON	-	Primary Progressive Optic Neuropathy
PPMS	-	Primary Progressive Multiple Sclerosis
pRNFL	-	Peripapillary Retinal Nerve Fibre Layer
PVEP	-	Pattern Visual Evoked Potential
RNFL	-	Retinal Nerve Fibre Layer
ROC	-	Receiver Operating Characteristic curve
RPE	-	Retinal Pigmented Epithelium
RRMS	-	Relapsing-Remitting Multiple Sclerosis
SERON	-	Steroid-responsive Epilepsy with Relapsing Optic Neuritis
SION	-	Single-episode Isolated Optic Neuritis
SPMS	-	Secondary Progressive Multiple Sclerosis
SVP	-	Superficial Vascular Plexus
T-α	-	Transducin α-Subunit

Publications arising from this thesis

Published

Kleerekooper I, Petzold A, Trip SA. Anterior visual system imaging to investigate energy failure in multiple sclerosis. Brain 2020; 143: 1999–2008.

Kleerekooper I, Herbert MK, Kuiperij HB, Sato DK, Fujihara K, Callegaro D, Marignier R, Saiz A, Senel M, Tumani H, De Jong B, Trip SA, Nakashima I, Verbeek MM, Petzold A. CSF levels of glutamine synthetase and GFAP to explore astrocytic damage in seronegative NMOSD. J Neurol Neurosurg Psychiatry 2020; 91: 605–611.

Kleerekooper I, Trip SA, Plant GT, Petzold A. Expanding the phenotype of MOG antibody-associated disease (MOGAD): half a century of epilepsy and relapsing optic neuritis. J Neurol Neurosurg Psychiatry 2020; 0: 1–3.

Kleerekooper I, Houston S, Dubis AM, Trip SA, Petzold A. Optical Coherence Tomography Angiography (OCTA) in Multiple Sclerosis and Neuromyelitis Optica Spectrum Disorder. Front Neurol 2020; 11: 1–17.

Marshall J, Kleerekooper I, Davagnanam I, Trip SA. Acute anosmia in neuromyelitis optica spectrum disorder. Mult Scler J 2020: 1–3.

Submitted / In preparation

Kleerekooper I, Del Porto L, Dell'Arti L, Guajardo J, Leo S, Robson AG, Trip SA, Petzold A, Plant GT, Holder GE. Macular structure and function in acute optic neuritis. *(Submitted)*

Kleerekooper I, Chua S, Foster PJ, Trip SA, Plant GT, Petzold A, Patel PJ, The UK Biobank Eye and Vision Consortium. Associations of alcohol consumption and smoking with disease risk and neurodegeneration in multiple sclerosis; a large UK cohort study. *(Submitted)*

Kleerekooper I, Traber GL, Dell'Arti L, Chapelle AC, Maillette de Buy Wenniger LJ, Chard D, Petzold A, Trip SA, Plant GT. Early Visual Failure in Multiple Sclerosis due to a Primary Progressive Bilateral Optic Neuropathy**.** *(Submitted)*

Kleerekooper I, Verschueren DV, Plant GT, Trip SA, Petzold A. Ellipsoid Zone reflectivity on OCT in neuroinflammatory and mitochondrial disease. *(In preparation)*

Further publications

Published

Dekker I, Leurs CE, Hagens MHJ, van Kempen ZLE, Kleerekooper I, Lissenberg-Witte BI, Barkhof F, Uitdehaag BMJ, Balk LJ, Wattjes MP, Killestein J. Long-term disease activity and disability progression in relapsing-remitting multiple sclerosis patients on natalizumab. Mult Scler Relat Disord 2019; 33: 82–87.

Wijburg MT, Kleerekooper I, Lissenberg-Witte BI, De Vos M, Warnke C, Uitdehaag BMJ, Barkhof F, Killestein J, Wattjes MP. Association of progressive multifocal leukoencephalopathy lesion volume with jc virus polymerase chain reaction results in cerebrospinal fluid of natalizumab-treated patients with multiple sclerosis. JAMA Neurol 2018; 75: 827–833.

Kleerekooper I, van Rooij SJH, van den Wildenberg WPM, de Leeuw M, Kahn RS, Vink M. The effect of aging on fronto-striatal reactive and proactive inhibitory control. Neuroimage 2016; 132: 51–58.

Vink M, Kleerekooper I, van den Wildenberg WPM, Kahn RS. Impact of aging on frontostriatal reward processing. Hum Brain Mapp 2015; 36: 2305–2317.

Jansen SA, Kleerekooper I, Hofman ZLM, Kappen IFPM, Stary-Weinzinger A, Van Der Heyden MAG. Grayanotoxin poisoning: 'Mad honey disease' and beyond. Cardiovasc Toxicol 2012; 12: 208–215.

Kleerekooper I, Van Kempen ZLE, Leurs CE, Dekker I, Rispens T, Lissenberg-Witte BI, van Munster CEP, de Jong BA, van Oosten BW, Uitdehaag BMJ, Wattjes MP, Killestein J. Disease activity following pregnancy-related discontinuation of natalizumab in MS. Neurol Neuroimmunol NeuroInflammation 2018; 5: 1–8

Submitted / In preparation

Verschueren DV, Kleerekooper I, Petzold A. Artificial intelligence in Neurology. *(In preparation)*

Kleerekooper I, Wagner S, Keane P, Khawaja A, Plant GT, Trip SA, Petzold A. Nasal atrophy of macular GCIPL thickness distinguishes pituitary lesions from glaucoma. *(In preparation)*

1. Introduction

This thesis aims to investigate neuroinflammatory disease, in particular the role of metabolic failure, through retinal imaging and biomarkers. In this chapter I will first introduce the neuroinflammatory diseases under investigation, multiple sclerosis (MS) and neuromyelitis optica spectrum disorder (NMOSD). This is followed by a brief discussion on anterior visual system anatomy from a neuro-ophthalmology perspective and its involvement in neuroinflammatory disease. Subsequently, the main retinal imaging technique used in this thesis, optical coherence tomography (OCT) will be introduced. Finally, the current understanding of the role of energy failure in neuroinflammatory disease will be summarised and the case for studying metabolic failure through retinal imaging will be made.

1.1. Neuroinflammatory disease

1.1.1. *Multiple Sclerosis*

Multiple sclerosis (MS) is an immune mediated demyelinating disorder of the central nervous system (CNS) that predominantly affects women in their childbearing years and is the most important cause of neurological disability in young adults (Reich *et al.*, 2018). The disease most commonly presents as relapsing-remitting MS (RRMS), which is characterised by fully or partly reversible episodes of subacute neurologic disability that last days to weeks. For about half of the RRMS patients the disease phenotype changes to a progressive accrual of disability without superimposed relapses, called secondary progressive MS (SPMS) after 10-20 years. A small proportion of patients (±15 %) presents with primary progressive MS (PPMS), exhibiting a progressive course from disease onset (Reich *et al.*, 2018, Thompson *et al.*, 2018*b*). Risk factors for MS are both genetic, with the strongest correlation being identified for the HLA-DRB1 locus on the major histocompatibility complex (MHC) (Gourraud *et al.*, 2012), and environmental, with important associations between low vitamin D concentrations, Epstein Bar virus infection and smoking having been reported (Reich *et al.*, 2018, Thompson *et al.*, 2018*b*). The prevalence of MS is approximately 285.8 per 100,000 women and 113.1 per 100,000 men in the UK (Mackenzie *et al.*, 2014) and as the disease can affect the entire CNS, clinical manifestations are diverse and range from physical disability and cognitive impairment to mood disturbance.

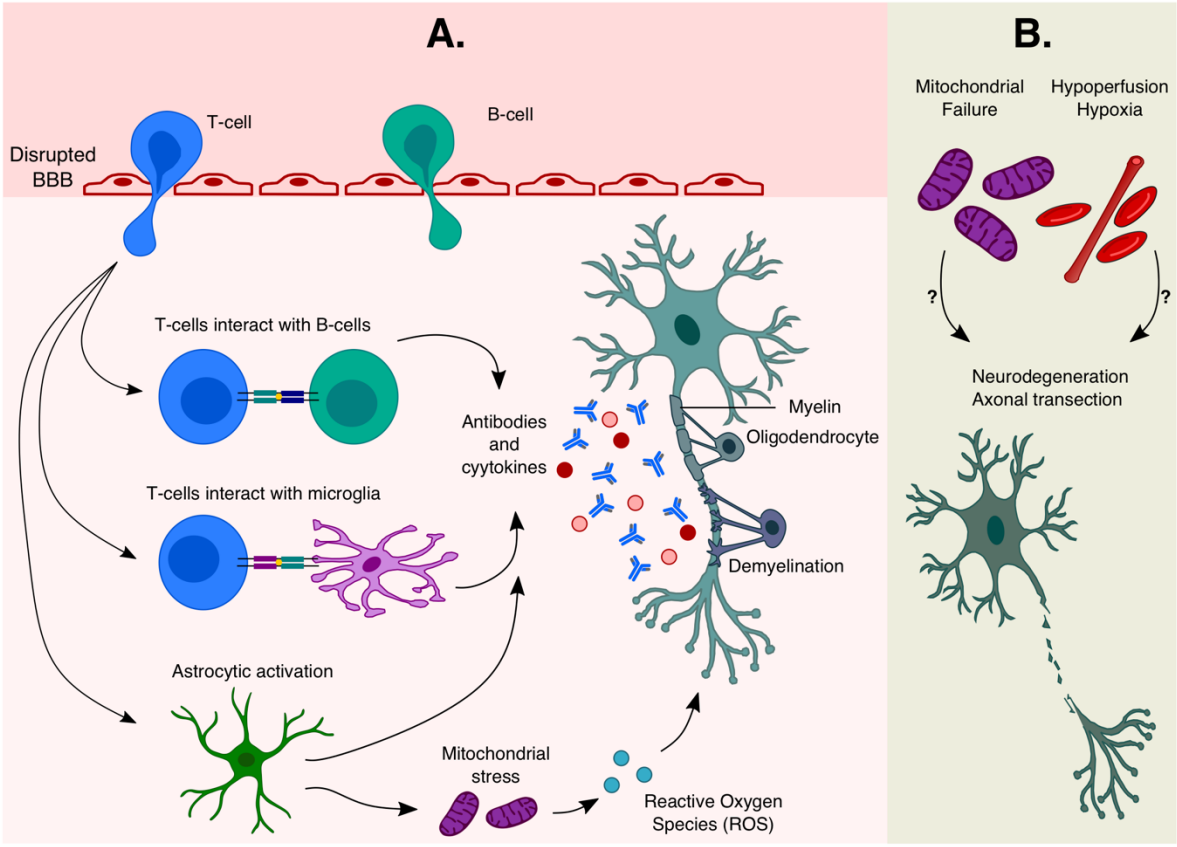

Figure 1.1 Schematic of multiple sclerosis pathophysiology. A: Adaptive immune cells migrate across the disrupted blood-brain barrier (BBB) to the central nervous system (CNS), where various interactions cause an inflammatory environment as antibodies and cytokines are released and likely cause demyelination. B: Mitochondrial failure, hypoperfusion and hypoxia are likely to play important roles in more progressive features of multiple sclerosis, such as neurodegeneration and axonal transection.

Many advances have been made in the field of MS, in particular with regard to the development of several highly effective immunomodulating drugs that successfully suppress disease activity in RRMS (Zhang *et al.*, 2014; Granqvist *et al.*, 2018; Kappos *et al.*, 2018; Derfuss *et al.*, 2020). However, most of the long-term disability is accrued in the progressive stages of MS, while there is still a sparsity of effective treatment options for these patients (Thompson, 2017). This is in part because MS pathophysiology has not yet been fully elucidated.

The most important and well-known pathologic process in RRMS remains demyelination associated with CNS inflammation, likely driven by T-cell infiltration (Frohman *et al.*, 2006; Lassmann, 2014). After disruption of the blood-brain-barrier (BBB) the CNS is infiltrated by T- and B-cells. Within the CNS these cells interact with each other, microglia and astrocytes

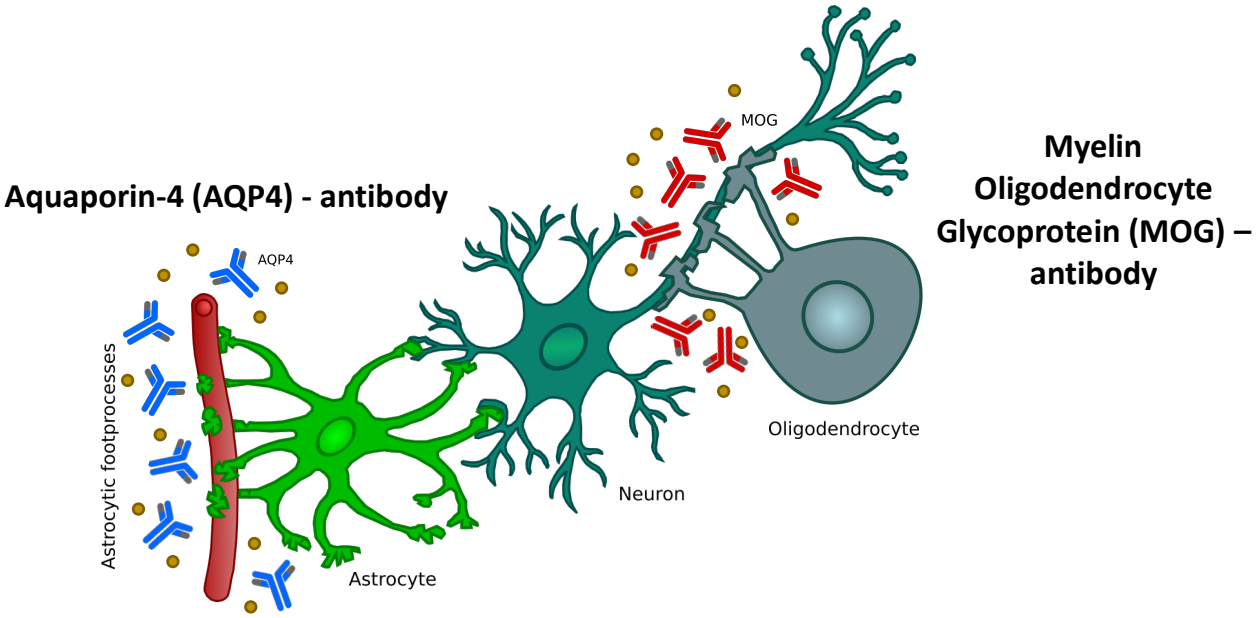

Figure 1.2 Schematic of the different pathologic processes in AQP4-antibody seropositive NMOSD and MOG-antibody associated disease. While AQP4-antibodies are associated with astrocytopathy, particularly at the perivascular foot processes, MOG-antibodies are associated with injury to the oligodendrocytes. The yellow circles visualize complement, which plays an important role in NMOSD associated injury.

which results in the release of antibodies, cytokines and other pro-inflammatory chemicals (Absinta *et al.*, 2021) (Figure 1.1-A). On the other hand, primary pathologic processes in progressive MS are thought to be axonal loss and atrophy (Lassmann *et al.*, 2012). The key pathologic processes driving these features of progressive MS are poorly understood, but mitochondrial failure and hypoperfusion are hypothesised to play important roles (Figure 1.1-B). However, axonal loss and atrophy are recognised to be present in RRMS as well (Kalkers *et al.*, 2002), and from the earliest stages of the disease. Histopathologic and radiologic studies have identified widespread axonal damage at the earliest clinical stages of MS and even in normal-appearing white matter of patients with acute MS (Mahad *et al.*, 2015; Balk *et al.*, 2016; Pietroboni *et al.*, 2017). This suggests that neurodegeneration in MS may not be the end-stage result of recurrent inflammatory damage, as previously believed, but is present from disease outset and can initially remain clinically silent. MS pathology is increasingly understood to not be exclusively driven by inflammation, and tissue energy failure has been steadily gaining traction as an important causal factor in the complex and likely multifactorial pathophysiology of MS (Desai and Smith, 2017).

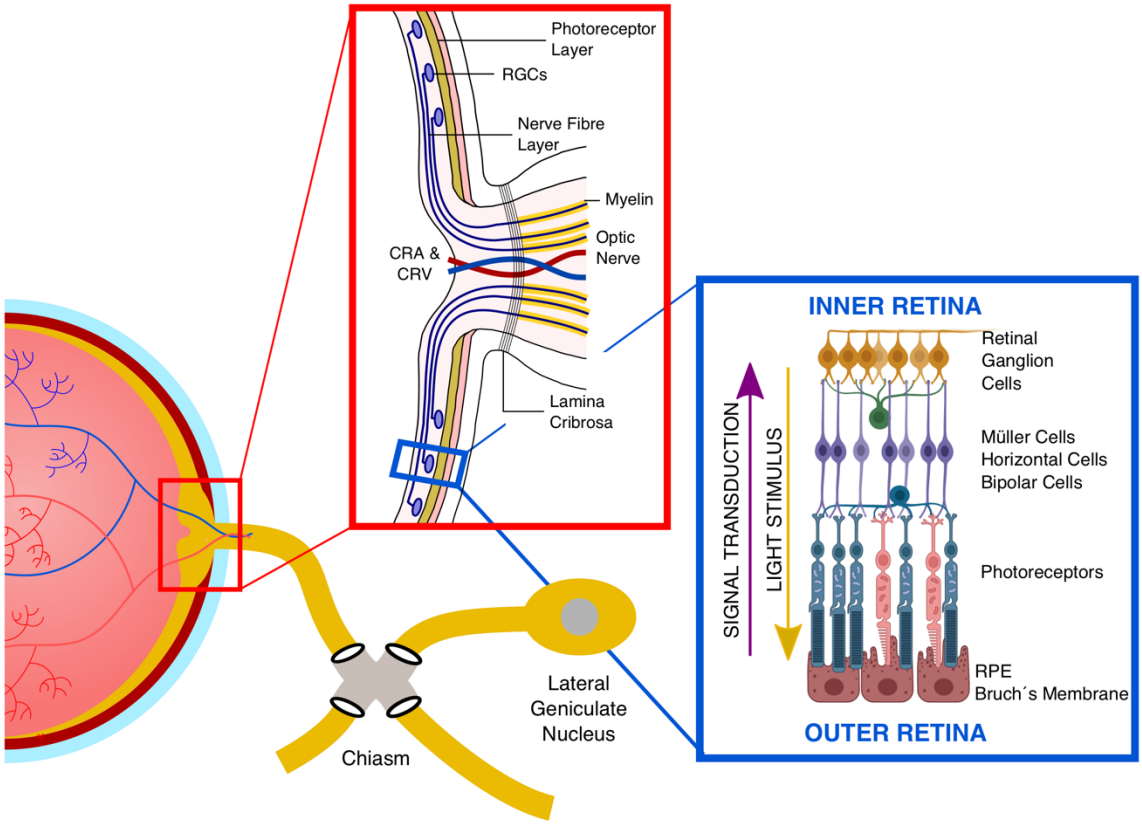

Figure 1.3 Schematic of retina and optic nerve anatomy. RPE: retinal pigmented epithelium. RGC: retinal ganglion cell. CRA: central retinal artery. CRV: central retinal vein. In part created with biorender.com.

1.1.2. *Neuromyelitis Optica Spectrum Disorders*

Neuromyelitis optica spectrum disorders (NMOSD) share cardinal features of optic neuritis (ON), longitudinally extensive transverse myelitis and area postrema syndrome that are often relapsing (Wingerchuk *et al.*, 2015; Fujihara, 2019). In most cases NMOSD is caused by the pathogenic effects of auto-antibodies targeting the water channel protein aquaporin-4 (AQP4), for which the majority of patients test positive. As AQP4 is predominantly expressed on perivascular astrocytic foot processes in the spinal cord and Müller cells in the retina, NMOSD has a predilection for the optic nerve and the spinal cord. NMOSD has a lower prevalence than MS, at 0.72-1.96 per 100,000 persons in the UK (Papp *et al.*, 2021), generally presents at a later age but also affects women to a greater extent than men.

A subset of NMOSD patients that test negative for AQP4 antibodies, test positive for antibodies against myelin oligodendrocyte glycoprotein (MOG) (Pache *et al.*, 2016). Histopathologically, MOG antibodies are associated with more predominant myelin injury

(Figure 1.2). Although patients with NMOSD may test positive for MOG antibodies, MOG associated disease (MOGAD) does not always fulfil NMOSD criteria (Höftberger *et al.*, 2020). MOGAD has a wide and not yet fully explored spectrum of disease, that includes epilepsy and acute disseminated encephalomyelitis, particularly in children. AQP4-associated disease has a higher predilection for affecting the spinal cord, while MOGAD is more often associated with ON. MOGAD is also more likely to present with bilateral ON, to be monophasic and has an approximately 1:1 sex ratio (Sato *et al.*, 2014*a*).

1.2. Anterior visual system anatomy from a neuro-ophthalmology perspective

This thesis will use 'the eye as a window to the brain' by making the most of the unique advantages that the anterior visual system has for studying the CNS, due to its anatomy and its frequent involvement in neurological diseases. Each optic nerve consists of approximately 1.2 million axonal fibres, most of which synapse in the lateral geniculate nuclei of the thalamus (Toosy *et al.*, 2014). The optic nerve fibres extend from the retinal ganglion cells (RGCs) in the inner retina, after which they initially form the unmyelinated retinal nerve fibre layer that relays information to the optic nerve head. The macular ganglion cell layer (GCL) contains the cell bodies of the RGCs, while the retinal nerve fibre layer (RNFL) is comprised of the axons of these cells that make up the optic nerve (Figure 1.3) (Strouthidis *et al.*, 2010). Posterior to the lamina cribrosa, the axons are wrapped by oligodendrocytes and the optic nerve becomes myelinated (Carelli *et al.*, 2004). The sclerae continue into the dura posterior of the globe, and the arachnoid and pia mater envelop the intraorbital section of the optic nerve as well (London *et al.*, 2013). These close anatomical links between the retina and CNS are further evidenced by the existence of retrograde degeneration, such as retinal atrophy as a result of optic nerve or visual cortex injury (Jindahra *et al.*, 2009; Balk *et al.*, 2014; Mühlemann *et al.*, 2020), and anterograde degeneration, such as thalamic and visual cortex atrophy as a result of optic nerve damage (You *et al.*, 2012).

Astrocytes are numerous around the optic nerve and serve important roles such as providing structural rigidity and maintaining the extracellular environment. Blood vessels in the CNS are ensheathed by the foot-processes of astrocytes, while vessels in the retina are enveloped similarly by Müller cells. Both retinal and cerebral blood vessels have continuous endothelial

tight junctions, resulting in selective permeability to various molecules (Shams and Plant, 2009; Campbell *et al.*, 2017).

Retinal and optic nerve circulation has the challenging goal of supplying nourishment and removing waste without compromising vision. There are two discrete vascular systems in the retina; the retinal and choroidal vessels. Blood supply for both systems comes from the ophthalmic artery, a branch of the internal carotid artery. The ophthalmic artery in turn branches out in two main vessel types that supply the retina, the central retinal artery and the posterior ciliary arteries. The central retinal artery runs with the optic nerve inside the optic nerve sheath and enters the globe through the optic disc after which it branches out to supply the inner retina (Campbell *et al.*, 2017; Joyal *et al.*, 2018).

1.3. Anterior visual pathway involvement in neuroinflammatory disease

1.3.1. *Prevalence of anterior visual pathway involvement*

Neuroinflammatory disease often affects the anterior visual pathway (Beck *et al.*, 2003; Okawa *et al.*, 2008). Post-mortem evidence indicates that anterior visual pathway involvement is virtually ubiquitous in MS (Toussaint *et al.*, 1983) and is also a major site of involvement in NMOSD (Hokari *et al.*, 2016).

Anterior visual pathway involvement often is the direct result of inflammatory insult, as approximately 25 % of MS patients present with ON (MSON), and the prevalence of symptomatic MSON increases to 70-80 % in later disease (Shams and Plant, 2009; Toosy *et al.*, 2014). This can also be subclinical, with structural or electrophysiological abnormalities evidencing previous ON that had gone clinically unnoticed (Halliday *et al.*, 1972; Petzold *et al.*, 2017). NMOSD even presents with ON in up to 50 % of cases (Levin *et al.*, 2013).

1.3.2. *Optic neuritis*

ON is an inflammatory optic nerve disorder that typically presents with unilateral subacute visual loss and pain that is exacerbated by eye movement. The visual loss has a gradual onset over hours to days, but the start can be experienced as quite sudden. Visual loss is usually described as blurry vision, after which a scotoma may develop. ON has been shown to be

associated with all different kinds and locations of scotomas, although these are usual central (Beck *et al.*, 2004; Pau *et al.*, 2011). Visual loss is variable, with visual acuity ranging from normal to no perception of light. Low contrast visual acuity and colour vision tests are usually more sensitive to picking up visual deficits compared with high contrast vision (Trobe *et al.*, 1996). ON mostly has an excellent spontaneous recovery of visual acuity. Mean time to recovering 6/6 vision is around 8 weeks, but vision can continue to improve for 6 months. However, visual function can remain low with acuities lower than 6/12 and 6/60 seen in 14 % and 5 % of patients after one year. Low contrast visual acuity and colour vision less frequently recovers completely and may remain suboptimal even if high contrast visual acuity recovers. Approximately 30 % of patients with ON experience positive visual symptoms, in the form of light flashes, called photopsias. These occur mainly in more anterior ON or neuroretinitis and tend to occur more frequently in the recovery phase than the acute stage of ON (Shams and Plant, 2009; Pau *et al.*, 2011).

ON is often associated with MS (Petzold *et al.*, 2014) but can also occur in association NMOSD, MOGAD, or in an isolated form, either single-episode isolated ON (SION) or relapsing. ON is usually clinically more severe in NMOSD compared with MS (Hokari *et al.*, 2016).

In the acute stage of ON, ophthalmoscopy reveals mild optic nerve oedema or hyperaemia in approximately 30 % of patients. Optic nerve oedema is transient and in later stages disc pallor, particularly in the temporal quadrant, can be observed. Pupillary light reflexes are reduced in the affected eye, causing a relative afferent pupillary deficit (RAPD). Magnetic resonance imaging (MRI) of the orbits is a sensitive investigation to confirm the diagnosis of ON. Typically, the radiological findings are most apparent in the retrobulbar intra-orbital segment of the optic nerve, which appears swollen with a high T2 signal. More than 90 % of ON patients that are scanned within 20 days of symptom onset show gadolinium contrast enhancement of the optic nerve (Miller *et al.*, 1988). After the acute insult, a high T2 signal usually persists and may be permanent. In the chronic stage the nerve will appear atrophied, which can be observed as a larger segment of fluid surrounding the nerve. Electrophysiological testing with pattern reversal visual evoked potentials (PVEP), used to record the conduction speed of light stimuli traveling from the retina to the occipital cortex, usually reveals a delay and reduced amplitude of the first positive deflection of the PVEP, called the P100, in ON. In some cases no

electrical response is observed at all, called conduction block. Another electrophysiological test sometimes used in the evaluation of ON is pattern electroretinography (PERG), which will be discussed in detail in chapter 2 of this thesis. Finally, as ON recovers retrograde degeneration can be observed in the retina with optical coherence tomography (OCT) (Box 1.1) as thinning of the macular ganglion cell and inner plexiform layer (mGCIPL) and the peripapillary retinal nerve fibre layer (pRNFL) (Petzold *et al.*, 2017). This atrophy mostly occurs during the three months following the onset of symptoms (Costello *et al.*, 2006).

***Box 1.1** Optical coherence tomography*

Optical coherence tomography (OCT) is a non-invasive and quick retinal imaging tool (Petzold *et al.*, 2017). OCT is highly effective in assessing retinal abnormalities, both qualitatively and quantitatively, and over the years OCT has emerged as a pivotal tool in expediting clinical diagnosis and optimising follow-up in neuroinflammatory disease (Jindahra *et al.*, 2010). OCT modalities have undergone rapid advances, and with the introduction of spectral-domain (SD) OCT high resolutions of approximately 3-7 µm are achieved. OCT can be described as an optical analogue to ultrasound-based imaging technology that uses low-coherence, near infrared light to measure the interference between backscattered light from microscopic constituents within tissue and a reference light beam reflected by a reference mirror to generate in vivo, two-dimensional structural images of biological tissue (Schuman *et al.*, 2004; Frohman *et al.*, 2008). The reference light beam and the sample beam are both directed towards the tissue of interest and the light that is reflected back is registered by a photo-detector in which the simultaneous registration of the two beams creates an interference signal (Figure 1.4). The first time-domain OCT images were obtained in 1991 by Huang and colleagues (Huang *et al.*, 1991). These days, the most commonly used OCT modality is SD-OCT, which uses a spectrometer instead of a photodetector to analyse all interference signals simultaneously instead of moving the reference beam splitter. The wavelength spectrum observed by the spectrometer is converted to time delay signals by the Fourier transform. As replacing the photodetector with a spectrometer allows full wavelength spectrum detection, this newer technique has faster acquisition speeds and is less sensitive to movement artefacts. Another important improvement specific to Heidelberg OCT is the active eye tracker, which observes eye movements on the infrared fundus image by recognising retinal features that make each retina unique like a fingerprint. The eye tracker corrects the OCT scan line for involuntary saccades away from target. Additionally, this setting allows for an automatic follow-up function that repositions the follow-up scan with only limited variability. Therefore, monitoring of minimal longitudinal changes is possible. Algorithms allow automated segmentation of individual retinal layers.

1.3.3. *Retinal abnormalities independent of optic neuritis*

Besides subacute inflammatory insult in the form of ON, neuroinflammatory disease is also associated with slowly progressive anterior visual pathway atrophy, as identified through mGCIPL and pRNFL thinning on OCT, that is independent of clinical ON (Trip *et al.*, 2006;

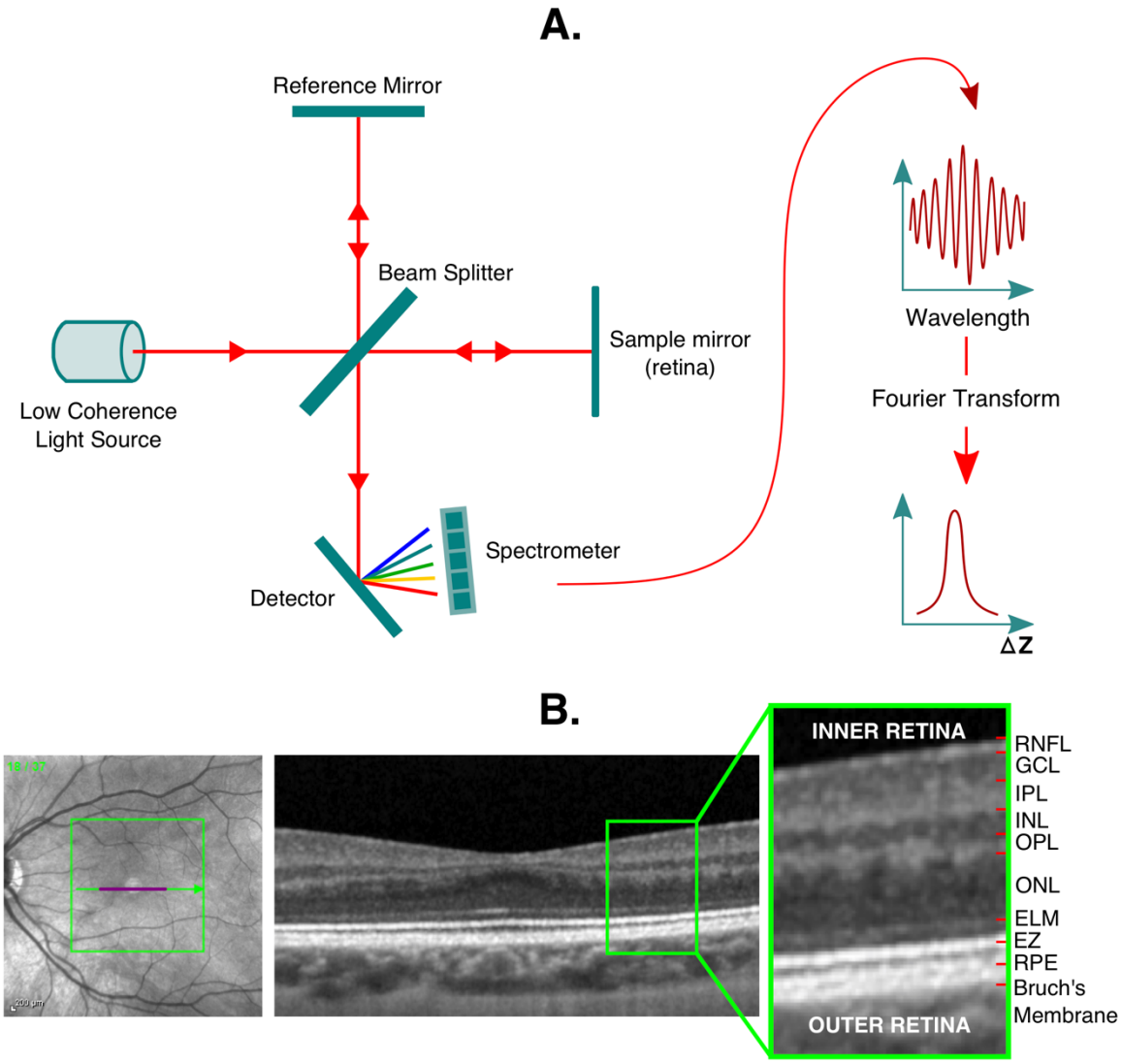

Figure 1.4 Optical coherence tomography (OCT). A: Schematic of the technical background of OCT including Fourier transform. B: Example healthy macular B-scan with inset noting layer nomenclature. Fundus photo on the left shows location of B-scan. RNFL = retinal nerve fibre layer. GCL = ganglion cell layer. IPL = inner plexiform layer. INL = inner nuclear layer. OPL = outer plexiform layer. ONL = outer nuclear layer. ELM = external limiting membrane. EZ = ellipsoid zone. RPE = retinal pigmented epithelium

Petzold *et al.*, 2017; Coric *et al.*, 2018). Retinal asymmetry of mGCIPL thickness has been found to increase the odds of having an MS diagnosis in patients without a history of clinical ON (Petzold *et al.*, 2020). It suggests that progressive features of MS, in particular neuronal loss and atrophy, can be captured in the retina. This is further evidenced by the fact that mGCIPL thickness measurements are associated with brain volume measurements on magnetic

resonance imaging (MRI) in the general population (Chua *et al.*, 2021*a*) and in MS (Saidha *et al.*, 2015*a*) as well as with MS disability scores (Martinez-Lapiscina *et al.*, 2016).

Although most damage to the optic nerve and retina occurs in the inner retinal layers, such as the discussed pRNFL and mGCIPL atrophy, there is evidence suggesting retinal involvement distal to these layers as well. Histopathological evaluation of retinal tissue of MS patients revealed that more outwardly located retinal layers, in particular the inner nuclear layer (INL), were important locations of pathology (Green *et al.*, 2010). INL thickness increases measured with OCT have been found to be associated with poor visual recovery after ON (Kaufhold *et al.*, 2013). Most data on INL involvement exist for the MSON subtype. INL changes may predict new enhancing radiological lesions and relapses in MS, suggesting an association with inflammatory disease activity (Balk *et al.*, 2019). The high incidence of retinal periphlebitis, especially in active disease (Lightman *et al.*, 1987), uveitis, particularly pars planitis (Messenger *et al.*, 2015), and activated microglia in MS retina (Green *et al.*, 2010), further document retinal inflammatory activity in MS. INL thickening may be related to microcystic macular oedema (MMO) (Gelfand *et al.*, 2013), present in approximately 10 % of ON eyes (Kaufhold *et al.*, 2013), and slightly more common in NMOSD associated ON compared with MSON and SION (Gelfand *et al.*, 2013). Some consider MMO to be a retrograde maculopathy, as it occurs in many forms of optic neuropathy (Abegg *et al.*, 2014). A better understanding of INL involvement in acute neuro-inflammatory disease is important given the discussed associations of INL thickening with important clinical parameters (Kaushik *et al.*, 2013) and treatment response in MS (Knier *et al.*, 2016). There are also treatment implications if the macula contributes to the visual loss in acute ON.

Furthermore, early unexplained findings of abnormal outer retinal function on electroretinography (ERG) in MS (Coupland and Kirkham, 1982; Falsini *et al.*, 1992) have been corroborated by more recent reports (Forooghian *et al.*, 2006; Sriram *et al.*, 2014; Janáky *et al.*, 2017; You *et al.*, 2018; Filgueiras *et al.*, 2019; Al-Nosairy *et al.*, 2021). Electrophysiological retinal dysfunction in MS has been found to be present even in the absence of ON or structural atrophy of the mGCIPL (Hanson *et al.*, 2018). There is some suggestion that retinal dysfunction is most pronounced during the acute stages of ON (Berninger and Heider, 1990; Holder, 2004). Some preliminary data suggest that outer retinal dysfunction is less pronounced in NMOSD

compared with MS (Filgueiras *et al.*, 2019). These functional changes may be accompanied by subtle structural changes to outer retinal layers, with a large meta-analysis of optical coherence tomography (OCT) scans from patients with MS finding a small but significant thickening of the combined outer nuclear layer (ONL) and outer plexiform layer (OPL) in eyes affected by ON compared with eyes that were not affected by ON (Petzold *et al.*, 2017). Not all MS patients seem to have structural outer retinal involvement to the same extent, and there is some evidence indicating that more prominent and early atrophy of outer retinal layers is associated with more aggressive disease and more severe disability (Saidha *et al.*, 2011). Despite these findings, the nature and clinical relevance of outer retinal pathology in ON and MS remains poorly understood.

1.4. Energy failure in neuroinflammatory disease

1.4.1. *Mitochondrial failure*

Although important advances have been made in the field of MS, many questions about its pathophysiology remain unanswered. Anita Harding's landmark paper, describing a group of patients with the mitochondrial disease Leber hereditary optic neuropathy (LHON) that developed demyelinating disease of the CNS, indicated that mitochondrial gene mutations may contribute to MS susceptibility and poor outcome (Harding *et al.*, 1992). Her work has prompted substantial expansion of research on mitochondrial failure in MS. Mitochondria are the key facilitators of oxidative phosphorylation, the most efficient metabolic pathway for producing energy in the form of ATP in aerobic organisms (Suomalainen and Battersby, 2018). Mitochondria also contribute to Ca2+ homeostasis, failure of which may lead to intracellular Ca2+ overload and apoptosis (Giorgi *et al.*, 2018). The close functional and structural association of glia and the neuro-axonal complex is an important factor in MS pathophysiology. Glia are a major source of inflammatory mediators such as reactive oxygen species (Nave, 2010; Fischer *et al.*, 2012), which in increased concentrations aggravate demyelination and metabolic dysfunction by damaging vulnerable oligodendrocytes and mitochondria (Smith *et al.*, 1999). Also, glia play important roles in adapting to variable energy demands by regulating glucose availability in MS lesions (Nijland *et al.*, 2014; Saab and Nave, 2017).

Mitochondrial dysfunction, particularly the accumulation of dysmorphic and swollen mitochondria, is among the first histopathological manifestations of the murine MS model experimental autoimmune encephalomyelitis (EAE) (Nikić *et al.*, 2011). Mitochondrial changes in EAE are related to clinical disease activity in time and severity (Sadeghian *et al.*, 2016). MS plaques contain high levels of oxidative damage, particularly to the vulnerable mitochondrial DNA (mtDNA) (Vladimirova *et al.*, 1998). One study found that neurons affected by MS lack an mtDNA-encoded catalytic subunit of respiratory chain complex IV, which could be brought back to high levels of clonally expanded mtDNA deletions on a single-neuron level (Campbell *et al.*, 2011). Furthermore, MS is associated with high levels of mtHSP70, a marker for mitochondrial stress (Witte *et al.*, 2009), and a significant decrease in mRNA of peroxisome proliferator-activated receptor gamma coactivator 1-alpha (PPARGC1A), an important regulator of metabolism and mitochondrial function (Witte *et al.*, 2013). Exposing neurons to cerebrospinal fluid (CSF) from individuals affected by MS in vitro leads to mitochondrial elongation and dysfunction of respiratory chain complexes I, III and IV. Interestingly, this neurotoxic effect could be reversed if extra glucose and lactate was supplied (Wentling *et al.*, 2019).

Studies investigating mitochondrial failure in MS in humans are relatively rare. However, patients with MS were found to have higher concentrations of extra-mitochondrial glucose metabolites, such as lactate, as well as ATP metabolites (such as purines and oxypurines) in their CSF and serum compared with control subjects (Amorini *et al.*, 2014; Albanese *et al.*, 2016; Lazzarino *et al.*, 2017). One study identified decreased respiratory chain complex IV activity in serum mononuclear cells of MS patients compared with control subjects (Hargreaves *et al.*, 2018). Finally, lower concentrations of N-acetyl-aspartate (NAA), a molecule believed to reflect mitochondrial function, have been shown to predict a worse clinical outcome in multiple sclerosis (Van Horssen *et al.*, 2012). However, as NAA is thought to reflect neuronal cell loss as well as dysfunction of mitochondria, these results might be partly confounded by CNS atrophy.

1.4.2. *Hypoxia and hypoperfusion*

Many studies have demonstrated the presence of hypoxia and hypoperfusion in the CNS of MS affected individuals clinically, radiologically, and histologically (Martinez Sosa and Smith, 2017). For example, cerebral type-III MS lesions histologically resemble hypoxic insult and MS lesions tend to form in watershed areas of the areas of the brain, suggesting a role for hypoxia in its pathophysiology (Haider *et al.*, 2016; Yang and Dunn, 2018). Several studies found a reduction in cerebral blood flow in MS affected individuals, even in the absence of structural damage (Juurlink, 2013; D'Haeseleer *et al.*, 2015). Cerebral circulation times are increased from a mean of 2.8 seconds in controls to 4.9 seconds in all types of MS (Monti *et al.*, 2015). Hypoperfusion in MS can be identified from very early in its disease course, with perfusion rates reduced even in patients with clinically isolated syndrome (CIS) (Varga *et al.*, 2009). Additionally, a study which used near-infrared spectroscopy (NIRS) showed that almost half of MS patients had haemoglobin saturation values that were significantly reduced compared with healthy controls (Yang and Dunn, 2015). Anaemia more than doubles the risk of developing MS and also doubles the risk of experiencing a relapse in MS (Tettey *et al.*, 2016). Furthermore, patients with MS have an increased risk of ischaemic heart disease and stroke, suggesting further susceptibility to microvascular damage (Jadidi *et al.*, 2013). Interestingly, one exploratory case study found evidence for transient reduced blood flow focally in the optic nerve during acute MSON (Haufschild *et al.*, 2003). Preliminary data suggests that blood flow in the retinal microcirculation is reduced in patients with RRMS compared with healthy controls (Modrzejewska *et al.*, 2007; Jiang *et al.*, 2016).

Animal work has shown that the inflamed spinal cord of EAE affected animals is severely hypoxic and hypoperfused (Nikić *et al.*, 2011; Davies *et al.*, 2013; Nathoo *et al.*, 2015; Sadeghian *et al.*, 2016). The level of hypoxia was temporally and spatially related to the clinical deficit, and predicted subsequent demyelinating damage. Investigations indicated that the hypoxia was caused by insufficient perfusion of the CNS, creating a shortage of oxygen delivery in the inflamed area (Davies *et al.*, 2013). Accordingly, it was found that therapeutic approaches aimed at alleviating hypoxia, with inspired oxygen, or alleviating hypoperfusion, with vasodilating agents, were related to improved neurologic outcome and reduced later stage demyelination in the affected animals (Desai *et al.*, 2020). These findings suggest that

hypoxia and hypoperfusion may render nerve cells inexcitable through depolarization, causing disability in the acute stage, but also damage oligodendrocytes, causing subsequent demyelination.

In addition to genuine hypoxia, the increased energy demands of saltatory conduction along demyelinated axons in MS may result in mitochondrial upregulation, causing increased numbers of mitochondria to be a continuous source of deleterious reactive oxygen species (Trapp and Stys, 2009). This situation, referred to as 'virtual hypoxia', initiates cellular signalling pathways affiliated with hypoxic and ischaemic conditions, resulting in oxidative stress, further mitochondrial dysfunction and increased intracellular Ca2+ concentrations through release of toxic Ca2+ from the axoplasmic reticulum (Trapp and Stys, 2009; Desai and Smith, 2017). Hypoxia and mitochondrial dysfunction can cause a vicious circle inducing axonal failure and neurodegeneration in multiple sclerosis, with one process impairing neuronal resilience to the other.

Although attention for vascular changes in neuroinflammatory disease has been primarily focused on MS, there is also evidence that NMOSD pathophysiology may be in part vascularly mediated (Marignier *et al.*, 2010; Kawachi and Lassmann, 2017). Neuropathology of AQP4-antibody seropositive NMOSD lesions show a perivascular pattern (Lucchinetti *et al.*, 2002; Roemer *et al.*, 2007), with rim deposits of activated complement components and macrophages found around thickened, fibrosed, and hyalinised vessels. Active spinal cord lesions may have an increased density of vascular structures (Lucchinetti *et al.*, 2002). Similar to MS lesions predominantly forming in watershed areas of the brain with poor perfusion, AQP4-antibody seropositive NMOSD lesions preferentially form in the hypo-perfused posterior and lateral spinal columns (Bradl *et al.*, 2018). AQP4 is expressed in a vasculocentric pattern in the optic nerve and spinal cord (Roemer *et al.*, 2007). Importantly, the predominantly perivascular location of is one of the key neuropathological features that can distinguish AQP4-antibody associated NMOSD from MS lesions at autopsy (Roemer *et al.*, 2007). One study found that retinal vascular changes identified through fundoscopy, such as attenuation of the peripapillary vascular tree (present in 3/40 MS eyes and 22/32 NMOSD eyes; $p = 0.001$) and focal arteriolar narrowing (present in 0/40 MS eyes and 9/32 NMOSD eyes; $p < 0.001$) could successfully distinguish NMOSD from MS patients (Green and Cree,

2009). Neuropathological studies of CNS lesions in MOG-antibody seropositive patients reveal features distinctly different from AQP4-antibody associated lesions. Although MOG associated lesions have a predilection for perivascular locations, this is less profound compared with AQP4-associated pathology. MOG lesions were found to share pathological characteristics with immunotype II and III MS lesions (Höftberger *et al.*, 2020). Type III pattern of demyelination shows similar tissue changes as observed in early stage white matter ischemia, and is therefore hypothesized to potentially be caused in part by hypoxia (Lassmann, 2013).

Although hypoxia and hypoperfusion are increasingly recognised as a possible important component in the multifactorial aetiology of neuroinflammatory, interpretation of its role is controversial. Ambiguity remains if it is a primary process, representing a causal factor in the disease mechanism, or a secondary process, developing in response to lower metabolic demand in atrophied tissue (Martinez Sosa and Smith, 2017). Retinal imaging may provide valuable new tools for future investigations in this field.

1.5. Retinal imaging to investigate metabolic function

1.5.1. *Retinal metabolic demand*

The anterior visual system provides an excellent location to study energy failure in neuroinflammatory disease, since it is one of the most metabolically active structures in the human body and is often affected (Beck *et al.*, 2004; Okawa *et al.*, 2008; Wong-Riley, 2010; Joyal *et al.*, 2018). The CNS has a very high energy demand, representing only 2 % of bodyweight, but 20 % of all resting state energy consumption (Lax et al., 2017). The retina consumes even more energy, its metabolic rate generally reported to exceed that of the brain (Okawa *et al.*, 2008; Warrant, 2009; Wong-Riley, 2010; Joyal *et al.*, 2018) (Figure 1.5). Accordingly, the choroid has the highest perfusion rate of any other structure within the human body and can rapidly adapt to changes in energy demand (Joyal *et al.*, 2018; Yu *et al.*, 2019).

The main function of the retina is the process of converting photons into an electrical retinal signal, called phototransduction. Human vision begins with photon absorption by visual

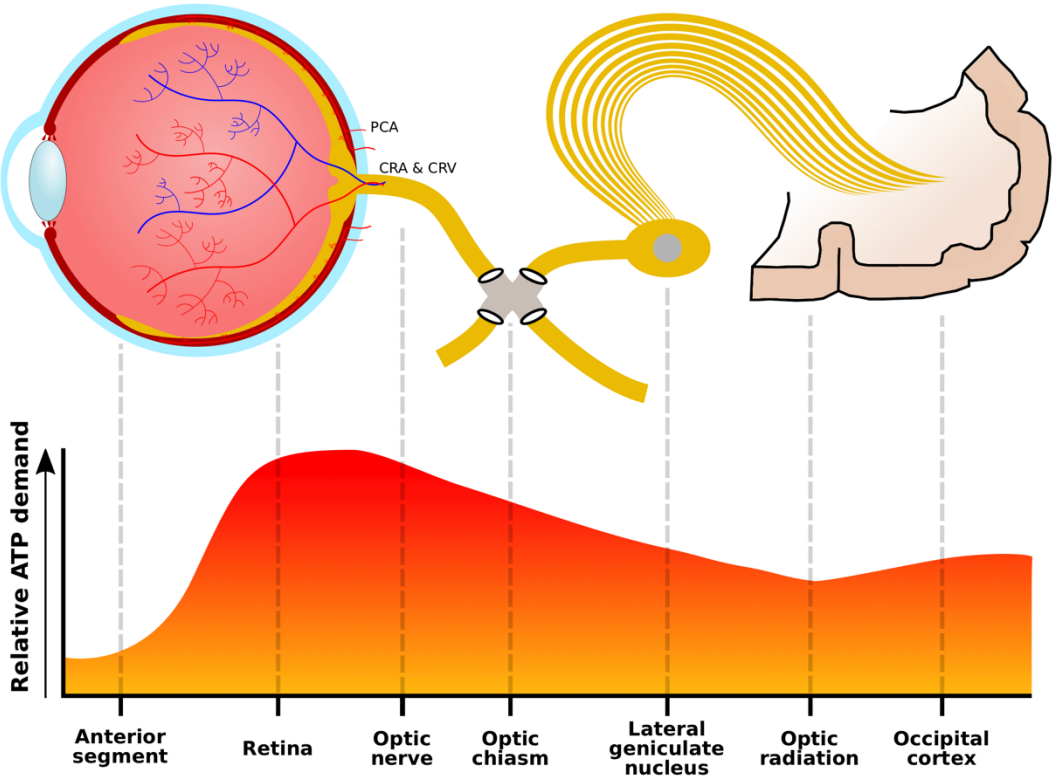

Figure 1.5 Schematic representation of energy demand along the length of the anterior visual system. CRA = central retinal artery. CRV = central retinal vein. PCA = posterior ciliary artery.

pigments in the photoreceptor outer segments, of which rhodopsin is the most abundant. Captured photons activate rhodopsin, after which rhodopsin binds to the G-protein transducin. As a result, the GDP molecule bound to the transducin a-subunit (T-a) is replaced by GTP, and the T-a GTP complex is released. The T-a GTP complex subsequently removes one c-subunit from inactive phosphodiesterase (PDE). A total of two c-subunits need to be removed to fully activate PDE. Activated PDE decreases the intracellular concentration of cyclic guanine monophosphate (cGMP) by hydrolysing cGMP to GMP. As a result of the lower cGMP concentration, ion channels in the cell membrane of the photoreceptor close, halting ion influx, which leads to subsequent hyperpolarization of the neuron. The hyperpolarized photoreceptor stops releasing excitotoxic neurotransmitter glutamate, resulting in the generation of an electrical potential in one or more bipolar cells (Okawa *et al.*, 2008; Wong-Riley, 2010).

Counterintuitively, in daylight, rods use ±75 % less energy than in scotopic conditions. In contrast, energy demand in cones is not affected by light conditions and is similar to that of

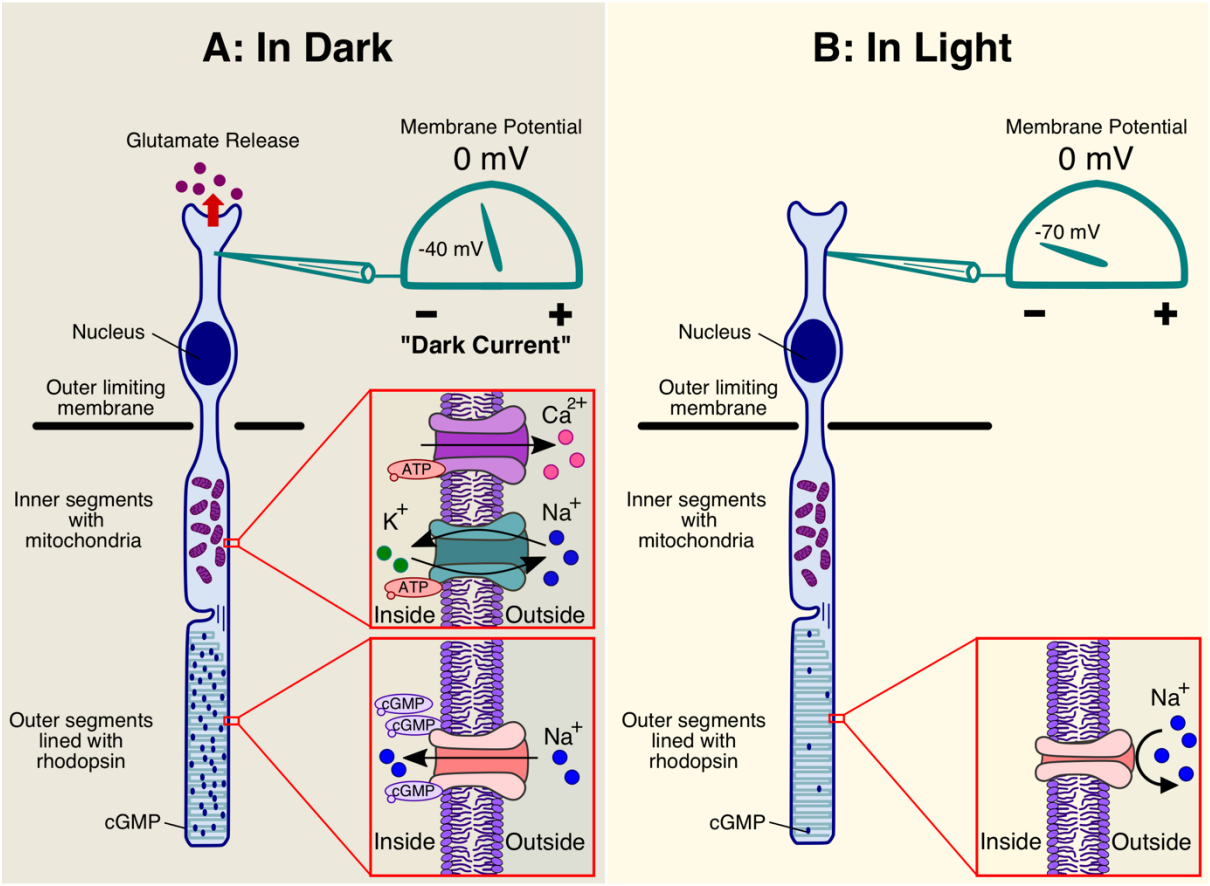

Figure 1.6 Schematic of processes occurring within rod photoreceptors in association with dark adaptation. A: situation during dark adaptation, including high concentration of cGMP, associated opening of the Na+ pore in the outer segment and activity of the Na+/K+ - ATPase and CA2+-ATPase transporters in the inner segment. B: situation in light, when there is a low concentration of cGMP and the Na+ ion pore is closed.

dark-adapted rods. Therefore, cones are more metabolically costly than rods on a cellular level, but because rods greatly outnumber cones, net retinal energy demand still decreases in daylight (Okawa *et al.*, 2008). In the dark, ion channels in the cell membrane of photoreceptors are open and allow influx of ions (Warrant, 2009). To maintain a relative depolarization of –40 mV, a state called the 'dark current', Na+ and Ca2+ ions are actively pumped out extracellularly against an ion-concentration gradient using two solute pumps, Na+/K+-ATPase and Ca2+-ATPase (Figure 1.6). Together, these two pumps account for almost all expended energy in dark-adapted photoreceptors. An additional factor contributing to the high energy demand in the anterior visual system is the fact that axons in the nerve fibre layer that conduct visual information are unmyelinated before they pass through the lamina cribrosa. This unmyelinated portion has slower conduction velocities and a markedly higher energy demand, as signified by marked cytochrome C oxidase (COX) staining locally (Carelli *et al.*,

2004). The energy consumption of a dark-adapted photoreceptor ranks top of all mammalian cells (Warrant, 2009; Wong-Riley, 2010). The majority of energy is created in the inner segments of the photoreceptors, where 60–65 % of all retinal mitochondria accumulate.

1.5.2. *Retinal imaging of metabolic function*

The intraorbital segment of the optic nerve contains most of the components of the cerebral environment, including oligodendrocytes and astrocytes, while the retinal segment differs in that it is unmyelinated and environmental homeostasis is maintained by Müller cells. The pathophysiology of MSON resembles that of MS plaque formation in the brain, as it involves perivascular cuffing, oedema of the nerve sheath and demyelination (Shams and Plant, 2009). The various aspects of MS pathophysiology, that involve neuronal and axonal loss, demyelination, oligodendrocytic loss and remyelination, can be identified in the optic nerve and the retina during and after an optic neuritis (London *et al.*, 2013). This brings into focus the possibility of using retinal imaging to study metabolic function in ON specifically and in neuroinflammatory disease in general.

Besides the use of OCT for imaging of retinal layer thickness as a marker of atrophy and structural qualitative changes such as MMO (Gelfand *et al.*, 2012), novel OCT modalities, focusing on the metabolically active photoreceptors, could indirectly provide insight into mitochondrial function. When studying energy failure in the retina, it is likely expedient to focus on dark-adaptation, given the discussed high metabolic demands that are associated with this process. Preliminary work with OCT has shown it is possible to visualise dynamic changes in outer retinal structure that occur during dark-adaptation. Photoreceptor outer segments increase in length in dark-adapted compared with photopic conditions (Lu *et al.*, 2017). This lengthening of retinal outer segments during dark adaptation was found to be reduced in vitelliform macular dystrophy (synonymous Best disease) (Abràmoff *et al.*, 2013). Considering the discussed very high energy demands of dark adaptation in the outer retinal layers, this observation warrants further exploration as it may be a valid indirect quantitative measure for metabolic failure in the retina. As discussed before, there is some electrophysiological data indicating that the photoreceptors may be particularly affected in acute ON, which is why pilot data in this thesis will focus on patients in the acute stages.

Furthermore, mitochondria have a high reflectivity index on OCT (Litts *et al.*, 2018). The second hyperreflective band seen on OCT, corresponding to the ellipsoid zone (EZ) of the photoreceptor inner segments, relates to local mitochondrial accumulation (Cuenca *et al.*, 2018). Reduced relative intensity or structural integrity of the EZ may reflect decreased numbers, altered morphology or function of mitochondria. In age-related macular degeneration (AMD), a decreased relative intensity of the EZ has indeed been reported (Tao *et al.*, 2016). This is an interesting observation as mitochondrial complex failure has been implicated in AMD (Nag and Wadhwa, 2016).

Additionally, OCT-angiography (OCTA), a novel OCT technique that images the retinal microvasculature, may provide an avenue for investigations into vascular changes in the CNS. Preliminary OCTA research shows the retinal microvasculature is affected in both MS and NMOSD, even in eyes unaffected by ON and in some cases in the absence of structural retinal atrophy (Murphy *et al.*, 2019; Chen *et al.*, 2020). Investigating when vascular changes occur relative to thinning of retinal layers in neuroinflammatory disease may help answer important questions about the role of hypoperfusion in their pathophysiology. Finally, certain qualitative characteristics of the retinal microvasculature on OCTA may provide information for diagnostic discrimination between different causes of ON (Petzold *et al.*, 2016), similar to how the “central vein sign” on high-field MRI is a valuable and very specific diagnostic marker for MS (Sati *et al.*, 2016).

As described, the anterior visual system has a high energy demand and is easily assessible with retinal imaging modalities. This makes it a potentially favourable location to study metabolic failure in neuroinflammatory disease. Mitochondria-targeted antioxidant agents are potential new therapeutic options in MS patients that could be effective early in the clinical disease course. Detection of mitochondrial dysfunction at the first manifestation of MS could provide further evidence for mitochondrial failure being a primary pathologic process in MS. Furthermore, if OCT could provide a non-invasive and quick functional measure of mitochondrial health, this could provide a valuable follow-up metric in trials aiming to salvage mitochondrial function in MS, such as those that have completed or started recently (Negrotto *et al.*, 2016; Chataway *et al.*, 2020).

1.6. Aims and outline of this thesis

This thesis aims to investigate neuroinflammatory disease through retinal imaging and biomarkers. Part 1 discusses the investigations of retinal dysfunction in acute ON, including the results of two pilot studies that aim to investigate metabolic failure in neuroinflammatory disease by developing novel OCT analysis techniques focusing on the outer retinal layers. Part 2 has a more clinical focus and discusses several studies that use retinal imaging and/or biomarkers to characterise phenotypes and environmental risk-factors in neuroinflammatory disorders.

1.6.1. *Outline Part 1*

In Chapter 2 the results of a study exploring structure-function correlates of retinal function in acute optic neuritis are reported.

Chapter 3 describes pilot work investigating dynamic thickness changes to the outer retinal layers that occur during dark-adaptation, and how these are affected by acute optic neuritis.

Chapter 4 details the development of a novel analysis tool that quantifies the reflectivity of the ellipsoid zone, and its associations with neuroinflammatory and mitochondrial disease.

Chapter 5 discusses the potential of OCT-angiography in the field of neuroinflammatory disease and presents limited preliminary data.

1.6.2. *Outline Part 2*

Chapter 6 describes the clinical and imaging characteristics of MS patients that present with primary progressive optic neuropathy in a retrospective cohort.

Research exploring the associations of smoking and alcohol consumption with retinal thickness, a substrate for neurodegeneration, in MS is described in Chapter 7.

Chapter 8 details an exceptional case of longstanding steroid-responsive epilepsy and relapsing optic neuritis in MOG antibody-associated disease.

A biomarker study reporting on evidence for astrocytic damage in seronegative neuromyelitis optica spectrum disorder is described in Chapter 9.

Finally, Chapter 10 will give a summary and a general discussion of the work discussed in this thesis.

Part 1

2. Macular structure and function in acute optic neuritis

ABSTRACT

Background Macular involvement in optic neuritis (ON) is well-recognised but its clinical relevance and structural correlates are poorly understood.

Objective Exploring macular structure-function correlates in acute and recovered ON.

Methods Twenty-six patients ON patients were recruited within 14 days of onset. Subjects underwent pattern electroretinography (PERG) and optical coherence tomography (OCT) imaging. PERG P50 and N95 components were correlated with OCT data. For 16 patients PERG measurements were repeated after approximately three months.

Results Eleven multiple sclerosis (MSON), six myelin oligodendrocyte glycoprotein associated (MOGON) and nine isolated acute ON cases were compared with 28 controls. PERG P50 component amplitudes, largely reflecting macular function, were reduced in affected eyes (median 2.3 µV; range 0.8–5.0 µV) compared with controls (3.3 µV; range 2.8-5.7 µV), and compared with fellow eyes (both $p<0.001$). There was consequent reduction in N95 amplitude. Eight cases (32 %) with subnormal P50 amplitudes (<2.0 µV) had poorer visual acuity ($p=0.020$). P50 amplitudes were positively correlated with INL thickness ($r_s=0.36$; $p=0.009$). After three months of follow-up N95/P50 ratios decreased significantly ($p=0.021$), while P50 amplitudes increased at trend ($p=0.064$) and there was no change in N95 amplitudes ($p=0.819$).

Conclusions P50 component reduction indicates macular involvement in acute ON, and correlates with structural alterations revealed by OCT. These early macular pathologic processes are likely to contribute to visual loss in the acute setting and show recovery during follow-up.

2.1. Background

Retinal involvement in optic neuritis (ON) is poorly understood, but may hold clinical relevance as thickening of the inner nuclear layer (INL) is related to poorer visual recovery (Kaushik *et al.*, 2013; Knier *et al.*, 2016; Petzold *et al.*, 2017). The pattern electroretinogram (PERG) is the retinal electrophysiological response to contrast stimulation, conventionally an isoluminant reversing black and white checkerboard. The PERG has two main components: a positivity at approximately 50ms (P50) followed by a larger negativity at 95ms (N95) (Holder, 1987) (Figure 2.1). The N95 component can be selectively affected in optic nerve disease, whereas P50 is affected in macular dysfunction. N95 is probably exclusively generated by the retinal ganglion cells (RGCs) (Holder, 1987; Viswanathan *et al.*, 2000). P50 origins are not fully ascertained, with approximately 70 % being generated by RGCs and 30 % more distally (Holder, 1991). However, P50 is "driven" by macular photoreceptors and is an accepted measure of macular function (Holder, 1987, 1991). Thus, the PERG facilitates the electrophysiological differentiation between macular and optic nerve dysfunction (Holder, 1987; Viswanathan *et al.*, 2000). The PERG is abnormal in approximately 40 % of recovered ON cases (Plant *et al.*, 1986; Holder, 1987), with most abnormalities confined to the N95 component (85 %) (Holder, 1991). However, P50 abnormalities, in addition to N95 reduction, can occur in acute ON (Berninger and Heider, 1990; Holder, 2001). This P50 reduction typically recovers over several weeks, possibly starting as soon as 7 days after symptom onset (Holder, 1991).

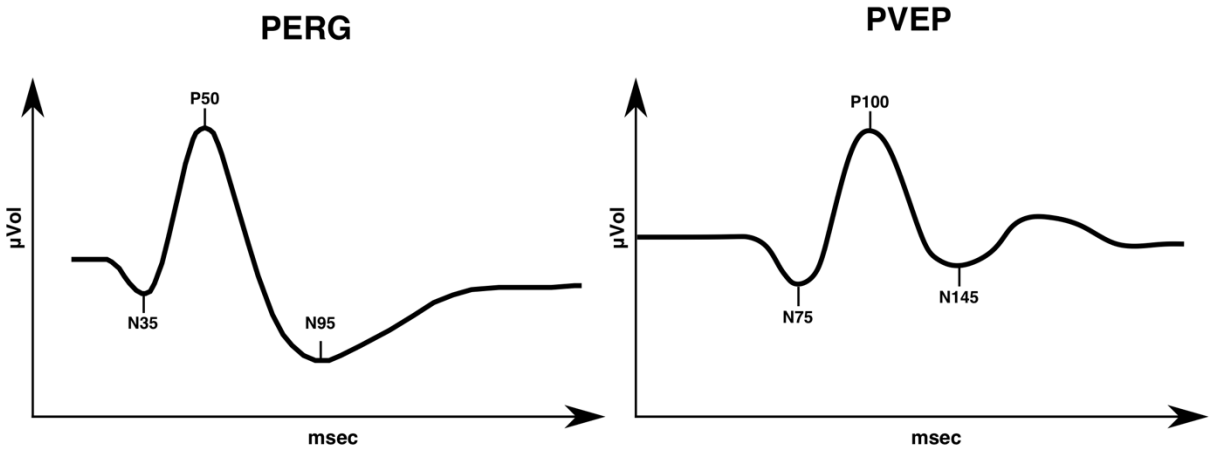

Figure 2.1 Example of normal PERG and PVEP electrophysiological responses. The PVEP traced is shown according to the ISCEV standards, with the P100 peak shown as an upward inflection.

In summary, structural INL changes and macular dysfunction evolve following ON but the underlying pathophysiological mechanisms are poorly understood. This study investigates the structural correlates of electrophysiologically demonstrable macular abnormalities in acute ON to elucidate the underlying retinal processes in the early phase of ON.

2.2. Aims, objectives and hypotheses

2.2.1. *Aims and objectives*

The aim of this study is to explore the structure-function correlates of macular dysfunction in acute ON how this evolves during follow-up to improve understanding of the role of macular involvement, in particular relating to the INL, in ON. Furthermore, associations of macular function with visual acuity in the acute stages of ON will be investigated.

2.2.2. *Hypotheses*

The main hypothesis of this study is that macular function, as measured through the PERG P50 amplitudes, is reduced in acute ON and shows associations with functional metrics, such as visual acuity, and with the thickness of the INL. A secondary hypothesis is that these data will show that macular function is most severe in the acute stages of ON and shows recovery during follow-up, as was reported in previous studies.

2.3. Methods

2.3.1. *Subjects*

Patients 18-60 years old with symptomatically unilateral ON, without a previous episode in the affected eye, were prospectively recruited from Moorfields Eye Hospital, London, UK. Diagnosis was made by a neuro-ophthalmologist (GTP, AP) using international consensus investigation protocols (Petzold *et al.*, 2014). Exclusion criteria included a diagnosis of other retinal or ocular disease.

Patients were recruited within 14 days of onset of visual loss and/or pain on eye movement, whichever was the earlier. Patients were classified as myelin oligodendrocyte glycoprotein (MOG) associated ON if seropositive for MOG antibodies (MOGON), as multiple sclerosis associated ON (MSON) if fulfilling the 2017 MS criteria and single episode isolated ON (SION) as described (Petzold *et al.*, 2014).

Controls consisted of cohorts of 28 and 29 healthy hospital staff, who had undergone PERG and pattern visual evoked potentials (PVEP) testing, respectively. Control OCT data were taken from a separate group of 13 healthy control subjects without ocular or retinal abnormalities.

2.3.2. *Ethics*

Approval for the study was obtained from the Ethics committee (study number 64861) and hospital R&D (FRAC0001). Subjects provided informed written consent, in accordance with the Declaration of Helsinki.

2.3.3. *Electrophysiology*

PERGs and PVEPs were obtained using the Espion E3 system (Diagnosys LLC) with protocols based on the ISCEV standard recommendations (Odom *et al.*, 2016). PERGs were recorded using gold foil electrodes referred to ipsilateral outer canthus gold-cup surface electrodes with a mid-forehead ground. The stimulus was a high contrast (>95 %), isoluminant checkerboard reversal, using 45’ checks in 15° x 12° field at 1.52 m viewing distance; amplifier bandpass was

1-100 Hz, stimulation rate was 4.2 reversals per second (rps) with white squares of ~100 cd/m^2 luminance.

PVEPs recording using gold cup electrodes with a midline channel of Oz-Fz (see (Holder, 1978) for lateral channel electrode positions). Responses were elicited by 55' checks, 1.8 rps, using the same field size, amplifier, luminance and contrast parameters as above. Regular calibration and service ensured stability of stimulus parameters. Reference ranges for PVEP and PERG measures were defined as the minimum to maximum ±5 % of the control range.

2.3.4. *OCT*

Optical coherence tomography (OCT) scans were recorded with Spectralis SD-OCT (Heidelberg Engineering, Inc, Heidelberg, Germany) with the eye tracking function enabled, on acquisition software version 6.7.13.0 (Petzold *et al.*, 2014). Participants were examined with a macular volume scan (1024 A-scans, 25 B-scans volume = 20° × 20°, automatic real-time function [ART] = 25) centred around the fovea and a circular 12° peripapillary scan (1536 A-scans, ART ~100) centred around the optic nerve head. Quality control (QC) of OCT scans was assessed using the quality criteria defined by the OSCAR-IB study (Tewarie *et al.*, 2012). One macular OCT scan did not pass QC due to poor fixation.

All B-scans were auto-segmented using Heidelberg Eye Explorer (version 6.15.7.0) followed by manual correction. The peripapillary retinal nerve fibre layer (pRNFL), ganglion cell layer (GCL), inner plexiform layer (IPL), INL, outer plexiform layer (OPL) and outer nuclear layer (ONL) were segmented. Compound macular ganglion cell and inner plexiform layer (mGCIPL) and compound OPL and ONL (OPNL) thicknesses were calculated. Mean layer thickness was computed within a 3.45 mm diameter circle centered around the fovea. Circular peripapillary scans were segmented for the pRNFL thickness measurement.

2.3.5. *Visual acuity testing*

Best corrected high-contrast LogMAR visual acuity (BCVA) was measured with a retro-illuminated chart at 4 meter viewing distance (Petzold *et al.*, 2014).

2.3.6. *Antibody testing*

MOG-IgG and AQP4-IgG Ab status were assessed locally using current cell-based assays (Petzold *et al.*, 2014).

2.3.7. *Follow-up evaluations*

PERG, OCT and BCVA measurements were repeated approximately three months after the baseline evaluation in the ON patients.

2.3.8. *Statistics*

Continuous variables were described by median and ranges, and categorical variables by counts and percentages. PVEP data of patients with undetectable responses were excluded from statistical analysis. A variable describing the interocular difference was created for OCT and PERG data by subtracting results in the affected eye from those in the fellow eye. Distributions of continuous variables and dichotomous variables across diagnosis groups were tested with the Kruskal-Wallis and Fisher exact tests, respectively. Post-hoc analysis for continuous variables was performed with Dunn Test, with p-values adjusted for multiple comparisons (Benjamini-Hochberg method). The Wilcoxon rank-sum test was used to compare distributions of continuous parameters between ON eyes and control left eyes, and the Wilcoxon signed-rank test to compare interocular differences in electrophysiological and structural parameters. To investigate changes during follow-up, comparisons between baseline and follow-up measurements were made with the Wilcoxon signed-rank test. The atrophy of the mGCIPL during follow-up was calculated by subtracting the follow-up from the baseline measurement in the affected eye. The association of mGCIPL atrophy during follow-up and electrophysiology measures at baseline were explored through linear regression for the affected eye. Correlations were performed by Spearman's rank analysis (r_s=Spearman's rho). To account for inter-eye correlations, only left eyes of control subjects were analysed. Data were analysed using R and Rstudio (RStudio Team 2021, http://www.rstudio.com/). Statistical significance threshold was set at $p<0.05$.

2.4. Results

Twenty-six patients with acute ON were recruited (Table 2.1). Females were overrepresented in the ON group as expected (Petzold *et al.*, 2014), but sex distribution did not differ from controls. Six patients were diagnosed with MOGON, 11 with MSON and nine cases with SION. Differences between the diagnosis groups are shown in Supplementary Table 2.1. Age, gender and BCVA were similar across ON types. Median time from symptom onset was 7 days (range 2 – 14) at recruitment, with MOGON cases trending towards earlier recruitment than SION cases (p=0.063). Three MSON and one MOGON case had a history of prior ON of the fellow eye. One MSON case had commenced oral steroid therapy (500mg once daily for 5 days) two days before trial investigations were performed, 13 others started afterwards. No MSON case was on disease modifying treatment. Serological testing for AQP4 was negative in all patients.

	Affected eye ON cases	**Fellow eye ON cases**	**Controls**	**Affected eye vs. controls**	**Affected eye vs. fellow eye**
N	26	--	28	--	--
Sex (F) N (%)	17 (65.4 %)	--	17 (60.7 %)	p=0.723[1]	--
Age median (range)	30.7 (18.1-59.2)	--	29.0 (17.0-50.0)	p=0.624[2]	--
Days since onset N (range)	7 (2-14)	--	n.a.	--	--
BCVA LogMAR median (range)	1.00 (-0.15 – 1.15)	0.90 (-0.20 – 0.50)	0.00 (-0.20 – 0.80)	p=0.012[2]	p<0.001[3]
mGCIPL µm median (range)	0.79 (0.56 – 0.98)	0.81 (0.55 – 0.95)	*0.89 (0.84 – 0.91)*	*p=0.004*[2]	p=0.345[3]
pRNFL µm median (range)	115 (72 – 329)	101 (78 – 250)	*103 (97 – 116)*	*p=0.059*[2]	p=0.002[3]
INL µm median (range)	0.35 (0.32 – 0.41)	0.35 (0.31 – 0.55)	*0.36 (0.34 – 0.43)*	*p=0.883*[2]	p=0.179[3]
P50 amplitude, µV median (range)	2.30 (0.80 – 5.00)	3.00 (1.00 – 4.70)	3.30 (2.80 – 5.70)	p<0.001[2]	p<0.001[3]
N95 amplitude, µV median (range)	3.4 (1.20 – 5.10)	4.80 (2.10 – 6.80)	5.00 (3.10 – 7.70)	p<0.001[2]	p<0.001[3]
Ratio N95/P50, median (range)	1.30 (0.95 – 3.00)	1.56 (1.05 – 2.80)	1.50 (1.18 – 2.39)	p=0.229[2]	p=0.220[3]
P50 peak time, msec median (range)	45 (40 – 55)	47 (44 – 56)	50 (46 – 56)	p<0.001[2]	p<0.001[3]

Table 2.1 Baseline cohort characteristics. 1= Fisher's exact test. 2= Wilcoxon rank-sum test. 3= Wilcoxon signed-rank test. 4= Kruskal-Wallis test. OCT results of controls (*in italic*) correspond to separate control group of 13 controls.

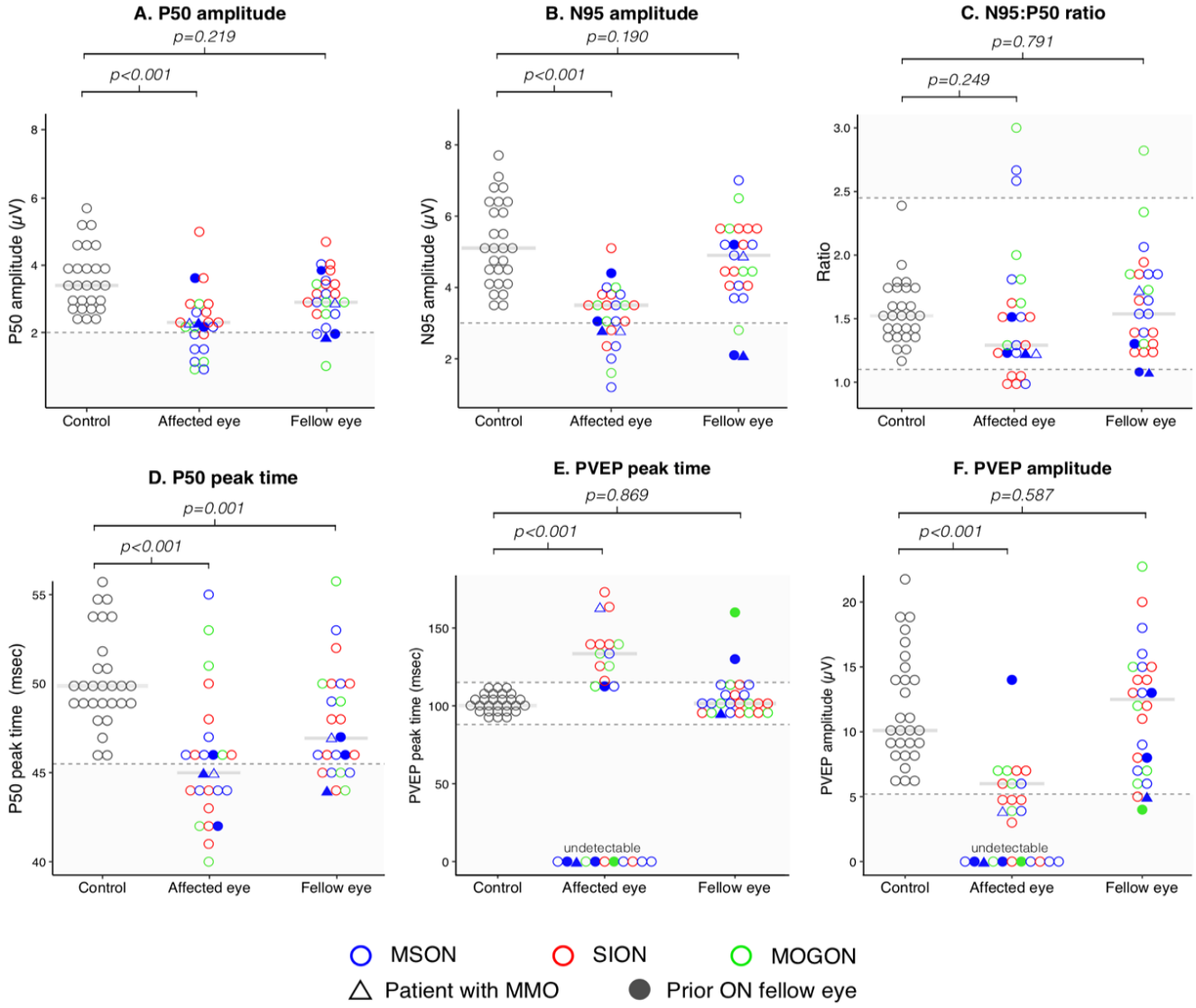

Figure 2.2 Electrophysiological data in acute ON and controls. PERG and PVEP parameters for control eyes (black) as well as the affected and fellow eyes of individuals with acute ON (blue=MSON, green=MOGON, red=SION). p-values represent the results of Wilcoxon rank-sum test. The grey horizontal bars represent group medians. (A) P50 amplitudes and (B) N95 amplitudes are significantly lower in affected eyes and fellow eyes (both p<0.001) of patients with acute ON patients than in controls. There is no significant difference in (C) the N95:P50 ratio between controls and individuals with acute ON. (D) P50 peak times are on average shorter in the affected eyes and fellow eyes of acute ON patients compared with controls (p<0.001). (E) and (F) PVEP peak time and amplitude both differ significantly between control eyes and affected eyes (both p<0.001). Normative ranges are shown (dashed horizontal reference line). Undetectable PVEPs are shown as "zero" values in the graph, but treated as "missing data" in statistical analyses.

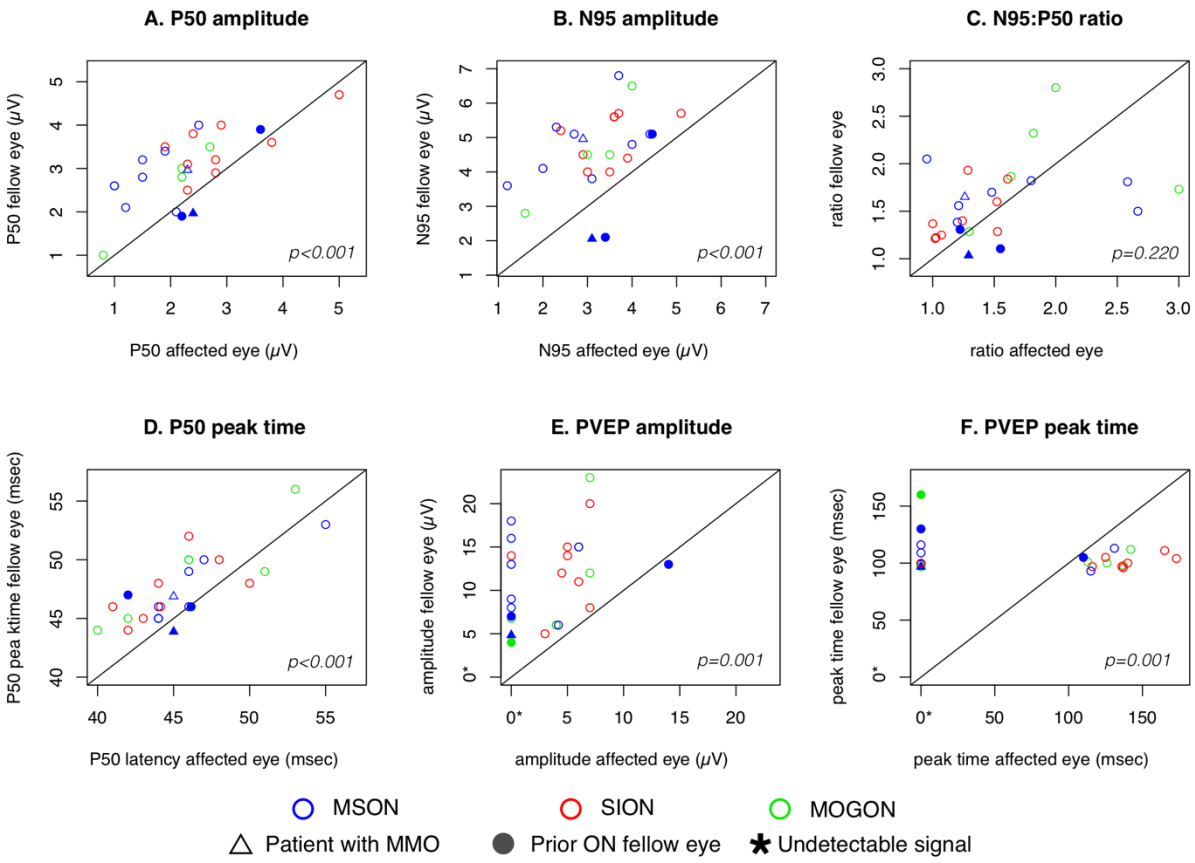

Figure 2.3 Electrophysiological data on inter-eye differences in acute ON. These figures show interocular differences in PERG and PVEP parameters. A central x=y line represents no difference. Observations to the upper-left of this line represent an interocular difference with the value higher in the fellow eye compared with the affected eye. p-values represent the results of Wilcoxon signed-rank test for group comparison. (A) P50 amplitudes and (B) N95 amplitudes are significantly lower in affected eyes compared with fellow eyes of acute ON patients (p<0.001). (C) There is no significant interocular difference in N95:P50 ratios. P50 peak times were significantly shorter in affected eyes compared to fellow eyes (p<0.001). (E) and (F) for both PVEP parameters there was a significant inter-eye difference (p=0.001 for both). Undetectable PVEPs are shown as "zero" values, but treated as "missing" in analyses.

BCVA

BCVA positively correlated positively with P100 peak times (r_s=0.58, p=0.003) and negatively with PVEP amplitude (r_s=-0.69, p=0.006). Eight ON cases with P50 amplitudes below the lower reference limit of 2.0 µV had worse median BCVAs (LogMAR 1.00; range 0.20 – 1.15) compared with other cases (LogMAR 0.40; range -0.15 – 1.10, p=0.020).

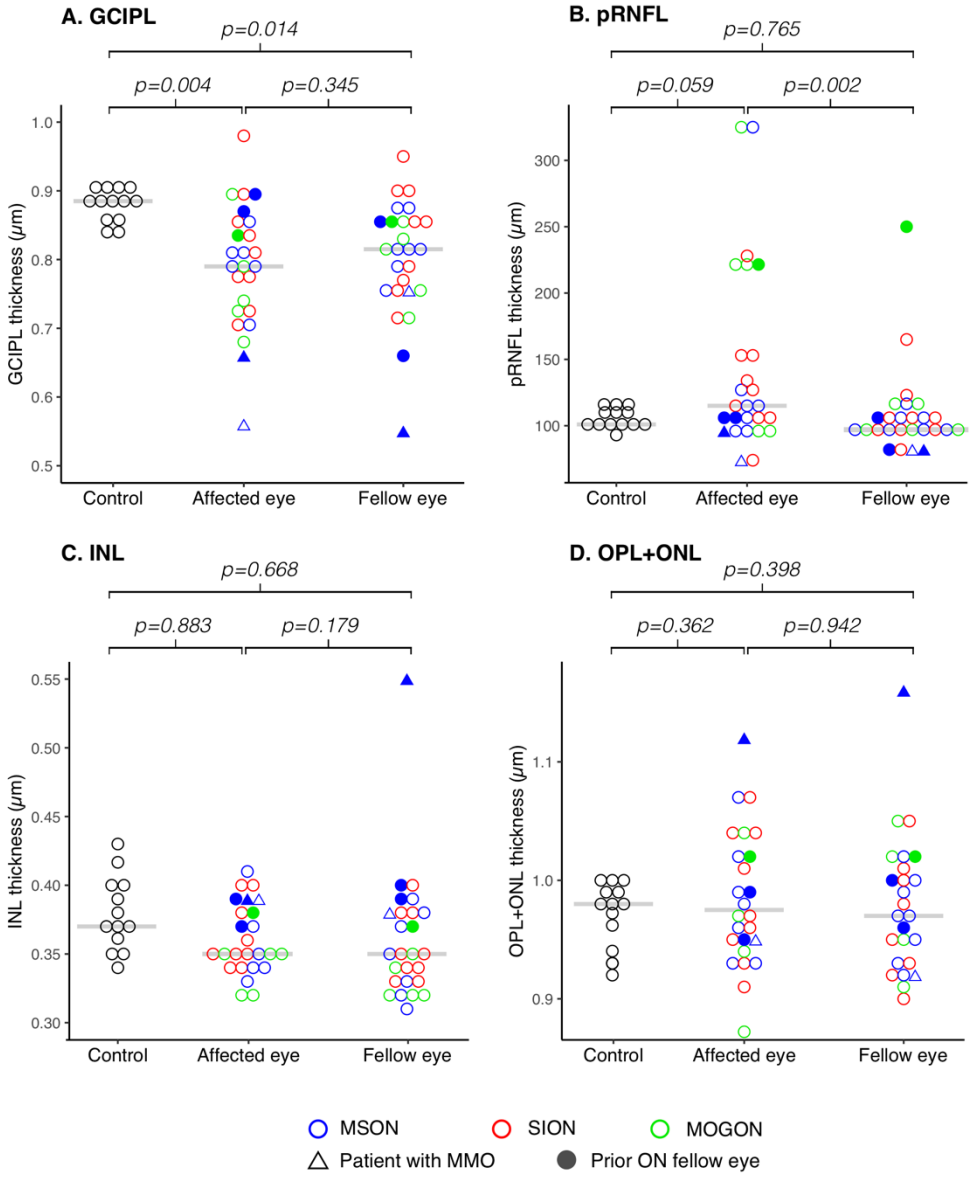

Figure 2.4 Dotplots showing structural (OCT) data in acute ON and controls. Structural data (OCT) on individual eyes and inter-eye differences in acute ON and controls. These figures show the OCT data for (A) mGCIPL, (B) pRNFL, (C) INL and (D) OPNL. Bars represent median observations.

2.4.1. *PVEP*

PVEPs were undetectable in 11 affected eyes of ON cases (42 %). When detectable, PVEP P100 was delayed (median 136 ms, range 110-173 ms) and amplitude reduced (median 6 µV, range 3-14 µV) in affected ON eyes compared with controls (median 11 µV, range 6-22 µV; both $p<0.001$). Median peak times and amplitudes did not significantly differ between fellow eyes of ON cases and control eyes (Figure 2.2), but did differ significantly between affected and fellow eyes ($p<0.001$ for both) (Figure 2.3). PVEP parameters did not differ across the three ON types. Abnormal fellow eye results were present in two and three patients for peak times

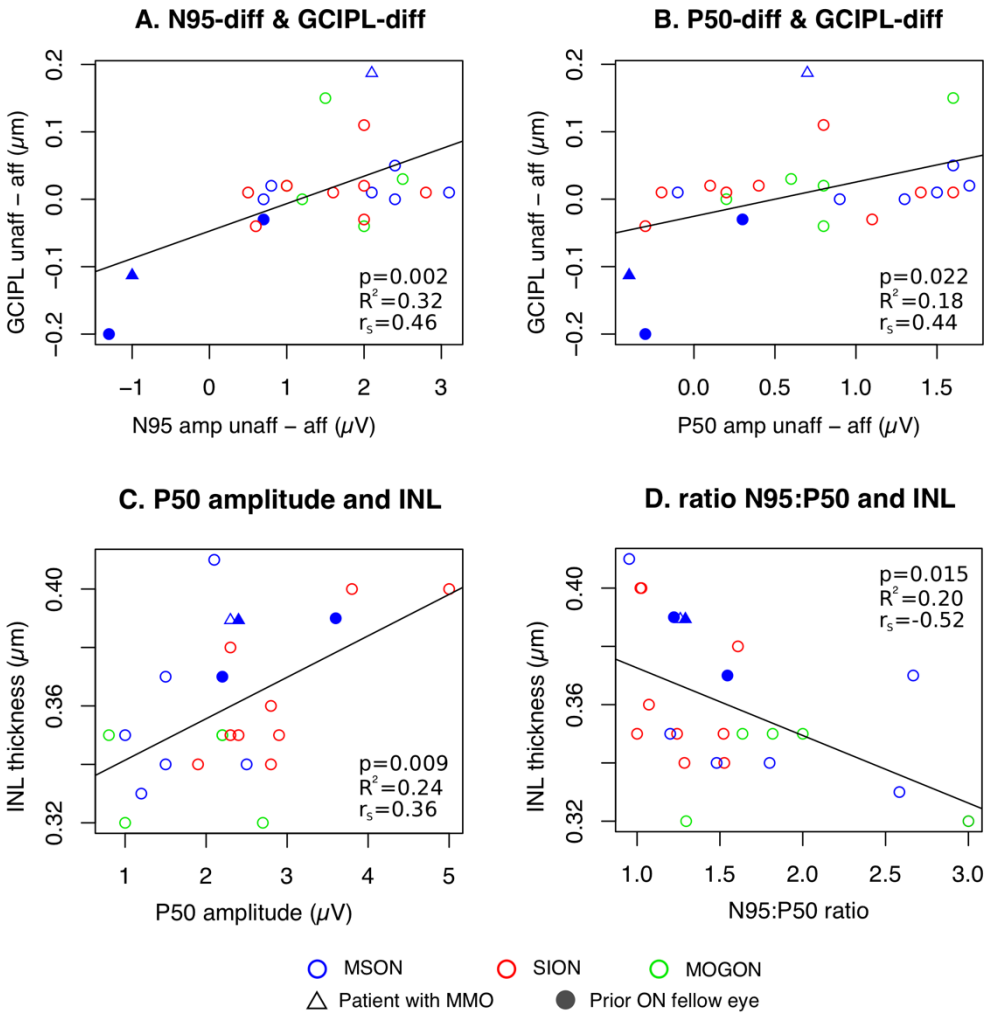

Figure 2.5 Structure-function correlations between retinal thickness and electrophysiological measures. Relationships between PERG parameters and retinal layer thickness measurements are shown in scatter plots with linear regression lines. r_s is the Spearman's rho, R^2 is the R-squared and p-values represent results of linear regression analysis. MSON, SION and MOGON are coloured blue, red and green, respectively. Symbols representing patients with a prior episode of ON in the fellow eye are filled and are triangular for patients with MMO. (A) Interocular differences for the fellow eye minus the affected eye for the N95 amplitude and (B) P50 amplitude are positively correlated with the interocular difference of mGCIPL thickness in ON cases. (C) Absolute P50 amplitudes were positively correlated with INL thickness and (D) N95:P50 ratios were correlated negatively with INL thickness.

and amplitudes, respectively. The fellow eye of one MSON patient had uninterpretable PVEPs despite good vision and was excluded from analysis.

2.4.2. *PERG*

P50 amplitudes, N95 amplitudes and P50 peak times fell outside reference limits in 8, 8 and 13 affected, and 4, 3 and 7 fellow eyes, respectively. For fellow eyes, these were

predominantly MS cases with previous ON in that eye (Figure 2.2). P50 amplitude and N95:P50 ratio differed significantly across ON types (p=0.026 and p=0.032, respectively). Post-hoc analysis showed this related to lower median P50 in MOGON (2.2 µV; range 0.8-2.7 µV) compared with SION (2.8 µV; 1.9-5.0 µV), while N95:P50 ratio was higher in MOGON (1.8; 1.3-3.0) compared with SION (1.24; 1.0-1.6) (Table 1).

Affected eyes of ON cases, but not fellow eyes, had lower median P50 amplitudes compared with controls (median 3.3 µV; range 2.8-5.7 µV, p<0.001). Median P50 amplitude in ON patients was significantly lower in affected eyes (2.3 µV; range 0.8-5.0 µV) compared with fellow eyes (3.0 µV; range 1.0-4.7 µV; p<0.001) (Figure 2.2 and 2.3). Nine cases (36 %) had abnormal relative P50 amplitudes (interocular ratio <0.70) (Holder, 1991) and eight cases (32 %) had subnormal absolute P50 amplitudes (<2.0 µV). These cases, comprising five MSON, two MOGON and one SION case, had a similar time from symptom onset as other cases (p=0.581) at a median of 6 days (range 2-14 days). Individual electrophysiology data of these eight cases are shown in Supplementary Figure 2.1.

Median N95 amplitude in control eyes (5.0 µV, range 3.1-7.7 µV) was higher compared with affected eyes (p<0.001) but not fellow eyes (p=0.190) of ON patients. N95 amplitudes in ON patients were significantly lower in affected eyes at 3.4 µV (range 1.2-5.1 µV) compared with fellow eyes at 4.8 µV (range 2.1 – 6.8; p<0.001). To ensure validity, outlier P50 and N95 amplitudes of one control subject were excluded from analysis due to high results.

There was no significant difference between N95:P50 ratios in controls (median 1.50, range 1.18-2.39) and either affected and fellow eyes of ON patients. Neither was there a significant difference in median N95:P50 ratios between affected and fellow ON eyes at 1.30 (range 0.95-3.00) and 1.56 (range 1.05-2.80), respectively, but there was a trend with eighteen cases (72 %) having a lower ratio in the affected than the fellow eye. The N95:P50 ratio was subnormal in 5 affected and 2 fellow eyes suggesting RGC dysfunction. In addition, 3 affected eyes and 1 fellow eye had an N95:P50 ratio above the reference limit. These eyes all had subnormal P50 amplitude results indicating macular dysfunction (supplementary Figure 2.1).

P50 peak times for affected and fellow ON eyes were variable but on average were shorter than control eyes (median 50ms, range 46-56ms; p<0.001 and p=0.001, respectively). Affected ON eyes had significantly shorter median P50 peak times at 45ms (range 40-55ms) compared with fellow eyes (median 47ms, range 44-56ms; p<0.001).

2.4.3. *OCT*

OCT control data were available from thirteen controls (median age: 28 years; range: 25 – 47). mGCIPL was thinner in both affected and fellow eyes of ON cases (median 0.79 µm and 0.81 µm, respectively) compared with controls (median 0.90 µm; p=0.004 and p=0.014, respectively), while pRNFL thickness was greater in affected compared with fellow ON eyes (median 115 µm and 101 µm, respectively; p=0.002) (Table 2.1; Figure 2.4). Two MSON patients (7.6 % of all ON cases) showed microcystic macular oedema (MMO), but INL thickness did not differ between ON cases and controls. OCT results did not differ across ON types.

2.4.4. *Structure-function associations*

Interocular differences of N95 and P50 amplitudes positively correlated with interocular differences in mGCIPL thickness (r_s=0.46, p=0.002 and r_s=0.44, p=0.022, respectively). P50 amplitudes were positively correlated with INL thickness (r_s=0.36, p=0.009) and N95:P50 ratios showed a negative correlation with INL thickness (r_s=-0.52, p=0.015) (Figure 2.5). OPNL

	Follow-up ON patients
N	16
Diagnosis, N (%)	MSON: 9 (56 %) SION: 4 (25 %) MOGON: 3 (19 %)
Age years, median (range)	32 (18 – 59)
Female sex, N (%)	10 (63 %)
Weeks follow-up, median (range)	14 (12 – 25)
BCVA, median (range)	0.20 (-0.10 – 1.00)
mGCIPL atrophy µm, median (range)	0.16 (0.10 – 0.49)

Table 2.2 Characteristics of ON patients with follow-up data available.

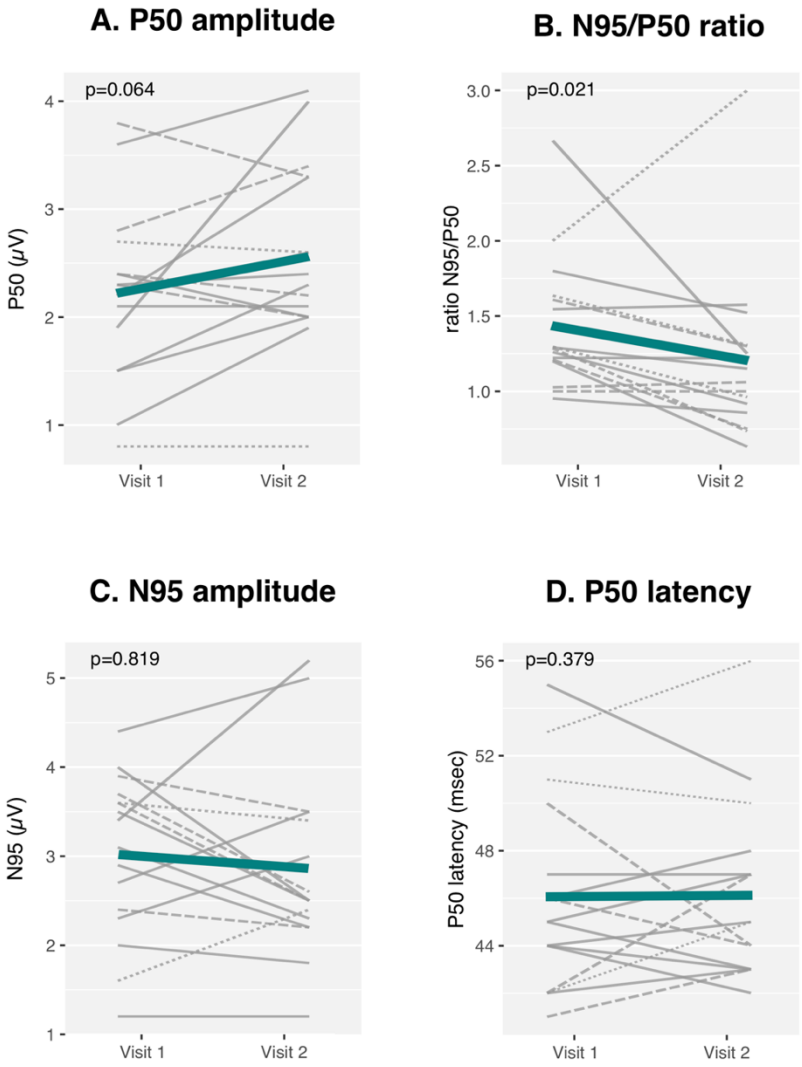

Figure 2.6 Repeated-measures plots showing follow-up PERG data in optic neuritis patients. Grey lines represent individual data and green lines represent group means. Dotted line = MOGON, striped line = SION and full line = MSON. p-values are results of Wilcoxon signed-rank tests.

thickness was associated neither with N95 amplitude, P50 amplitude nor with the N95:P50 ratio.

P50 peak times and PVEP parameters did not correlate with any retinal layer thickness parameters, and did not differ significantly between patients with subnormal and normal electrophysiology results.

2.4.5. *Time since symptom onset*

Time since symptom onset did not correlate with any electrophysiological measure (all p>0.05). Time since onset also did not differ for cases with subnormal P50 results (all p>0.05), with five out of the 8 cases presenting before 7 days. As PERG abnormalities in ON may start recovering after as little as 7 days (Holder, 1987, 1991), a subgroup analysis of the 18 ON patients that were included ≤7 days from symptom onset was performed. The above-described inter-group differences and structure-function associations remained significant within this subgroup (Supplementary Figures 2.2 and 2.3).

2.4.6. *Follow-up electrophysiology data*

Characteristics of the 16 ON patients that had electrophysiological follow-up data available are shown in Table 2.2. There was a significant reduction in median N95:P50 ratio from baseline (1.29, range: 0.95 – 2.67) to follow-up (1.11, range: 0.63 – 3.00; p=0.021) (Figure 2.6). This was accompanied by a near-significant increase in median P50 amplitude from baseline (2.25 µV, range: 0.80 – 3.80) to follow-up (2.35 µV, range: 0.80 – 4.10; p=0.064). On the other hand, there were no significant temporal differences in N95 amplitudes and P50 latencies (p=0.819 and p=0.379, respectively). In contrast to the baseline measurements, there is a significant difference between N95:P50 ratio of the affected eye (1.11, range: 0.63 – 3.00) and the fellow eye (1.47, range: 1.00 – 2.50) at follow-up (p=0.005). Despite the slight recovery of P50 amplitude during follow-up, this measure is still significantly reduced in the affected eye (2.35 µV, range: 0.80 – 4.10) compared to the fellow eye (3.00 µV, range: 1.00 – 3.90; p=0.002).

2.4.7. *mGCIPL atrophy and BCVA at follow-up*

Patients showed a median of 0.16 µm (range: 0.10 – 0.49) of mGCIPL atrophy during follow-up. This was not associated with any of the results of either electrophysiological tests, PERG or PVEP, at baseline. BCVA at follow-up was LogMAR 0.20 (range: -0.10 – 1.00) and was not associated with electrophysiological measures at baseline. There was no significant difference in mGCIPL atrophy rates or BCVA at follow-up across the different diagnosis groups (p=0.802 and p=0.880, respectively).

2.5. Discussion

These data demonstrate both structural and functional macular changes in acute ON. PERG P50 amplitudes, reflecting macular function, were reduced in affected eyes and showed associations with impaired visual acuity and mGCIPL as well as with INL thicknesses. There was an expected correlation between the RGC generated N95 component and mGCIPL thickness.

The finding of reduced P50 amplitudes in this series of acute ON cases confirms limited earlier findings (Berninger and Heider, 1990; Holder, 1991). The observed reduction in the N95 component is expected as a consequence of reduction in P50. It is notable that in 4 eyes (3 affected, 1 fellow) the N95:P50 ratio was greater than normal, indicating a greater effect on P50. These eyes had subnormal P50 components signifying macular dysfunction. Some patients showed N95 reduction without significant P50 involvement, in keeping with the selective loss of N95 that can occur in RGC dysfunction in optic neuropathy (Holder, 2004). Although these patients suffered acute visual loss, this does not preclude previous sub-clinical optic nerve involvement, which is long-established in MS (Halliday *et al.*, 1972). In general, N95 involvement without P50 involvement occurs in early or mild disease; P50 involvement becomes evident in more severe disease and/or later in the course of the disorder (Holder, 2001, 2004). Although P50 origins are not fully ascertained, it is likely in part generated by retinal structures distal to the RGCs (Holder, 1987, 1991). The correlation between P50 and INL thickness suggests a localised functional impairment in acute ON and is further consistent with a contribution of the INL to P50 generation.

Herein is the first demonstration that P50 reductions occur in acute ON of various aetiology, including MOGON. There was some suggestion that P50 amplitudes were more reduced in MOGON compared with SION. However, MOGON cases tended to present earlier in their disease course, and as P50 reduction in acute ON may start recovering after a week (Holder, 1987, 1991; Berninger and Heider, 1990), earlier presentation may be relevant.

Importantly, macular dysfunction may contribute to the visual loss in acute ON, as cases with subnormal P50 amplitudes had poorer visual acuities, consistent with earlier preliminary data

(Holder, 1987). Visual acuity measures were restricted to high-contrast, and low-contrast measurements may have shown greater sensitivity (Balcer *et al.*, 2017).

The data show a structure-function relationship between P50 amplitude and INL thicknesses in acute ON. This correlation, combined with the identified association of impaired P50 amplitude with visual dysfunction, suggests clinically significant changes in the INL within the acute stages of ON. INL thickness was not increased in ON eyes, in contrast to some previous reports (Kaushik *et al.*, 2013; Knier *et al.*, 2016). However, OCT imaging in those studies was not performed acutely but 50-100 months after ON. INL thickening could conceivably occur later in the disease course.

Here, mGCIPL thicknesses showed associations with the P50 and N95 components of the PERG. Macular GCL thickness in various pathologies, including advanced MS, has previously shown positive correlation with N95 amplitude, but not P50 amplitude (Hokazono *et al.*, 2013). As most ON patients showed moderate to severe optic disc swelling, no structure-functional association was evident between pRNFL thickness and PERG measures, although, as expected, this occurs in chronic MSON for the N95 (Parisi, 2003; Trip *et al.*, 2005). A recent publication (Al-Nosairy *et al.*, 2021) addressed multi-focal PERG (mfPERG) in MS patients and found evidence suggestive of foveal axonal dysfunction, with relationships for OCT data with mean central reduction in the second negative (N2) component of the mfPERG and shorter peak time of the positive P1 component in the grouped ring 2 mfPERG. Whether mfPERGs and conventional PERGs entirely reflect the same underlying processes has yet to be clinically determined and may be technique dependent (Al-Nosairy *et al.*, 2021).

These data show that a shortened PERG P50 peak time can occur in acute ON. P50 shortening is associated with marked loss of RGC function (Holder, 1997), and has been reported in recovered ON, presumably due to direct retrograde degeneration (Holder, 1987; Monsalve *et al.*, 2018). It also occurs in non-human primates (NHPs) following intravitreal tetrodotoxin (TTX) injection (Viswanathan *et al.*, 2000), which blocks spiking cell function but spares the INL and photoreceptors. Although data on P50 peak time in acute optic nerve dysfunction are limited, shortening of P50 peak time has been reported in advanced but not early stages of Leber Hereditary Optic Neuropathy (LHON) (Wang *et al.*, 2020) and dominant optic atrophy

(DOA) (Holder *et al.*, 1999). PERG abnormalities in DOA are confined to the N95 component in the early stages, but with increasing severity there is amplitude reduction and subsequent shortening of P50 peak time (Holder *et al.*, 1999). This conforms with the understanding of the origins of the PERG components, with N95 originating in RGCs and P50 originating partly in RGCs and partly from more distal structures (Viswanathan *et al.*, 2000; Holder, 2001) As RGC dysfunction advances, an initial reduction confined to the RGC derived N95 is followed by progressive loss of the RGC contribution to P50. Those elements of P50 generated more anteriorly than the RGCs in the visual pathway therefore become more dominant and P50 component therefore appears both earlier and of lower amplitude. This is entirely consistent with the experimental shortening of P50, associated with amplitude reduction, that occurs following TTX in NHPs (Viswanathan *et al.*, 2000).

The finding of a reduced P50 peak time in acute ON indicates that loss of RGC function may be present earlier than some other investigated optic nerve diseases (Mauguiere *et al.*, 1995; Holder *et al.*, 1999; Wang *et al.*, 2020). However, retrograde degeneration to the RGCs due to prior subclinical optic nerve involvement cannot be excluded as ON patients overall had thinner mGCIPL thickness than controls. The significantly shorter P50 component in affected compared with fellow eyes in ON cases suggests that the acute event, either through acute retrograde signalling or inflammatory activity in the macula, contributes to the finding.

PVEP findings corresponded with optic nerve dysfunction, showing delayed peak times and reduced amplitudes. Abnormalities were mostly restricted to affected eyes, but were present in some clinically asymptomatic eyes with a history of previous ON in keeping with previous reports (Halliday *et al.*, 1972).

After approximately three months of follow-up following ON onset, an increase in N95/P50 ratio was observed, which appeared to be driven by recovery of the P50 amplitude. On the other hand, there was no change in N95 amplitude over time. This is in line with earlier observations (Berninger and Heider, 1990; Holder, 1991) and indicates that macular dysfunction is most severe acutely and recovers as time elapses. This time course would be most consistent with macular dysfunction being caused by acute metabolic failure or inflammatory activity which recovers after the acute event, while it appears to be inconsistent

with it being caused by retrograde degeneration. It is interesting to note that animal work has found evidence for hypoxia and hypoperfusion in the acute stages of experimental autoimmune encephalomyelitis (EAE) which recovers subsequently, mirroring the timing of macular dysfunction identified in acute ON here (Davies *et al.*, 2013; Desai *et al.*, 2020).

These data corroborate earlier reports that macular involvement in neuroinflammatory disease may extend beyond the pRNFL and RGCs (Saidha *et al.*, 2011). Previous studies identified that increased INL thickness is associated with poorer clinical outcomes in ON and MS (Kaufhold *et al.*, 2013; Balk *et al.*, 2019). Although not replicated in this acute cohort, P50 amplitudes were reduced, indicative of macular dysfunction, and were associated with visual acuities and with INL thickness. The nature of macular involvement in ON remains uncertain. There may be early pathophysiological processes which have functional but not structural consequences. It seems unlikely this reflects retrograde degeneration, as that typically occurs at a later stage and does not involve the INL (Balk *et al.*, 2014). Different, more acute retrograde effects such as changes in metabolic demand and signalling are not excluded. However, a marked effect on P50 amplitude would involve a trans-synaptic effect anterior to the RGCs in the visual pathway, and is thus more likely to reflect primary alteration in macular function synchronous with the inflammatory effect on the optic nerve rather than a retrograde effect. Given the known incidence of inflammatory changes in the retinae of MS patients, there may be local inflammatory processes, such as activated microglia (Rucker, 1945; Green *et al.*, 2010), or vascular changes, such as hypoperfusion or focal arteriolar narrowing (Davies *et al.*, 2013), that contribute to macular dysfunction.

2.6. Conclusion

This study documents macular dysfunction in acute ON, as shown by reduction in the PERG P50 component and structure-function correlations between PERG parameters and thickness of both INL and mGCIPL on OCT imaging. During follow-up, an increase in N95/P50 ratio was observed, which was driven by some recovery in P50 amplitude. This finding of transient macular dysfunction in the acute stage of ON could be due, separately or in combination, to breakdown of the blood-retina barrier at the level of the superior vascular plexus, metabolic failure, activation of microglia, or, less likely, the retrograde effects of optic nerve damage.

Cases with subnormal P50 amplitudes had poorer visual acuities, suggesting that macular dysfunction may, in some cases, contribute to the visual loss in acute ON. This is an important consideration for clinical trials aimed at rescuing optic nerve dysfunction in ON and suggests that such clinical trials should consider the inclusion both of structural and functional macular parameters.

2.7. Supplementary data

	MOG-ON	MSON	SION	P-value group variance
N	6	11	9	
Gender (F) N (%)	4 (66.6 %)	8 (72.7 %)	5 (55.6 %)	p=0.867[1]
Age median (range)	41.3 (27.0 – 59.2)	32.7 (18.1 – 49.5)	26.5 (19.1 – 35.6)	p=0.075[2]
Days since onset N (range)	6 (2 – 7)	6 (3 – 13)	8 (3 – 14)	p=0.200[2]
BCVA LogMAR median (range)	0.25 (0.00 – 1.10)	1.00 (-0.15 – 1.15)	0.90 (0.15 – 1.05)	p=0.464[2]
mGCIPL µm median (range)	0.77 (0.68 – 0.90)	0.80 (0.56 – 0.89)	0.81 (0.70 – 0.98)	p=0.687[2]
pRNFL µm median (range)	221 (98 – 329)	107 (72 – 321)	125 (76 – 228)	p=0.204[2]
INL µm median (range)	0.35 (0.32 – 0.38)	0.37 (0.33 – 0.41)	0.35 (0.34 – 0.40)	p=0.308[2]
P50 amplitude, µV median (range)	2.20 (0.80 – 2.70)	2.10 (1.00 – 3.60)	2.80 (1.90 – 5.00)	**p=0.026[2]** MOG – SION[3]
N95 amplitude, µV median (range)	3.50 (1.60 – 4.00)	3.10 (1.20 – 4.40)	3.60 (2.40 – 5.10)	p=0.500[2]
Ratio N95/P50, median (range)	1.82 (1.30 – 3.00)	1.29 (0.95 – 2.67)	1.24 (1.00 – 1.61)	**p=0.032[2]** MOG – SION[3]
P50 peak time, msec median (range)	46 (40 – 53)	45 (42 – 55)	44 (41 – 50)	p=0.820[2]

Supplementary Table 2.1 Baseline characteristics for the three diagnosis groups. Only affected eyes are included in analyses in this table. 1= Fisher's exact test. 2= Kruskal-Wallis test. 3= groups that post-hoc Dunn test identified significant difference between.

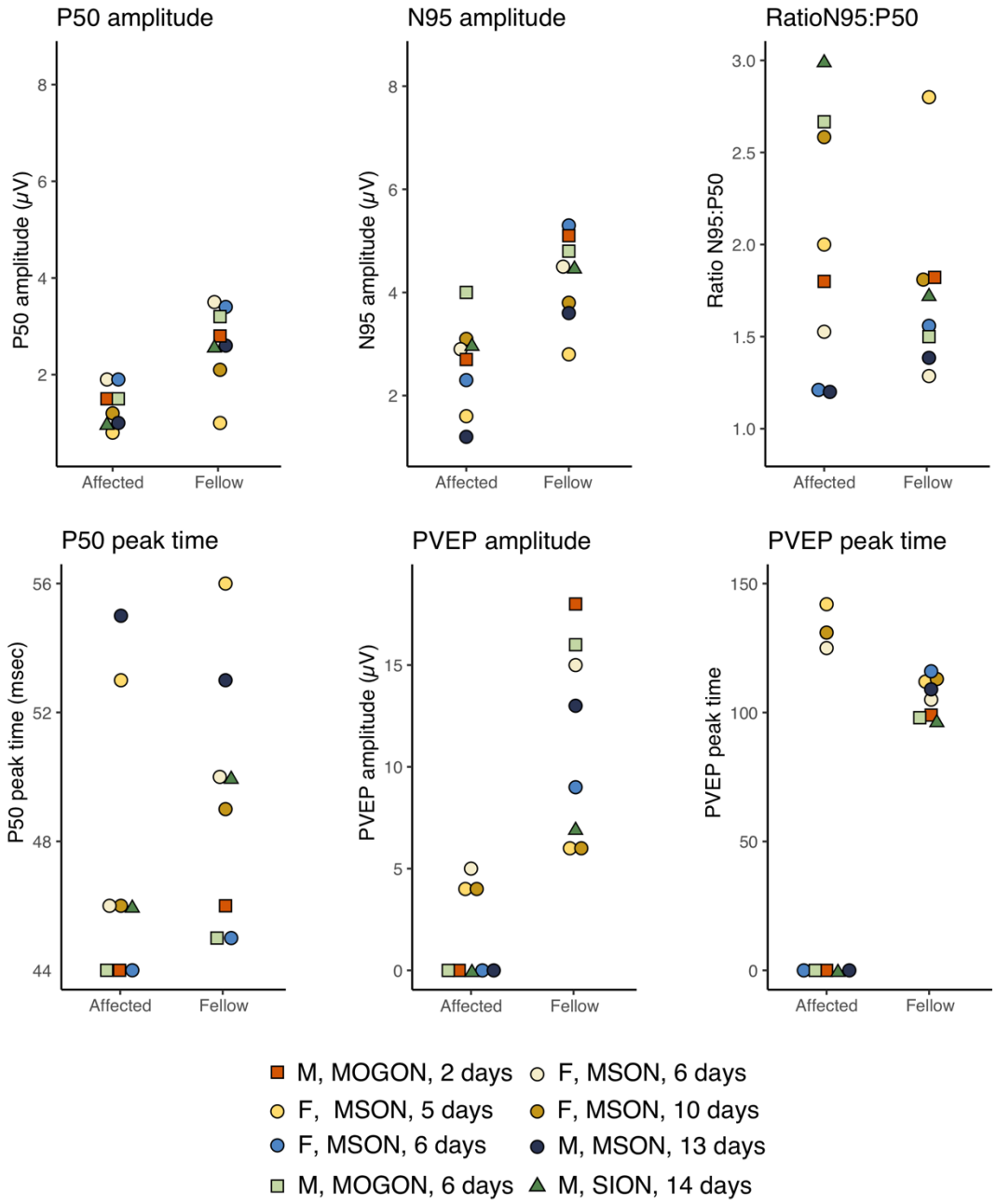

Supplementary Figure 2.1 Electrophysiological data for ON patients with subnormal P50 amplitude. These figures show individually identifiable electrophysiology results for the eight cases with a subnormal P50 amplitude (<2.0 µV). Each individual case with an abnormal P50 is identified through colour-coding, and additional electrophysiological results of these patients are shown.

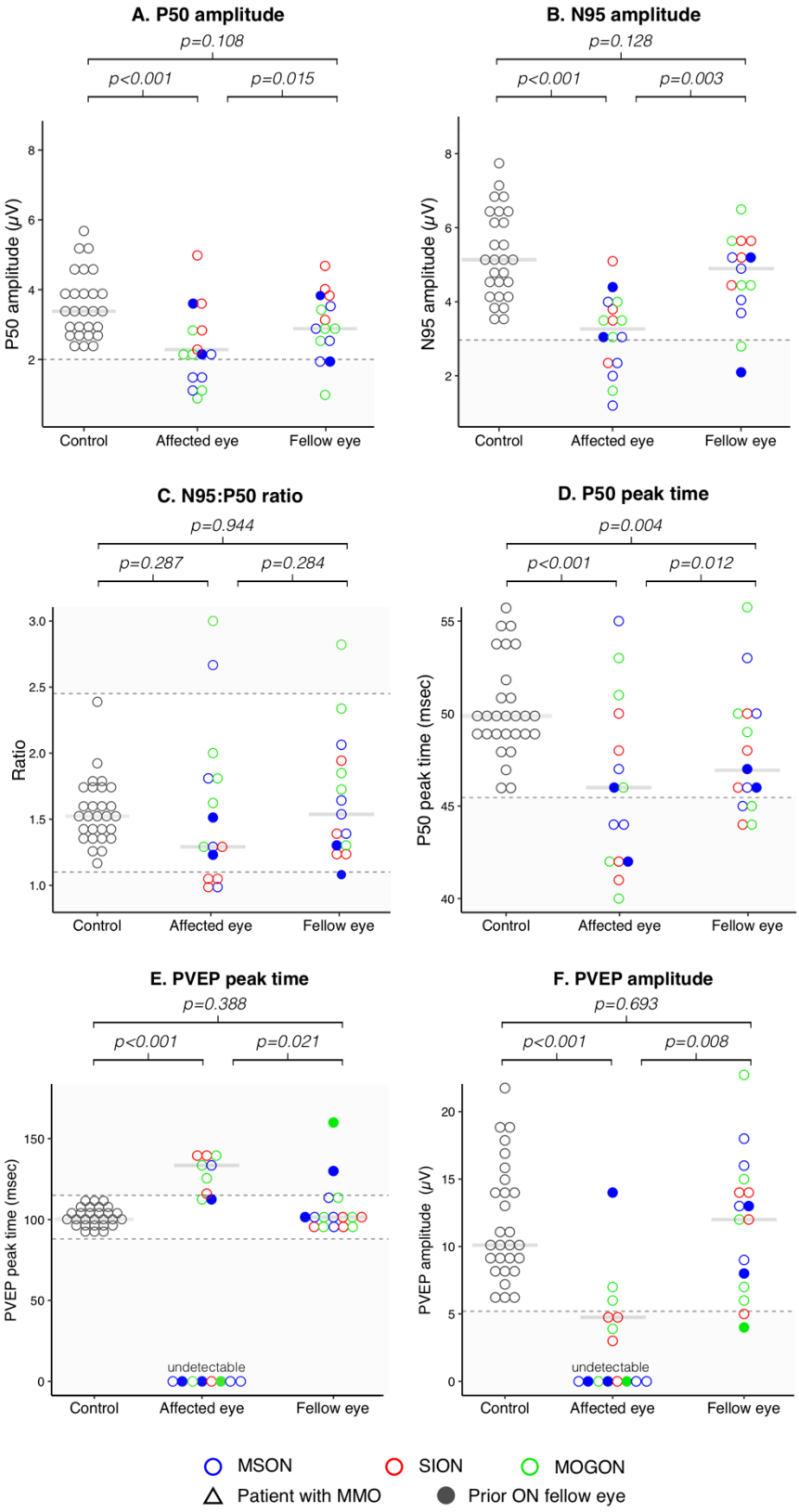

Supplementary Figure 2.2 Interocular differences in subgroup ON patients included ≤7 days. (A) P50 amplitudes and (B) N95 amplitudes are significantly lower in affected eyes compared with fellow eyes of acute ON patients (p=0.015 and p=0.003 respectively). (C) There was no interocular difference in N95:P50 ratios. (D) P50 peak times were significantly faster in affected eyes compared to fellow eyes (p=0.012). (E) and (F) for both PVEP parameters there was a significant inter-eye difference (p=0.021 and p=0.008).

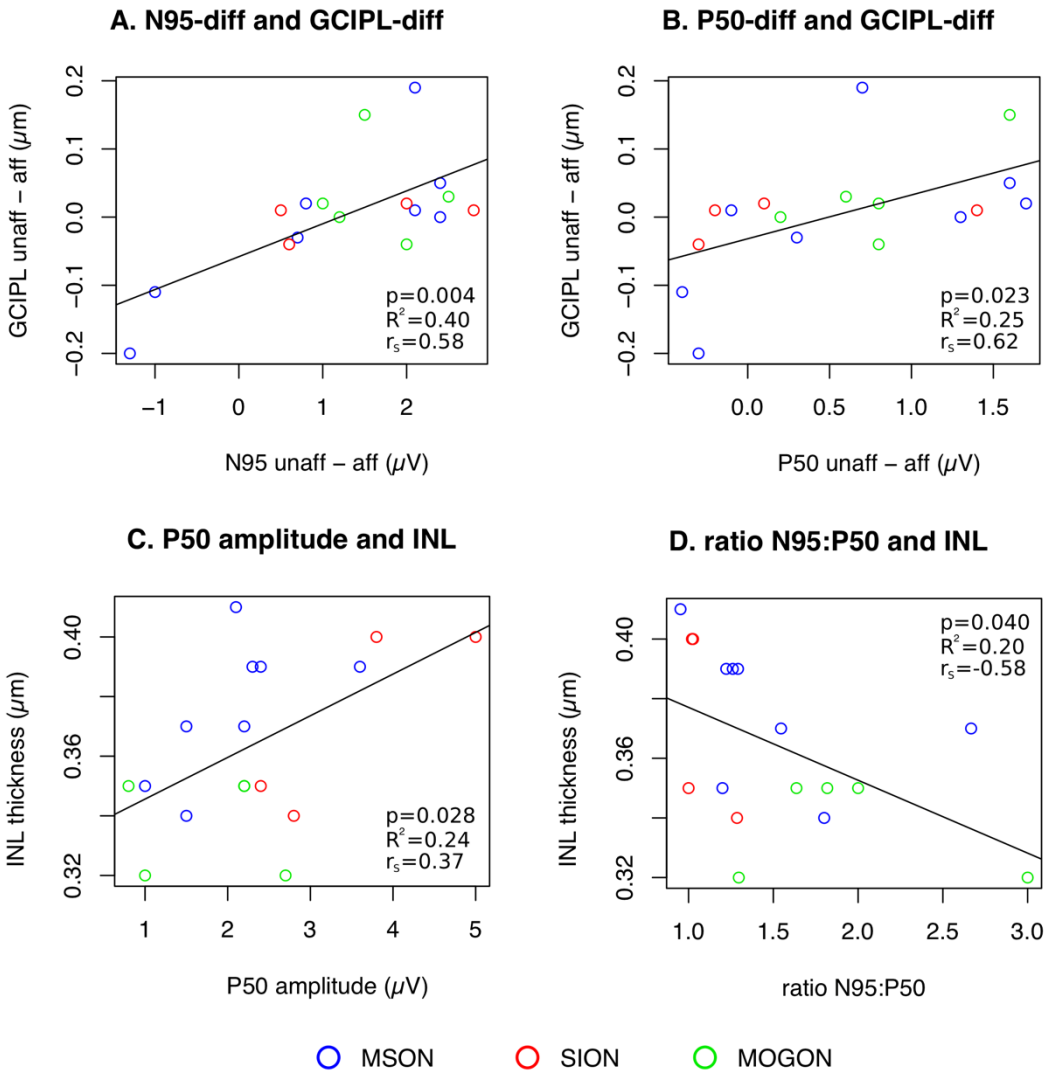

Supplementary Figure 2.3 Structure-functional correlations in subgroup ON patients included ≤7 days. Relationships between PERG parameters and retinal layer thickness measurements are shown in scatter plots with linear regression lines. r_s is the Spearman's rho, R^2 is the R-squared and p-values represent results of regression analysis. Multiple sclerosis, isolated optic neuritis and MOGON cases are coloured blue, red and green, respectively. (A) Interocular differences (fellow eye – affected eye) of N95 amplitude and (B) P50 amplitude are positively correlated with the interocular difference of mGCIPL thickness. (C) Absolute P50 amplitude and (D) N95:P50 ratio are positively and negatively correlated with absolute INL thickness, respectively. (E) Interocular differences of N95:P50 amplitude are negatively correlated with interocular differences in INL thickness. For these final analyses one outlier with MMO was excluded.

3. Dynamic changes to the thickness of outer retinal layers during dark-adaptation

ABSTRACT

Background The energy-costly process of dark-adaptation coincides with thickness changes in the outer retina. This process may be impaired in acute optic neuritis (ON), given the potential associations with metabolic dysfunction.

Objectives To develop a dark-adaptation protocol and explore outer retinal thickness changes with optical coherence tomography (OCT) in health and in ON.

Methods Healthy control subjects and acute ON patients, with symptom onset within 14 days, were recruited at Moorfields Eye Hospital. Macular OCT was repeated in five dark- and light adaptation blocks of varying time lengths in a pilot group of three control subjects. Changes to the outer segment equivalent layer (OSEL) were visualised. The most efficient protocol was repeated in the subsequently recruited controls and ON patients. The differences in outer retinal layer thickness during dark- and light-adapted states (light – dark) were visualised and this 'light-associated compression' was compared between controls and ON patients.

Results Nine healthy control subjects and three acute ON patients were recruited. Based on pilot data from three healthy controls a dark- and light-adaptation protocol comprising 20 minutes of dark-adaptation and 10 minutes of light-adaptation was chosen as most efficient. On average, OSEL thickness decreased with a median of -1.41 µm (range: -4.65 – 0.08 µm) between dark- and light-adaptation across all healthy control eyes and unaffected eyes of ON patients ($p<0.001$). Light-associated compression of the OSEL appeared to be greater for healthy controls at -2.45 µm (range: -4.65 – 0.08 µm) compared with acute ON eyes at +0.43 µm (range: -1.71 – 1.67 µm; $p=0.100$).

Conclusions This pilot study identified that light-associated compression of the OSEL thickness can be detected with an easy and patient-friendly protocol. These preliminary data suggest that dynamic dark-adaptation associated thickness changes may be reduced in ON.

3.1. Background

As discussed in the introduction, metabolic failure may interfere with the high energetic needs of dark adaptation during acute optic neuritis (ON). Dark- and light-adaptation are associated with functional changes that can be measured electrophysiologically, with tests such as the electroretinography (ERG) and electro-oculography (EOG) (Robson *et al.*, 2018). In recent years it has been identified that structural changes may also occur, with dynamic thickness changes identified to the outer retinal layers using high resolution OCT systems (Abràmoff *et al.*, 2013; Lu *et al.*, 2017). Preliminary data revealed a consistent dark-associated expansion of the photoreceptor outer segment equivalent layer (OSEL) (Abràmoff *et al.*, 2013) (Figure 3.1). The maximum thickness of the OSEL was observed approximately 20 minutes after dark adaptation, while the thinnest level was observed 17 minutes after introduction to light.

The layer containing the outer segments of the photoreceptors was by far the most sensitive to thickness changes in response to dark adaptation. Structural changes in photoreceptor outer segments thickness were temporally associated with changes of the electro-oculogram, suggesting they are related to functional processes (Abràmoff *et al.*, 2013). However, functional light-adaptation occurs very quickly, within seconds, while the maximum compression of the outer retinal layers seems to take more than 10 minutes. The exact factors that cause this change in outer segment thickness change during dark adaptation are unknown. The thickness change could be caused by swelling of the photoreceptor matrix (potentially related to opening of the ion pumps in the photoreceptor membrane in dark) or swelling of the interphotoreceptor matrix. A change in refractive characteristics of the photoreceptor outer segments may also play a part. The border between RPE and outer segments could become less clear because of an interaction between the outer tips of photoreceptors and the RPE. Finally, there may be a change in position or orientation of the RPE melanosomes. There is a circadian shedding process within the photoreceptors, in which the RPE facilitates the phagocytosis of photoceptor outer segment discs. The greatest part of this phagocytic activity occurs in the morning when night turns into day. It is unclear what the effect of this circadian process is on outer segment thickness.

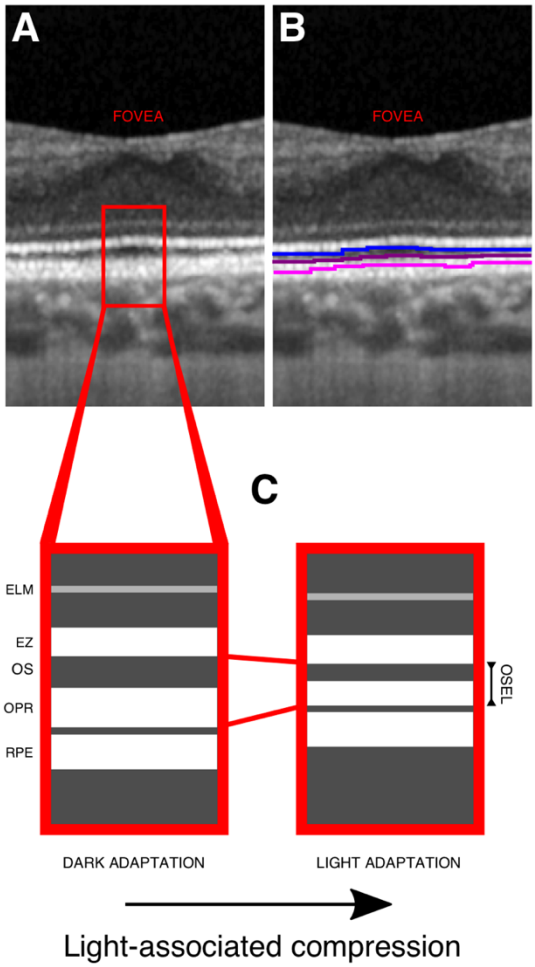

Figure 3.3.1 Schematic visualising the light-associated compression of the OSEL that has been identified by Abramoff al. (2013). A: Foveal OCT B-scan with a red insert indicating the four highly reflective outer retinal bands. B: Foveal OCT B-scan showing the segmentation of the outer segments (OS) and the OPR (outer segments photoreceptor and retinal pigmented epithelium complex) which make up the outer segment equivalent layer (OSEL). C: enlarged visualization of thickness changes that occur during light-adaptation to the outer segment equivalent layer (OSEL). ELM: external limiting membrane. EZ: ellipsoid zone. RPE: retinal pigmented epithelium.

The nature of outer retinal pathology in ON and MS remains poorly understood. Given the known high energetic demands of dark-adaptation (Wong-Riley, 2010; Joyal *et al.*, 2018), this process may lose efficiency when mitochondrial function is reduced due to hypoxia or hypoperfusion. In ON there is indirect evidence for hypoperfusion and mitochondrial failure, as measured by increased serum lactate (Haufschild *et al.*, 2003), and visual pathway neurodegeneration in MS is associated with increased serum lactate concentrations (Petzold *et al.*, 2015).

3.2. Aims, objectives and hypotheses

3.2.1. *Aims and objectives*

Here, outer retinal layer thickness changes in response to a dark-adaptation protocol will be explored in healthy controls and acute ON patients. This pilot study is primarily aimed at establishing the reproducibility of the results by Abràmoff et al. (2013) in healthy control subjects with a protocol that is easy, patient-friendly and yields consistent results. The objective is to create a functional measure that can quantify the retinal response to the highly energy dependent dark-adaptation process.

The secondary aim of this pilot study is to explore how these dynamic thickness changes associated with dark-adaptation differ between the eyes of healthy controls and patients with acute ON. An objective is to contribute to the understanding of outer retinal involvement in ON by investigating how dynamic light-associated changes in outer retinal thickness are affected in ON.

3.2.2. *Hypotheses*

The primary hypothesis of this study is that a simple dark-adaptation OCT protocol is sensitive to picking up thickness changes in the outer retinal layers induced by consecutive dark- and light-adaptation. More specifically, the hypothesis is that outer retinal layer thickness will be greater in a dark-adapted state compared with a light-adapted state.

The secondary hypothesis is that the magnitude of this light-associated compression will be smaller for patients with acute ON compared with healthy controls, particularly so for the clinically affected eye of ON patients.

3.3. Methods

3.3.1. *Participants*

Healthy control participants were recruited from Moorfields Eye Hospital staff. Control subjects had best corrected visual acuities (BCVA) of ≥6/6 in both eyes, no pre-existing eye disease, did not use any medication, had a normal fundus appearance and had basic structural OCT measurements (pRNFL and mGCIPL) within normal limits.

Patients aged 18-60 years with a symptomatically unilateral ON, without a previous episode in the affected eye, were prospectively recruited from Moorfields Eye Hospital (see Chapter 2). Diagnosis was made by a neuro-ophthalmologist (AP) using an international consensus investigation protocol. Patients presenting within 14 days of onset of visual loss and/or pain on eye movement, whichever was the earlier, were recruited. Patients were classified as MOG associated ON if seropositive for MOG antibodies (MOGON), as MS associated ON if fulfilling the 2017 MS criteria (MSON) and single episode isolated ON (SION) as described.

3.3.2. *Ethical approval*

Approval for the study was obtained from the Ethics committee (study number 64861) and hospital R&D (FRAC0001). Informed consent in writing was obtained from all subjects, in accordance with the Declaration of Helsinki.

3.3.3. *OCT protocol*

All OCT measurements were performed with Spectralis SD-OCT (Heidelberg Engineering, Inc, Heidelberg, Germany) with the eye tracking function enabled, on acquisition software version 6.7.13.0. Macular volume scan (1024 A-scans, 37 B-scans volume = 15x15°, automatic real-time function [ART] = 25) centered around the fovea with high-resolution setting enabled were performed, with subsequent scans performed on follow-up mode. Scans were consistently performed for the left eye first. Quality control (QC) of OCT scans was assessed using the quality criteria defined by the OSCAR-IB study (Tewarie *et al.*, 2012).

3.3.4. *OCT layer segmentation*

All B-scans were segmented using two different segmentation software programs. First, the Heidelberg Eye Explorer (version 6.15.7.0) was employed which segmented the retinal nerve fiber layer (RNFL), ganglion cell layer (GCL), inner plexiform layer (IPL), inner nuclear layer (INL), outer plexiform layer (OPL), outer nuclear layer (ONL), outer retinal layers (ORL; external limiting membrane to Bruch's membrane) and retinal pigmented epithelium (RPE). One final layer was calculated by subtracting the RPE from the ORL, to represent the photoreceptor layer (PL). Subsequently, scans were segmented using OCTExplorer (Version 3.8.0 (x64)) from IOWA Reference Algorithms. This algorithm segmented the RNFL, GCL, IPL, INL, OPL, ONL, ellipsoid zone (EZ), outer segments (OS), outer segment of the photoreceptor/RPE complex including subretinal potential space (OPR) and RPE. An additional layer was created by combining the OS and the OPR, called the outer segment equivalent layer (OSEL). For both segmentation algorithms the macular ganglion cell and inner plexiform layer (mGCIPL) was created by combining the GCL and the IPL.

Both segmentation algorithms used the Early Treatment Diabetic Retinopathy Study (ETDRS) grid of 1, 3 and 6 mm grid size allowing calculation of mean layer thicknesses for each of the nine grid-defined regions. Using OCTExplorer, mean retinal thickness was calculated

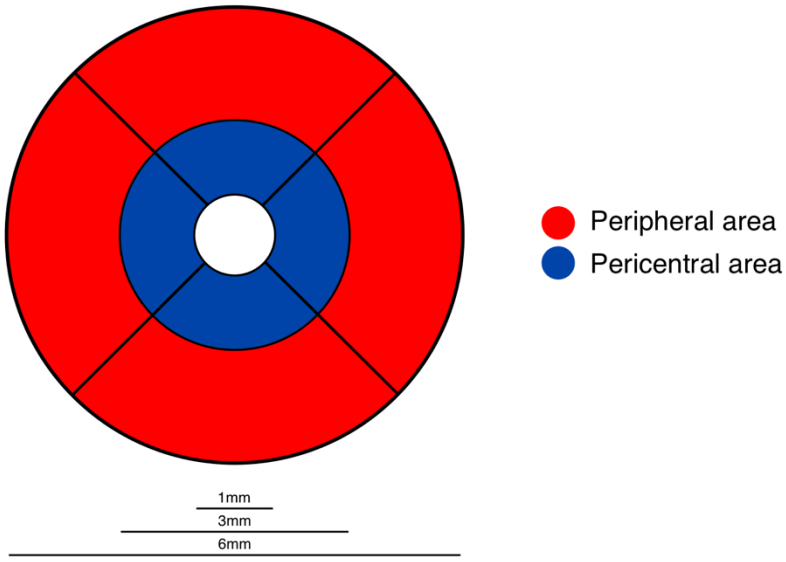

Figure 3.2 Early Treatment Diabetic Retinopathy Study (ETDRS) grid that was used to analyse retinal thicknesses. The combined four red segments correspond to the peripheral area comprise the peripheral area while the four blue segments comprise the pericentral area.

separately for three retinal areas that were defined according to the ETDRS grid: the whole macular region (full ETDRS grid size), the pericentral region (donut-shaped ring centred on the fovea with an inner diameter of 1 mm and an outer diameter of 3 mm) and the peripheral region (an inner diameter of 3 mm and an outer diameter of 6 mm) (Figure 3.2).

3.3.5. *Dark adaptation*

During the dark-adapted measurements room lights were turned off and participants were asked to put on a padded eye mask. Subjective total darkness was verified verbally. The eye mask had a padded excavation in front of the eyes, ensuring no pressure was put on the eye balls. A timer was set for the protocol required time of dark-adaptation. No scans were made during dark-adaptation but only after the full dark-adaptation block was complete. This was done to ensure no stray light from screens or other electronics was observed by participants. After the dark-adaptation block was complete, participants and OCT machine were covered with a cloth that was impermeable to light to ensure no stray light was observed from the computer screen. The OCT machine uses near infrared light for retinal scanning, which (almost) does not activate rhodopsin receptor proteins. Therefore, OCT scanning itself should not alter the dark-adapted state of the retina. No restrictions were put on daylight exposure prior to study measurements.

3.3.6. *Light adaptation*

During the light adaptation block, participants were asked to look in the direction of a 250-lumen light of 20x20 cm at a distance of 50 cm with room lights switched on.

Block	Dark-adaptation scan	Light-adaptation scan 1	Light-adaptation scan 2	Light-adaptation scan 3
1.	5 minutes	5 minutes		
2.	10 minutes	10 minutes		
3.	20 minutes	10 minutes	20 minutes	
4.	30 minutes	10 minutes	20 minutes	30 minutes
5.	5 minutes	5 minutes		

Table 3.1 Summary of employed dark-adaptation protocol when acquiring first pilot data.

3.3.7. *Development of dark- and light-adaptation block timings*

The goal was to create an efficient study protocol to investigate structural changes to outer retinal layers in dark-adaptation, which was done stepwise as described below.

Step 1: First, three healthy control subjects were scanned with a protocol of 5 blocks of alternating dark- and light adaptation. After the baseline scan participants were dark-adapted for 5 minutes and subsequently light adapted for 5 minutes. Secondly, a block of 10 minutes dark adaptation was followed by 10 minutes of light adaptation. Thirdly, a block of 20 minutes of dark adaptation was followed by two light adapted scans at 10 and 20 minutes. The longest block was 30 minutes of dark adaptation followed by three light adapted scans at 10, 20 and 30 minutes. Finally, the block of 5 minutes dark adaptation followed by 5 minutes of light adaptation was repeated. This protocol is shown in the Table 3.1. Thicknesses of the OSEL and the PL were plotted in repeated measures plots to visualise light-induced changes.

Step 2: The most efficient protocol, being the shortest protocol that was associated with dynamic changes to the OSEL and/or the PL during dark-adaptation, that was identified in the first three subjects was repeated in the subsequently recruited healthy control subjects and the acute ON patients.

3.3.8. *Electrophysiology*

ON cases had pattern electroretinography (PERG) performed, for which the methods are detailed in chapter 2 of this thesis.

3.3.9. *Statistical analysis*

OCT layer thicknesses of one eye per subject were analysed, to account for inter-eye correlations (Aytulun *et al.*, 2021). For analyses including all subjects, this was the left eye for healthy control eyes, as this was the eye that was scanned first, and the clinically unaffected eye for the acute ON patients. Continuous data were explored using histograms and dot-plots, while categorical data was explored using cross-tabulations. Summary statistics for continuous variables were given with medians and ranges, and non-parametric tests were used.

First, thicknesses for the full ETDRS grid for the OSEL and the PL were visualised using repeated measures plots for the various time blocks for the three first scanned healthy control subjects. Results were inspected visually.

Subsequently, outer retinal layer thicknesses (OSEL, OS, OPR and PL) were compared between the dark- and light-adapted states with the Wilcoxon signed-rank test for all subjects. Absolute and percentage light-induced thickness change (calculated by dividing the thickness difference by the thickness in dark-adapted state) in layer thickness were calculated. In addition, absolute and percentage changes for the pericentral and peripheral areas were analysed separately. For the outer retina it is expected that layer thickness will be reduced in light-adapted state compared with dark-adapted state, and this effect will be referred to as 'light-associated compression'. These analyses were repeated for all remaining retinal layers and the full retinal thickness to identify dark-induced changes to other layers of the retina.

Finally, absolute and percentage change in dark-associated OSEL thickness were compared between 1) healthy control eyes and acute ON eyes and 2) affected and fellow eyes of acute ON patients using repeated measures plots. Results were inspected visually. A preliminary analysis exploring the differences in absolute and percentage light-associated compression seen in the outer retinal layers between affected ON eyes and healthy control eyes will be performed with the Mann-Whitney U test.

Significance thresholds were Bonferroni corrected for multiple comparisons (31 layers) and set to $p<0.0016$ (=0.05 / 31). Statistical analysis was performed with R and Rstudio (RStudio Team 2021, http://www.rstudio.com/).

3.4. Results

3.4.1. *Participants*

A total of nine healthy control subjects and three acute ON patients were recruited. Baseline characteristics are summarised in Table 3.2. Subjects were scanned on different times on the day, varying from 10:00 to 19:00. BCVA for healthy controls was ≥6/6 in both eyes. The acute ON patients had a median BCVA of 6/5 (6/4 – 6/5) in the fellow eye and of 6/9 (6/6 – 6/60) in the affected eye. Two of the acute ON patients were diagnosed with MS and one tested positive for MOG antibodies, leading to diagnoses of MSON and MOGON, respectively. The low number of patients was in part a consequence of the COVID19 pandemic as this line of research was stopped by MEH R&D

	Healthy controls	**Acute ON patients**
N	9	3
Sex, F (%)	5 (56 %)	3 (100 %)
Age, median (range)	29 (28 – 47)	25 (24 – 28)
Baseline mGCIPL thickness, median (range)	83.60 µm (72.74 – 94.97)	80.51 µm (74.25 – 92.10)
Baseline mRNFL thickness, median (range)	30.57 µm (26.25 – 33.66)	28.66 µm (27.87 – 29.94)
Baseline OSEL thickness, median (range)	29.68 µm (23.52 – 32.41)	28.77 µm (25.64 – 30.90)

Table 3.2 Baseline characteristics of the included cohort.

3.4.2. *OCT*

One (right) eye of a healthy control subject did not meet quality control criteria as it was not centred at the fovea, resulting in a total of 17 healthy control eyes that were included in analysis.

3.4.3. *Development of the dark-adaptation protocol*

As the first step of this study, five blocks of dark- and light-adaptation (Table 3.1) were performed in three healthy subjects, and six eyes. Two of these subjects were male (66 %) and two and one subjects were 29 years and 28 years old, respectively. Thickness changes during these five dark-adaptation blocks are represented visually in Figure 3.3.

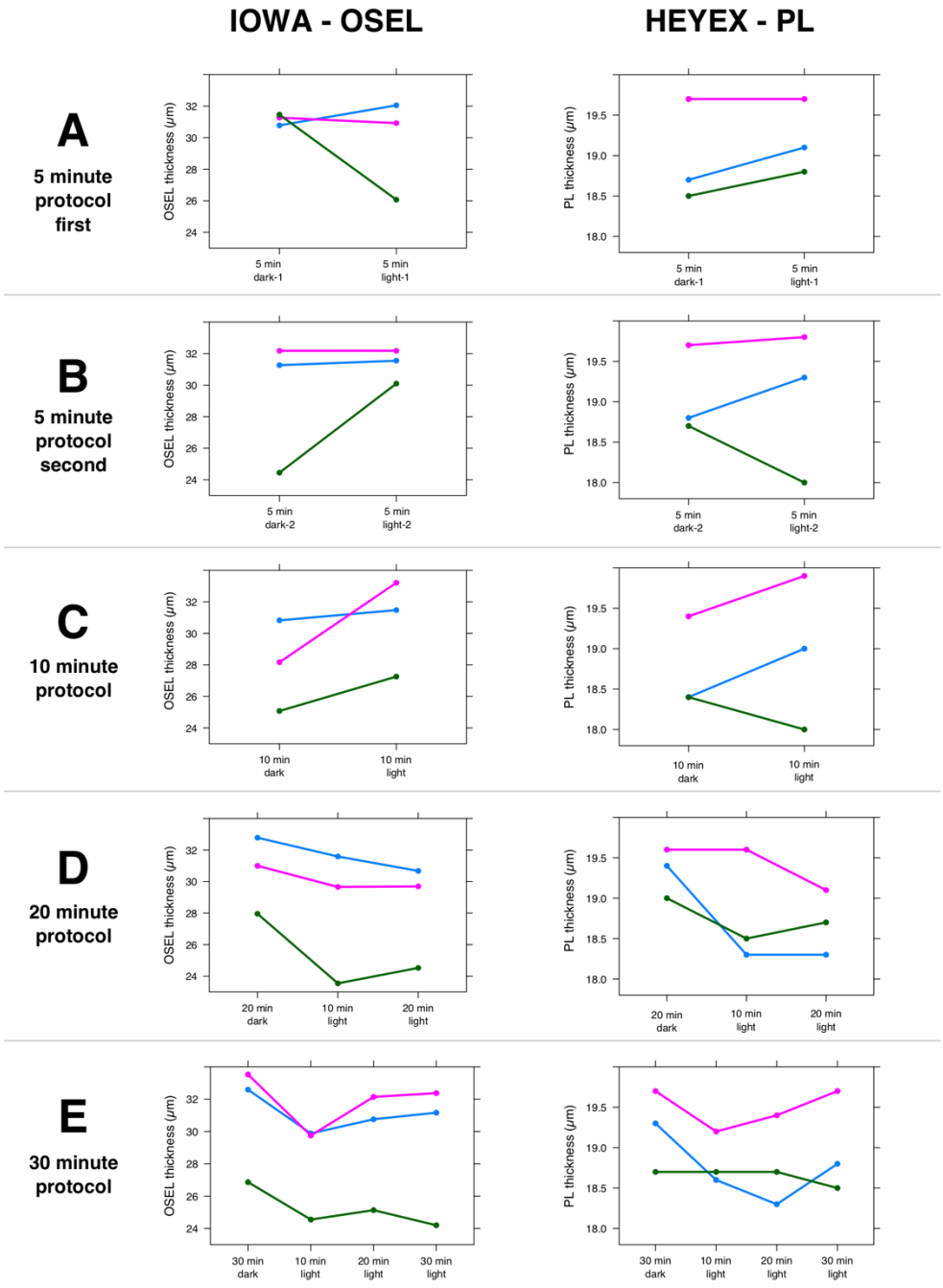

Figure 3.3 Repeated-measures plots visualising pilot data on thickness changes in three healthy controls during dark-adaptation blocks of various length. Left column shows the changes in OSEL thickness (as segmented with IOWA OCTExplorer) and the right column shows the changes in PL thickness (as segmented with Heyex.

For the 5-minute and 10-minute protocols no consistent thickness change was observed. In contrast, for both the 20-minute and 30-minute dark-adaptation block followed by 10 minutes of light adaptation, there was a consistent reduction of OSEL and PL thickness during light adaptation for all three subjects, except for one subject that showed no thickness change for the PL in the 30-minute block. As the 20-minute block is shorter and therefore more efficient than the 30-minute block, the 20-minute block was tested in the subsequently recruited subjects.

Layer	Change in Layer 20 min dark – 10 min light	Full ETDRS grid
OSEL (µm)	Wilcoxon signed-rank test	**p<0.001**
	Δ absolute, median (range)	-1.41 (-4.65 – 0.08)
	Δ percentage, median (range)	-4.62 % (-15.78 – 0.31)
OS (µm)	Wilcoxon signed-rank test	p=0.204
	Δ absolute, median (range)	-0.09 (-2.14 – 0.25)
	Δ percentage, median (range)	-0.81 % (-2.49 – 17.12)
OPR (µm)	Wilcoxon signed-rank test	**p<0.001**
	Δ absolute, median (range)	-1.35 (-4.90 – 1.37)
	Δ percentage, median (range)	-7.07 % (-23.48 – 9.71)
PL (µm)	Wilcoxon signed-rank test	p=0.041
	Δ absolute, median (range)	-0.50 (-7.00 – 1.00)
	Δ percentage, median (range)	-2.66 % (-36.60 – 5.56)

Table 3.3 Dynamic light-associated changes in the outer retinal layers as measured in the full ETDRS grid. OSEL = outer segment equivalent layer. OS = outer segments. OPR = outer segments photoreceptor and retinal pigmented epithelium complex. PL = photoreceptor layer. Δ = thickness change when comparing dark-adapted with light-adapted state.

3.4.4. *Dynamic light-associated changes to the outer retina*

Six additional healthy control and three acute ON subjects were scanned with a protocol comprising 20 minutes of dark adaptation and 10 minutes of light adaptation. Changes in thickness of outer retinal layers were explored. Layers of interest were the OSEL, OS, OPR and PL (Table 3.3). The OSEL showed a significant (p<0.001) light-associated compression of -1.41

	Change in Layer 20min dark – 10min light	Full ETDRS grid	Pericentral area	Peripheral area
RNFL (µm)	Signed-rank test	p=0.012	p=0.002	p=0.052
	Δ absolute, median (range)	-1.03 (-3.5 – 1.2)	-0.86 (-2.9– 0.6)	-0.99 (-4.7 – 2.1)
	Δ percentage, median (range)	-3.27% (-10.3 – 4.5)	-3.06% (-9.1 – 2.4)	-2.80% (-11.3– 6.3)
INL (µm)	Signed-rank test	p=0.027	p=0.034	p=0.029
	Δ absolute, median (range)	0.39 (-0.4 – 1.8)	0.65 (-0.7 – 3.3)	0.48 (-1.1 – 1.5)
	Δ percentage, median (range)	0.98% (-1.3 – 5.7)	1.55% (-1.7 – 9.8)	1.55% (-3.0 – 4.0)
EZ (µm)	Signed-rank test	p=0.012	p=0.034	p=0.129
	Δ absolute, median (range)	-0.31 (-1.53 – 0.21)	-0.40 (-2.2 – 0.6)	-0.18 (-1.8 – 0.3)
	Δ percentage, median (range)	-2.28% (-9.7 – 1.6)	-2.64% (-12.9– 4.2)	-1.46% (-11.5– 2.3)
Whole retina (µm)	Signed-rank test	**p<0.001**	**p<0.001**	**p=0.001**
	Δ absolute, median (range)	-2.76 (-0.9 – -7.2)	-2.66 (-1.5 – -4.6)	-2.63 (-11.3 – 0.4)
	Δ percentage, median (range)	-0.88% (-0.3 – -2.4)	-0.82% (-0.4 – -1.4)	-0.83% (-3.9 – 0.1)

Table 3.4 Dynamic light-associated thickness changes in the macular retinal nerve fibre layer (RNFL), inner nuclear layer (INL), ellipsoid zone (EZ) and the whole retina. p-values are in **bold** if values remained significant after Bonferroni correction.

µm, corresponding with -4.62 % in the full-grid measurement. When looking at the two individual layers that comprise the OSEL, it appeared that the majority of the light-associated changes in layer thickness occurred in the OPR (diff: -1.35 µm, percentage: -7.07 %, p<0.001) and not the OS (diff: -0.09 µm, percentage: -0.81 %, p=0.204). There was no clear difference in light-associated changes occurring in the pericentral and peripheral areas of the outer macular layers (Supplementary Table 3.1). The dark-adaptation protocol was not associated with a significant change in the thickness of the PL (p=0.041).

3.4.5. *Dynamic light-associated changes to other retinal layers*

Structural changes of other retinal layers during the dark- and light-adaptation protocol were explored. There was a near-significant light-associated compression of the pericentral area of the RNFL (diff: -0.86 µm, percentage: -3.06 %, p=0.002) and some suggestion of light-

associated expansion of the INL (diff: 0.39 µm, percentage 0.98 %, p=0.027) and light-associated compression of the EZ (diff: -0.31 µm, percentage -2.28 %, p=0.012). Furthermore, there was a highly significant reduction in total retinal thickness across the full ETDRS grid

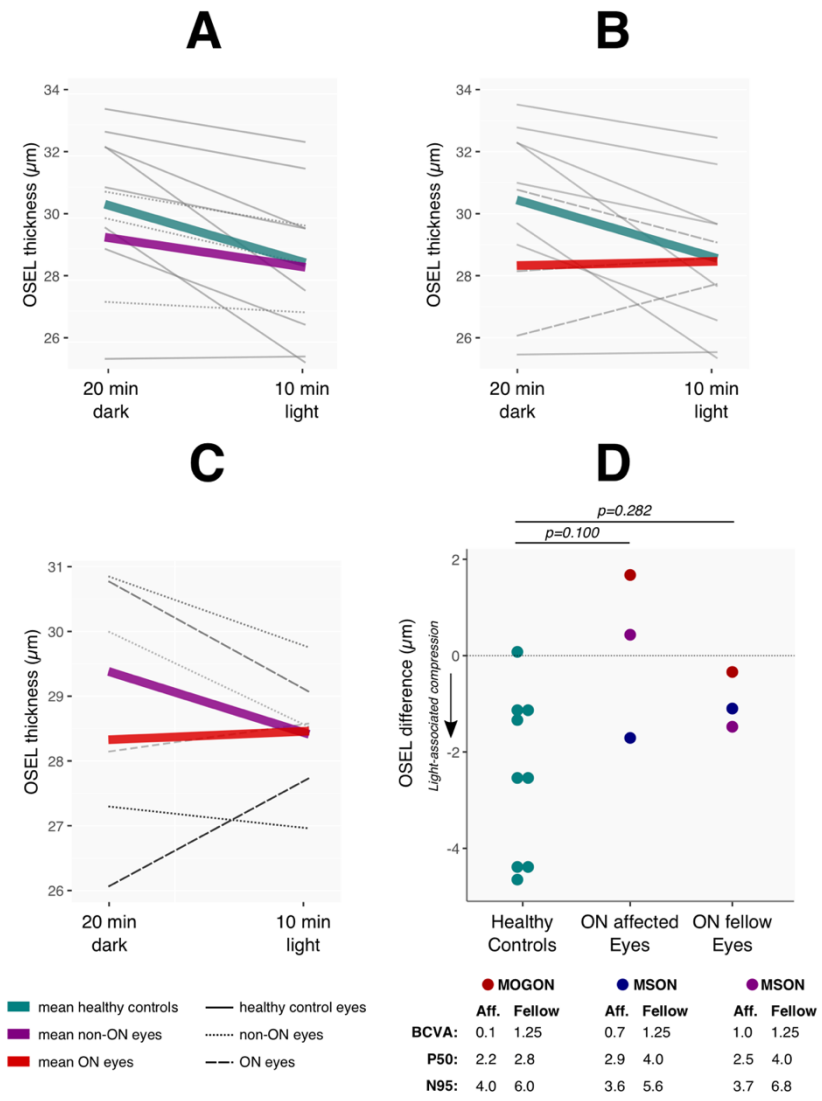

Figure 3.4 Light-associated compression of the OSEL in controls and in ON cases. A: repeated-measures plot showing mean light-associated thickness change in the OSEL for healthy controls (green line) and fellow eyes of ON cases (purple line). Thickness changes for individual subjects are shown in grey. B: repeated-measures plot showing mean light-associated thickness change in the OSEL for controls (green line) and affected eyes of ON cases (red line). C: repeated-measures plot showing light-associated thickness change in OSEL for fellow (purple) and affected (red) eyes of ON patients. D: Dot-plot showing absolute thickness change for healthy controls (green) and ON cases. For ON cases the affected and fellow eyes are colour-coded per subject. Dotted line represents no change. p-values represent results of Wilcoxon rank sum test. Diagnosis (MOG-associated ON or MSON), best corrected visual acuity (BCVA), P50 amplitude and N95 amplitudes are given for the ON cases below D.

(diff: -2.86 µm, percentage: -0.88 %, p<0.001), as well as in the pericentral (diff: -2.66 µm, percentage: -0.82 %, p<0.001) and peripheral areas (diff: -2.63 µm, percentage: -0.83 %, p<0.001) (Table 3.4). No dynamic changes were observed for the other retinal layers (Supplementary Table 3.2).

3.4.6. *Healthy controls versus acute ON patients*

Figure 3.4 visualises the OSEL thicknesses during 20-minute dark-adaptation and subsequent 10-minute light-adaptation for healthy control eyes and acute ON eyes in repeated measures plots. Individual acute ON eyes are shown in dotted lines and individual healthy control eyes are shown in full lines. Mean thickness changes are shown in green, purple and red lines for healthy control eyes, fellow eyes of acute ON patients and affected eyes of acute ON patients, respectively. Plot A visualises the changes in the healthy control eyes and the fellow eyes of acute ON patients. This shows a smaller sized change in OSEL thickness for fellow eyes of acute ON patients compared with healthy control eyes. Plot B visualises the changes in healthy control eyes and the affected eyes of acute ON patients, which showed a greater difference in light-associated thickness changes between these groups with acute ON eyes showing no light-associated compression. Plot C shows the intra-individual differences in light-associated changes between affected and fellow eyes. This plot shows a light-associated compression of the OSEL for fellow eyes but not for affected eyes of ON patients.

The magnitude of light-associated change in OSEL thickness was a median of -2.45 µm (range: -4.65 – 0.08) for healthy controls and +0.43 µm (range: -1.71 – 1.67) for acute ON eyes. This corresponded to a percentage change in OSEL thickness of -8.03 % (range: -14.39 – 0.31) and +0.81 % (range: -5.55 – 6.43) for healthy controls and acute ON eyes, respectively. Fellow eyes of ON patients showed a light-associated reduction of -1.10 µm (range: -1.48 – -0.34), corresponding to a -3.56 % (range: -4.92 – -1.24) change, in OSEL thickness. Both the absolute and percentage light-associated thickness change differed at trend (p=0.100) between healthy controls and acute ON eyes. Figure 3.4-D visualises these differences in light-associated compression of the OSEL between controls and ON cases. Almost all controls showed light-associated compression of the OSEL, except for one subject that showed no change, while two out of the three affected eyes of ON cases showed some expansion of the OSEL. The ON case showing the greatest OSEL expansion was the only MOGON case, and also displayed the

lowest BCVA. PERG evaluation showed relatively similar macular function for all three ON cases, with P50 amplitudes ranging from 2.2 to 2.9 µV. Interestingly, most severe P50 amplitude reduction was seen for the MOGON case showing the greatest light-associated OSEL expansion.

3.5. Discussion

This pilot study identified a consistent and significant light-associated compression of the OSEL in healthy controls and fellow eyes of ON patients, using a protocol that comprised 20 minutes of dark adaptation followed by 10 minutes of light adaptation. Furthermore, these pilot data suggest that acute ON might be associated with a reduction in the dynamic thickness changes that occur within the outer retina during dark-adaptation.

These findings are in line with two previous studies that explored the effects of dark- and light-adaptation on outer retinal layer thickness in humans. The first study (Abramóff et al., 2013) used a similar protocol in healthy controls and showed an average light-associated reduction in OSEL thickness of -1.48 µm. This is very close to the effect sizes observed in this pilot work, with an observed light-associated reduction in OSEL size of -1.41 µm across all eyes, and of -2.45 µm when only looking at healthy control eyes. This indicates that the protocol employed here had a similar efficiency, even though subjects studied by Abramóff et al. were all scanned in the early morning before sunrise to account for circadian effects. Another study that employed ultrahigh-resolution OCT similarly identified a maximum reduction of OSEL thickness after approximately 10-15 minutes of light-adaptation, depending on the level of rhodopsin bleach (Lu *et al.*, 2017). The fact that the finding of light-associated compression in the OSEL is consistent with prior work, supports the existence of structural thickness changes to the outer segments of the photoreceptors in response to dark-adaptation.

Further supportive of the existence of structural thickness changes to the outer segments of the photoreceptors in dark-adaptation is animal work that showed histopathological differences in the size of the outer segments of photoreceptors between rodents that were light-adapted and dark-adapted (Li *et al.*, 2016). Interestingly, these findings were counter-directional to the findings presented here in human subjects, as the researchers identified light-associated expansion of the photoreceptor outer segments. This could be due to differences between rodent and human retinal anatomy and function. Another reason for the dissimilarity could be the difference in study protocol, with the investigated animals being adapted to dark conditions for much longer (up to eight days).

However, other explanations for these findings should be considered. An important consideration is the possibility of optical artefacts due to pupillary size changes in response to

light conditions. As the pupils of the subjects were not dilated, pupillary changes due to dark- and light-adaptation could have caused an optical effect leading to changes in thickness measurements. However, existing data suggests that mydriasis does not influence retinal layer thicknesses measured by OCT (Cheng *et al.*, 2011; Tanga *et al.*, 2015). Furthermore, it would be unlikely that these optic effects would cause such selective changes in OSEL thickness measurements as identified in this study. Light-associated compression of the OSEL represented ±5 % of the baseline layer thickness, a considerably greater effect size compared with other retinal layers. OCT thickness measures generally have an excellent repeatability for the inner as well as the outer retinal layers (Çetinkaya *et al.*, 2017).

Although the dynamic structural changes observed here are referred to as 'light-associated compression', it should be noted that it is unclear if these structural changes are primarily driven by responses to dark-adaptation or light-adaptation. It is likely that the OSEL shows a constant dynamic range of compression and expansion in response to light conditions.

Further analysis of the two individual layers that make up the OSEL, the OPR (containing the subretinal potential space) and the OS, revealed that the dynamic thickness changes are primarily confined to the OPR. Light-associated compression of the OPR represented ±7 % of the initial layer thickness, while this was only ±1 % for the OS. This suggests that the light-associated thickness changes are located either in the outermost tips of outer segments of the photoreceptors or are the results of changes in the size of the subretinal potential space. This is an interesting observation with regard to identifying the underlying mechanisms that cause the thickness changes of the OSEL. Because the main thickness change was observed in the OPR, a possible swelling of the subretinal potential space seems to be relatively more likely as an explanation for the findings presented here. This could be the result of shedding within the photoreceptor outer segments and phagocytosis facilitated by the RPE. However, it is important to recognise that changes in refractive characteristics of photoreceptors or the photoreceptor outer tips may play a role in these findings.

This pilot study provides limited evidence that the light-associated compression of the OSEL is disturbed in patients with acute ON. On visual inspection of repeated-measure plots, mean light-associated compression of the OSEL was almost absent in eyes affected by ON. Furthermore, two out of the three ON patients showed light-associated expansion of the

OSEL, while this was not observed in any of the healthy control subjects. The magnitude of light-associated compression differed at trend between eyes affected by ON and healthy control eyes (p=0.100). To a lesser extent, light-induced compression was also reduced in fellow eyes of patients with acute ON compared with healthy controls. These findings might relate in part to the electrophysiological findings presented in chapter 2, which were suggestive of outer retinal dysfunction in acute ON. Additional studies have also reported findings of outer retinal dysfunction in ON and MS, which are largely unexplained (Berninger and Heider, 1990; Holder, 2004; Hanson *et al.*, 2018; Al-Nosairy *et al.*, 2021).

There are several potential explanations for the finding of decreased light-associated compression of the OSEL in ON. Importantly, the possibility of a chance effect, due to the small sample size, cannot be discarded. It should be noted that one out of the three ON cases investigated here did show light-associated compression of the OSEL, which was actually relatively reduced in the fellow eye for this case, highlighting the necessity to validate these findings in a bigger cohort. Furthermore, patients with ON could have a reduced ability to focus effectively on the target during OCT scanning due to impaired visual acuity or a central scotoma. However, scan quality was excellent for the three ON cases and did not seem disturbed by poor focus. There might be temporal changes in the dynamics of light-induced structural changes, with ON patients reaching trough thicknesses at an earlier or later time than healthy controls. This could have meant that the employed protocol was not adequately timed to pick up changes in ON. However, the most interesting hypothesis is that retinal processes associated with dark-adaptation are affected by ON. During ON there are certain changes to the retinal environment that are recognised. Firstly, there is evidence for localised inflammation, with increased numbers of activated glial cells (Green *et al.*, 2010) and perivenous cuffing (Lightman *et al.*, 1987). In addition, there is evidence for mitochondrial dysfunction, hypoxia and hypoperfusion in early neuroinflammatory disease in animal work (Desai *et al.*, 2016, 2020) as well as in human patients with ON (Haufschild *et al.*, 2003). Given the known high energetic cost of dark-adaptation, metabolic disturbances could theoretically disturb this process and might explain the findings of this study.

This study could provide some explanation for some poorly understood visual symptoms of ON patients, as ON patients sometimes report having photopsias, or have difficulty adjusting to changes in light conditioning and might also experience ‘bleaching’ symptoms. It would be

interesting to explore how light-associated compression of the OSEL evolves when ON resolves as well as if this is affected in patients with MS that have not experienced ON.

An important limitation of this work relates to the low sample size, and findings need to be corroborated in larger groups of subjects. Future research is also necessary to identify the intra-individual reproducibility of light-induced thickness changes. How structural thickness changes relate to electrophysiological metrics of dark-adaptation could be investigated through simultaneous OCT and ERG examination. To further investigate if metabolic failure is an important factor in determining the magnitude of light-associated compression in ON, future studies should relate light-associated compression to serum measures of metabolic function (such as lactate) and OCT-angiography metrics.

3.6. Conclusion

These results indicate that OCT may be used as a functional measure as it is sensitive to dynamic changes in the outer segments of the photoreceptors that occur in response to dark-adaptation. These changes can be elicited consistently with a relatively quick and subject-friendly protocol, with OSEL thicknesses being greater in the dark-adapted compared with the light-adapted state. Pilot data in this study indicate that light-associated compression of the OSEL may be less pronounced or even absent in acute ON. Although this finding needs to be confirmed in bigger cohorts, it suggests that dark-adaptation processes may be disturbed in acute ON. A hypothesis is that the energy-costly process of dark-adaptation is affected by metabolic failure in acute ON.

3.7. Supplementary material

Layer	Change in Layer 20 min dark – 10 min light	Pericentral area	Peripheral area
OSEL (µm)	Wilcoxon signed-rank test	**p<0.001**	**<0.001**
	Δ absolute, median (range)	-1.40 (-4.52 – 0.11)	-1.90 (-5.77 – -0.27)
	Δ percentage, median (range)	-4.34 % (-14.67 – 0.42)	-6.25 % (-19.09 – -1.02)
OS (µm)	Wilcoxon signed-rank test	p=0.677	p=0.050
	Δ absolute, median (range)	-0.15 (-1.88 – 1.01)	-0.34 (-2.60 – 0.45)
	Δ percentage, median (range)	-1.40 % (-14.70 – 8.88)	-3.42 % (-23.49 – 5.29)
OPR (µm)	Wilcoxon signed-rank test	p=0.003	p=0.003
	Δ absolute, median (range)	-1.59 (-5.13 – 0.91)	-1.38 (-5.23 – 1.00)
	Δ percentage, median (range)	-7.49 % (-23.46 – 6.39)	-6.56 % (-26.23 – 7.00)
PL (µm)	Wilcoxon signed-rank test	n/a	n/a
	Δ absolute, median (range)	n/a	n/a
	Δ percentage, median (range)	n/a	n/a

Supplementary Table 3.1 Dynamic light-associated changes in the outer retinal layers as measured in the pericentral and peripheral areas of the ETDRS grid. OSEL = outer segment equivalent layer. OS = outer segments. OPR = outer segments photoreceptor and retinal pigmented epithelium complex. PL = photoreceptor layer. Δ = thickness change when comparing dark-adapted with light-adapted state.

	Change in Layer 20min dark – 10min light	Full ETDRS grid	Pericentral area	Peripheral area
GCIPL (µm)	Signed-rank test	p=0.569	p=0.970	p=0.470
	Δ absolute, median (range)	-0.33 (-1.8 – 1.0)	0.09 (-1.9 – 2.0)	-0.33 (-5.9 – 2.9)
	Δ percentage, median (range)	-0.41 % (-2.4– 1.2)	0.10 % (-1.9 – 2.1)	-0.40 % (-8.3 – 4.3)
ONL (µm)	Signed-rank test	p=0.470	p=0.151	p=0.910
	Δ absolute, median (range)	-0.30 (-5.2 – 4.6)	-0.57 (-5.1 – 6.9)	-0.05 (-1.6 – 3.0)
	Δ percentage, median (range)	-0.34 % (-6.1 – 4.7)	-0.64 % (-5.2 – 7.8)	-0.06 % (-1.8 – 4.0)
RPE (µm)	Signed-rank test	p=0.110	p=0.151	p=0.064
	Δ absolute, median (range)	0.45 (-1.2 – 3.9)	0.21 (-1.2 – 3.8)	0.73 (-2.9– 4.3)
	Δ percentage, median (range)	2.5 % (-5.8 – 22.4)	1.22 % (-4.9 – 22.4)	3.63 % (-13.6 – 24.4)

Supplementary Table 3.2 Dynamic light-associated thickness changes in the macular ganglion cell and inner plexiform layer (GCIPL), outer nuclear layer (ONL) and retinal pigmented epithelium (RPE).

4. Ellipsoid Zone Reflectivity in Neuroinflammatory and Mitochondrial Disease

ABSTRACT

Background: The ellipsoid zone (EZ), the second hyperreflective band on optical coherence tomography (OCT) scans, is thought to derive its high intensity profile from light scattering of mitochondria. Structural or functional changes to mitochondria may affect its reflectivity.

Objective: To develop an analysis tool that extracts relative EZ reflectivity with good reliability and to explore if EZ reflectivity is affected in multiple sclerosis (MS) and mitochondrial disease.

Methods: Control subjects and acute optic neuritis (ON) patients were recruited prospectively while patients with MS associated primary progressive optic neuropathy (PPON), chronic progressive external ophthalmoplegia (CPEO) and dominant optic atrophy (DOA) were identified retrospectively. A Python script that extracted median reflectivity from segmented B-scans was purpose built. EZ reflectivity was normalised to the retinal pigmented epithelium (RPE) and to the outer nuclear layer (ONL). Reliability of the EZ reflectivity measures was evaluated with intraclass correlation coefficients (ICC). Group differences in EZ reflectivity were investigated through multivariable linear regression, adjusted for relevant confounders.

Results: Twelve controls, 23 acute ON, seven CPEO, 13 DOA and 13 PPON patients were included. Test-retest reliability of the EZ/RPE and EZ/ONL ratios were 0.76 ($p<0.001$) and 0.63 ($p=0.013$), respectively. Multivariable regression analysis, adjusted for age, sex and inner retinal layer thickness, revealed that the median EZ/RPE and EZ/ONL ratio were reduced in CPEO (Beta=-0.12 ($p=0.036$) and Beta=-0.59 ($p=0.011$)), DOA (Beta=-0.16 ($p=0.049$) and Beta=-0.55 ($p=0.088$)) and PPON (Beta=-0.17 ($p=0.014$) and Beta=-0.57 ($p=0.037$), respectively) compared with controls. EZ/RPE and EZ/ONL ratios were reduced in affected eyes of acute ON patients (Beta=-0.11 ($p=0.013$) and Beta=-0.42 ($p=0.006$), respectively) compared with healthy controls.

Conclusions: EZ reflectivity can be determined with good reliability from OCT scans and is reduced in acute and chronic neuroinflammatory disease, such as in acute ON and PPON, and in mitochondrial disorders, such as CPEO and DOA. These results suggest that EZ reflectivity may be an indirect non-invasive in-vivo biomarker for mitochondrial function.

4.1. Background

Optical coherence tomography (OCT) images the structure of retinal tissue and delineates the boundaries between the retinal layers based on changes in the refractive index. As the retina has a highly structured anatomical organisation of cell types with variable reflective properties, this information can be used to calculate individual retinal thicknesses for quantitative analysis. However, the analysis of a layer's reflective index itself is a novel and currently under-explored technique within the field of OCT scanning. Although the analysis of reflectivity metrics has certain technical complexities, in particular associated with the instability of the measure in response to changes in image acquisition protocols or quality, it holds exciting potential for studying cellular function in vivo.

Four individual hyperreflective bands can be identified in the outer retina on macular OCT imaging. Research combining histopathological analysis and OCT images of retinal tissue from human donor eyes indicates that the high reflectivity index of the second of these bands (the ellipsoid zone (EZ)) is caused by local mitochondrial accumulation (Cuenca *et al.*, 2018; Litts *et al.*, 2018). Cytochrome C oxidase (COX) staining of the EZ on histopathological imaging correlates with the second highly reflective layer on OCT (Figure 4.1) (Cuenca *et al.*, 2018). This is in line with the anatomical structure of the EZ, which consists almost entirely of accumulated mitochondria in the outer portion of the inner segments of the photoreceptors. Although mitochondria seem to contribute to some extent to the high reflectivity index of the retinal pigmented epithelium (RPE) as well, the reflectivity of this layer appears to be also driven by local phagosomes and melanosomes (Cuenca *et al.*, 2018; Curcio *et al.*, 2018).

Mitochondria have been identified as one of the organelles that scatter the most light (Wilson *et al.*, 2007). In vitro research indicates that the optical properties of mitochondria, specifically their scattering coefficients, are associated with their structural integrity and functional status. Scattering of light has been found to correlate with the activity of succinate dehydrogenase (Complex II of the electron transport chain) as well as with the mitochondrial protein content of tissue (Beauvoit *et al.*, 1995). In vitro work has shown that the light scattering ability of mitochondria is affected by metabolic state. Refractivity of mitochondria reduces in response to energy depletion (Tychinsky, 2009) and subjecting cell cultures to

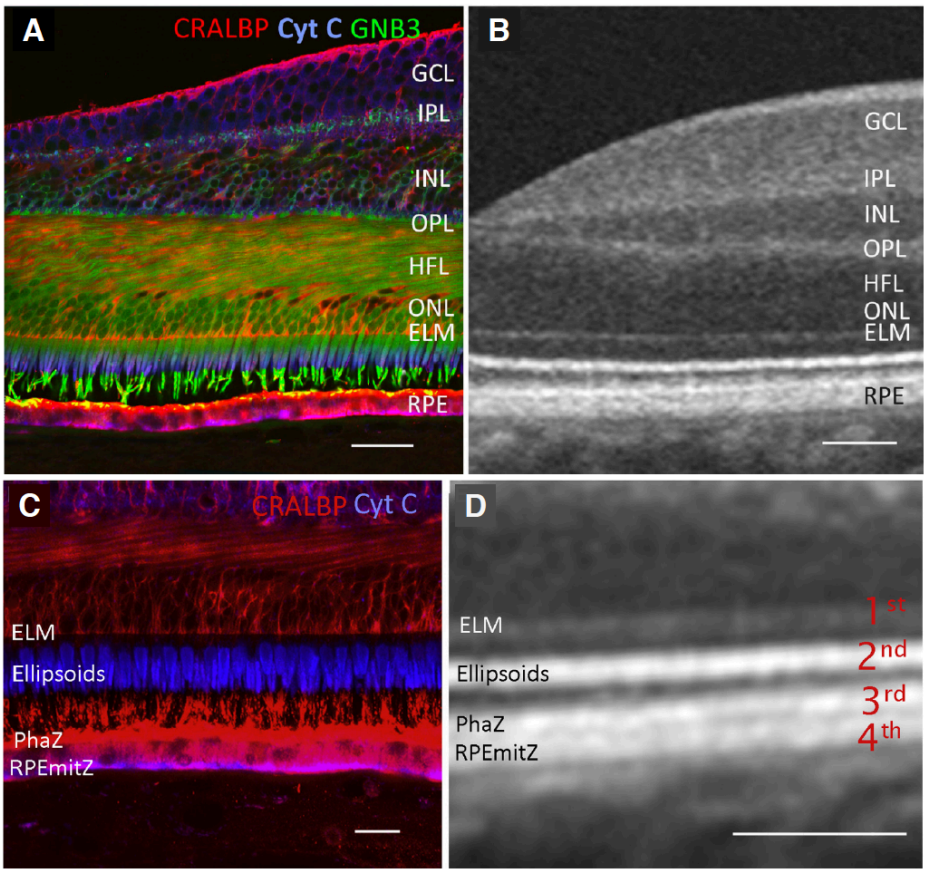

Figure 4.1 Correlations between histopathological analysis and OCT images of retinal tissue. A and C: histopathological analysis of full retinal tissue (A) and the outer retinal layers (B) with blue staining for cytochrome C oxidaxe (COX) as a measure of mitochondrial accumulation, red staining for cellular retinaldehyde-binding protein (CRALBP) and green staining for guanine nucleotide-binding protein b 3 (GNB3). Figure C and D show that the accumulation of mitochondria in the ellipsoid, as visualized through COX staining, corresponds with the second hyperreflective band on OCT. Scale bar in A and B 10microns, in C 20 microns and in D 100 microns. Figure adapted from Cuenca et al., 2018, used with permission.

oxidative stress has been shown to both alter mitochondrial morphology and light scattering patterns (Wilson *et al.*, 2005). These associations of refractivity with changes in mitochondrial morphology are relevant as mitochondrial morphology is constantly highly dynamic and involves constant processes of fission and fusion to maintain energy homeostasis (Karbowski and Youle, 2003). Fission, resulting in smaller mitochondria, has been shown to be associated with increased backscattering or reflectivity on OCT (Pasternack *et al.*, 2010, 2011; Farhat *et al.*, 2011). These associations of light scattering properties of mitochondria with their functional status and morphology, bring into focus the possibility of using EZ reflectivity to monitor mitochondrial health in vivo.

There is limited data on the associations of EZ reflectivity on OCT with pathology in humans. Preliminary data suggest that relative EZ reflectivity reduces with increasing age (Wu *et al.*, 2013). Furthermore, a decreased relative intensity of the EZ has been reported in glaucoma (Ha *et al.*, 2018) and age-related macular degeneration (AMD) (Wu *et al.*, 2013; Tao *et al.*, 2016; Toprak *et al.*, 2017; Thiele *et al.*, 2020). These are interesting observations as mitochondrial complex failure has been implicated in AMD (Nag and Wadhwa, 2016) and glaucoma (Kong *et al.*, 2009). EZ reflectivity was also reduced in retinitis pigmentosa (Gong *et al.*, 2021) and Best disease (Romano *et al.*, 2020), while showing a trend reduction in patients with pseudoxanthoma elasticum (PXE) compared with controls (Risseeuw *et al.*, 2020).

EZ reflectivity has not been investigated in multiple sclerosis (MS). However, given the important questions about the role of mitochondrial failure in the pathophysiology of MS (Campbell *et al.*, 2014; Desai and Smith, 2017), it might provide a valuable tool. This study will investigate EZ reflectivity in individuals affected by neuroinflammatory disease affecting the optic nerves, as well as in two mitochondrial disorders, dominant optic atrophy (DOA) and chronic progressive external ophthalmoplegia (CPEO). DOA is a dominant autosomal genetic disorder that is often associated with mutations to the OPA1-gene, which encodes mitochondrial membrane proteins, and has a specific predilection for affecting the function of mitochondria in the retinal ganglion cells (RGCs) (Yu-Wai-Man *et al.*, 2010). CPEO is characterised by reduced ocular motility and is associated with several mitochondrial DNA mutations. Although the mutations are present throughout the body, the extraocular muscle groups are primarily affected given their high volume of mitochondria (Gorman *et al.*, 2016). While DOA is associated with prominent macular ganglion cell and inner plexiform layer (mGCIPL) atrophy, this is not the case in CPEO. By exploring EZ reflectivity across these various disorders, it might be possible to disentangle the contribution of retinal atrophy to the EZ reflectivity profile.

As absolute reflectivity measures are affected by lighting, scanning quality and acquisition protocols, EZ reflectivity should be normalised to another retinal layer (Chen *et al.*, 2013). There are several considerations to recognise when deciding on an appropriate reference layer. Importantly, this layer should be unaffected by the disease that is under investigation, to ensure that findings are exclusively the result of changes to the EZ. As MS and DOA are well-

known to be associated with changes to the mGCIPL and the RNFL, these layers are likely poor reference layers in this regard. Furthermore, ideally the reference layer is spatially close to the EZ, relatively large, to ensure stability, and has a similar absolute reflectivity index as the EZ, to prevent small measurement errors in- or deflating the ratio to a large extent. Most suitable reference layers to normalise EZ reflectivity when studying MS are likely the RPE, due to its similar intensity, and the outer nuclear layer (ONL), due to its relatively great thickness.

4.2. Aims, objectives and hypotheses

4.2.1. *Aims and objectives*

The primary aim of this study was to develop an automated analysis tool that extracts reflectivity data from macular OCT scans. Subsequently, the goal was to explore the reproducibility of the resulting measure of relative EZ reflectivity.

The secondary aim of this study was to explore the utility of relative EZ reflectivity as an in vivo metric of mitochondrial health by investigating if EZ reflectivity is affected in MS, ON, CPEO and DOA.

4.2.2. *Hypotheses*

The primary hypothesis of this study is that a reproducible measure of relative EZ reflectivity, normalised to either the RPE or the ONL and calculated from the median grey value of individual retinal layers, can be created.

The secondary hypothesis of this study is that relative EZ reflectivity is reduced in MS, ON, CPEO and DOA, given the known involvement of mitochondrial genetic mutations and/or metabolic failure in these disorders.

4.3. Methods

4.3.1. *Participants*

Healthy control participants were recruited from Moorfields Eye Hospital staff. Most of these healthy control subjects also underwent the dark-adaptation testing that was discussed in chapter 3. Control subjects had best corrected visual acuities (BCVA) of ≥6/6 in both eyes, no pre-existing eye disease, did not use any medication, had a normal fundus appearance and had basic structural OCT measurements (pRNFL and mGCIPL) within normal limits.

Symptomatically unilateral ON patients aged 18-60 years, without a previous episode in the affected eye, were prospectively recruited from Moorfields Eye Hospital. These were the same subjects as discussed in detail in chapter 2, but only patients with OCT scans of sufficient quality in both eyes were included here. Diagnosis was made by a neuro-ophthalmologist (AP) using an international consensus investigation protocol. Patients presenting within 14 days of onset of visual loss and/or pain on eye movement, whichever was the earlier, were recruited. Patients were classified as MOG associated ON if seropositive for MOG antibodies (MOGON), as MS associated ON if fulfilling the 2017 MS international diagnostic criteria (MSON) (Thompson *et al.*, 2018*a*) and single episode isolated ON (SION) as described.

In addition, patients that had a primary progressive optic neuropathy (PPON), referring to early and pronounced optic nerve involvement in MS that is described in detail in chapter 6 of this thesis, were retrospectively identified from chart review at Moorfields Eye Hospital and at the Amsterdam University Medical Centre. Finally, patients diagnosed with CPEO and DOA with sufficient quality macular OCT scans available were retrospectively identified from chart review at Moorfields Eye Hospital. Age, sex, BCVA and additional medical history were noted for these retrospectively identified subjects.

4.3.2. *Ethical approval*

Approval for the study was obtained from the Ethics committee (study number 64861) and hospital R&D (FRAC0001 & CaRS_23). Informed consent in writing was obtained from prospectively recruited subjects, in accordance with the Declaration of Helsinki. The analysis of retrospective data was exempt from review by NHS ethical committee in the UK. The

Amsterdam institutional review board issued a waiver stating that the requirements of the Medical Research Involving Human Subjects Act did not apply for the use of the clinical and imaging data for this study.

4.3.3. *OCT protocol*

For healthy controls and ON patients the OCT measurements were performed prospectively with Spectralis SD-OCT (Heidelberg Engineering, Inc, Heidelberg, Germany) with the eye tracking function enabled, on acquisition software version 6.7.13.0. Macular volume scan (1024 A-scans, 37 B-scans volume = 15x15°, automatic real-time function [ART] = 25) centred around the fovea with high-resolution setting enabled were performed, with subsequent scans performed on follow-up mode. The dark-adaptation protocol as detailed in chapter 2 of this thesis was performed in a subset of subjects.

Clinically performed OCT scans were retrospectively identified for patients with PPON, CPEO and DOA. Macular volume scans centred on the fovea that passed OSCAR-IB quality control criteria were included and analysed in this study (Tewarie *et al.*, 2012). Scan quality was approximated through the signal-to-noise ratio and was set at a minimum of 20 dB for inclusion.

4.3.4. *OCT layer segmentation*

Macular OCT scans were segmented for quantitative thickness data with OCTExplorer (Version 3.8.0 (x64)) from IOWA Reference Algorithms. This algorithm segmented the retinal nerve fibre layer (RNFL), ganglion cell layer (GCL), inner plexiform layer (IPL), inner nuclear layer (INL), outer plexiform layer (OPL), outer nuclear layer (ONL), EZ, outer segments (OS), outer segment of the photoreceptor/RPE complex including subretinal potential space (OPR) and RPE. The mGCIPL was created by combining the GCL and IPL. The inner retinal layers (IRL) were created by combining all layers that were located above the EZ, being the RNFL, GCL, IPL, INL, OPL and ONL. Thicknesses were calculated in a 1, 3 and 6 mm ETDRS grid. Layer segmentation was inspected visually for errors. However, manual correction was not required for these data.

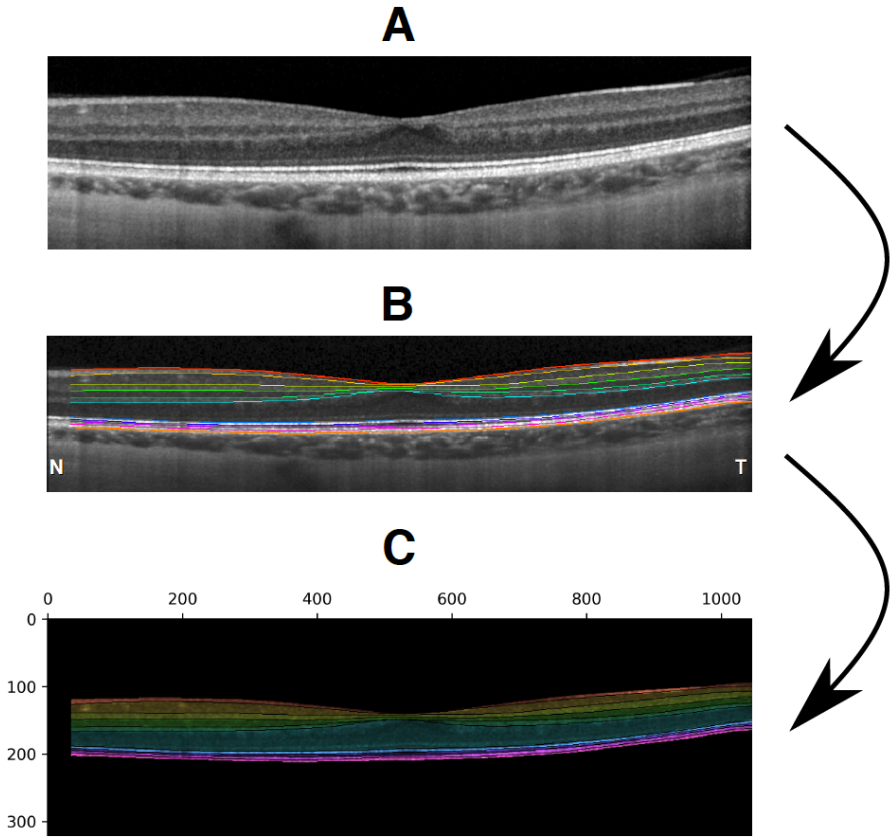

Figure 4.2 Flowchart showing the process of reflectivity data analysis. A: Good quality OCT scans centred on the fovea were identified in Heyex. B: Layer segmentation was performed in OCTExplorer and the foveal image with colour-delineated layer segmentation was exported to be analysed with Python. C: Python identified the layer boundaries and calculated the median pixel intensity of each layer. This image was created as a check to be visually inspected for errors. Units on the axes refer to pixels.

4.3.5. *Reflectivity analysis*

To prepare for reflectivity analysis, RAW macular OCT scans (.vol) were exported from Heyex in 8-bit colour depth (256 grayscale values). Images were not changed in brightness or contrast. Subsequently, images were imported in OCTExplorer (Version 3.8.0 (x64)) from IOWA Reference Algorithms to be segmented. OCTExplorer instead of Heyex software was used for segmentation, as Heyex does not segment the EZ separately. Segmentation was inspected for errors and could be manually corrected where required. However, no manual correction was required in this dataset. The B-scan of interest was identified and this segmented scan showing coloured layer delineation (Figure 4.2) was exported from

OCTExplorer as .tif. Subsequently, OCT reflectivity data were extracted from this segmented image using a custom-built script in Python (Python Software Foundation; http://www.python.org/). This script extracted the grey value (0=black to 255=white) of each pixel within the segmented layers and calculated the median grey score of each layer. For the RPE the median of the top 20 % highest reflective pixels were calculated as well. Relative EZ reflectivity was calculated by normalising to other retinal layers separately through taking the ratio (EZ reflectivity / other layer reflectivity). Choice of reference layer is complex and each layer has advantages and disadvantages. Therefore, EZ reflectivity was normalised to both the ONL and the RPE (with both the reflectivity of the entire layer and of the top 20 % highest intense pixels analysed) separately. The RPE and the ONL were chosen because of their similar intensity profile to the EZ and their large size, respectively. Analysing these two ratios together gives more certainty that identified changes are the result of changes in EZ reflectivity, instead of in the reference layer.

For prospectively recruited participants that completed the dark-adaptation protocol (chapter 2) both the foveal B-scan and a peripheral B-scan (5th B-scan from most inferior B-scan) were analysed. These subjects also had both eyes analysed. For additional subjects (PPON, CPEO and DOA) only the foveal B-scan of the left eye was analysed.

4.3.6. *Data exploration*

Continuous data were explored visually using histograms and dot-plots, while categorical data was explored using cross-tabulations. Given the low sample size non-normal distributions were assumed without formal testing; summary statistics for continuous variables were given with medians and ranges, and non-parametric tests were used. EZ reflectivity was analysed for one eye per subject, to account for inter-eye correlations, except when inter-eye differences or correlations were analysed (Aytulun *et al.*, 2021). For analyses including all subjects, either the left eye or the clinically unaffected eye for ON patients were included, except when explicitly stated otherwise.

4.3.7. *Reliability of EZ reflectivity measurement*

Reliability performance of the relative EZ reflectivity metrics was analysed from the repeated-measures data that was available in the prospectively recruited cohort of controls and acute ON patients that completed the dark-adaptation protocol (chapter 3). Three measures of reliability were calculated with intraclass correlation coefficients (ICC), a measure that reflects not only the correlation but also the degree of agreement between measurements (Koo and Li, 2016). Test-retest reliability was approximated by comparing the two light-adapted scans (baseline and light-adapted) in the dark-adaptation protocol, which were performed within one hour from one another. Interocular correlation was analysed by comparing the foveal B-scans of the right and left eye. Finally, intra-ocular correlation was investigated by comparing the EZ reflectivity ratio between the foveal and the peripheral B-scans. For visualisation purposes, dot-plots with Spearman's correlation coefficients and associated p-value from linear regression for the association were created for these three metrics. Bland-Altman plots were used to visualise test-retest reliability. To explore if macular location influences the EZ reflectivity ratio, EZ reflectivity was compared between B-scans centred foveally and peripherally within the same eye using Wilcoxon signed-rank tests.

The strength of correlation was considered as good-to-excellent (ICC / $\rho > 0.75$), moderate-to-good (ICC / $\rho = 0.5–0.75$), fair (ICC / $\rho = 0.2–0.49$), or not correlated (ICC / $\rho < 0.25$) (Cicchetti, 1994) .

4.3.8. *EZ reflectivity in disease*

Differences in relative EZ reflectivity were compared between the healthy controls and patients with chronic disease (PPON, CPEO and DOA) with the Kruskal-Wallis test. If statistically significant, post-hoc evaluation was performed with the Dunn-test with p-values adjusted for multiple comparisons with the Benjamin-Hochberg method. Relative EZ reflectivity (normalised to the ONL and the RPE) was compared between the healthy controls and both the affected and the fellow eyes of acute ON patients with the Wilcoxon rank-sum test. Interocular differences in EZ reflectivity in the acute ON patients were explored through the Wilcoxon signed-rank test.

To account for potential confounding by age, sex, retinal thickness and scan quality, multivariable linear regression models were built. Three relevant confounding metrics of retinal thickness were considered, being mGCIPL, EZ and IRL thickness. Associations of potential confounders (age, retinal thickness and scan quality) with the outcome (EZ reflectivity) were explored through univariable linear regression. Differences in EZ reflectivity across sex were investigated with the Wilcoxon rank-sum test.

Subsequently, a multivariable linear regression model was built that included a variable for pathology (control, CPEO, DOA and PPON) with additional covariates for identified potential confounders. Finally, two multivariable linear regression analyses that were adjusted for relevant confounders were built to compare EZ reflectivity between controls and affected as well as fellow eyes of acute ON patients.

For acute ON patients with follow-up OCT data available evolution of EZ reflectivity over time was investigated with Wilcoxon signed-rank tests. Furthermore, EZ reflectivity during the acute stage of ON was related to subsequent mGCIPL atrophy with linear regression, to explore its potential predictive value.

Group comparisons were performed for EZ reflectivity normalised tot the RPE as well as to the ONL. This was done to check for consistency across these two metrics, to affirm that observed group differences are the result of changes to the EZ and not to either reference layer.

4.3.9. *EZ reflectivity during dark- and light-adaptation*

Given the known changes in metabolic demand during the energy-costly process of dark-adaptation, an analysis exploring differences in EZ reflectivity between dark-adapted and light-adapted states was performed. Changes in EZ reflectivity values between the 20-minute dark-adapted scan and the 10-minute light-adapted scans were visualised using repeated-measure plots and tested with the Wilcoxon signed-rank test. Differences in dynamic EZ reflectivity changes between healthy controls and ON patients were inspected visually through repeated measures plots.

4.3.10. *Statistical analysis*

Significance thresholds were set to $p<0.05$. Statistical analysis was performed with R and Rstudio (RStudio Team 2021, http://www.rstudio.com/).

4.4. Results

4.4.1. *Participants*

A total of 12 healthy control subjects (of which 9 were included in chapter 3), 23 acute clinically unilateral ON patients (included in chapter 2), seven CPEO patients, 13 DOA patients and 13 PPON patients were included in this study. Baseline characteristics are summarised in Table 4.1. The 23 acute ON patients had a median BCVA of 6/5 (6/4 – 6/5) in the fellow eye and of 6/9 (6/6 – 6/60) in the affected eye. Nine of the acute ON patients were diagnosed with MSON, six with MOGON and eight with SION.

	Healthy controls	Acute ON patients	CPEO	DOA	PPON	p-value
N	12	23	7	13	13	
Sex, F (%)	6 (50 %)	18 (78 %)	3 (43 %)	8 (61.5 %)	2 (15 %)	0.018[1]
Age years, median (range)	28.1 (27 – 46)	28.4 (25 – 28)	68.3 (18 – 80)	27.6 (7 – 70)	37.9 (22 – 60)	0.044[2]
GCIPL µm, median (range)	84.5 (72.7 – 95.0)	74.7 (52.6 – 92.1)	76.9 (52.5 – 81.9)	41.0 (32.3 – 57.6)	46.8 (32.8 – 64.7)	<0.001[2]
IRL µm, median (range)	311 (288 – 331)	293 (263 – 332)	283 (256 – 304)	234 (217 – 257)	250 (217 – 298)	<0.001[2]
EZ µm, median (range)	14.7 (13.6 – 16.3)	14.2 (12.9 – 15.9)	14.3 (12.8 – 15.3)	14.7 (13.5 – 15.4)	14.6 (13.3 – 15.4)	0.367
Scan quality dB, median (range)	38 (27 – 43)	35 (20 – 43)	27 (21 – 33)	28 (25 – 31)	27 (20 – 38)	0.007[2]

Table 4.1 Baseline characteristics of cohort. GCIPL = ganglion cell and inner plexiform layer. IRL = inner retinal layers. 1 = Fisher's exact test. 2 = Kruskal-Wallis test.

4.4.2. *Reliability EZ reflectivity metric*

The reliability of the created EZ reflectivity metrics was analysed by calculating the ICC between the two light-adapted scans (test-retest reliability), between the right and left eye (inter-ocular correlation) and between the foveal and the peripheral B-scan on the same eye (intra-ocular correlation). For this analysis the 12 subjects included in the dark-adaptation analyses of chapter 2 were used (9 healthy controls, 3 acute ON patients). The results are shown in Table 4.2. When using the RPE as the reference layer, the best repeatability performance was achieved when using the median of the 20 % most intense pixels (EZ/RPE20% ratio). Test-retest and interocular ICCs were slightly better for the EZ/RPE20%

Ratio	Test-retest ICC	p-value	Inter-ocular ICC	p-value	Intra-ocular ICC	p-value
EZ/RPE	0.75	**<0.001**	0.73	**0.003**	0.16	0.294
EZ/RPE20%	0.76	**<0.001**	0.73	**0.003**	0.35	0.219
EZ/ONL	0.63	**0.013**	0.65	**0.009**	0.37	0.102

Table 4.2 Performance on reliability metrics (intra-class coefficients) for the EZ/RPE and EZ/ONL ratios. Test-retest ICC: baseline and light-adapted scan. Interocular ICC: right and left eye. Intra-ocular ICC: foveal and peripheral scan within one eye. ρ = Spearman's correlation coefficient. EZ/RPE20% and EZ/ONL ratios showed the best performance overall.

ratio at 0.76 (p<0.001) and 0.73 (p=0.003), respectively, compared with the EZ/ONL ratio at 0.63 (p=0.013) and 0.65 (p=0.009). These results correspond to a 'good-to-excellent' and a 'moderate-to-good' reliability performance for the EZ/RPE20% and EZ/ONL ratios, respectively (Cicchetti, 1994). Intra-ocular reliability was poorer, with ICCs of 0.35 (p=0.219) and 0.37 (p=0.102) for the EZ/RPE20% and EZ/ONL ratios, respectively.

Results of Spearman's correlations are visualised in Figure 4.3. Test-retest and interocular correlations were roughly similar for the EZ/RPE20% and the EZ/ONL ratios, with interscan correlations of ρ=0.72 (p<0.001) and ρ=0.73 (p<0.001) and interocular correlations of ρ=0.74 (p=0.016) and ρ=0.73 (p=0.036), respectively. The intra-ocular correlation (foveal and peripheral scan) again showed a poorer performance, with a ρ of 0.34 (p=0.133) for the EZ/RPE20% ratio and a ρ of 0.45 (p=0.001) for the EZ/ONL ratio.

	EZ/RPE20%		**EZ/ONL**	
	median	range	median	range
Controls	0.75	0.64 – 0.91	2.95	1.94 – 3.45
CPEO	0.62	0.57 – 0.74	2.29	2.06 - 2.63
DOA	0.68	0.52 – 0.79	2.54	1.69 – 3.18
PPON	0.60	0.44 – 0.77	2.37	2.03 – 2.72
p-value	0.003		0.003	

Table 4.3 EZ/RPE20% ratio and EZ/ONL ratio across the groups. CPEO = chronic progressive external ophthalmoplegia. DOA = dominant optic atrophy. PPON= primary progressive optic neuropathy.

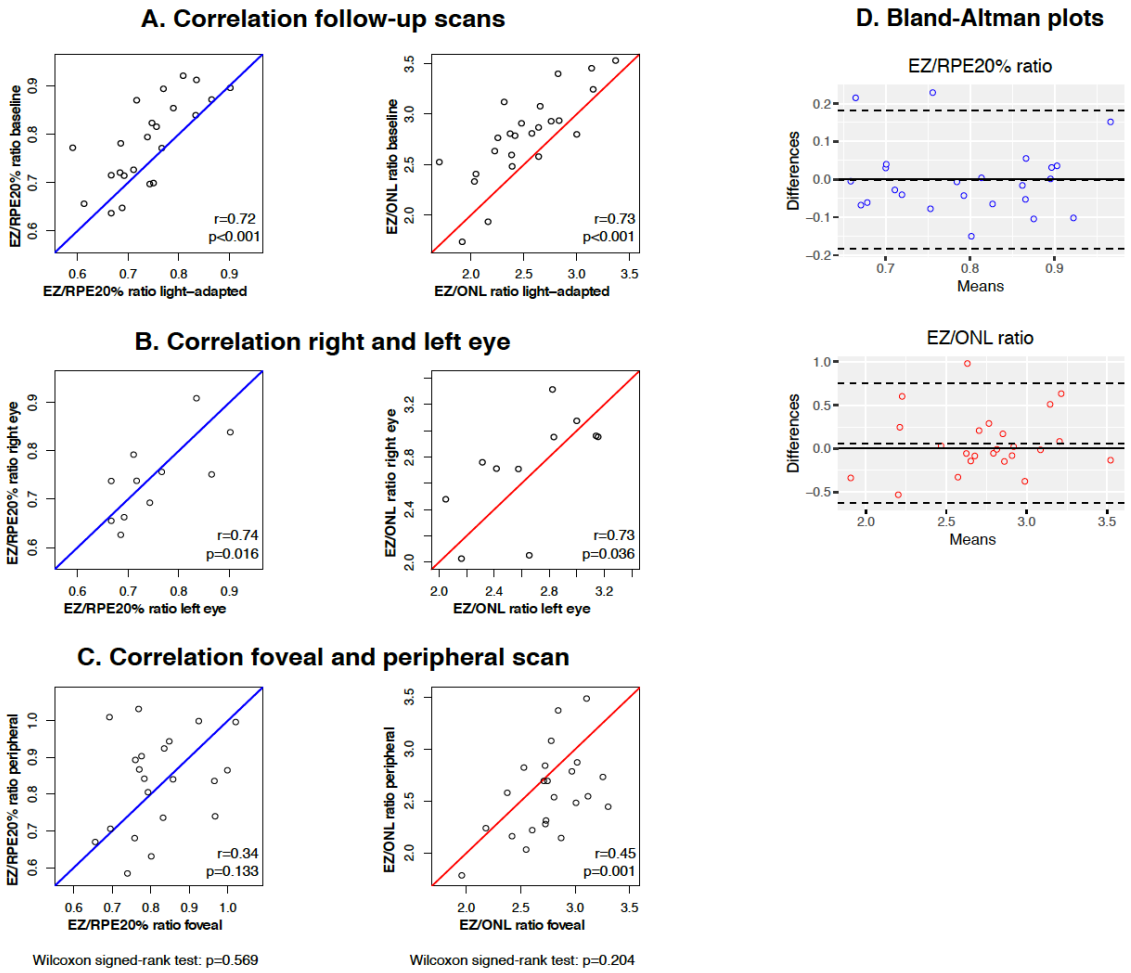

Figure 4.3 Reproducibility of relative EZ reflectivity metrics. A: Interscan reproducibility performance is visualized by comparing the baseline scan and the light-adapted scan for controls. B: Interocular correlations are visualized by comparing the right and left eye. C: Intra-ocular correlations are visualized by comparing the foveal and peripheral scans. In A-C: lines represent x=y, blue lines correspond to the EZ/RPE20% results and red lines to EZ/ONL results, r=Spearman's correlation coefficient and p-value is the result of linear regression analysis. For C results of Wilcoxon signed-rank test comparing foveal and peripheral locations is given as well. Although both eyes are plotted separately in plot A and C for visualisation purposes, statistical inferences were made on one eye per subject. D: Bland-Altman plots comparing the two follow-up scans for EZ/RPE20% ratio (blue dots) and EZ/ONL ratio (red dots).

Dot-plots showed a greater dispersion for the peripheral scan location but gave no indication of a clear direction of effect. Foveal or peripheral location was not associated with a higher or lower relative EZ reflectivity, which was further evidenced by there being no significant difference between these locations (Wilcoxon signed-rank test: p=0.569 and p=0.204 for EZ/RPE20% ratio and EZ/ONL ratio, respectively).

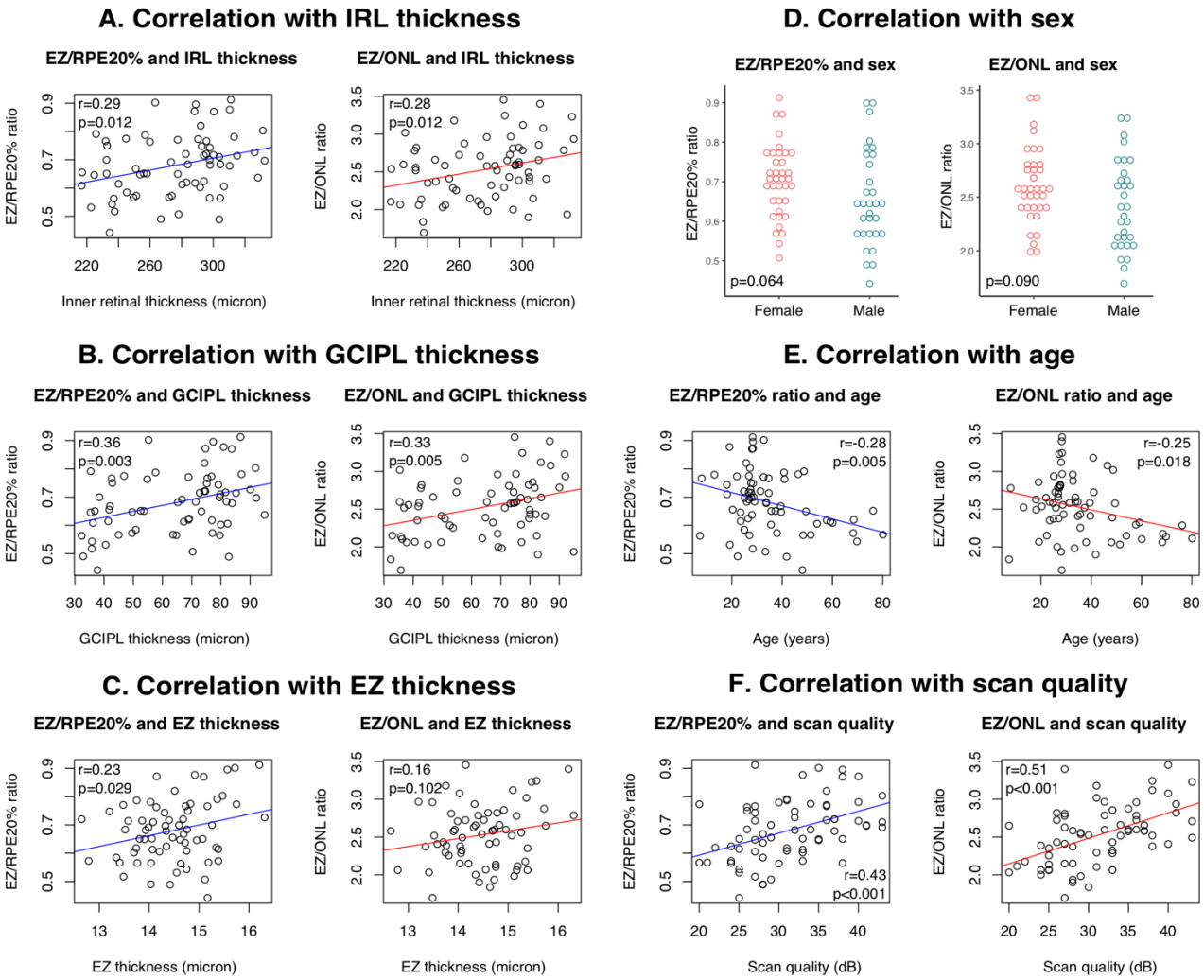

Figure 4.4 Correlations of relative EZ reflectivity with covariates. Correlations of EZ/RPE20% (blue lines) and EZ/ONL (red lines) with age (A), inner retinal layer thickness (B) and ganglion cell layer thickness (C) are shown. r=Spearman's correlation coefficient and p-value is the result of linear regression analysis. D shows the distribution of EZ reflectivity across sex and D visualizes the association of EZ reflectivity with scan quality. p-values are the result of Wilcoxon rank-sum tests.

4.4.3. *Associations EZ reflectivity and covariates*

As shown in Table 4.1, the investigated groups were not matched on baseline characteristics. Univariable regression analyses were performed to explore associations of covariates with relative EZ reflectivity (visualised in Figure 4.4). This revealed a negative linear association of age with EZ/RPE20% (Beta=-0.00, p=0.005) and EZ/ONL (Beta=-0.01, p=0.018). EZ reflectivity was on average lower in males compared with females (EZ/RPE20%: 0.71 vs. 0.64; p=0.064 and EZ/ONL: 2.67 vs. 2.36; p=0.090), but not significantly. Furthermore, there were significant

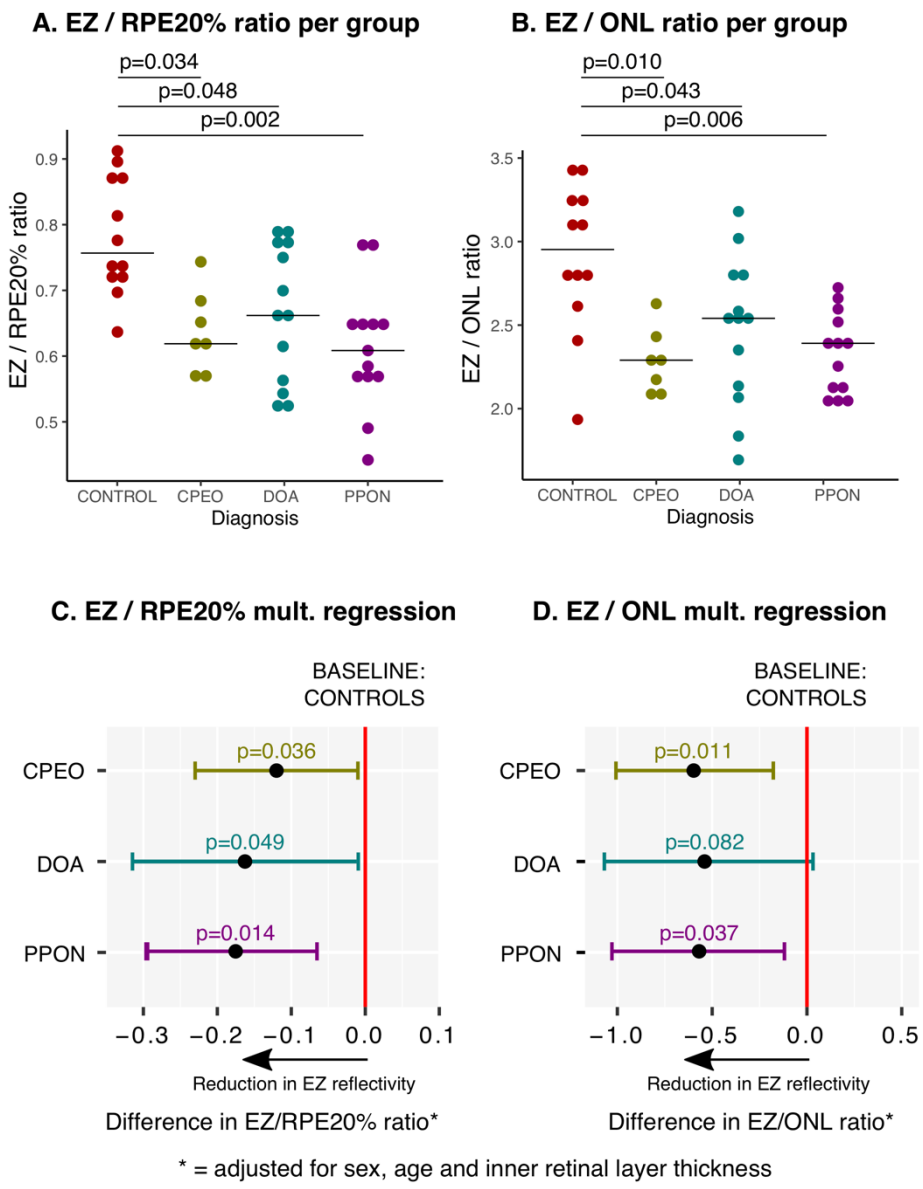

Figure 4.5 Relative EZ reflectivity across controls and patients with CPEO, DOA and PPON. A and B show distributions across these groups for the RZ/RPE20% ratio and the EZ/ONL ratio, respectively. p-values correspond to post-hoc analysis with the Dunn-test (adjusted for multiples comparisons). C and D visualise the results of multivariable regression analysis, adjusted for sex, age and inner retinal layer thickness using Forest plots. The vertical line (red) indicates the reference (control) group and is set to "zero". Horizontal bars represent 95% confidence intervals.

associations with IRL thickness (EZ/RPE20%: Beta=0.03; p=0.018 and EZ/ONL: Beta=0.05; p=0.018), mGCIPL thickness (EZ/RPE20%: Beta=0.08; p=0.003 and EZ/ONL: Beta=0.06; p=0.005)) and EZ thickness (EZ/RPE20%: ρ=0.23; p=0.029 and EZ/ONL: ρ=0.16; p=0.102). Finally, when exploring the association between reflectivity and OCT scan quality (measured in signal-to-noise ratio in dB), significant associations were identified for both the EZ/RPE20%

ratio (Beta=0.03; p<0.001) and the EZ/ONL ratio (Beta=0.05; p<0.001). However, when repeating these analyses only for the healthy controls and unaffected eyes of the ON patients there were only significant associations between EZ/RPE20% and age (Beta=-0.00; p=0.045) as well as EZ thickness (Beta=0.04; p=0.043), but not for the other covariates (all p>0.100).

4.4.4. *EZ reflectivity in CPEO, DOA and PPON*

The Kruskal-Wallis test indicated there was strong evidence for differences between the control group, CPEO patients, DOA patients and PPON patients for both the EZ/RPE20% and the EZ/ONL ratios (both p=0.003). Post-hoc analysis revealed there was a significant difference

		EZ/RPE20% ratio		**EZ/ONL ratio**	
		Estimate	**p-value**	**Estimate**	**p-value**
Multivariable linear regression adjusted for age, sex and IRL thickness					
Diagnosis (BL=control)	**CPEO**	-0.12	**0.036**	-0.59	**0.011**
	DOA	-0.16	**0.049**	-0.55	0.082
	PPON	-0.17	**0.014**	-0.57	**0.037**
Multivariable linear regression adjusted for age, sex and GCIPL thickness					
Diagnosis (BL=control)	**CPEO**	-0.09	0.096	-0.52	**0.022**
	DOA	-0.05	0.577	-0.28	0.443
	PPON	-0.08	0.286	-0.35	0.270
Multivariable linear regression adjusted for age, sex and EZ thickness					
Diagnosis (BL=control)	**CPEO**	-0.10	0.063	-0.51	**0.015**
	DOA	-0.12	**0.003**	-0.45	**0.004**
	PPON	-0.13	**0.002**	-0.45	**0.006**
Multivariable linear regression adjusted for signal-to-noise ratio					
Diagnosis (BL=control)	**CPEO**	-0.09	0.071	-0.42	**0.034**
	DOA	-0.06	0.147	-0.25	0.148
	PPON	-0.12	**0.009**	-0.38	**0.026**
Signal-to-noise ratio (dB)		0.01	0.075	-0.02	**0.042**

Table 4.4 Results of multivariable linear regression analysis investigating the associations of EZ/RPE20% and EZ/ONL with disease status (controls, CPEO, DOA and PPON) adjusted for sex, age and inner retinal layer thickness (model 1), ganglion cell and inner plexiform layer thickness (model 2) or ellipsoid zone layer thickness (model 3) and adjusted for signal-to-noise ratio (model 4). No independent significant associations were identified for sex, age or retinal layer thickness, but a near-significant association with signal-to-noise ratio is shown.

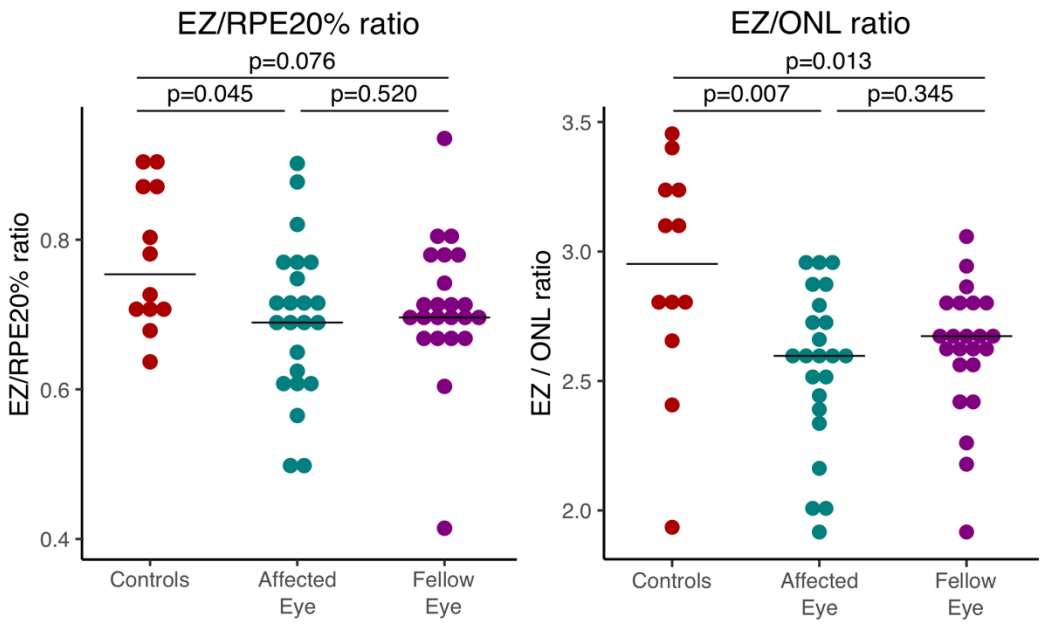

Figure 4.6 Relative EZ reflectivity (normalised to RPE20% and ONL) in controls, affected eyes and fellow eyes of acute ON patients.

between the control group and the CPEO group (p=0.034 and p=0.010), the DOA group (p=0.048 and p=0.043) and the PPON group (p=0.002 and p=0.006) for both the EZ/RPE20% and the EZ/ONL ratios, respectively. These results are visualised in Figure 4.5.

Age, sex, retinal thickness metrics (IRL and mGCIPL) and signal-to-noise ratio all showed significant associations with both the outcome (EZ reflectivity) and the explanatory variable (disease status), while EZ thickness was only associated with the EZ reflectivity. Multivariable linear regression models were built to account for the potential confounding effects of these covariates. Results of these models are shown in Table 4.4 and visualised in Figure 4.5. CPEO, DOA and PPON showed significant reductions in EZ reflectivity, both when normalised to the RPE20% layer and the ONL layer, when adjusted for age, sex and IRL thickness. In the subsequent model, adjusted for age, sex and GCIPL thickness, only CPEO was associated with a significant reduction in the EZ/ONL ratio (p=0.022) but not the EZ/RPE20% ratio. The final model, adjusted for signal-to-noise ratio, revealed significant and independent reductions in the EZ/RPE20% for PPON and the EZ/ONL ratio for PPON and CPEO. When combining the retinal thickness and scan quality covariates in one model there were no significant associations of EZ reflectivity with pathology.

4.4.5. *EZ reflectivity in acute optic neuritis*

Median EZ/RPE20% and the EZ/ONL ratios were lower in the affected eyes (0.70; range: 0.49 – 0.90 and 2.58; range: 1.90 – 2.97) and the fellow eyes (0.70; range: 0.41 – 0.94 and 2.67; range: 1.92 – 3.06) of acute ON patients compared with controls (0.75; range: 0.64 – 0.91 and 2.95; range: 1.94 – 3.45) (Figure 4.6). Affected eyes of ON patients had significantly lower EZ/RPE20% (p=0.045) and EZ/ONL ratios (p=0.007). Similarly, there was a near-significant reduction in EZ/RPE20% (p=0.076) and a significant reduction in EZ/ONL (p=0.013) in fellow eyes of ON patients compared with healthy controls. Wilcoxon signed-rank tests found no evidence for interocular differences in EZ reflectivity between the affected and fellow eyes of ON patients (EZ/RPE20%: p=0.520 and EZ/ONL: p=0.345). Subsequently, the associations of EZ reflectivity with ON status were adjusted for the relevant potential confounders using multivariable linear regression (Table 4.5). This analysis identified a significant reduction of -0.11 in the EZ/RPE20% ratio (p=0.013) and of -0.42 in the EZ/ONL ratio (p=0.006) in affected eyes of acute ON patients compared with controls, when adjusted for scan quality, age, sex

		EZ/RPE20% ratio		**EZ/ONL ratio**	
		Estimate	**p-value**	**Estimate**	**p-value**
Multivariable linear regression adjusted for age, sex, GCIPL thickness and scan quality					
Diagnosis (BL=control)	**Acute ON (affected eye)**	-0.11	**0.013**	-0.42	**0.006**
Scan quality (dB)		0.00	0.335	0.02	**0.027**
Age (per year)		-0.00	**0.029**	-0.01	0.182
Sex	**Male**	0.00	0.929	-0.09	0.519
GCIPL (per micron)		-0.00	0.081	-0.01	0.209
Multivariable linear regression adjusted for age, sex, GCIPL thickness and scan quality					
Diagnosis (BL=control)	**Acute ON (fellow eye)**	-0.09	0.268	-0.35	0.316
Scan quality (dB)		0.00	0.535	0.03	0.292
Age (per year)		-0.00	0.872	-0.00	0.870
Sex	**Male**	-0.05	0.436	-0.21	0.469
GCIPL (per micron)		-0.00	0.400	-0.01	0.457

Table 4.5 Results of multivariable linear regression analysis investigating the associations of EZ/RPE20% and EZ/ONL with optic neuritis status. Analysis is adjusted for scan quality, age, sex and GCIPL thickness. Healthy controls are compared with the affected eyes (model 1) and the fellow eyes (model 2) of ON patients.

and mGCIPL thickness. There was no significant difference in EZ reflectivity between controls and fellow eyes of acute ON patients.

4.4.6. *Evolution of EZ reflectivity during ON recovery*

Follow-up macular OCT scans of sufficient quality were available for 16 ON patients. There were 12 female patients (75%) and the median age was 29.9 years (range: 18.1 – 59.1 years). Two cases were diagnosed with single-episode isolated ON, five cases were myelin oligodendrocyte glycoprotein (MOG) antibody seropositive and nine cases were diagnosed with MS associated ON. Follow-up scans were made after a median of 13.9 weeks (range: 5 – 199 weeks).

In the affected eyes of ON patients EZ/RPE20% decreased non-significantly from 0.71 to 0.68 (p=0.632), while median EZ/ONL decreased non-significantly from 2.58 to 2.51 (p=0.159), between the baseline and the follow-up scan. The fellow eyes of ON patients also did not show a significant change in EZ reflectivity during follow-up, with EZ/RPE20% being a median of 0.72 both at baseline and follow-up (p=0.782) and median EZ/ONL being 2.65 at baseline and 2.61 at follow-up (p=0.349). Similar to at the baseline measurements, there was no significant interocular difference in EZ reflectivity at follow-up, with median EZ/RPE20% being 0.68 in the affected eye and 0.72 in the fellow eye (p=0.348) and median EZ/ONL being 2.51 in the affected eye and 2.61 in the fellow eye (p=0.211).

To explore if EZ reflectivity in the acute stage of ON is predictive of subsequent atrophy of the mGCIPL during recovery, a linear regression model was created investigating the association between the amount of mGCIPL thinning (mGCIPL at baseline – mGCIPL at follow-up) and EZ reflectivity at baseline. These models did not identify significant associations, both for the EZ/RPE20% (ρ=0.03, p=0.517) and EZ/ONL ratios (ρ=0.07, p=0.330).

4.4.7. *EZ reflectivity during dark-adaptation*

Overall, there was a significant reduction in relative EZ reflectivity when comparing the foveal dark-adapted scan with the light-adapted scan for both the EZ/RPE20% ratio (p=0.016) and the EZ/ONL ratio (p=0.027) (Figure 4.7). The EZ/RPE20% ratio reduced by 0.07 (±10 %) across these conditions, while there was a reduction of 0.21 (±7 %) in the EZ/ONL ratio.

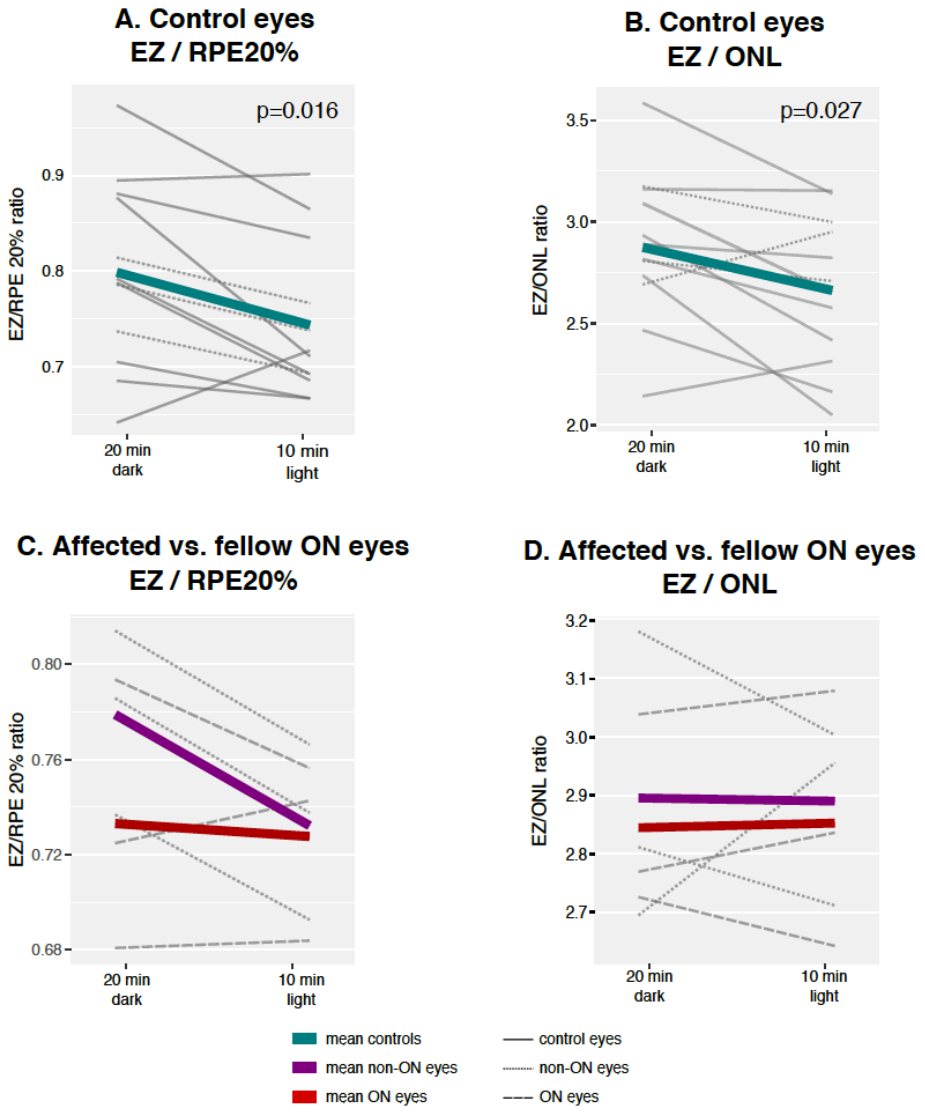

Figure 4.7 Repeated-measure plots visualising dynamic changes in EZ reflectivity during dark-adaptation. A and B show the overall EZ reflectivity change from the dark-adapted scan to the light-adapted scan for all control eyes for the EZ/RPE20% and the EZ/ONL ratio, respectively. p-values correspond to results of Wilcoxon signed-rank tests. C and D visualise the interocular differences in these dynamic changes for patients with acute ON. Red lines indicate mean change for affected eyes, while purple lines show mean changes for fellow eyes.

These dynamic changes in EZ reflectivity were inspected visually for the affected and fellow eyes of the ON patients in repeated-measures plots (Figure 4.6). For both the EZ/RPE20% and the EZ/ONL ratio, the ON affected eyes did not show dynamic changes in relative EZ reflectivity across the lighting conditions.

4.5. Discussion

In this chapter it was presented that EZ reflectivity can be determined from macular OCT scans with a novel automated analysis tool with good-to-excellent test-retest reliability. Furthermore, it was shown that relative EZ reflectivity was significantly reduced both in acute neuroinflammatory disease, as evidenced by a reduction in eyes affected by ON of recent onset, and in patients with chronic disease associated with mitochondrial failure, such as PPON, an early and severe optic neuropathy associated with MS, as well as CPEO and DOA.

Test-retest reliability was good-to-excellent for the EZ/RPE20% ratio in particular, while reliability of the EZ/ONL ratio was moderate-to-good (Cicchetti, 1994; Koo and Li, 2016). Although most previous studies did not report on reproducibility data, test-retest reliability was comparable to another method created earlier (Risseeuw *et al.*, 2020). It should be noted that the test-retest protocol used here was suboptimal, as the lighting conditions during baseline and light adaptation were similar but not entirely equal. There appeared to be a trend with EZ reflectivity being higher at baseline compared with light adaptation (Figure 4.3), and a more standardised test-retest protocol might have resulted in even higher reproducibility performance. The lower test-retest reliability of the EZ/ONL may be because the ONL includes the Henle Fibre layer, which is known to have a variable intensity depending on scanning angle (Lujan *et al.*, 2011). Advantages of the EZ reflectivity analysis technique employed here are the availability of reliability data, the normalisation to more than one reference layer and the fact that segmentation was performed entirely in an automated, non-manual, fashion meaning that the scope for human error or the introduction of human observer bias is limited. Disadvantages are that only one B-scan is analysed per eye, instead of the full volume scan and that focal differences cannot be identified.

This is the first study that evaluated relative EZ reflectivity in neuroinflammatory and mitochondrial disease and identified evidence for EZ reflectivity reductions in acute ON, PPON, CPEO and DOA. Findings were consistent for the EZ/RPE20% ratio and the EZ/ONL ratio, increasing the evidence that the identified associations are due to changes in the EZ and not to the reference layers. These findings are in line with previous work indicating that EZ reflectivity is reduced in glaucoma (Ha *et al.*, 2018), AMD (Wu *et al.*, 2013; Tao *et al.*, 2016;

Toprak *et al.*, 2017; Litts *et al.*, 2018; Thiele *et al.*, 2020), retinitis pigmentosa (Gong *et al.*, 2021) and Best disease (Romano *et al.*, 2020).

There are several possible explanations for the reductions in EZ reflectivity reported here. As histopathological studies have shown that the high reflectivity of the EZ on OCT is most likely the result of local accumulations of mitochondria (Cuenca *et al.*, 2018; Litts *et al.*, 2018) and light scattering properties of mitochondria change when put under oxidative stress (Wilson *et al.*, 2005; Tychinsky, 2009) or mitochondrial morphology alters (Pasternack *et al.*, 2010, 2011), the reduction in EZ reflectivity may be the result of changes in mitochondrial health or in metabolic function. The results presented here show that the EZ reflectivity is reduced across disorders with known mitochondrial dysfunction, indicating that this OCT metric might be an in-vivo non-invasive measure of metabolic function. EZ reflectivity may also be a more general measure of photoreceptor health, as it was shown to correlate with cone density (Saleh *et al.*, 2017) and electrophysiological retinal function (Wu *et al.*, 2013). Finally, it cannot be excluded that the findings are confounded by image quality or optical effects, such as the Stiles-Crawford effect which is discussed in more detail below.

It needs to be recognised that this study had several limitations in its design which means its findings need to be interpreted with caution. A limitation was the retrospective analysis of clinical OCT scans for PPON, CPEO and DOA patients, with scan quality generally being poorer in disease compared with controls. Furthermore, PPON, CPEO and DOA had different age and sex distributions compared with controls. This means that the findings could be partly the result of confounding. Efforts were made to account for these baseline differences in group characteristics through multivariable regression analysis adjusting for these potential confounders. Although EZ reflectivity was associated with scan quality, age and sex, the investigated diseases mostly remained significantly associated with EZ reflectivity reductions after adjustment for these factors in multivariable analysis. Importantly, the healthy control and acute ON cohorts were more equally matched on baseline-criteria and EZ reflectivity showed a strongly significant reduction in the affected eyes of acute ON eyes, after adjustment for all potential confounders.

Patients with PPON, DOA and acute ON had significantly thinner IRL and mGCIPL thicknesses compared with controls, which raises the possibility that EZ reflectivity may be reduced in these disorders as a result of differences in the thickness of tissue that light travels through before reaching the EZ. EZ reflectivity was indeed associated with both IRL and mGCIPL thickness. Group comparisons were adjusted for IRL thickness which did not make a difference to the results of group comparisons. However, after adjusting for mGCIPL thickness only EZ/ONL reflectivity was significantly reduced in CPEO and acute ON compared with controls. There may be specific optical properties of the mGCIPL that mean atrophy of this layer causes a reduction of EZ reflectivity. However, the fact that patients with CPEO had reduced EZ reflectivity in the absence of mGCIPL atrophy hints at the existence of independent pathologic changes to EZ. EZ reflectivity and mGCIPL atrophy may be interrelated, but similar to findings of reduced vascular density in retinas of individuals with MS (Kleerekooper *et al.*, 2020), it is difficult to disentangle 'cause and effect'. EZ reflectivity might be reduced due to lower metabolic demand as a result of retinal atrophy or there might be retinal atrophy due to metabolic failure, which is observed through EZ reflectivity loss. It is important to recognise that this is particularly difficult to disentangle this in these data, as PPON and DOA patients all had profound mGCIPL atrophy, while controls had normal mGCIPL thicknesses. However, it is interesting to note that mGCIPL or IRL atrophy would reduce the attenuation of light to the EZ layer, which would hypothetically be associated with an increase in its reflectivity, a finding opposite to the observed data.

EZ reflectivity was not reduced in fellow eyes of ON patients compared with controls. This finding suggests that EZ reflectivity may be somewhat more reduced in the affected compared with the fellow eye, even though mGCIPL thicknesses were roughly equal in both eyes of ON patients (Figure 2.4). This may be suggestive of an association with acute metabolic failure. But EZ reflectivity was not reduced in the affected compared with the fellow eyes of patients with acute ON, and also did not show further reductions over follow-up. This is in line with EZ reflectivity being related to a disease process separate from acute inflammation or with subclinical prior injury. This is different from mGCIPL atrophy, which primarily occurs during the three months following ON onset (Costello *et al.*, 2006).

Further limitations to the interpretation of EZ reflectivity across groups in this study relate to limited sample size and residual confounding, with healthy controls having no comorbidities, while some of the investigated CPEO, DOA and PPON cases had other microvascular and metabolic comorbidities independent from the disorders under investigation, such as hypertension and smoking. Selection bias may have played a role in the retrospective identification of patients with mitochondrial disease, in particular regarding CPEO. This disorder is not often associated with retinal involvement, and OCT scanning in these patients may have been prompted by visual complaints, although no retinal abnormalities were identified in the investigated eyes. Furthermore, controls were all scanned with the same OCT protocol while patients had scans with variable technical specifications, sometimes scanning 20x20° macular fields while controls all had 15x15° scans. Although exploratory analysis revealed no consistent difference in relative EZ reflectivity for foveal and peripheral macular locations, this could have influenced the results. Prospectively acquired OCT data with a set scanning protocol is necessary to confirm these results. Furthermore, future studies investigating differences in EZ reflectivity in relapsing-remitting MS, secondary-progressive MS and primary-progressive MS as well as associations of EZ reflectivity with clinical disability scores and serum lactate or other serum measures of mitochondrial function might give insight in its role as biomarker. An alternative to reflectivity analysis such as presented here is the analysis of the attenuation coefficient (Vermeer *et al.*, 2014; Ghafaryasl *et al.*, 2020), which calculates how quickly light attenuates when traveling through examined tissue.

Finally, this study found some evidence for a reduction in EZ reflectivity when going from a dark-adapted to a light-adapted state. As mitochondria are known to undergo constant dynamic changes to their morphology as a result of fusion and fission when adapting to local metabolic demand (Karbowski and Youle, 2003), this might be a result of dynamic changes in the EZ maintaining energy homeostasis during dark-adaptation. However, it may also be the result of light-associated changes in pupillary size or the directionality of photoreceptors, as reflectivity of retinal tissue is known to be dependent on the directionality of light hitting photoreceptors, known as the Stiles-Crawford effect (Snyder and Pask, 1973). The repeated-measure plots of patients with acute ON suggested that this light-associated dynamic change in EZ reflectivity was reduced or absent in affected eyes. Given the low sample size these findings should not be overinterpreted, but it is notable that these findings mirror the

identified reduction of dynamic light-associated compression of the outer retinal layers in ON that was described in chapter 2. Finally, there was an association between EZ thickness and EZ reflectivity, with both reducing in light-adapted state compared with dark-adapted state (Table 3.4 and Figure 4.7). It is unclear if both structural and functional changes occur in dark-adaptation, or if either finding is confounded by the other. For example, EZ structural measurement might increase due to differences in segmentation as reflectivity increases, or EZ reflectivity measures might reduce as a result of compression of the EZ.

4.6. Conclusion

Relative EZ reflectivity can be determined with good test-retest reliability from macular OCT scans. These data suggested that EZ reflectivity may be reduced in MS associated progressive optic neuropathy, acute ON and the mitochondrial disorders CPEO and DOA. Interpretation of the results of this study are complicated due to limitations in design and sample size, but the presented preliminary findings warrant further investigation in larger prospective cohort studies to establish the usefulness of EZ reflectivity as a non-invasive in-vivo biomarker of mitochondrial health.

5. OCTA to investigate MS and MOG associated acute optic neuritis

ABSTRACT

Vascular changes are increasingly recognised as important factors in the pathophysiology of neuroinflammatory disease, especially in multiple sclerosis. The relatively novel technology of optical coherence tomography angiography (OCTA) images the retinal and choroidal vasculature non-invasively and in a depth-resolved manner. OCTA provides an alternative quantitative measure of retinal damage, by measuring vascular density instead of structural atrophy. Here, a review of studies using OCTA in multiple sclerosis and neuromyelitis optica spectrum disease is given. Data to date consistently reveal lower densities of the retinal microvasculature in both these disorders compared with healthy controls, particularly in eyes affected by optic neuritis but even in the absence of prior optic neuritis. Limited pilot OCTA data in acute optic neuritis is presented here. Findings in two patients show an increased foveal avascular zone in patients with acute optic neuritis, indicative of a reduced vascular density. Although these data represent the first report of OCTA findings in acute optic neuritis, these findings would be in line with previous reporting of reduced vascular densities in multiple sclerosis and neuromyelitis optica spectrum disorder in the absence of optic neuritis. Future studies exploring the timing of vascular changes relative to structural atrophy may help answer important questions about the role of hypoperfusion in the pathophysiology of neuroinflammatory disease.

5.1. Background

Optical coherence tomography (OCT) angiography (OCTA) expands upon the technique of OCT by looking at temporal changes in the quality of backscattered light to distinguish locations of static tissues from blood flow. It detects blood vessels based on differences in amplitude, intensity, or phase variance between sequential OCT B-scans in the same position of the retina. Sequential B-scans are taken at the same transverse location and compared. The difference in signal between images reflects blood cells flowing through vessel lumen. Therefore, blood movement is used as an intrinsic contrast agent to create a vascular map (see Figure 5.1). Because of its reliance on picking up tiny temporal changes, a high sampling frequency is necessary to create OCTA images of sufficient quality (Kim *et al.*, 2011; Schwartz *et al.*, 2014).

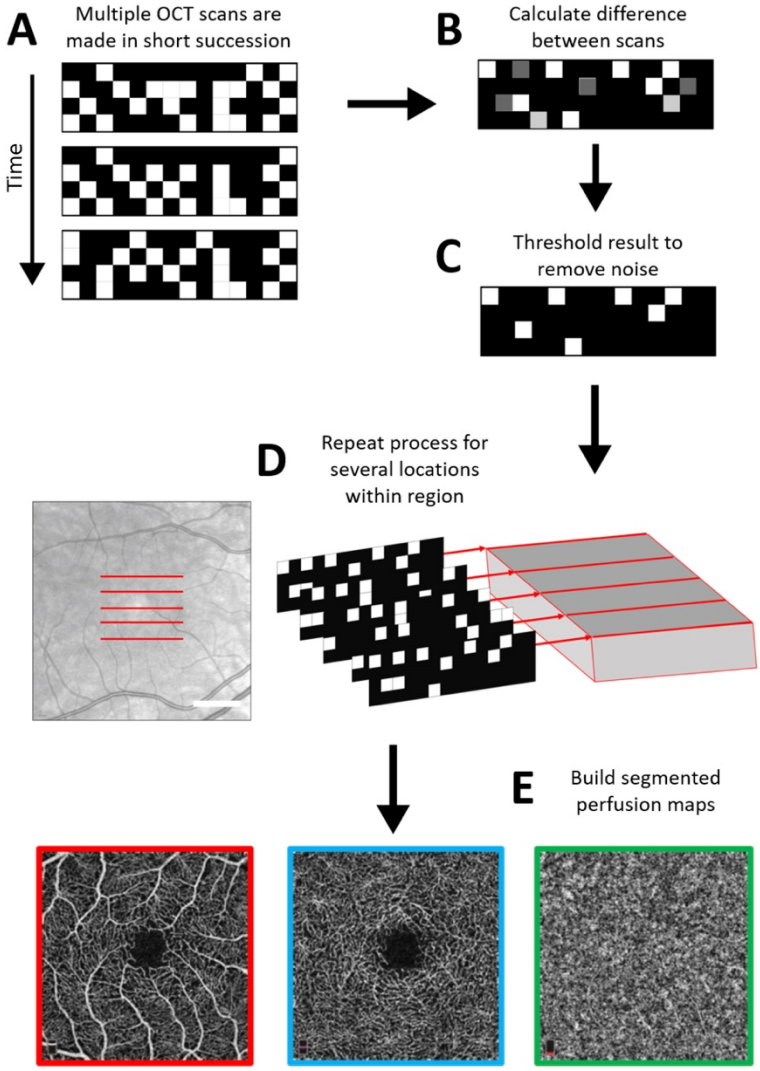

Figure 5.1 Schematic visualization of the process of OCTA scan acquisition. Below the SVP, DPV and choroidal plexi are shown from left to right. Taken from Kleerekooper et al., 2020 (Frontiers of Neurology).

5.2. Aims, objectives and hypotheses

5.2.1. *Aims and objectives*

The aim of this chapter is to summarise the current understanding of changes to the retinal microvasculature as measured through OCTA in neuroinflammatory disease. Furthermore, novel pilot data of OCTA scans in patients with acute optic neuritis (ON) will be presented.

5.2.2. *Hypotheses*

The main hypothesis of this chapter is that OCTA is capable of identifying changes in the retinal microvasculature, both in quantitative and qualitative analysis, in neuroinflammatory disease.

5.3. Literature review

All currently published studies found a significant reduction in retinal vessel density, in the macular area, the peripapillary area, or both, in multiple sclerosis (MS) patients compared with controls. Most also identified correlations between structural OCT measurements and vessel density (Feucht *et al.*, 2019; Murphy *et al.*, 2019; Jiang *et al.*, 2020; Ulusoy *et al.*, 2020; Yilmaz *et al.*, 2020). The largest study cohort to date found a significant reduction in superficial vascular plexus (SVP) density from 29.1 % in controls to 24.1 % in MS eyes ($p<0.001$) (Murphy *et al.*, 2019). Furthermore, MS eyes affected by ON (MSON) had a lower SVP vessel density at 21.7 % compared with non-ON (MSNON) eyes at 26.0 % ($p<0.001$). Finally, the difference between vessel densities in MSNON eyes and control eyes just reached significance ($p=0.03$). These results are corroborated by several other studies, that identified reduced macular SVP vessel densities in eyes of MS patients compared with controls (Feucht *et al.*, 2019; Jiang *et al.*, 2020; Ulusoy *et al.*, 2020; Yilmaz *et al.*, 2020), with a significant reduction in SVP vessel density in MSON compared with MSNON eyes identified in the two larger cohorts (Lanzillo *et al.*, 2017; Yilmaz *et al.*, 2020). Reductions in vessel density around the optic nerve head (ONH), called “capillary dropout” have been identified in MS eyes compared to control eyes, as well as in MSON eyes compared with MSNON (Wang *et al.*, 2014; Spain *et al.*, 2018). OCTA data captured in the acute stages of ON is currently lacking, although one small case series of seven MSON patients did find significantly reduced SVP macular and ONH vessel densities in affected compared with fellow eyes 2–8 months after the episode (Higashiyama *et al.*, 2017).

A lower vessel density of the macular SVP was found to be related to a higher expanded disability status score (EDSS) and lower low-contrast visual acuity in MS patients (Murphy *et al.*, 2019). Interestingly, in this study results of other clinical outcomes like the 9-hole peg test, the timed 25-foot walk test and the multiple sclerosis functional composite (MSFC) were related to macular SVP vessel density, but not to combined ganglion cell and inner plexiform layer (GCIPL) thickness. Another study describes an inverse correlation between visual evoked potential latency times and vessel density of the SVP and DVP (Yilmaz *et al.*, 2020).

A limited number of studies on OCTA in NMOSD exist, which all found profound decreases in microvascular densities (Kwapong *et al.*, 2018; Huang *et al.*, 2019; Chen *et al.*, 2020). A recent study found a significant reduction in vessel density of the peripapillary region and the macular SVP in patients with aquaporin-4 (AQP4) seropositive NMOSD compared with controls. There were also significant reductions in vessel density in the macular and ONH region when comparing NMOSD patient without previous ON to controls ($p = 0.023$ and $p = 0.029$), while retinal thickness were similar (Chen *et al.*, 2020). This suggests OCTA may be more sensitive to ON-independent damage in NMOSD than OCT. Additionally, these findings of vascular dropout in the absence of structural thinning argue against the hypothesis that reductions in microvascular density are a result of reduced demand in atrophied tissue and, if replicated, may provide evidence for a role of microvascular dysfunction as an independent disease process in NMOSD. Macular SVP and deep vascular plexus (DVP) densities have been found to correlate negatively to visual acuity measures in NMOSD (Kwapong *et al.*, 2018). The potentially more profound vascular changes in the anterior visual system of NMOSD compared with MS patients might be the result of the reduced metabolic demand associated with more severe structural atrophy in NMOSD related ON, although the reduction in vascular density in the absence of atrophy argue against this. Furthermore, it might be the result of mechanical constriction at the ONH due to more severe papilledema. However, the fact that vascular density reductions are also identifiable in patients without ON is incongruous. OCTA data in myelin oligodendrocyte glycoprotein associated disease (MOGAD) is very limited, but also show reductions in vascular density (Yu *et al.*, 2020).

5.4. Pilot OCTA data in acute optic neuritis

Heidelberg OCTA scanning of a 3x3 mm square regions centred on the fovea was performed on a subset of the acute ON (N = 3) and healthy control subjects (N = 2) included in the study presented in chapter 2 of this thesis. Automated vascular layer segmentation of the SVP and

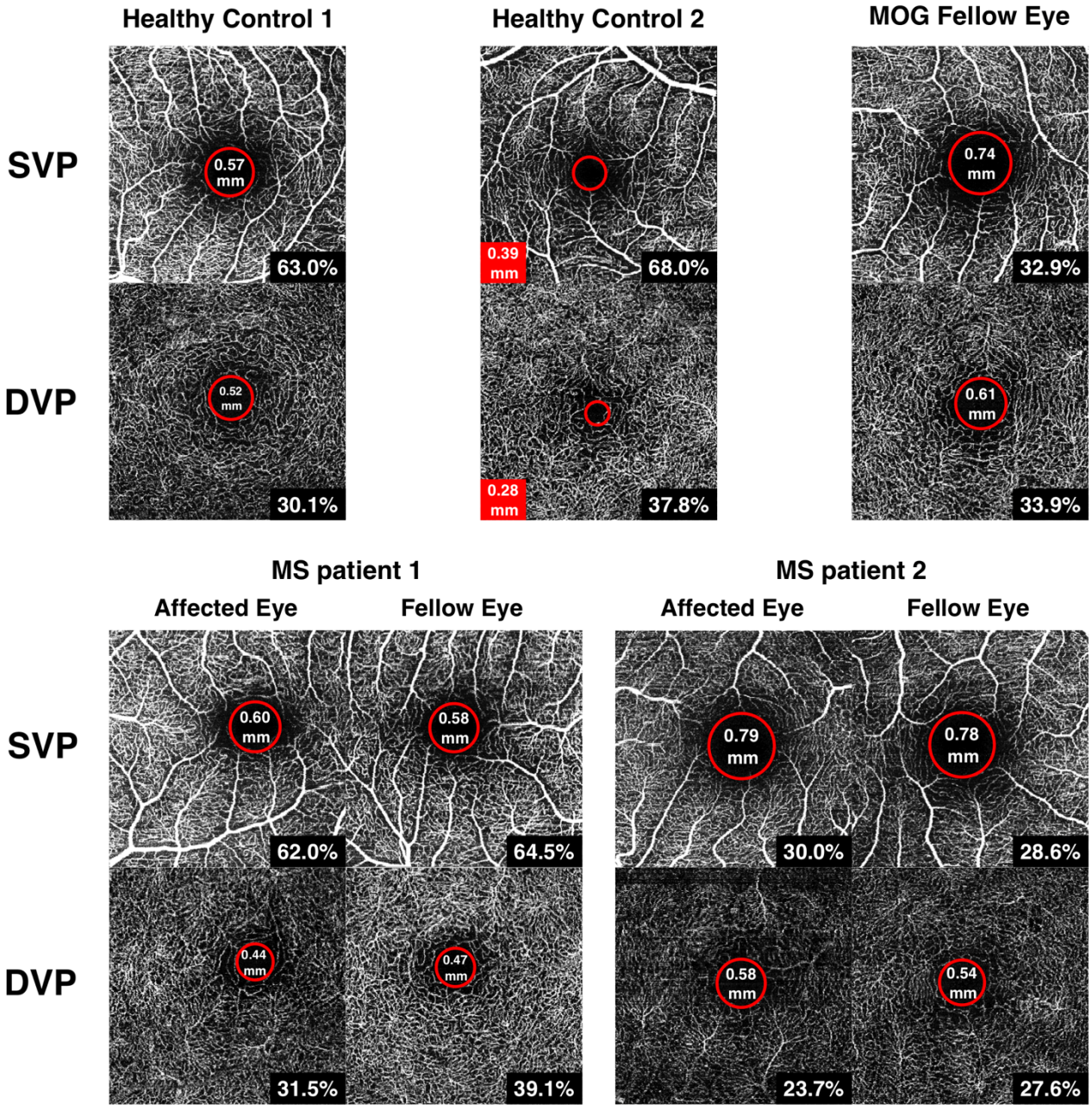

Figure 5.2 Pilot OCTA data. Foveal 3x3mm en face images of superficial vascular plexus (SVP) and deep vascular plexus (DVP) of two healthy controls (healthy control 1 (male 47 years) and healthy control 2 (female 28 years)), one fellow eye of a MOG seropositive patient and both the affected and fellow eyes two MS patients with acute optic neuritis. Foveal avascular zone measurements are shown in red circles with size in millimeters. Vessel density measurements (%) are given in black in the right lower corner.

DVP with subsequent creation of en face maps was performed through Heyex software. Quality control was evaluated manually and scans with significant and clear motion artefacts were not included in analysis. Macular OCTA scans that were of sufficient image quality in the fellow eye of one female MOG-antibody seropositive acute ON patient of 25 years old and the fellow and affected eyes of two female acute MSON patients of 24 and 29 years old were included. For comparison, the OCTA images of two healthy control subjects (one female of 28 years old and one male of 47 years old) were included. Analysis of foveal avascular zone size (FAZ) was performed with Inkscape and the diameter of the foveal avascular zone (FAZ) was calculated in millimetres. Vessel density metrics were calculated with ImageJ. First images were binarised, and subsequently the ratio of pixels representing blood vessels (white pixels) and the total number of pixels was taken. Vessel density was presented as percentages (%). Given the very low sample size of included patients no statistical analysis was performed, but en face OCTA scans including the FAZ measurements of these subjects are visualised for comparison in Figure 5.2. This figure shows an appreciably greater size of the FAZ for the SVP and the DVP in both the MOG-ON and the MSON affected subjects compared to the control subjects, particularly healthy control 2. Similar observations are made with regard to the SVP and DVP vessel density metrics. The SVP vessel density is 63.0 % and 68 % in healthy controls, and ranges from 28.6 % to 64.5 % in acute ON patients. Similarly, DVP vessel density is 30.1% and 37.8 % in healthy controls and ranges from 23.7 % and 39.1 % in acute ON patients. There appears to be no clear difference between the affected and fellow eyes of the acute MSON patients for both the FAZ or the vessel density metrics.

5.5. Discussion

In this chapter existing data on the use of OCTA in studies investigating neuroinflammatory disease were summarised. As discussed, OCTA consistently reveals reductions in vascular density of the SVP, DVP and the ONH area in MS, particularly in subjects affected by ON, and in NMOSD. OCTA metrics correlate with clinical disability outcome metrics in MS, potentially more strongly than structural OCT measures. Finally, for AQP4-seropositive NMOSD there is some evidence that vascular density reduction occurs before structural atrophy of retinal thickness measurements.

Furthermore, limited novel data on OCTA in acute ON were presented which show that the FAZ may be of greater size in three patients with acute ON, related to MOG-seropositivity and to MS, compared with healthy controls. This is particularly appreciable when comparing the younger healthy control to the individuals with ON. This could potentially be due to age-related decreases in vascular density in the older healthy control individual. Increased size of the FAZ reflects reductions in vascular density, as it is reported to be correlated with density metrics of the SVP and DVP (Yilmaz *et al.*, 2020). These data represent the first reports of OCTA imaging in acute ON, to the best of my knowledge, and seem to suggest that retinal vascular density can be reduced during these acute stages. However, no appreciable difference between the affected and fellow eyes is observed. These findings should not be overinterpreted, given the very limited sample size, the slight motion artefacts and the out-of-centre fixation for some scans. However, these results would be in line with prior research identifying that vascular density is reduced even in eyes unaffected by ON in MS and NMOSD.

5.6. Conclusion

OCTA provides an alternative quantitative measure for retinal damage in MS and NMOSD. MS and NMOSD patients, both with and without ON, consistently reveal lower densities of the retinal microvasculature compared with healthy controls. In line with these prior findings, pilot data suggesting that retinal vessel density is reduced in acute ON are presented here. Future research exploring the temporality of vascular relative to structural changes may help answer important questions about the role of hypoperfusion in the pathophysiology of neuroinflammatory disease.

Part 2

6. Early Visual Failure in Multiple Sclerosis due to Primary Progressive Bilateral Optic Neuropathy

ABSTRACT

Background Although involvement of the anterior visual system in multiple sclerosis (MS) is almost ubiquitous, primary progressive visual failure commencing before disease onset is rare.

Methods This multi-centre international retrospective chart review, based at two tertiary referral neuro-ophthalmology clinics (Moorfields Eye Hospital, London, UK and Amsterdam University Medical Centre, Amsterdam, the Netherlands), described demographic, clinical and imaging features of patients with progressive visual failure presenting before or less than one year after multiple sclerosis onset. All cases fulfilled McDonald MS diagnostic criteria and had alternative causes for progressive optic neuropathy excluded.

Results Sixteen MS patients (13 male; 81 %) with early visual failure were identified between 1996 and 2019. The median age at onset of visual symptoms was 25 years (range 15 – 48). Eight patients (50 %) were diagnosed with primary progressive MS, and out of eight cases initially diagnosed with relapsing-remitting MS, two developed secondary progressive disease during follow-up. Follow-up was available for a median of 6.5 years (range 1 – 23 years) since onset. Visual loss was bilateral in all cases. Eleven patients (69 %) reported Uhthoff phenomenon. Five out of the eleven (45 %) cases who received methylprednisolone treatment experienced improvement (although transient in four cases). Optical coherence tomography revealed severe retinal atrophy, with a median peripapillary retinal nerve fibre layer thicknesses of 62 µm (range: 49 – 91) and a median macular ganglion cell and inner plexiform layer of 45 µm (range: 35 – 72). Microcystic macular oedema was present in 50 % of macular scans.

Conclusion This study suggests that progressive visual failure in early MS predominantly affects males and is a bilateral disease mostly associated with primary progressive MS. Some patients benefit from glucocorticoid treatment.

6.1. Background

The most common cause of visual loss in multiple sclerosis (MS) is optic neuritis (MSON), which generally has an excellent spontaneous visual recovery. Though infrequently reported, progressive, non-resolving, visual loss is sometimes seen as a feature of MS (Ashworth, 1967; Jasse *et al.*, 2013). Rarely, insidious visual failure is a presenting symptom of MS. This phenotype has been described in a total of eight cases (Ormerod and McDonald, 1984; Read *et al.*, 1996), for whom painless, bilateral and severe progressive visual loss was a harbinger of subsequent MS and no alternative cause was identified. These cases were predominantly male (62.5 %), suggesting that this particular phenotype affects a demographic that more resembles that of primary progressive MS (PPMS) than relapsing remitting MS (RRMS).

The presence of progressive optic nerve injury in MS has been established by optical coherence tomography (OCT) studies, that show that progressive inner retinal atrophy occurs following MSON (Trip *et al.*, 2005) but also independently from MS onset (Petzold *et al.*, 2017; Seitz *et al.*, 2018). These studies are corroborated functionally by the finding of subclinical visual impairment in individuals with early stage RRMS (Rohowetz *et al.*, 2020) and almost 70 % of MS patients reporting visual disability (Salter *et al.*, 2012). Optic atrophy and subsequent inner retinal thinning in MS is likely mediated through inflammatory episodes of (clinical and subclinical) MSON (Trip *et al.*, 2006; Petzold *et al.*, 2017); transsynaptic retrograde degeneration due to lesions in the cerebral optic radiations (Jindahra *et al.*, 2009; Balk *et al.*, 2014); and a background level of axonal loss (Haider *et al.*, 2016; Petzold *et al.*, 2017). PPMS is reported to be associated with higher annualised rates of peripapillary retinal nerve fibre layer (pRNFL) and macular ganglion cell and inner plexiform layer (mGCIPL) atrophy compared with both RRMS and secondary progressive MS (SPMS) (Henderson *et al.*, 2010; Sotirchos *et al.*, 2020).

6.2. Aims, objectives and hypotheses

6.2.1. *Aims and objectives*

The aim of this retrospective cohort study is to describe a cohort of MS cases in which early, progressive visual failure occurred without prior inflammatory anterior visual system involvement, which is referred to as primary progressive optic neuropathy (PPON) from now

on. When previous reports were written, many autoimmune antibody and genetic tests, as well as OCT imaging, were not yet available. The objective is to better characterise PPON, by describing demographic data, long-term follow-up of visual function, retinal structure and treatment response.

6.2.2. *Hypotheses*

Given the primary progressive course of optic neuropathy in these patients the clinical characteristics of PPON may resemble those of PPMS. Therefore, a hypothesis is that PPON cases are primarily male and exhibit pronounced neurodegeneration and atrophy, as evidenced by reduced retinal thickness measurements.

6.3. Methods

This is a retrospective case review that was conducted at the Neuro-Ophthalmology Departments of the National Hospital for Neurology and Neurosurgery, London, UK and the Amsterdam UMC, Amsterdam, The Netherlands.

6.3.1. *Ethics*

The study was registered at Moorfields Eye Hospital (CaRS_23) and was exempt from review by NHS ethical committee in the UK. The Amsterdam institutional review board issued a waiver stating that the requirements of the Medical Research Involving Human Subjects Act did not apply for the use of the clinical and imaging data for this study (METc number 2021.0462). This study was performed in agreement with local law on human research and the Declaration of Helsinki.

6.3.2. *Inclusion criteria*

Cases were selected if 1) there was a history of insidious visual loss for at least 12 months, 2) visual failure commenced before or no longer than 1 year after any MS related neurological symptom, 3) there was no prior symptomatic MSON and 4) a diagnosis of MS based on appropriate panel consensus criteria was made (McDonald *et al.*, 2001, Thompson *et al.*, 2018*a*) (Table 6.1). Alternative causes for optic neuropathy needed to have been excluded through exhaustive investigation (Petzold *et al.*, 2014; Biousse and Newman, 2016).

6.3.3. *Exclusion criteria*

Patients with a family history suggestive of hereditary optic neuropathy or a presumed increased risk for nutritional and toxic optic neuropathy were excluded. Results for common genetic variants associated with Leber Hereditary Optic Neuropathy (LHON) (G11778A, T14484C and G3460A) and dominant optic atrophy (OPA1 gene) testing were described. In addition, results for cell-based assays for aquaporin-4 (AQP4) antibody and myelin oligodendrocyte glycoprotein (MOG) antibody, as well as results for anti-nuclear antibodies (ANA), vitamin B12, vitamin D and folate were noted.

6.3.4. *Clinical data*

1)	**Clinical**
a)	Progressive, painless visual loss for one year minimum (retrospectively or prospectively determined), without previous symptomatic optic neuritis;
b)	Onset of visual loss before, or no longer than 1 year later than, other relapsing or progressive multiple sclerosis associated symptoms.
2)	**MS Diagnosis**
a)	Fulfilling appropriate panel consensus MS diagnostic criteria (Thompson *et al.*, 2018*a*).
3)	**Neuro-ophthalmological evaluation**
a)	Clinical evidence for optic neuropathy; - e.g. best corrected visual acuity (BCVA), visual fields, optic atrophy, dyschromatopsia, pRNFL and/or mGCIPL atrophy, PVEP peak time delay, relative afferent pupillary deficit (RAPD; where visual loss is asymmetric)
b)	No family history suggestive of a potentially hereditary optic neuropathy;
c)	Exclusion of other hereditary, autoimmune, structural and inflammatory causes of optic neuropathy guided clinically (Petzold *et al.*, 2014; Biousse and Newman, 2016), including (but not-exhaustively): - known hereditary optic neuropathies through genetic testing, in particular LHON - nutritional-toxic optic neuropathy; - structural lesions in visual pathways through MRI of brain and orbits; - chiasmitis; - other autoimmune or inflammatory causes of progressive optic neuropathy.

Table 6.1 Applied diagnostic criteria for MS patients with primary progressive optic neuropathy.

Descriptive characteristics of PPON cases including sex, age at onset, time to MS diagnosis, MS subtype, presence of retrobulbar pain and the Uhthoff phenomenon were summarised. Initial neurological symptoms and signs were described.

6.3.5. *Neuro-ophthalmological evaluation*

Patient charts were reviewed for results of routine investigations performed in the neuro-ophthalmology clinic. High-contrast best corrected visual acuity (BCVA) as measured monocularly with a Snellen chart and colour vision as evaluated with Ishihara charts were noted. Findings in fundoscopy (swollen or pale disc), visual fields (automated perimetry or by

confrontation) and pattern visual evoked potentials (PVEP) were summarised if available. Temporal evolution of symptoms was described.

6.3.6. *OCT*

Macular volume scans centred around the fovea and a circular 12° peripapillary scans (1536 A-scans, ART ~100) centred around the optic nerve head recorded with Spectralis SD-OCT (Heidelberg Engineering, Inc, Heidelberg, Germany) were analysed. Quality control (QC) of OCT scans was assessed using the quality criteria defined by the OSCAR-IB study by two authors (IK, AP) (Tewarie *et al.*, 2012).

All B-scans were segmented using segmentation software of the Heidelberg Eye Explorer (version 6.15.7.0) followed by manual correction. Macular layer thickness was computed by averaging the inner four sectors of the 3.45 mm EDTRS grid centred on the fovea. Macular volume scans and circular optic nerve scans were analysed for mGCIPL, inner nuclear layer (INL) and pRNFL thicknesses. Each macular B-scan was inspected for the presence of microcystic macular oedema (MMO) (Gelfand *et al.*, 2012), also termed retrograde maculopathy (Abegg *et al.*, 2014). Control OCT data was acquired with a similar protocol on healthy control subjects recruited from hospital staff.

6.3.7. *Radiology*

Brain MRI scans were reviewed with regard to presence of compressive lesions affecting the anterior visual pathways and demyelinating lesions, including gadolinium-enhancement. Spinal cord MRI scans were reviewed for presence of cervical and thoracic demyelinating lesions and gadolinium-enhancement. Orbital MRI scans were reviewed for atrophy, T2 hyperintensity and gadolinium-enhancement of the optic nerves. T2 hyperintensity of the optic nerve was not considered a sign of acute optic neuropathy since it is commonly observed in chronic neuropathy of any cause (Filippi *et al.*, 2019).

6.4. Results

6.4.1. *Cohort characteristics*

Sixteen patients that presented between 1997 and 2019 were identified, 13 of whom were male (81 %). Cases had a median age of 25 (range 15 – 48) at onset of visual symptoms (Table 6.2).

6.4.2. *Clinical features*

Patients reported a history of painless, progressive and non-resolving visual deterioration for at least one year. Visual loss was bilateral in all patients, developing simultaneously in 10 cases and with an interval of up to 9 years in the remaining six cases. Eleven patients (69 %) described presence of Uhthoff phenomenon.

Fourteen patients tested negative to common mutations associated with LHON, fourteen tested negative to AQP4-antibodies, eleven tested negative to MOG-antibodies and seven tested negative to OPA1 mutations. Vitamin D was in normal range for seven out nine tested cases and mildly subnormal in two. Folate and vitamin B12 were found to be in normal range for all six and seven available results, respectively. One case was found to be weak-positive to ANA, in the absence of features suggestive of a rheumatological disorder, while six others were negative.

6.4.3. *Neuro-ophthalmological evaluation*

Median BCVA was 6/36 (range 6/6 – hand movement (HM)) in the worse eye with median Ishihara plates correctly read to 1/17 (range 0/17 – 15/17) plate at the initial visit. The fellow eye had a median BCVA of 6/12 (range 6/5 – count finger (CF)) and could correctly identify a median of 6/17 (range 0/17 – 16/17) Ishihara plates.

Visual fields abnormalities were largely non-specific, but 12 cases (71 %) had a central scotoma in one or both eyes. Fundoscopy revealed optic disc pallor in all patients. Optic disc swelling was not observed. Conduction speeds were severely delayed for two patients with PVEP results (median: 155.4 ms, range: 112.8 – 163.3 ms).

Case	Sex	Age at onset	Uhthoff	Pain	Time to MS diagnosis (months)*	MS type	OCB	LHON	OPA1	MOG	AQP4
1	M	40	no	no	27	PPMS	no LP	-	-	-	-
2	M	29	yes	no	16	RRMS → SPMS	+	-	-	-	-
3	M	33	yes	no	12	PPMS	+	-	nd	nd	nd
4	M	25	yes	no	32	PPMS	+	-	-	nd	nd
5	M	17	no	no	12	RRMS → SPMS	+	-	nd	nd	-
6	M	22	yes	no	12	PPMS	+	-	-	-	-
7	M	40	yes	no	11	RRMS	matched	-	-	-	-
8	M	24	yes	no	3	RRMS	+	-	-	-	-
9	M	24	no	no	72	PPMS	+	-	nd	-	-
10	M	34	no	no	16	PPMS	+	-	nd	nd	-
11	M	48	yes	no	6	RRMS	no LP	-	-	-	-
12	M	35	yes	no	36	PPMS	+	-	nd	nd	-
13	F	15	no	no	84	PPMS	+	-	nd	-	-
14	F	18	yes	no	5	RRMS	no LP	nd	nd	-	-
15	F	21	yes	no	-6	RRMS	+	nd	nd	-	-
16	M	21	yes	no	7	RRMS	+	-	nd	-	-

Table 6.2 Baseline characteristics of 16 patients included in the PPON cohort. OCB = oligoclonal bands. nd = not done. *Time to MS diagnosis since start of visual symptoms in months.

6.4.4. *Evolution over time*

Follow-up was available for a median of 6.5 years (range 1 – 23 years) since onset (Table 6.3). BCVA at the final timepoint in the worst affected eye was a median of 6/36 (range 6/6 – no perception of light (NPL)), with a median 1/17 Ishihara plates (range 0/17 – 17/17) correctly identified. One case reported severe progressive visual deterioration which could not be reliably measured due to nystagmus.

Overall, visual function deteriorated or remained the same for fourteen cases over follow-up. Six of these cases used disease modifying treatment (DMT), comprising dimethylfumarate, teriflunomide, sequential interferon beta 1a and dimethylfumarate, and sequential glatiramer acetate, interferon beta 1a, natalizumab and alemtuzamab.

Some visual improvement during follow-up was experienced by two PPMS cases, one in response to intravenous methylprednisolone (IVMP). Case four experienced some spontaneous improvement, without taking IVMP or DMT, despite having progressive visual symptoms for two years. Some variability in measurements due to prominent Uhthoff in this patient may have been partly responsible for this finding.

6.4.5. *Treatment response*

IVMP was administered in eleven cases. This resulted in improvement in visual acuity for five patients (45 %), although this was transient in four. Case six experienced significant and lasting recovery after IVMP, with vision improving from bilateral CF vision to 6/18 and 6/12 visual acuity, despite having progressive visual symptoms for over one year. This case was not treated with DMT and had tested negative to both MOG and AQP4 antibodies.

6.4.6. *MS diagnosis*

Non-visual neurological symptoms presented a median of 7 months (range -11 months – 6 years) following onset of visual symptoms. In four cases there were signs of mild neurological

Case	First available evaluation		Final available evaluation		Time FU (yrs)	Years PPON final FU	Δ VA FU	IVMP	Treatment effect IVMP
	BCVA worst – better eye	Ishihara worst – better eye	VA worst – better eye	Ishihara worst – better eye					
1	6/24 – 6/9	6/17 – 12/17	6/36 – 6/9	1/17 – 6/17	4	6	↓	yes	no
2	6/6 – 6/5	6/17 – 1/17	6/12 – 6/9	7/17 – 7/17	7	8	↓	yes	transient
3	6/60 – 6/24	1/17 – 3/17	3/60 – 3/36	0/17 – 2/17	1	1	↓	no	-
4	6/9 – 6/9	14/17 – 16/17	6/6 – 6/6	17/17 – 17/17	2	4	→	no	-
5	6/60 – 6/18	0/17 – 4/17	CF – CF	1/17 – 1/17	7	8	↓	yes	transient
6	CF – CF	0/17 – 0/17	6/18 – 6/12	3/17 – 6/17	2	3	→	yes (x3)	yes
7	6/18 – 6/9	15/17 – 15/17	6/12 – 6/9	1/17 – 1/17	5	8	↓	yes (x2)	transient
8	6/18 – 6/18	deuteranope	3/60 – 1/60	deuteranope	4	7	→	yes	no
9	3/60 – 6/60	1/17 – 2/17	6/36 – 6/18	0/17 – 0/17	8	13	↓	yes	no
10	6/60 – 6/18	1/17 – 10/17	NPL – 6/9	4/13 – 8/13	2	2	→	yes	no
11	HM – 6/12	0/17 – 0/17	6/24 – 6/18	0/17 – 0/17	1	1	↓	no	-
12	6/18 – 6/12	1/17 – 5/17	nystagmus	Nystagmus*	2	5	↓	yes	no
13	6/36 – 6/12	3/17 – 14/17	6/24 – 6/18	3/17 – 6/17	1	7	→	no	-
14	6/60 – 6/9	-	CF – 6/15	-	8	8	↓	no	-
15	6/6 – 6/6	-	6/30 – 6/7.5	-	23	23	↓	yes	no
16	3/60 – 6/24	1/17 – 1/17	CF – 6/36	1/17 – 1/17	1	1	↓	yes (x2)	transient

Table 6.3 Follow-up data with regards to visual acuity metrics and treatment effect. BCVA and Ishihara colour vision measurements are given for the first available evaluation and for the final follow-up evaluation. Time in years between this first measure and the follow-up measurement is given in the Time FU column. The number of years clinical PPON was present at final follow-up was given in the years PPON final FU column. Δ VA FU indicates if visual function decreased, remained the same or improved during follow-up. *VA could not be reliably assessed due to severe nystagmus, worsening on unilateral eye closure due to a positive Heimann-Bielschowsky phenomenon.

impairment at presentation without history of previous symptoms. Eight cases were diagnosed with PPMS (47 %), while nine patients were initially diagnosed with RRMS, of which two converted to secondary progressive disease during follow-up. All 13 patients that underwent lumbar puncture and cerebrospinal fluid (CSF) analysis provided evidence for oligoclonal bands (OCBs), present in approximately 90 % of MS cases (Dobson *et al.*, 2013), which were isolated ("unmatched OCBs") in 12 while in one case there was evidence for inflammatory IgG response matching the oligoconal IgG pattern seen in the serum ("matched OCBs").

The nature of symptoms and signs related to the diagnosis of multiple sclerosis was varied and included walking difficulties, cognitive impairment, pyramidal signs, paraesthesia, impaired balance and cerebellar eye signs. Bladder, bowel and/or erectile dysfunction were present in 12 cases (71 %).

		PPON cases	**Controls**
Peripapillary ring scans	N (cases)	13	13
	pRNFL µm, median (range)	60.5 (49 – 91)	103 (94 – 112)
	pRNFL nasal µm, median (range)	49 (32 – 100)	77 (52 – 109)
	pRNFL temporal µm, median (range)	28 (15 – 63)	61 (58 – 92)
	pRNFL N/T ratio, median (range)	1.87 (0.60 – 4.47)	1.50 (0.76 – 1.88)
Macular scans	N (cases)	12	13
	GCIPL µm, median (range)	45 (35 – 72)	88 (69 – 91)
	INL µm, median (range)	39 (34 – 51)	37.5 (33 – 41)
	MMO, n (%)	6 (50 %)	0 (0 %)
Disease duration at OCT scan	Years since onset visual symptoms, median (range)	7 (1 – 20)	NA

Table 6.4 OCT data of PPON cases and 13 age- and sex-matched controls.

6.4.7. *OCT*

Thirteen patients had at least one OCT scan available. The first acquired OCT scans revealed median thicknesses of the pRNFL and mGCIPL of 60.5 µm (range: 49 – 91 µm) and 45 µm

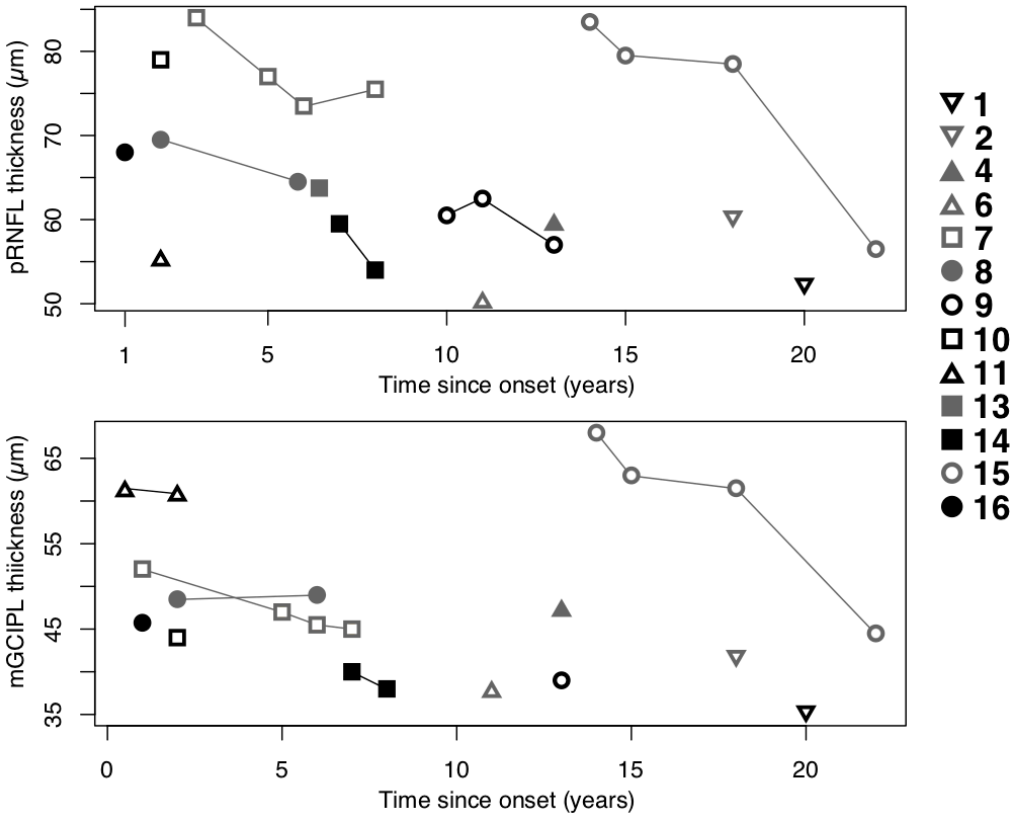

Figure 6.1 Follow-up OCT data in PPON cohort.

(range: 35 – 72 µm), respectively. Peripapillary atrophy predominantly affected the temporal quadrant (Table 4). Median INL thickness was 39 µm (range: 34 – 51 µm). In 13 age- and sex-matched controls, the median pRNFL, mGCIPL and INL thicknesses were 103 µm (range: 94 – 112 µm), 88 µm (range: 69 – 91 µm) and 37.5 µm (range: 33 – 41 µm).

Follow-up OCT revealed thinning of pRNFL and mGCIPL over time (Figure 6.1). MMO was present in six out of twelve cases with macular scans available (50 %) (see Figure 6.2 for examples), and was unilateral in four cases and bilateral in the other two cases.

6.4.8. *Radiology*

All cases had at least one MRI brain scan available. No structural compression of the anterior visual system was observed. Typical demyelinating lesions were seen in periventricular, juxtacortical and infratentorial regions. Evidence for gadolinium enhancement was found in two patients, both showing “faint” enhancement of one or more supratentorial lesions.

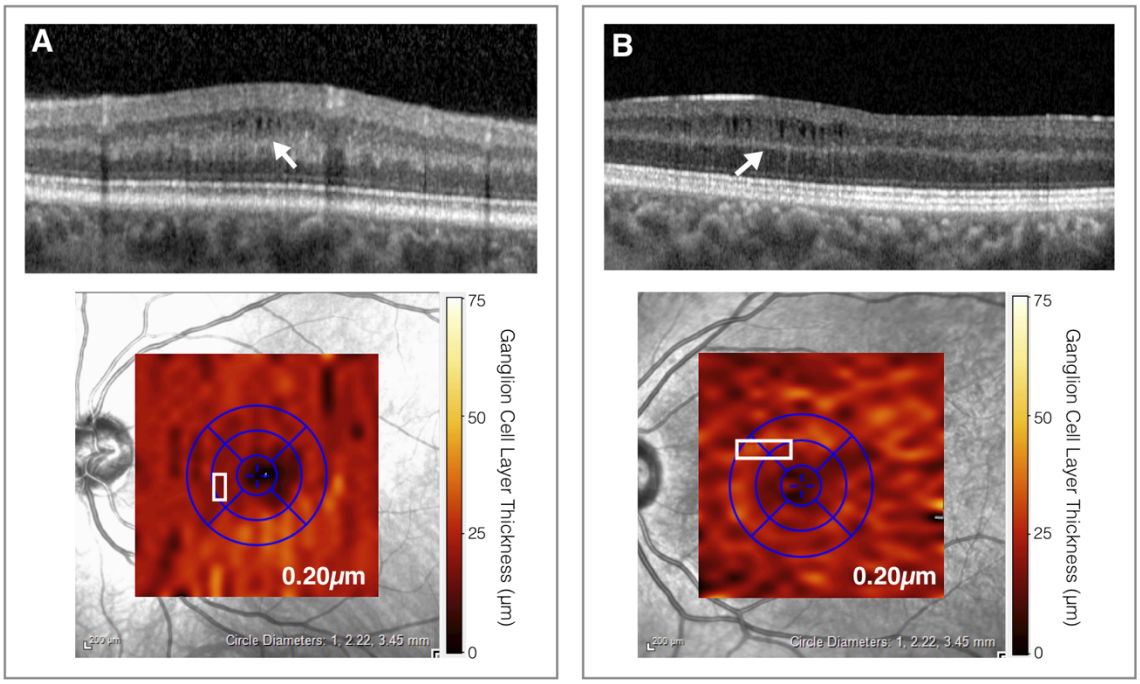

Figure 6.2 Examples of microcystic macular oedema (or retrograde maculopathy) on OCT. Macular scans of the left eyes from case 10 (A) and case 14 (B) both showing severe ganglion cell layer atrophy (20 µm) and MMO of the inner nuclear layer (indicated with white arrows). The white square in the fundus photo indicates the location of MMO.

Thirteen cases had spinal cord imaging available, which showed extensive involvement with multiple (confluent) lesions in the cervical and thoracic spinal cord in 9 cases (69 %), one case had only one cervical lesion and two cases had extensive cervical spinal cord involvement with one and no thoracic lesions, respectively. One final RRMS case showed no abnormalities on spinal cord imaging. One case showed gadolinium-enhancement of two spinal cord lesions.

Orbital imaging showed atrophic or slender optic nerves in all cases with orbital imaging. Optic nerves were atrophic without signal change in six cases, although one case developed T2 signal hyperintensities in both optic nerves during follow-up. In the other six cases T2 signal hyperintensities were present in the intraorbital segment of the optic nerve, which was bilateral in all cases. No optic nerve enhancement was observed in the eight patients that underwent gadolinium enhanced dedicated orbital imaging.

6.5. Case vignettes

Case 2 A 30-year old man presented with insidious, painless, bilateral visual loss with Uhthoff phenomenon for 15 months. Visual acuities were 6/6 and 6/5, while reading 1 and 6 out of 17

Ishihara plates, respectively. OCTs showed pRNFL atrophy with a mean thickness of 60 µm and bilateral MMO. IVMP caused transient improvement of colour vision. More than a year after onset of visual loss he developed paraesthesia, vertigo and ocular movement deficits. MRI showed multiple infra- and supratentorial demyelinating lesions typical of MS and CSF was positive for unmatched OCBs. During follow-up he developed aggressive RRMS, for which many different DMTs were trialled. This included β-interferons, glatiramer acetate, natalizumab and alemtuzumab. He had up to six relapses per year, experiencing break-through relapses even while treated with natalizumab. He was diagnosed with secondary progressive MS after six years of disease duration. Visual acuities deteriorated slightly to 6/12 and 6/9 over time.

Case 9 A 29-year old man presented with a 5-year history of progressive, painless and bilateral visual loss without Uhthoff phenomenon. Visual acuity was poor at 3/60 and 6/60, while reading 1/17 and 2/17 Ishihara plates. OCT revealed severe pRNFL and mGCIPL atrophy at a mean of 60 µm and 39 µm, respectively. During an 8-year follow-up visual acuities deteriorated to 3/60 and 1/60, while reading 0 Ishihara plates bilaterally. IVMP was administered without effect. One year after presentation he developed paraesthesia of both hands, progressive walking difficulty and occasional bladder and bowel incontinence. He was diagnosed with PPMS, based on unmatched OCBs and typical demyelinating lesions on MRI.

Case 13 A 22-year old woman reported a history of progressive, painless visual loss, primarily of the right eye starting when she was 15 years old. There was no Uhthoff's. Visual acuities were 6/36 and 6/12, reading 3/17 and 6/17 Ishihara plates. OCTs showed pRNFL atrophy at a mean of 65 µm. She followed a vegetarian diet, but serum B12 and folate levels were within the reference range, not taking supplements. At 20 years of age she developed fluctuating, progressive sensory symptoms of the right arm and was diagnosed with PPMS based on unmatched OCBs and typical demyelinating lesions on MRI. Treatment with ocrelizumab was proposed.

6.6. Discussion

Here the clinical, radiological and OCT features of 16 MS patients with early progressive visual failure due to PPON were described. These data suggest that this rarely reported MS phenotype is associated with male sex, a primary progressive disease course and severe optic atrophy as evidenced by thinning of the pRNFL and mGCIPL layers of the retina and a high prevalence of MMO. Visual function improved after corticosteroid treatment in 45 % of patients, although this was transient for most. One patient in particular experienced an important and lasting visual recovery after IVMP treatment. Presence of the Uhthoff phenomenon was relatively high at 69 % suggesting a high proportion of intact but demyelinated axons.

A strong male predominance was identified in this cohort, with 81 % being men. This broadly corresponds to the eight cases described by Read et al. (Read *et al.*, 1996) and Ormerod and McDonald (Ormerod and McDonald, 1984), of which five cases were male. Given that females are overrepresented in MS and optic neuritis demographics (Braithwaite *et al.*, 2020), the male predominance in this PPON cohort is remarkable and mirrors the demographics of PPMS (Thompson *et al.*, 2018*b*). There is some evidence suggesting that males may be more susceptible to anterior visual system damage in multiple sclerosis, with more axonal loss after MSON than in females (Costello *et al.*, 2012; Burton *et al.*, 2017) and persistent visual loss in MS being more common in males (Jasse *et al.*, 2013).

PPMS cases comprised 50 % of this cohort, a considerable overrepresentation of this subtype that makes up approximately 15 % of all MS cases (Thompson *et al.*, 2018*b*). Despite the clear progressive nature of PPON, half of the cases were diagnosed with RRMS. At least three patients out of the previously reported eight PPON cases appear to have relapsing remitting disease, although MS subtypes are not specified (Ormerod and McDonald, 1984; Read *et al.*, 1996). This partial overlap between progressive and relapsing disease activity occurs incidentally, as described by the “progressive relapsing” MS phenotype (Miller and Leary, 2007) and 28 % of PPMS cases in a large cohort experiencing one or more relapses throughout the disease course (Cottrell *et al.*, 1999).

Additional reporting on progressive visual loss in MS is scarce, but one study found that 21 % patients out of a cohort of MS patients with optic nerve involvement reported a history of progressive visual loss without superimposed visual relapses (Kahana *et al.*, 1973) and a different cohort containing three RRMS patients with progressive optic neuropathy in the absence of prior MSON (Jasse *et al.*, 2013). Two case reports also describe progressive visual failure in multiple sclerosis (Gasperini *et al.*, 1991; Giordano *et al.*, 2018).

In this cohort corticosteroid therapy improved visual acuity in 45 % of patients in which it was administered, despite the known poor effects of corticosteroid treatment in PPMS (Thompson *et al.*, 2018*b*). However, for four out of five patients this improvement in visual acuity was transient, in line with the known lack of long-term efficacy of corticosteroid treatment in MS (Zipp *et al.*, 2000). Ocrelizumab is now available for treatment of PPMS (Montalban *et al.*, 2017), and may be of value in PPON patients, in particular those for whom IVMP was effective. The finding of some spontaneous visual recovery during follow-up in one patient may be partly related to increased white and grey matter network connectivity compensating for structural decline (Fleischer *et al.*, 2016), but may also be related to variable visual acuity results due to Uhthoff. PPON is a rare finding in MS and should only be diagnosed after exhaustive exclusion of other causes for optic neuropathy. However, this should not necessarily preclude commencing treatment in MS patients with progressive visual failure while differential diagnoses are simultaneously excluded, as these data indicate this could prevent or slow permanent damage to the optic nerves.

OCT data revealed severe optic atrophy in this cohort, with median pRNFL and mGCIPL thicknesses of 60.5 µm and 45 µm in patients compared with 103 µm and 88 µm in controls, respectively. When controlling for disease duration, retinal thickness measures in individuals with PPMS are generally slightly thinner than in RRMS (Henderson *et al.*, 2010; Sotirchos *et al.*, 2020). The majority of retinal atrophy after MSON occurs in the first three months (Costello *et al.*, 2006) and independently from MSON, retinal atrophy in multiple sclerosis occurs at a rate of approximately 0.4-0.7 % per year (Balk *et al.*, 2016; Sotirchos *et al.*, 2020). In this cohort, longitudinal OCT data seem to suggest that atrophy occurred at a higher rate and for a longer period after the onset of visual symptoms than is generally seen in MS.

The INL thickness of 37 µm that was observed in this cohort roughly corresponds with observations in other MS phenotypes (Balk *et al.*, 2016; Petzold *et al.*, 2017). MMO was observed in 50 % of macular scans. This is substantially higher than the 1-4.7 % reported in MS (Balk *et al.*, 2012; Gelfand *et al.*, 2012), possibly due to the severe optic nerve atrophy in PPON, as retrograde degeneration has been postulated to be an important factor in MMO development (Abegg *et al.*, 2014).

The early onset of optic neuropathy in MS in this cohort is in line with the well-understood fact that neurodegeneration and axonal loss commences at disease onset, in addition to inflammatory demyelinating insults (Zipp *et al.*, 2013). It is unclear if visual loss in PPON is primarily driven by demyelination or axonal loss. The severe retinal atrophy indicates axonal loss, but the high prevalence of Uhthoff phenomenon in this cohort suggests additional presence of demyelination (Frohman *et al.*, 2013). Post-mortem histological investigation of 13 advanced multiple sclerosis patients, with and without prior MSON, showed that visual acuity was highly correlated to the extent of optic nerve demyelination (Ulrich and Groebke-Lorenz, 1983). Lesions of PPMS patients contain less inflammation and more ongoing axonal damage compared to those in RRMS and SPMS (Revesz *et al.*, 1994; Lucchinetti and Bruck, 2004; Tallantyre *et al.*, 2010; Lassmann *et al.*, 2012). Given the profound level of optic atrophy and absence of MSON, PPON probably has underlying pathophysiological mechanisms similar to PPMS. It is not possible to localise the damage within the anterior visual pathway (optic nerves, chiasm or optic tracts) and a contribution of retrograde transsynaptic degeneration following damage to the optic radiations cannot be excluded. Metabolic failure may play an important role in the pathophysiology of PPON, as energy failure implicated in PPMS in general and given the clear and profound reductions in ellipsoid zone (EZ) reflectivity in PPON that were described in chapter 4 in this thesis.

The initial disease course in PPON resembles a visual variant of progressive solitary sclerosis, in which one critically located demyelinating lesion causes insidious and progressive accumulation of motor disability (Keegan *et al.*, 2016). However, all cases described here developed radiological lesion dissemination. The predilection of spinal cord and optic nerve involvement seen in this cohort appears in line with the opticospinal MS variant (Eikelenboom

et al., 2004), although all cases did have brain MRIs with several lesions typical for demyelination.

Harding disease, the combination of LHON and MS (Harding *et al.*, 1992), presents similarly to PPON but occurs primarily in females (Palace, 2009; Pfeffer *et al.*, 2013). Most patients in this cohort tested negative for known mutations associated with LHON and one male patient was excluded from the cohort because he was found to have the mtDNA 11778 mutation. More extensive studies of the mDNA genome, of nuclear mitochondrial genes and of mitochondrial function may be revealing in this cohort as in MS more generally (Mao and Reddy, 2010).

The main limitation of this study is the retrospective data collection from case note review. The phenotype is rare (16 cases identified over ±20 years in two tertiary neuro-ophthalmology clinics) and the cohort may not represent all incident cases over the recruitment period. Only high-contrast visual acuity was available, while low-contrast visual acuities would have probably been more sensitive to visual deficits (Balcer *et al.*, 2017). This study is unique due to the long follow-up and extensive laboratory, OCT and MRI information available overall.

6.7. Conclusion

Here, the rare phenomenon of progressive visual loss as an early symptom of MS is described in a cohort of sixteen cases. The phenotype predominantly occurs in male individuals and is associated with a primary progressive disease course. A (transient) effect of intravenous corticosteroids was observed in 45 % of patients. PPON should be a differential-diagnostic consideration in patients with progressive visual failure, but should only be diagnosed after other more common causes of optic neuropathy have been confidently excluded and MS diagnostic criteria are fulfilled.

7. Alcohol consumption and smoking in multiple sclerosis; a large UK cohort study

ABSTRACT

Background Understanding the effects of modifiable risk factors on multiple sclerosis (MS) risk and associated neurodegeneration is important to guide clinical counselling.

Objective Investigate the associations of alcohol use and smoking with odds of having an MS diagnosis and with macular ganglion cell layer and inner plexiform layer (mGCIPL) thickness.

Methods This cross-sectional study analysed data from the community-based United Kingdom Biobank (UKBB) study on smoking status (never, previous, currently, passive) and alcohol consumption (low, moderate, high), obtained through questionnaires, and retinal thickness (measured by optical coherence tomography (OCT)) in individuals aged 40-69 years. Multivariable logistic regression analyses were used to identify risk factors for MS diagnosis by calculating odds ratios (ORs) and 95% confidence intervals (CI). Multivariable generalised estimating equations (GEEs) were used to explore the associations of alcohol use and smoking with mGCIPL thickness in individuals with MS. Finally, interaction models explored if the correlations of alcohol and smoking with mGCIPL thickness were modified by MS diagnosis.

Results 72,101 individuals were included (20,065 healthy, 51,737 with comorbidities and 179 with MS). Modifiable risk factors significantly associated with the odds of MS diagnosis were smoking (OR 3.05; 95% CI 1.95 – 4.64), moderate alcohol intake (OR 0.62; 95% CI 0.43 – 0.91) and obesity (OR 1.72; 95% CI 1.15 – 2.56). High alcohol consumption was associated with thinner mGCIPL thickness in individuals with MS (beta=-3.09 µm; p=0.020), with a significant trend effect across the alcohol intake levels (p=0.021). The effects of high alcohol intake on mGCIPL thickness trended towards being more severe in MS compared with controls (beta=-2.27 µm, p=0.074 vs. beta=-0.91 µm, p<0.001, respectively). Smoking was not associated with mGCIPL thickness in MS. However, there was suggestion of effect modification in the interaction model, with smoking being associated with greater mGCIPL thickness in controls (beta=0.87 µm, p<0.001), but a negative trend in MS (beta=-2.14 µm, p=0.077).

Conclusion High alcohol consumption was associated with retinal features indicative of more severe neurodegeneration while smoking was associated with higher odds of MS diagnosis.

7.1. Background

The pathophysiology of multiple sclerosis (MS) has not been fully elucidated, but both genetic and environmental factors are known to play important roles (Olsson *et al.*, 2016, Thompson *et al.*, 2018*b*; Jacobs *et al.*, 2021). Understanding the role of modifiable risk factors, such as smoking and alcohol intake, is important to guide counselling of patients in clinic (Pakpoor *et al.*, 2014; Rosso and Chitnis, 2020). Smoking in particular is known to increase the risk of developing MS (Manouchehrinia *et al.*, 2013) and advising patients to stop smoking to lessen the risk of conversion from clinically isolated syndrome (CIS) to MS has become an important part of patient guidance (Brownlee and Miller, 2014). Less is known about how these health behaviours influence neurodegeneration once the diagnosis has been established. Ameliorating neurodegeneration and brain atrophy is an important treatment goal in MS, given the known associations with physical and cognitive disability (Kappos *et al.*, 2016).

Studies investigating brain atrophy in MS are hampered by long MRI scanning protocols necessary to acquire brain volume measures. Retinal thickness measures have been identified as a surrogate for brain volume (Saidha *et al.*, 2015*b*; Mejia-Vergara *et al.*, 2021), as the retina is developmentally and anatomically part of the central nervous system but has the advantage of being more easily assessable for imaging. Thickness of the macular ganglion cell and inner plexiform layer (mGCIPL) as measured with optical coherence tomography (OCT) correlates with brain volume measures in the general population (Chua *et al.*, 2021*a*) and in MS (Saidha *et al.*, 2015*b*). As with brain volume, retinal thickness measures are associated with performance on MS disability scores (Martinez-Lapiscina *et al.*, 2016; Birkeldh *et al.*, 2019).

As smoking and alcohol are highly correlated behaviours (Jiang *et al.*, 2014; Beard *et al.*, 2017), it is difficult to disentangle their respective effects on health outcomes. In the general population, smoking and alcohol intake separately have been found to be related to brain atrophy (Kubota *et al.*, 2001; Mukamal *et al.*, 2001; Taki *et al.*, 2004; Anstey *et al.*, 2006; Paul *et al.*, 2008; Topiwala *et al.*, 2017, 2021; Dougherty *et al.*, 2020; Ning *et al.*, 2020), and daily alcohol intake has also been found to be associated with thinner mGCIPL thickness (Khawaja *et al.*, 2020).

Smoking is known to be associated with a higher risk of developing MS (Manouchehrinia *et al.*, 2013) and may also drive increased disease activity, disability progression (Manouchehrinia *et al.*, 2013) and neurodegeneration (Rosso and Chitnis, 2020) in MS. However, some studies investigating associations between smoking and brain volume in MS found inconclusive results (Kvistad *et al.*, 2016; Rosso *et al.*, 2019; Rosso and Chitnis, 2020), and none of these studies adjusted for the potential confounding effects of concomitant alcohol use. How alcohol affects MS is less clear, with both protective (Hedström *et al.*, 2014; Weiland *et al.*, 2014) and adverse effects (Pakpoor *et al.*, 2014; Abdollahpour *et al.*, 2018) reported and the association between alcohol consumption and brain atrophy in MS not yet being investigated. Correlations of alcohol intake with health outcomes are complex, frequently following a U-shaped curve. Moderate alcohol consumption may be protective to developing cardiac infarction (Wood *et al.*, 2018) and cataract (Chua *et al.*, 2021*b*) for example. However, with regard to brain volume (Topiwala *et al.*, 2017, 2021) and mortality (Wood *et al.*, 2018) most evidence points to a linear negative correlation with alcohol, without a protective effect of moderate consumption.

7.2. Aims, objectives and hypotheses

7.2.1. *Aims and objectives*

The aim of this study is to investigate the associations of alcohol consumption and smoking with having a diagnosis with MS and mGCIPL thickness measures in a large community-based cohort study comprising more than 70,000 adults in the United Kingdom. The objective is that better understanding of the roles of these modifiable risk factors as their successful management may lead to better health outcomes and quality of life in MS.

7.2.2. *Hypotheses*

The main hypothesis of this study is that modifiable risk factors, smoking and alcohol consumption, show associations with thinner mGCIPL thickness measures in a cohort of MS patients. A further hypothesis of this study is that previously identified associations of smoking with an increased odds of having a diagnosis with MS will be replicated.

7.3. Methods

7.3.1. *Participants*

Participants were adults aged 40-69 registered in the National Health Service (NHS) who participated in expanded ophthalmic protocol, including OCT, of the regular UK Biobank baseline visit between 2009-2010 at six study assessment centres across the United Kingdom (Chua *et al.*, 2019). Subjects were categorized as 'multiple sclerosis', 'non-comorbid' or 'comorbid' based on clinician controlled ICD-10 disease codes, available through record-linking with the NHS, as in previous studies (Petzold *et al.*, 2020). The ICD-10 code for MS, G35, is applicable to all forms of MS diagnosed by clinicians within the NHS, but does not specify which tests were used to reach a diagnosis. The cumulative disease burden was calculated by counting the number of ICD-10 codes per participant. Individuals without MS were categorised as 'healthy' if this cumulative disease burden was 0 and 'comorbid' if it was ≥1. It should be noted that patients with a CIS, such as optic neuritis, are unlikely to be categorised as having MS at the time of the study. However, the relatively older age range recruited will have reduced the proportion of individuals in the CIS category.

7.3.2. *Ethical approval*

The North West Multi-Centre Research Ethics Committee approved the UK Biobank study protocol (reference no. 06/MRE08/65), in accordance with the tenets of the Declaration of Helsinki. All participants gave written informed consent.

7.3.3. *Data collection*

Detailed overall study protocols, as well as protocols specifically for the ophthalmic investigations are available online (http://www.ukbiobank.ac.uk/resources/). In brief, undilated macular spectral domain OCT scans were carried out in a dark room with the Topcon 3D OCT-1000 Mk-II (Topcon Corp), in line with APOSTEL guidelines (Cruz-Herranz *et al.*, 2016; Aytulun *et al.*, 2021) as described in detail before (Patel *et al.*, 2016). An extensive quality-control protocol, combining both automated and manual checks, was used to ensure sufficient image quality, complying with OSCAR-IB criteria (Tewarie *et al.*, 2012), and accurate

layer segmentation (Patel *et al.*, 2016; Khawaja *et al.*, 2020). mGCIPL thickness was reported in microns (µm).

Participants completed a self-administered touch-screen questionnaire informing on health-related behaviours, demographics and socio-economic data. Smoking and alcohol status were inferred from the answers to "Do you smoke tobacco?" (Never, Previously, Currently) and "How often do you drink alcohol?" (Never, Special occasions only, 1-3 times per month, 1-2 times per week, 3-4 times per week, Daily or almost daily). The responses to the alcohol related question were collapsed into 'low' (never or special occasions only), 'moderate' (drinking once per month up to 4 times per week) and 'high' (daily or almost daily). In addition, household passive smoking was recorded ("Do any household members smoke tobacco?"). Ethnicity responses were recoded into four categories; White ('British', 'White', 'Irish' or 'Other white background'), Asian ('Indian', 'Pakistani', 'Asian or Asian British', 'Bangladeshi', 'Chinese' or 'Other Asian background'), Black ('Caribbean, 'African', 'Black or Black British' or 'Other black background') and Other/Mixed ('Other mixed background', 'Do not know', 'Mixed', 'Other ethnic group', 'White and black African', 'White and Black Caribbean' and 'White and Asian'). Corneal compensated intraocular pressure measurements were performed with the Ocular Response Analyzer (Reichert) from either the left or right eye. Weight and height were measured with BV-418 MA body composition analyser (Tanita, Arlington Heights, IL) and Seca 202 height measure (Seca, Birmingham, United Kingdom), respectively. Based on weight and height measurements BMI was calculated (kg/m^2). BMI was transformed into a categorical variable based on accepted health-related limits (<18 underweight, 18-24 healthy, 24-30 overweight, >30 obese). Postcode of the participant was used to determine Townsend Deprivation Score, which was transformed into a categorical variable based on quartiles of equal group size.

7.3.4. *Data exploration*

Data distributions were described using summary statistics for continuous variables (median and interquartile range (IQR), or mean and standard deviation (SD) when normally distributed) and cross-tabulations (including percentages) for categorical variables in the baseline table.

Visual inspection (using dot-plots, histograms) and data ranges were used to inspect for normality and inconsistencies. Missing data were shown in the baseline table.

7.3.5. *Logistic regression*

Univariable followed by multivariable logistic regression was used to identify factors associated with the odds of having a MS diagnosis. The 'healthy' and 'comorbid' control groups were used separately. Covariates considered besides alcohol use and smoking were age, sex, Townsend deprivation score, ethnicity and BMI. Odds ratios (OR) and 95% confidence intervals (CI) were represented visually using Forest plots.

7.3.6. *mGCIPL thickness in MS*

Subsequently, the goal was to build a multivariable model investigating the respective effects of alcohol use and smoking on mGCIPL thickness measures in individuals with MS, adjusted for relevant confounding factors. To account for inter-eye correlations generalised estimating equations (GEEs) were used (Cruz-Herranz *et al.*, 2016; Aytulun *et al.*, 2021). Spearman's correlations were performed between all covariates to identify evidence for multicollinearity (ρ>0.5). Identification of potential confounding factors was explored by performing univariable analyses of the association of covariates with mGCIPL thickness separately. Subsequently, the association of potential confounders with alcohol use and smoking were tested using Chi-squared tests for categorical variables and Kruskal-Wallis tests for continuous variables. Age, sex and intraocular pressure are included in the final multivariable GEE model 'a priori'. Dose-response effects of alcohol use and smoking were investigated by testing for linear trend estimations across the variable levels. To explore potential multiplicative effects of combined smoking and alcohol use, a model including interaction terms for the alcohol and smoking variables was tested.

7.3.7. *Effect modification MS*

Finally, it was explored if associations of smoking and alcohol use with mGCIPL thickness differ between controls and individuals with MS. To this end, GEE analyses were run on the complete cohort, including individuals with and without MS. Two models were used, including variables

for MS diagnosis, alcohol intake and smoking status as well as an interaction term for MS and either smoking status (model 1) or alcohol intake (model 2). These models were inspected for significant ($p<0.05$) or trending ($p<0.10$) results for the Wald test of the interaction terms.

7.3.8. *Statistical analysis*

A statistical significance threshold of $p<0.05$ was used. Statistical analyses were performed with R and R Studio. The exchangeable correlation structure was used in GEE.

7.4. Results

7.4.1. *Participants*

A total of 179 individuals with MS, 20,065 healthy controls and 51,737 comorbid controls were included (Figure 7.1). Baseline characteristics are shown in Table 7.1. Sex distributions were in line with the known overrepresentation of females in MS demographics (Thompson *et al.*, 2018*b*). As only three MS cases were classified as 'underweight', this BMI level was collapsed with 'normal weight'.

7.4.2. *Odds of MS diagnosis*

Factors associated with the odds of being diagnosed with MS were investigated by performing univariable logistic analysis (suppl. Table 7.1) and subsequent multivariable logistic regression (Figure 7.2-A, suppl. Table 7.2) using the 'healthy' and 'comorbid' control group separately.

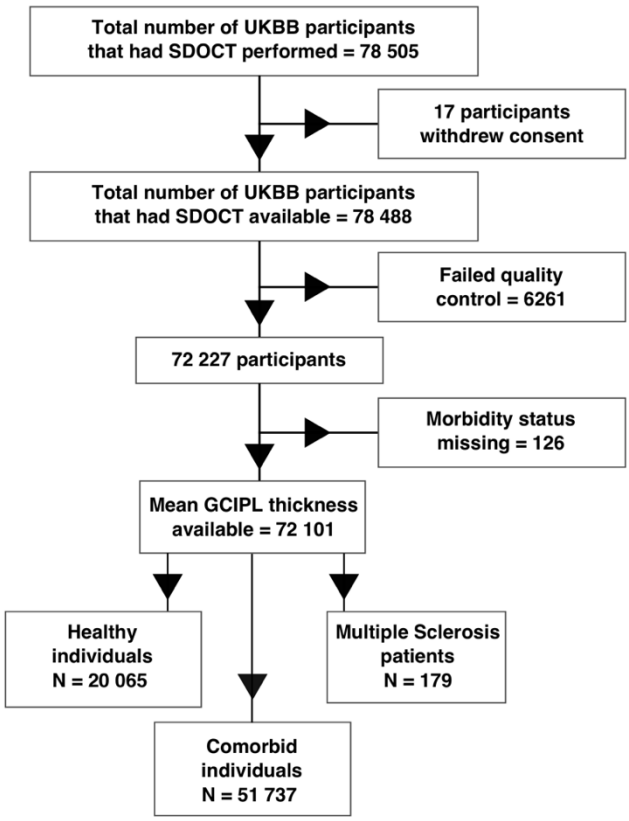

Figure 7.1 Inclusion flowchart. Flowchart of subject inclusion. MS patients were defined as those with a 'G35' ICD-10 disease code. Healthy control individuals were those that had zero ICD-10 disease codes registered, while comorbid control individuals had one or more (non-MS) ICD-10 disease codes registered. SDOCT = spectral domain optical coherence tomography. GCIPL = ganglion cell and inner plexiform layer.

		Healthy	Comorbid	MS cases
N		20,065	51,737	179
Sex, M (%)		10,001 (49.8 %)	23,246 (44.9 %)	49 (27.4 %)
Age, mean (sd)		55.2 (7.9)	57.2 (8.0)	55.6 (7.7)
Age group, n (%)	40-49 years	5423 (27.0 %)	10,878 (21.0 %)	44 (24.6 %)
	50-59 years	7594 (37.8 %)	16,132 (31.2 %)	73 (40.8 %)
	60-70 years	7048 (35.1 %)	24,724 (47.8 %)	62 (34.6 %)
Smoking status, n (%)	Never	12,071 (60.2 %)	27,896 (53.9 %)	81 (45.3 %)
	Previous	6210 (30.9 %)	18,666 (36.1 %)	63 (35.2 %)
	Current	1702 (8.5 %)	4858 (9.4 %)	33 (18.4 %)
	Missing / no answer	82 (0.4 %)	317 (0.6 %)	2 (1.1 %)
Alcohol consumption, n (%)	Low	3267 (16.3 %)	10,832 (20.9 %)	47 (26.3 %)
	Moderate	12,228 (60.9 %)	10,832 (58.5 %)	89 (49.7 %)
	High	4515 (22.5 %)	10,489 (20.3 %)	41 (22.9 %)
	Missing / no answer	55 (0.3 %)	165 (0.3 %)	2 (1.1 %)
Ethnicity, n (%)	White	18,232 (90.9 %)	47,333 (91.5 %)	168 (93.9 %)
	Black	537 (26.8 %)	1394 (26.9 %)	3 (1.7 %)
	Asian	705 (3.5 %)	1594 (3.1 %)	4 (2.2 %)
	Other / Mixed	560 (2.8 %)	1306 (2.5 %)	3 (1.7 %)
	Missing / no answer	31 (0.2 %)	110 (0.2 %)	1 (0.6 %)
Townsend deprivation index, n (%)	Lowest quartile	5234 (26.1 %)	12,720 (24.6 %)	33 (18.4 %)
	Low-middle quartile	4975 (24.9 %)	12,958 (25.0 %)	46 (25.7 %)
	High-middle quartile	5063 (25.2 %)	12,865 (24.9 %)	43 (24.0 %)
	Highest quartile	4770 (23.8 %)	13,135 (25.4 %)	57 (31.8 %)
	Missing / no answer	23 (0.1 %)	59 (0.1 %)	0 (0 %)
BMI group, n (%)	Low or normal weight (<25)	7841 (39.1 %)	16,731 (32.3 %)	60 (33.5 %)
	Overweight (25-30)	8549 (42.6 %)	21,767 (42.1 %)	68 (37.4 %)
	Obese (>30)	3603 (18.0 %)	13,026 (25.2 %)	43 (24.0 %)
	Missing	72 (0.4 %)	213 (0.4 %)	9 (5.0 %)
Intraocular pressure	Mean mmHg (sd)	16.0 (4.3 %)	15.9 (4.3)	15.1 (3.7)
	Missing, n (%)	657 (3.3 %)	1618 (3.1 %)	12 (6.7 %)
Household passive smoking, n (%)	Yes	1820 (9.1 %)	4896 (9.5 %)	21 (11.7 %)
	No	16,979 (84.6 %)	42,926 (83.0 %)	134 (74.9 %)
	Missing	1266 (6.3 %)	3915 (7.6 %)	23 (13.4 %)
mGCIPL thickness, µm mean (SD)		72.8 (6.0)	72.2 (6.0)	67.8 (6.3)
mGCIPL IEPD, mean (sd)		2.63 (3.43)	2.82 (3.61)	6.37 (6.34)
mGCIPL IEAD, µm mean (sd)		1.95 (2.55)	2.08 (2.67)	4.54 (4.73)

Table 7.1 Baseline characteristics of included cohort. mGCIPL = macular ganglion cel land inner plexiform layer. IEPD = inter-eye percentage difference. IEAD = inter-eye absolute difference.

Ethnicity was not included as a variable in this analysis, given the low number of non-White ethnic MS cases (5.5 %). Household passive smoking was not significantly associated with a change in odds of MS (suppl. table 7.1), and this variable was not included in multivariable analysis.

		Mean mGCIPL µm (sd)	beta	p-value	Trend	Observations (n)
Sex, n (%)	Female	68.2 (6.2)	-	-		
	Male	66.8 (6.5)	-1.37	0.200	-	179
Age per unit increase		-	0.00	0.990	-	179
Smoking status, n (%)	Never	68.3 (6.2)	-	-		
	Previous	67.9 (6.6)	-0.34	0.750		
	Current	67.0 (5.9)	-1.26	0.300	0.330	177
Alcohol consumption, n (%)	Low	68.7 (6.4)	-	-		
	Moderate	68.5 (6.4)	-0.15	0.900		
	High	65.7 (5.6)	-2.94	**0.020**	**0.024**	177
Townsend deprivation index, n (%)	Lowest quartile	68.5 (7.3)	-	-		
	Low-middle quartile	67.6 (5.5)	-0.91	0.540		
	High-middle quartile	67.2 (6.0)	-1.34	0.390	0.880	179
	Highest quartile	68.2 (6.5)	-0.34	0.820		
BMI per unit increase		-	0.04	0.680	-	170
BMI groups	Low/normal weight		-	-		
	Overweight (25-30)		-0.41	0.720		170
	Obese (>30)		-0.41	0.770		
IOP per unit increase		-	1.61	0.290	-	167
Household passive smoking	No	-	-	-	-	-
	Yes	-0.76	0.610	-	156	

Table 7.2 Univariable generalised estimating equations (GEEs) investigating associations with mGCIPL thickness in multiple sclerosis. Results of univariable generalized estimating equations (GEEs) investigating associations with explanatory variables (alcohol consumption and smoking status) and other covariates with mGCIPL thickness in individuals diagnosed with MS. Significant results in **bold.** mGCIPL = macular ganglion cell and inner plexiform layer.

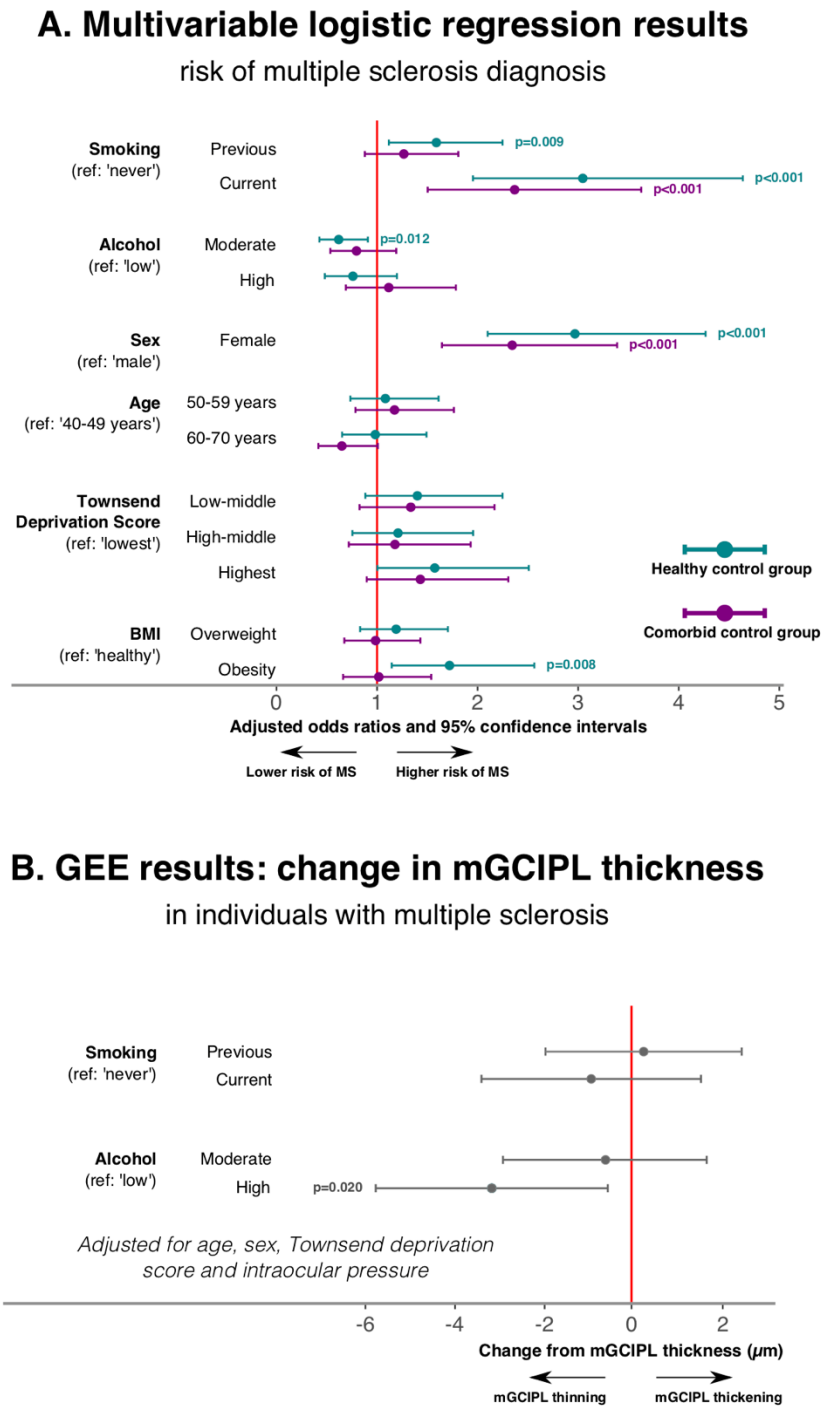

Figure 7.2 Forest plots visualising associations of modifiable risk factors with MS risk and mGCIPL thickness. A: Multivariable logistic regression results visualising factors associated with risk of being diagnosed with multiple sclerosis. Circles represent odds ratios and bars represent 95% confidence intervals. Green bars show analyses with the healthy control group and blue bars show analyses with the comorbid control group. B: Multivariable generalised estimating equations results visualising the associations with smoking status and alcohol intake (adjusted for age, sex, Townsend deprivation score and intraocular pressure) with mGCIPL thickness in individuals with multiple sclerosis. mGCIPL = macular ganglion cell and inner plexiform layer.

Compared with never having smoked, being a current or previous smoker was associated with a 3.05 (95% CI: 1.95 – 4.64) and a 1.59 (95% CI: 1.12 – 2.25) times higher odds of having an MS diagnosis when using a 'healthy' control group, and a 2.30 (95% CI: 1.48 – 3.51) and a 1.25 (95% CI: 0.88 – 1.77) times higher odds when using a 'comorbid' control group. Moderate alcohol intake was associated with lower odds of being diagnosed with MS using the 'healthy' (OR: 0.62, 95% CI: 0.43 – 0.91) but not the 'comorbid' control group (OR: 0.81, 95% CI: 0.56 – 1.18). Obesity was associated with increased odds of MS when comparing with the 'healthy' control group (OR: 1.72, 95% CI: 1.15 – 2.56). Female sex was associated with higher odds of MS, both for the 'healthy' (OR: 2.97, 95% CI: 2.10 – 4.27) and the 'comorbid' (OR: 2.28, 95% CI: 1.62 – 3.28) control group.

7.4.3. *mGCIPL thickness in MS*

Univariable associations of mGCIPL thickness with smoking status, alcohol intake, sex, age, Townsend deprivation score, BMI and intraocular pressure in individuals with MS using GEEs

		mGCIPL change µm	p-value	Trend p-value	Observations (n)
Smoking status	Never	-	-	-	164
	Previous	0.37	0.743		
	Current	-0.66	0.615		
Alcohol consumption	Low	-	-	**0.021**	
	Moderate	-0.56	0.630		
	High	-3.09	**0.020**		
Sex (male)		-1.02	0.370		
Age, per unit increase		-0.04	0.368		
Townsend deprivation score	Lowest quartile	-	-	-	
	Low-middle quartile	-0.32	0.840		
	High-middle quartile	-1.45	0.380		
	Highest quartile	-0.30	0.850		
Intraocular pressure (mmHg), per unit increase		0.21	0.170		

Table 7.3 Final multivariable generalised estimating equation (GEE) investigating the associations of smoking and alcohol with mGCIPL thickness in multiple sclerosis. Results of multivariable generalised estimating equation (GEE) model investigating the associations between alcohol consumption and smoking status with mGCIPL thickness in individuals diagnosed with MS, adjusted for confounders. Significant results in **bold.** mGCIPL = macular ganglion cell and inner plexiform layer.

are shown in table 7.2. The only significant finding was a negative association of mGCIPL thickness with high alcohol consumption (beta=-2.94 µm, p=0.020). Twenty-one individuals with MS, out of whom 17 did not smoke themselves, reported household passive smoking. Household passive smoking was not significantly associated with mGCIPL thickness (beta=-0.76 µm, p=0.615).

Exploring for potential confounders within the MS cohort revealed significant or trend associations of sex with smoking (p=0.020) and alcohol (p=0.060), Townsend deprivation index with smoking (p=0.070) and intraocular pressure with alcohol use (p=0.050). BMI was not associated with mGCIPL or either explanatory variable and was therefore not taken forward for multivariable analysis. There was no evidence of multicollinearity.

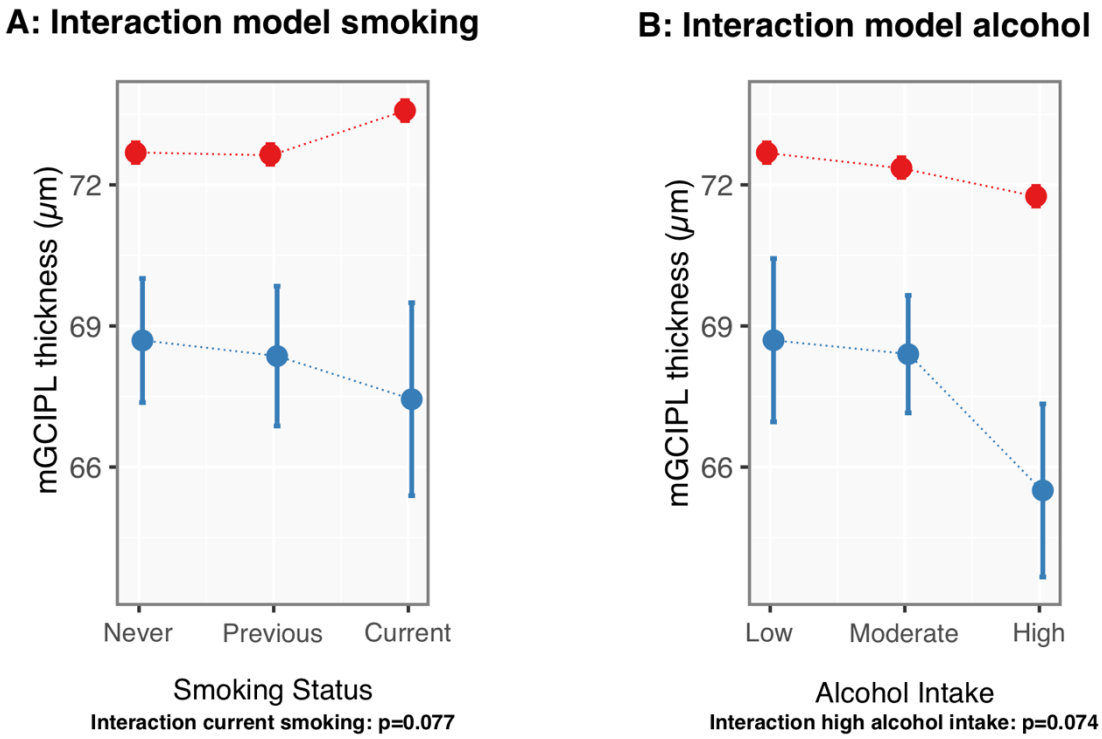

Figure 7.3 Effect modification by MS Modelled estimates of the associations of mGCIPL with alcohol consumption and smoking status for the entire cohort, plotted for individuals with multiple sclerosis and controls separately. A: interaction model including interaction term for smoking status and multiple sclerosis diagnosis. B: interaction model including interaction term for alcohol intake and multiple sclerosis diagnosis. Blue represents individuals with multiple sclerosis and red represents controls. Bars represent 95% confidence interval limits.

To explore potential multiplicative effects of combined high alcohol intake and smoking on mGCIPL thickness, a model with interaction terms for alcohol intake and smoking status variables was created (suppl. Table 7.3). None of the interaction parameters came close to the significance threshold (all p>0.100).

		mGCIPL µm change	p-value	Observations
Model 1: interaction smoking with multiple sclerosis				
Smoking status	Never	-	-	
	Previous	-0.04	0.437	
	Current	0.89	<0.001	
Alcohol consumption	Low	-	-	
	Moderate	-0.33	<0.001	
	High	-0.93	<0.001	
Multiple sclerosis diagnosis		-4.00	<0.001	
Interaction MS and smoking	MS + smoking previously	-0.29	0.784	
	MS + smoking currently	-2.14	**0.077**	72,101
Model 2: interaction alcohol use with multiple sclerosis				
Smoking status	Never	-	-	
	Previous	-0.04	0.428	
	Current	0.89	<0.001	
Alcohol consumption	Never or special occasions only	-	-	
	Drinking moderately	-0.33	<0.001	
	Daily or almost daily	-0.93	<0.001	
Multiple sclerosis diagnosis		-3.99	<0.001	
Interaction terms	MS + moderate alcohol intake	0.03	0.979	
	MS + alcohol daily or almost daily	-2.27	**0.074**	72,101

Table 7.4 Effect modification of alcohol and smoking effects by multiple sclerosis diagnosis. Interaction multivariable generalized estimating equation (GEE) models investigating if the association of smoking status (model 1) and alcohol consumption (model 2) with mGCIPL thickness is modified by a diagnosis with multiple sclerosis (MS). Model 1 includes an interaction term for MS diagnosis and smoking status, while model 2 includes an interaction term for MS diagnosis and alcohol consumption. These analyses included the entire cohort (including both the healthy and comorbid control groups).

The final multivariable GEE model, adjusted for smoking status, sex, age, Townsend deprivation score and intraocular pressure, identified a significant association of high alcohol consumption with a thinner mGCIPL thickness in individuals with MS (beta=-3.09 µm, p=0.020) (Table 7.3, Figure 7.2-B). There was a significant linear trend effect across the alcohol consumption parameters (beta=-1.55 µm, p=0.021). No significant effects were identified for previous smokers (beta=0.37 µm, p=0.743) or current smokers (beta=-0.66 µm, p=0.615), compared with never smokers. Sex, age, Townsend deprivation score and intraocular pressure were not associated with mGCIPL thickness. As a sensitivity analysis, this final GEE model was repeated after excluding the 10 non-White ethnic participants. The effect of high alcohol intake remained significant (beta=-3.01 µm, p=0.031) in this cohort, as did the dose-response effect for alcohol intake (beta= -1.52 µm, p=0.029).

7.4.4. *Effect modification MS*

The possibility of the associations of smoking and alcohol with mGCIPL thickness being modified by MS diagnosis was investigated with interaction models (Table 7.4). GEE models including individuals with and without MS were created with interaction terms for MS diagnosis and smoking status (model 1) or alcohol intake (model 2). The results of model 1 suggested that the association of smoking with mGCIPL thickness was modified by MS diagnosis, as current smoking was associated with thicker mGCIPL thickness in controls (beta=0.89 µm, p<0.001), but a thinner thickness in MS (beta=-2.14 µm, p=0.077). In model 2, high alcohol intake was associated with thinner mGCIPL thickness in control individuals (-0.89 µm, p<0.001), but the effect size of this association was substantially greater in MS (beta=-2.27 µm, p=0.074). These models suggest that the associations of high alcohol intake and current smoking with mGCIPL thickness may be modified by MS diagnosis, with both interaction terms trending towards significance (Figure 7.3).

7.5. Discussion

In this large community-based cohort, smoking was associated with increased odds of having an MS diagnosis while high alcohol consumption was associated with more severe neurodegeneration, observed as thinner mGCIPL thickness, in individuals with MS. Paradoxically, moderate alcohol intake was associated with lower odds of having been diagnosed with MS. The associations of smoking and alcohol with mGCIPL thickness may be modified by MS, as these adverse health behaviours were associated with greater relative reductions in mGCIPL thickness in individuals with MS compared with controls.

These findings replicate the well-known associations of smoking and obesity with increased odds of MS diagnosis (Marrie *et al.*, 2009; Manouchehrinia *et al.*, 2013, Thompson *et al.*, 2018*b*). Only smoking remained significantly associated with odds of having an MS diagnosis when using the comorbid instead of the healthy control group, illustrating the importance of choice of control group. Risk factors as well as protective factors associated with MS may be similar across various morbidities, which obscures associations.

In contrast, moderate alcohol consumption was associated with a lower odds of having an MS diagnosis, although this was only apparent using the healthy control group. A protective effect of moderate alcohol consumption with regards to MS risk has been described before (Hedström *et al.*, 2014; Weiland *et al.*, 2014), although an increase in MS risk associated with alcohol use has been reported as well (Pakpoor *et al.*, 2014; Abdollahpour *et al.*, 2018). In line with these findings, moderate alcohol consumption has been shown to be associated with a lower risks of cataract surgery and cardiovascular events (Rimm *et al.*, 1991; Mukamal *et al.*, 2001; Bell *et al.*, 2017; Wood *et al.*, 2018, Chua *et al.*, 2021*b*). One of the largest studies to date, that included prospective data, reported that this protective effect of alcohol is likely due to the effects of alcohol on pathways related to HDL-cholesterol (Wood *et al.*, 2018). Due to the cross-sectional nature of the current study the 'sick-quitters' effect, the tendency to quit or profoundly limit alcohol intake when ill, could have influenced these findings as this can create the impression that 'moderate' drinkers are healthier than 'never' drinkers (Davis *et al.*, 2014).

This study identified a novel association of high alcohol consumption with thinner mGCIPL thickness in MS, while there was no association with smoking. This seems to be in line with a large recent population-based study which found that alcohol consumption explained 7.7 % of variance in grey matter volume, compared with only 1.7 % that was explained by smoking status (Topiwala *et al.*, 2021). Accordingly, a previous study found that smoking was not associated with retinal thickness in MS (Rosso *et al.*, 2019). Other studies did identify significant correlations of smoking with brain atrophy in MS (Rosso and Chitnis, 2020), but these studies were not adjusted for alcohol consumption. The data reported in this study suggest that alcohol may have divergent effects on various disease processes in MS. With regards to neurodegeneration, a linear effect of alcohol on mGCIPL thickness was observed in MS, with no protective effects of moderate alcohol consumption identified. This resembles previously reported associations of alcohol consumption with brain volume in the general population (Topiwala *et al.*, 2017, 2021). However, a potential non-linear, U-shaped association was observed with regard to MS risk, with odds being lower for individuals with moderate alcohol consumption, resembling the associations of alcohol consumption with cardiac infarction and cataract surgery (Wood *et al.*, 2018, Chua *et al.*, 2021*b*).

Even though an association of high alcohol consumption with lower mGCIPL thickness was observed in MS, this is an imperfect surrogate finding for more clinically relevant metrics such as brain volume loss, disease severity or higher disability load in MS. Smoking has been shown to be associated with increased disease severity (Manouchehrinia *et al.*, 2013). In contrast, alcohol has been reported to ameliorate MS disease severity and progression (Weiland *et al.*, 2014; Hedström *et al.*, 2021), particularly in smokers (Ivashynka *et al.*, 2019), while at the same time being associated with increased cerebral lesion load (Diaz-Cruz *et al.*, 2017). But like this study, these studies were cross-sectional and the sick-quitters effect, with patients with more severe disease more likely to limit their alcohol consumption, could have influenced the results. The association of alcohol consumption with MS disease severity is complex and future prospective studies using clinically relevant outcome measures of physical and cognitive disability are needed to elucidate these questions. Importantly, it is important to recognise that the results of the current study do not provide evidence for the existence of a health benefit for MS patients to refrain from alcohol completely.

The data reported in this study suggest that associations of both smoking and alcohol with mGCIPL thickness may be modified by MS diagnosis, with individuals diagnosed with MS appearing to be more susceptible to the neurodegenerative effects of these adverse health behaviours. Although these findings just failed to reach statistical significance at the <0.05 level, these may still represent clinically important processes given their large effect sizes and known low power of interaction terms. This effect was particularly interesting for smoking, as current compared to never smokers on average had an 0.95 µm greater mGCIPL thickness in control participants, but a larger mGCIPL thickness reduction of approximately -2.14 µm in individuals with MS. Similarly, individuals with high compared with low alcohol consumption had approximately -0.89 µm thinner mGCIPL thicknesses in controls, while this difference was -2.27 µm in individuals with MS. These findings suggest that neurodegenerative processes occurring in MS may interact with neurotoxic effects of alcohol and smoking, resulting in greater neuronal cell death and axonal loss. This is biologically plausible because, although the mechanisms causing alcohol-related neurodegeneration are unclear, animal studies suggest that ethanol and its metabolite acetaldehyde are directly neurotoxic (Arendt *et al.*, 1988; McIntosh and Chick, 2004). In addition, both alcohol and smoking are related to microvascular dysfunction and oxidative stress (Ambrose and Barua, 2004; Das and Vasudevan, 2007) which could aggravate MS pathophysiological processes, given the known role of energy failure and mitochondrial dysfunction (Su *et al.*, 2013; Desai and Smith, 2017).

The strengths of this study were the large community-based dataset comprising extensive and high-quality data. Although the questionnaire on exposure status has not been formally validated, previous studies demonstrated good performance (Wood *et al.*, 2018, Chua *et al.*, 2021*b*). However, the self-reported nature of exposure status classification could have caused misclassification. This would have most likely been non-differential misclassification, biasing effect estimates to zero, although MS patients could potentially have had different likelihoods of over- and underestimating their health behaviours compared with healthy controls. Furthermore, alcohol consumption in this study was determined with regard to frequency of intake but not with regard to quantity of alcohol units consumed, as this information was missing for a large proportion of the individuals with MS. This means alcohol intake could not be more precisely quantified and the distinctive effects of binge-drinking or various alcoholic beverage types could not be distinguished, even though red wine may have specific effects on

health outcome measures, as was shown before in relation to cataract (Chua *et al.*, 2021*b*). A further limitation was the low response rate of the UKBB, with an underrepresentation of ethnic minorities and individuals with a lower socio-economic status. In particular, individuals with MS participating in the UKBB may not have been representative of the general MS population as participants may have had milder disease enabling them to travel more easily to study centres. Also, there was not sufficiently reliable information on optic neuritis status, disease duration or disability to take these factors into account which could have caused residual confounding.

7.6. Conclusion

In this large community-based cohort investigating the effects of modifiable risk factors in MS, high alcohol consumption was associated with more pronounced retinal features of neurodegeneration, even though moderate alcohol consumption was associated with lower odds of being diagnosed with MS. Smoking was strongly associated with increased odds of having an MS diagnosis. Further research is necessary to confirm the results of this study, in particular relating to the complex associations of alcohol consumption with MS disease severity. The presented findings suggest that current recommendations that exist for the entire population regarding smoking and moderating alcohol consumption may hold additional relevance for people at risk of or diagnosed with MS.

7.7. Supplementary information

		Healthy control group			Comorbid control group		
		OR	**95% CI**	**p-value**	**OR**	**95% CI**	**p-value**
Smoking status	Never	-	-	-	-	-	-
	Previous	1.51	1.08 – 2.10	0.014	1.16	0.83 – 1.61	0.370
	Current	2.89	1.90 – 4.30	<0.001	2.34	1.54 – 3.48	<0.001
Alcohol consumption	Low	-	-	-	-	-	-
	Moderate	0.51	0.36 – 0.73	<0.001	0.68	0.48 – 0.97	0.032
	High	0.63	0.41 – 0.96	0.032	0.90	0.59 – 1.37	0.626
Sex	Male	-	-	-	-	-	-
	Female	2.64	1.92 – 3.70	<0.001	2.16	1.60 – 3.03	<0.001
Age group	40-49 years	-	-	-	-	-	-
	50-59 years	1.18	0.82 – 1.74	0.380	1.12	0.77 – 1.64	0.557
	60-70 years	1.08	0.74 – 1.61	0.680	0.62	0.42 – 0.92	0.015
Townsend deprivation index	Lowest quartile	-	-	-	-	-	-
	Low-middle quartile	1.47	0.94 – 2.31	0.095	1.37	0.88 – 2.16	0.170
	High-middle quartile	1.35	0.86 – 2.14	0.200	1.29	0.82 – 2.04	0.274
	Highest quartile	1.90	1.24 – 2.94	0.004	1.67	1.10 – 2.60	0.019
BMI	Low/healthy	-	-	-	-	-	-
	Overweight	1.02	0.72 – 1.46	0.893	0.86	0.61 – 1.22	0.390
	Obese	1.56	1.05 – 2.31	0.027	0.92	0.62 – 1.36	0.680
Household passive smoking	No	-	-	-	-	-	-
	Yes	1.46	0.90 – 2.27	0.110	1.37	0.84 – 2.13	0.180

Supplementary Table 7.1 Univariable logistic regression – odds of multiple sclerosis. Results of univariable logistic regression analysis investigating the associations of modifiable risk factors (smoking status and alcohol consumption) and other covariates with the odds of having a diagnosis of multiple sclerosis (MS). Alcohol consumption is defined as follows: never or special occasions only (low), drinking once per month up to 4 times per week (moderate) or daily or almost daily (high).

		Healthy control group			Comorbid control group		
		OR	**95% CI**	**p-value**	**OR**	**95% CI**	**p-value**
Smoking status	Never	-	-	-	-	-	-
	Previous	1.59	1.12 – 2.25	0.009	1.25	0.88 – 1.77	0.200
	Current	3.05	1.95 – 4.64	<0.001	2.30	1.48 – 3.51	<0.001
Alcohol consumption	Low	-	-	-	-	-	-
	Moderate	0.62	0.43 – 0.91	0.012	0.81	0.56 – 1.18	0.258
	High	0.76	0.48 – 1.20	0.237	1.11	0.70 – 1.75	0.650
Sex	Male	-	-	-	-	-	-
	Female	2.97	2.10 – 4.27	<0.001	2.28	1.62 – 3.28	<0.001
Age group	40-49 years	-	-	-	-	-	-
	50-59 years	1.08	0.74 – 1.61	0.691	1.17	0.79 – 1.73	0.438
	60-70 years	0.98	0.65 – 1.49	0.935	0.67	0.44 – 1.01	0.051
Townsend deprivation index	Lowest quartile	-	-	-	-	-	-
	Low-middle quartile	1.40	0.88 – 2.25	0.155	1.32	0.83 – 2.11	0.240
	High-middle quartile	1.21	0.75 – 1.96	0.432	1.17	0.73 – 1.89	0.514
	Highest quartile	1.57	1.00 – 2.51	0.051	1.41	0.90 – 2.25	0.137
BMI	Low/healthy	-	-	-	-	-	-
	Overweight	1.19	0.83 – 1.71	0.342	0.99	0.69 – 1.41	0.936
	Obese	1.72	1.15 – 2.56	0.008	1.02	0.68 – 1.51	0.934

Supplementary Table 7.2 Multivariable logistic regression – odds of multiple sclerosis. Results of multivariable logistic regression analysis investigating the associations of modifiable risk factors (smoking status and alcohol consumption) with the odds of having a diagnosis of multiple sclerosis (MS), adjusted for confounders. Alcohol consumption is defined as follows: never or special occasions only (low), drinking once per month up to 4 times per week (moderate) or daily or almost daily (high).

		MS cohort			
		GCIPL change	**p-value**	**Trend p-value**	**Observations (n)**
Smoking status	**Never**	-	-		
	Previous	-1.68	0.410		
	Current	-2.26	0.280	-	
Alcohol consumption	**Low**	-	-		
	Moderate	-1.32	0.430		
	High	-4.21	**0.020**	-	
Interaction terms	**Previous smoking + drinking moderately**	1.91	0.450		
	Previous smoking + drinking daily	2.27	0.430		
	Current smoking + drinking moderately	2.54	0.360		
	Current smoking + daily drinking	1.65	0.560	-	176

Supplementary Table 7.3 Testing for multiplicative effects of Alcohol and Smoking in multiple sclerosis. Generalised estimating equation (GEE) model exploring potential multiplicative effects of alcohol consumption and smoking status on mGCIPL thickness in individuals with multiple sclerosis. The model includes an interaction term for smoking status and alcohol consumption. mGCIPL = macular ganglion cell and inner plexiform layer.

8. A 50-year history of synchronised epilepsy and relapsing optic neuritis in MOG associated disease

8.1. Background

The clinical phenotype of myelin oligodendrocyte glycoprotein (MOG) antibody associated disease (MOGAD) is diverse and ever expanding. In this brief chapter a new phenomenon in MOGAD is illustrated: the temporal synchronisation of relapsing, steroid responsive epilepsy and optic neuritis (ON) in a patient that has experienced these symptoms for almost 30 years. Retinal imaging through optical coherence tomography (OCT) is used to characterise features of this syndrome further. The 47 year long follow-up period with repeated MRI, EEG, and laboratory tests of blood and cerebrospinal fluid permits to exclude with confidence that this phenotype is due to the more commonly described association of seizure activity with ON in acute encephalitis (Foiadelli *et al.*, 2020). Autoimmune disease has opened a field for discovery of new phenotypes in clinical neurology and the unravelling of the autoimmune pathophysiology has led to successful novel treatment strategies including long-term immune suppression (Stellmann *et al.*, 2017).

8.2. Case report

A 69-year old woman with MOG associated relapsing ON reports these attacks to be often preceded by clusters of seizures. Originally, she was diagnosed with epilepsy, at the age of 22 years, after experiencing a grand-mal tonic-clonic seizure. Her seizure phenotype evolved over the years, and currently she has strictly nocturnal, complex partial seizures, with occasional tongue biting and/or brief jerking of all limbs (Figure 8.1-A). The following day she is fatigued, but she has never been encephalopathic. She also suffers from periodic limb movements during sleep which rouse her with sleep paralysis. Repeated electroencephalograms and polysomnography demonstrated a suspected left temporal epileptogenic zone with a possible spike and a run of theta activity. MRIs of the whole brain did not show signs of a focal encephalitis. Her epilepsy was treatment refractory to carbamazepine in spite of being compliant and repeated blood levels being in the therapeutic range. Her seizure frequency remained at three to four times per month. However, of interest, her seizure frequency reduced to 3-5 per year up to the present time after a second diagnosis of relapsing ON was made which changed her overall management to include steroid treatment.

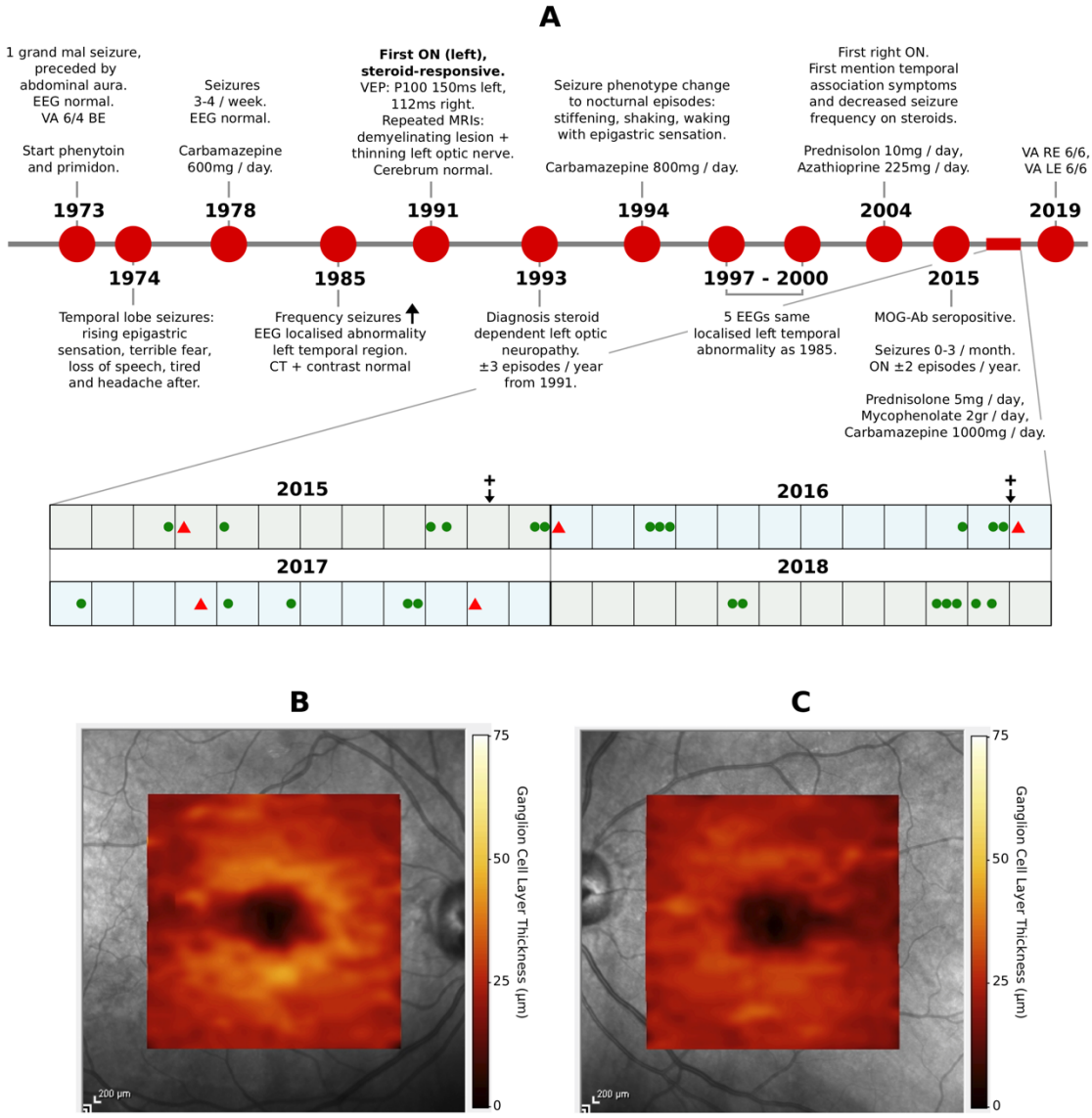

Figure 8.1 (A) Detailed timeline of evolution of clinical symptoms of the patient from 1973 to 2019. Inset below represents the diary kept by patient between 2015 and 2018, with epileptic attacks shown with green dots and ON episodes in red triangles. Within a four year period, three out of five ON relapses were preceded by increased epilepsy activity by only 1-2 days. Both seizures and optic neuritis stopped after increasing corticosteroid dosing. On some occasions seizures re-occurred upon steroid taper, as is the case with the seizures seen in October and November 2018. The timing of both positive MOG serum tests is noted with a **+**. OCT documented severe ganglion cell layer atrophy in (B) the right macula (volume 0.25mm^3 on 1, 2.22, 3.45 mm grid) and (C) more profoundly in the left macula (volume 0.20mm^3). This remained stable over the past six years. EEG: Electroencephalogram. VA: visual acuity. BE: both eyes. ON: optic neuritis. VEP: visual evoked potentials. RE: right eye. LE: left eye. MOG-Ab: myelin oligodendrocyte glycoprotein antibody.

Eighteen years after having been diagnosed with epilepsy, an independent diagnosis of left relapsing ON was made (case #14 in (Petzold *et al.*, 2019)). Serial MRI scans revealed isolated

enhancement of the left optic nerve in attacks. Brain imaging was normal and there was no evidence for a myelopathy. The ON was corticosteroid responsive and dependent (threshold at prednisolone 5.5 mg once daily), which led to a clinical diagnosis of chronic relapsing inflammatory optic neuropathy (CRION) (Kidd *et al.*, 2003). Her maintenance therapy has now been combined prednisolone and mycophenolate for over ten years. It was not until MOG-antibodies were rediscovered that evidence for the presumed autoimmune pathology underlying the clinical diagnosis of CRION could be demonstrated in 2015 (Kidd *et al.*, 2003). She tested MOG seropositive twice (Figure 8.1-A). At the time, the just reported association of MOG disease with epilepsy in acute encephalitis was considered and excluded. Panel analysis came back normal for antibodies targeting aquaporin-4, N-methyl-D-aspartate (NMDA) and voltage-gated potassium channels (CASPR-2 and LGI-1) as well as ANA, ANCA and paraneoplastic antibodies. Her cerebrospinal fluid examination was normal on two occasions, including absence of oligoclonal bands.

The patient highlighted that her ON relapses are typically synchronised with an increase in epileptic activity. Clinical advice over the past 20 years has been to increase her corticosteroid dosage immediately when noticing first ON symptoms, to protect vision (Plant *et al.*, 2011). Remarkably, this typically also arrested seizure activity. She then started to keep a detailed diary of her seizure and ON attacks. Over the four-year observation period from her diary it became evident that episodes of ON were indeed preceded by seizures 1-2 days prior for three out of five events (Figure 8.1-A). Importantly, the increased corticosteroid dose (10-20 mg once daily) always stopped the seizures and on three occasions seizures re-occurred upon oral corticosteroid taper.

At her last assessment (4/12/2019) she reported left red desaturation and had a left relative afferent pupillary deficit. Visual acuities were well preserved at 0.00 LogMAR, potentially attributable to the high-dose corticosteroid treatment that she was instructed to consistently self-initiate immediately at ON relapse (Plant *et al.*, 2011). There was bilateral optic disc pallor. Optical coherence tomography of the macula showed severe atrophy of the ganglion cell and inner plexiform layers which has remained stable over the past six years (Figure 8.1-B).

8.3. Discussion

Improved antibody detection techniques have widened the clinical spectrum of MOGAD. MOGAD currently includes ON, neuromyelitis optica spectrum disorder (NMOSD), acute or multiphasic disseminated encephalomyelitis (ADEM or MDEM), focal encephalitis and seizures (Foiadelli et al., 2020; Sato et al., 2014). A possible explanation for the wide-ranging spectrum of clinical phenotypes in MOGAD is that the MOG-antibody might not be pathogenic, but is released as a result of CNS injury. Some uncertainty remains if the MOG-antibody causes CNS injury, such as has been confidently ascertained for the AQP4-antibody, or is released as an epiphenomenon of myelin damage that occurs due to an unknown cause.

Seizures are relatively common in MOGAD, with a prevalence of 5-21 %, compared with 0.4-1 % in AQP4-antibody seropositive NMOSD (Foiadelli *et al.*, 2020). Seizure phenotypes in MOG autoimmune disease are diverse, although most have a focal onset, are monophasic and are associated with isolated or disseminated encephalitis on MRI. The majority of reported cases represents children. Several cases of concurrent ON and epilepsy in MOGAD have been reported, but these all describe mono- or biphasic disease with inflammatory lesions on MRI (Foiadelli *et al.*, 2020). Some patients have normal imaging at initial presentation but develop more extensive clinical and radiological disease shortly after. Here, a long-lasting syndrome of corticosteroid responsive epilepsy mostly synchronised with relapsing ON in adult MOGAD is described. This suggests that both conditions may be immune mediated and summarised as synchronised steroid responsive epilepsy with relapsing ON (SERON). Although this patient tested negative for antibodies associated with autoimmune epilepsy, it cannot be excluded that there is a different, unidentified, pathogenic auto-antibody. Importantly, this case highlights that MOG antibodies may be present in presumed auto-immune mediated, antibody negative epilepsy with normal brain imaging.

In conclusion, early recognition of SERON requires investigation for MOG-antibody and prompt initiation of corticosteroid treatment. The likely critical interval for starting steroids is within about 48 hours of symptoms onset (Plant *et al.*, 2011). This should be followed by a slow oral taper of corticosteroids to test for corticosteroid dependence. Epileptic activity in

patients with MOGAD may prove to commonly show a corticosteroid-responsive phenotype, as in this case.

Although ON is common and seizures are reported to occur relatively frequently in MOG-Ab seropositive patients, this is the first description of such a strong temporal association between focal seizure activity preceding ON. Early recognition of SERON will guide appropriate investigations and vision saving treatment. In this patient it has taken half a century to figure out that the synchronisation of paroxysmal attacks affecting different parts of the central nervous system were interdependent and that both disorders responded to immune suppression. It is therefore intriguing to speculate if a more careful revision of the sometimes poorly understood plethora of paroxysmal symptoms in certain patients may indeed reveal other novel phenotypes. The recognition of the synchronous appearance of such paroxysmal symptoms provides an important clinical clue. Testing for auto-antibodies and a corticosteroid trial is recommended in such cases.

9. Glutamine synthetase and GFAP to explore astrocytic damage in double seronegative NMOSD

ABSTRACT

Objective To explore levels of astrocytopathy in neuromyelitis optica spectrum disorder (NMOSD) by measuring levels of the astrocytic enzyme glutamine synthetase (GS) and glial fibrillay acidic protein (GFAP).

Methods Cerebrospinal fluid concentrations of GS and GFAP were measured by ELISA in patients with NMOSD (n=40, 28 aquaporin-4 (AQP4)-Ab-seropositive, 3 double-Ab-seronegative, 4 myelin oligodendrocyte glycoprotein (MOG)-Ab-seropositive, and 4 AQP4-Ab-seronegative with unknown MOG-Ab-serostatus), multiple sclerosis (MS) (n=69), optic neuritis (n=5) and non-neurological controls (n=37).

Results GFAP and GS concentrations differed significantly across groups (both $p<0.001$), showing a similar pattern of elevation in AQP4-Ab-seropositive NMOSD patients. GS and GFAP were significantly correlated, particularly in AQP4-Ab-seropositive NMOSD patients ($r_s=0.70$, $p<0.001$). Interestingly, GFAP levels in some double-Ab-seronegative NMOSD patients were markedly increased.

Conclusions These data indicate astrocytic injury in some double-Ab-seronegative NMOSD patients, which hints at the possible existence of yet undiscovered astrocytic autoimmune targets. Elevated GS and GFAP levels could identify those double-Ab-seronegative patients that are suitable for autoimmune screening.

9.1. Background

Neuromyelitis optica spectrum disorder (NMOSD) refers to a heterogenous group of immune mediated CNS diseases that share optic neuritis, transverse myelitis and area postrema syndrome as key clinical features (Wingerchuk *et al.*, 2015).

In recent years understanding of NMOSD has considerably advanced through the identification of two autoimmune targets. The first auto-antibody that was recognised targets aquaporin-4 (AQP4), a water channel which is expressed in astrocytic foot processes (Lennon *et al.*, 2004). Accordingly, AQP4 targeted autoimmune activity results in profound astrocytopathy, a feature that is distinct from multiple sclerosis (MS) (Papadopoulos and Verkman, 2012, Wei *et al.*, 2018*a*). The subsequently identified myelin-oligodendrocyte glycoprotein (MOG) auto-antibodies damage oligodendrocytes and myelin, but do not cause astrocytic injury (Sato *et al.*, 2014*a*; Ikeda *et al.*, 2015; Kaneko *et al.*, 2016; Wang *et al.*, 2016).

Identification of these antibodies has facilitated diagnostic procedures, broadened the clinical spectrum and helps guide treatment decisions in NMOSD (Fujihara, 2019; Pittock *et al.*, 2019). However, some patients present with a clinical phenotype that is consistent with NMOSD, but do not express AQP4 or MOG antibodies (Ab) (Jiao *et al.*, 2013). The response to immunosuppression in these patients suggests a possible autoimmune pathology, but the autoimmune target remains unknown (Mealy *et al.*, 2018).

Glial Fibrillary Acidic Protein (GFAP), a part of the astrocyte cytoskeleton, is a very useful biomarker when investigating astrocytic damage (Petzold, 2015). A very substantial increase in cerebrospinal fluid (CSF) GFAP levels during AQP4-Ab-seropositive NMOSD relapses has consistently been reported, and some reports also show low levels of GFAP in MOG-Ab-seropositive disease (Misu *et al.*, 2009; Petzold *et al.*, 2010; Takano *et al.*, 2010; Ikeda *et al.*, 2015; Kaneko *et al.*, 2016, Wei *et al.*, 2018*b*, *a*; Watanabe *et al.*, 2019).

One disadvantage of using GFAP as a biomarker, however, is its poor solubility which limits the sensitivity of the test (Petzold, 2015). In order to strengthen the laboratory approach for characterising the widening spectrum of autoimmune astrocytopathies, a novel assay to

detect the predominantly astrocytic enzyme glutamine synthetase (GS) was developed (Herbert *et al.*, 2012). In contrast to GFAP, GS is highly soluble, facilitating detection (Tumani *et al.*, 1995; Bernstein *et al.*, 2014).

9.2. Aims, objectives and hypotheses

9.2.1. *Aims and objectives*

The main aim of this international multicentre study is to investigate astrocytopathy across the full NMOSD spectrum, including double-Ab-seronegative patients, to gain insight into the pathophysiological processes at play. The objective is to better characterise the pathophysiology of seronegative NMOSD.

9.2.2. *Hypotheses*

The main hypothesis of this study is that if astrocytopathy is a feature of seronegative NMOSD, this will be reflected by increased level of CSF GFAP in these patients. A subsidiary hypothesis is that complement mediated damage to astrocytes would not only release GFAP but also GS. Therefore, CSF levels of GS in NMOSD should reveal a similar pattern to what is observed for GFAP (Marignier *et al.*, 2010; Petzold, 2015).

9.3. Methods

9.3.1. *Patients and non-neurological controls*

This retrospective study included patients with NMOSD, MS and optic neuritis (ON) from five centres. These were Hôpital Neurologique Pierre Wertheimer (Lyon, France), Clinic of Neurology (Dietenbronn, Ulm, Germany), Radboud Medical Centre (Nijmegen, Netherlands), Hospital das Clinicas da Faculdade de Medicina (Sao Palo, Brazil) and IDIBAPS (Barcelona, Spain) (Supplementary table 9.1). Diagnosis of NMOSD was made according to criteria published by Wingerchuk et al. (2015) (Wingerchuk *et al.*, 2015). MS patients that had undergone lumbar puncture as part of diagnostic procedure were recruited. MS patients were diagnosed according to criteria published by Polman et al. (2005) and all had a long clinical follow-up, during which they displayed a typical disease phenotype (Polman *et al.*, 2005). ON patients were diagnosed according to published criteria (Petzold *et al.*, 2014) and did not fulfil diagnostic criteria for NMOSD or MS.

Age-matched non-neurological controls were selected from a database of patients referred to the Neurology department in the Radboud University Medical Centre in Nijmegen during the period 2001 to 2009, who underwent lumbar puncture as part of the diagnostic work-up and were confirmed to not have neurological disease. For these patients all routine CSF parameters were normal.

9.3.2. *Approvals and consents*

The CSF samples were collected according to standard protocols with local ethics approval (Teunissen *et al.*, 2009). At the time of collection all patients from the Nijmegen centre gave informed consent to lumbar punctures, including later use for scientific purposes but written consent from the patients was legally not required for these analyses. Written informed consent was obtained from all patients from other participating centres.

9.3.3. *CSF samples*

CSF samples were collected in polystyrene or polypropylene tubes, centrifuged (5 minutes, 860 g at room temperature), and stored at -80 °C. For storage purposes, 20 MS samples had

been moved to storage at -20°C, but not more than six months prior to analysis. Patient information was encoded to maintain confidentiality.

9.3.4. *GFAP ELISA*

GFAP levels were measured using a home-made sandwich ELISA (linear up to 250 µg/L; inter-assay variation coefficient <14 %) as previously described (Geel *et al.*, 2002).
For six French patients with NMOSD, GFAP levels have been published previously and sample volumes were too small to repeat the test (Petzold *et al.*, 2011). These data were excluded from analysis, because these data were based on a different method and GFAP levels were not directly comparable. Because of insufficient CSF material GFAP measurements could not be performed for nine additional subjects (2 AQP4-Ab-seropositive, 2 MOG-Ab-seropositive, 1 double-Ab-seronegative NMOSD, 2 MS patients and 2 controls).

9.3.5. *GS ELISA*

GS levels in CSF were measured using the previously published home-made sandwich ELISA incorporating an acidification and neutralisation step for enhanced detection (Herbert *et al.*, 2012).

9.3.6. *AQP4-IgG antibody assay*

State of the art cell-based assays were used for AQP4-Ab in the French (Marignier *et al.*, 2013), German (Waters *et al.*, 2016), Brazilian (Sato *et al.*, 2014*b*) and Spanish cohorts (Höftberger *et al.*, 2013, 2015).

9.3.7. *MOG-IgG antibody assay*

MOG-Ab-serostatus was retrospectively identified from chart study. MOG-IgG Ab status was assessed in local laboratories by cell-based assay.

9.3.8. *Statistical analysis*

Categorical variables were described by counts and percentages, and continuous variables by median and interquartile ranges (IQRs). Distribution of age and gender was tested with the

Kruskal-Wallis test and Fisher exact test respectively. GS and GFAP levels were compared across groups by the Kruskal-Wallis test. Post-hoc analysis was performed with Dunn Test, with p-values adjusted for multiple comparisons with the Benjamini-Hochberg method. Correlations were performed by Spearman's rank analysis (r_s = Spearman's rho). Multivariate logistic regressions were used to check for distributions of CSF GS and GFAP across groups with two potential confounding factors, age and gender. Results were given with odds ratios (OR) and p-values. In the figures GFAP has been log transformed after adding 1 (log10(GFAP+1)) for visualisation purposes. Performance of GFAP and GS in discriminating for both NMOSD status and AQP4-Ab-seropositive NMOSD status were analysed by plotting receiver operating characteristics (ROC) curves and calculating associated area under curve (AUC) with corresponding 95% confidence interval (CI). Optimally effective cut-off values were calculated using the Youden Index. Statistical threshold of $p<0.05$ was used and data were analysed using R and RStudio.

9.4. Results

9.4.1. *Subject characteristics*

Forty patients with NMOSD were recruited. Out of these, 28 were AQP4-Ab-seropositive, four were MOG-Ab-seropositive, three were double-Ab-seronegative and four were AQP4-Ab-seronegative but had an unknown MOG-Ab-serostatus. Additionally, 69 patients with MS, five patients with ON and 37 non-neurological control subjects were included (Table 9.1). The baseline characteristics are summarised in Table 9.1. Mean age trended towards being lower for MOG-Ab seropositive patients, but this was not significant (p=0.057). There was a female predominance in the MS and NMOSD groups compared to controls, as is demographically expected, but this difference just failed to reach significance (p=0.051). For all NMOSD patients, and for most MS and ON patients, CSF was obtained acutely during a clinical relapse without concomitant treatment.

	Controls	MS	Optic Neuritis	AQP+ NMOSD	MOG+ disease	Double-Ab neg NMOSD	Unknown MOG NMOSD	p-value
N	37	69	5	28	4	3	4	
Gender F/M (%F)	19/18 (51 %)	52/17 (75 %)	4/1 (80 %)	22/5 (81 %*)	3/1 (75 %)	1/2 (33 %)	2/2 (50 %)	0.051[a]
Mean age (sd)	43.2 (11.1)	42.1 (10.6)	39.8 (9.5)	48.11 (17.5)	25.0 (24.1)	56.0 (4.4)	37.3 (14.0)	0.057[b]
GFAP ng/mL median (IQR)	0.500 (0.825)	0.60 (0.750)	0.20 (0.40)	5.40 (37.85)	0.00 (0.00)	76.7 (46.85)	0.68 (0.08)	<0.001[b]
GS µg/L median (IQR)	235.4 (249.0)	329.4 (315.0)	223.4 (131.0)	490.7 (407.2)	246.4 (74.0)	452.0 (309.0)	487.2 (221.2)	<0.001[b]

Table 9.9.1 Baseline cohort characteristics and CSF parameters.[a] Fisher exact test. [b] Kruskall-Wallis test for non-parametric data. * Gender data missing for 1 AQP4-Ab-seropositive NMOSD patient. GFAP: Glial Fibrillary Acidic Protein; GS: Glutamine Synthetase; MS: multiple sclerosis; NMO+: AQP4-Ab-seropositive NMOSD; NMO-: AQP4-Ab-seronegative NMOSD; ON: optic neuritis; IQR: interquartile range.

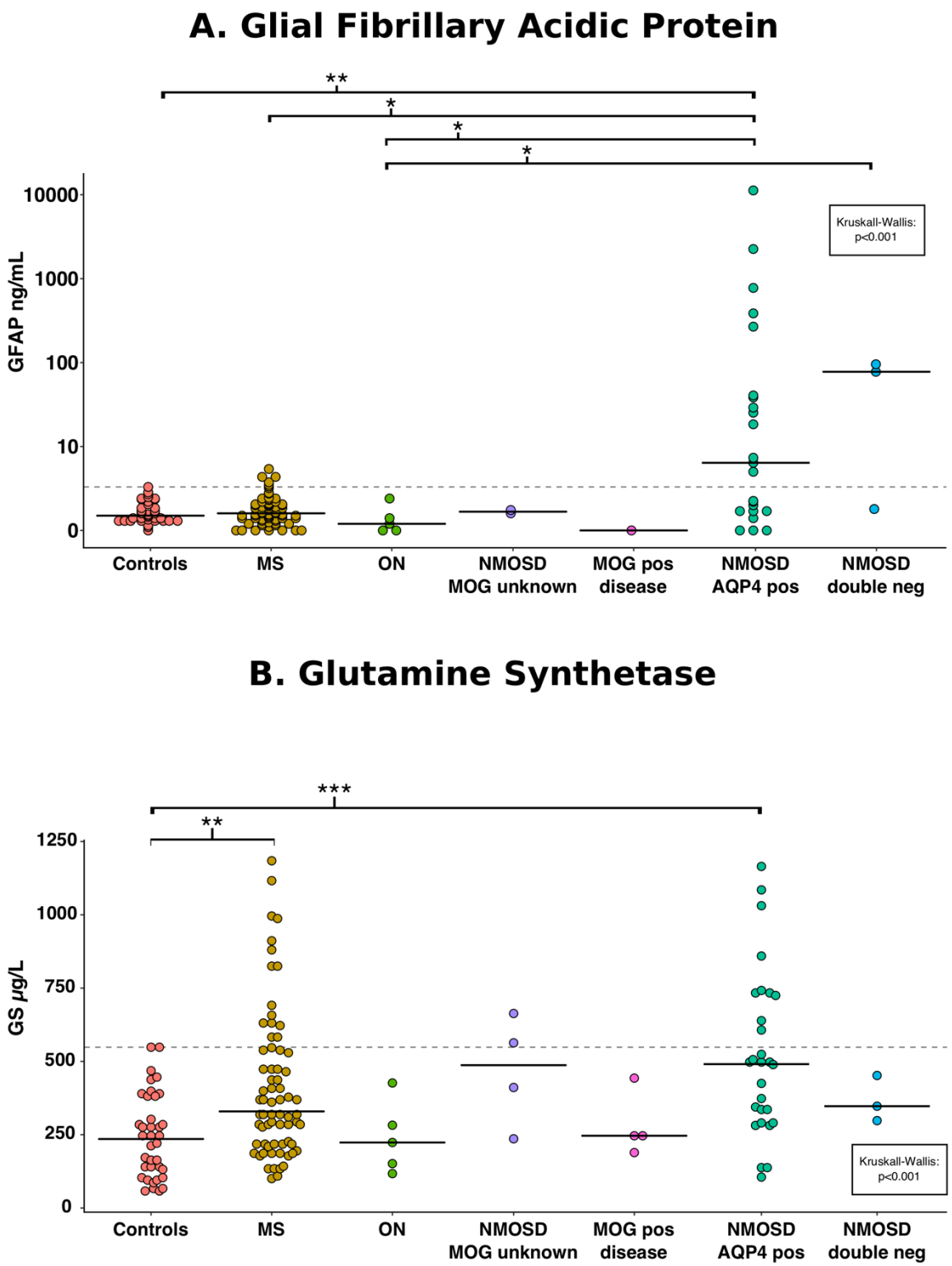

Figure 9.1 GFAP and GS levels across groups. A: CSF GFAP levels in ng/mL of non-neurological control subjects, patients with MS, ON and NMOSD (sub-grouped into AQP4-Ab-seropositive, MOG-Ab-seropositive, double-Ab-seronegative and AQP4-Ab-seronegative with unknown MOG-Ab serostatus). GFAP has been log transformed after adding 1 (log10(GFAP+1)) for visualisation purposes. B: CSF GS levels in µg/L across groups. The grey dotted lines represent the highest measured GFAP and GS concentrations in non-neurological control subjects.* = p<0.05; ** = p<0.01; *** = p<0.001; Controls = non-neurological control subjects; MS = Multiple Sclerosis; NMOSD = neuromyelitis optica spectrum disease; NMO+ = AQP4-Ab-seropositive NMOSD, NMO- = AQP4-Ab-seronegative NMOSD; ON = optic neuritis.

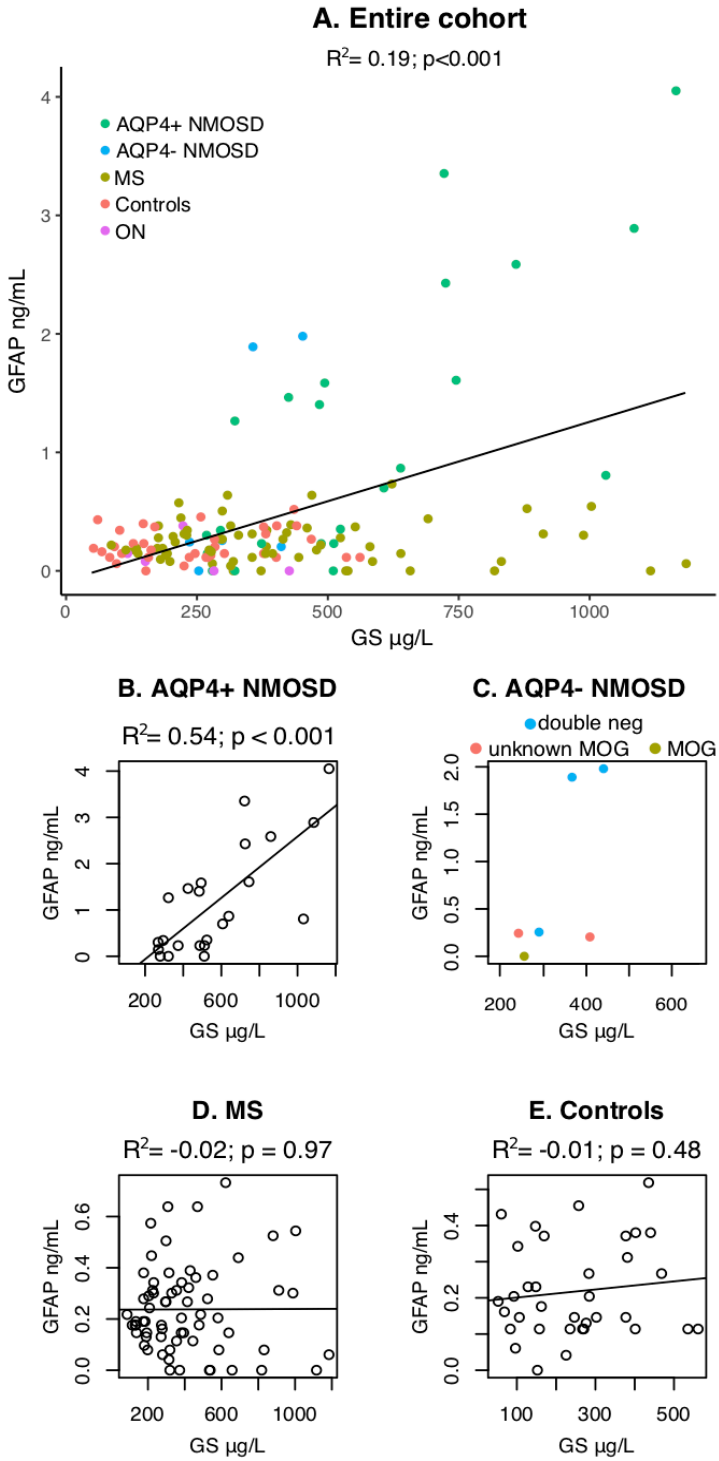

Figure 9.2 Correlations GFAP and GS.A. linear regression showing significant positive relationship of GFAP and GS in the entire cohort with colour coding of the dots for the different subgroups. **B**. scatter plot with linear regression line showing the particularly strong positive relationship of GFAP and GS in the AQP4-Ab seropositive NMOSD group. **C**. colour coded scatter plot of GFAP versus GS levels across groups. **D**. non-significant relationship between GFAP and GS in the multiple sclerosis (MS) cohort. **E**. non-significant relationship between GFAP and GS in the non-neurological control cohort. GFAP + 1 was log transformed for visualisation purposes.

9.4.3. *Storage conditions*

Neither GS nor GFAP levels were influenced by the storage conditions (-20^{o} C versus -80^{o} C; p>0.05).

9.4.4. *CSF GFAP levels*

Distribution of GFAP levels differed significantly across groups (p<0.001). Median GFAP levels were significantly higher for patients with AQP4-Ab-seropositive NMOSD (5.40 ng/mL) compared with MS patients (0.60 ng/mL, p=0.010), ON patients (0.20 ng/mL, p=0.014) and non-neurological controls (0.50 ng/mL, p=0.007).

Interestingly, GFAP concentrations that were substantially higher than the highest measured in non-neurological controls (2.30 ng/mL) were observed exclusively in AQP4-Ab-seropositive NMOSD and double-Ab-seronegative NMOSD (Figure 9.1), although there were six MS patients with a slightly higher GFAP concentration. Furthermore, median GFAP levels for double-Ab-seronegative patients were significantly increased compared with ON patients (p=0.046).

Multivariate logistic regression showed that GFAP levels predicted diagnosis of NMOSD (OR=1.59; p=0.0257) independent of age and gender (OR=0.99; p=0.657 and OR=0.79; p=0.704). Additionally, prediction of AQP4-Ab-seropositive NMOSD specifically was nearly significant (OR=1.34; p=0.060) independent of age and gender (OR=1.05; p=0.163 and OR=2.41; p=0.096)

9.4.5. *CSF GS levels*

Like GFAP, distribution of GS levels differed significantly across groups (p<0.001). GS levels were significantly higher for patients with AQP4-Ab-seropositive NMOSD (median 490.7 µg/L; p<0.001) and MS (median 329.4 µg/L, p=0.003) compared with non-neurological controls (median 235.4 µg/L).

Multivariate logistic regression showed that GS levels predicted diagnosis of NMOSD (OR=1.10; p=0.003) independent of age and gender (OR=1.03; p=0.098 and OR=0.97; p=0.939). Furthermore, GS was a significant predictor of AQP4-Ab-seropositive NMOSD

(OR=1.12; p<0.001) specifically, alongside age (OR=1.05; p=0.006) but independent of gender (OR=0.65; p=0.442).

Interestingly, an overall positive correlation between GS and GFAP levels was observed (r_s=0.23, p<0.001), which was particularly strong in AQP4-Ab-seropositive NMOSD (r_s=0.70, p<0.001) but absent for the MS group (r_s=-0.02, p=097) and controls (r_s=0.07, p=0.48) (Figure 9.2)

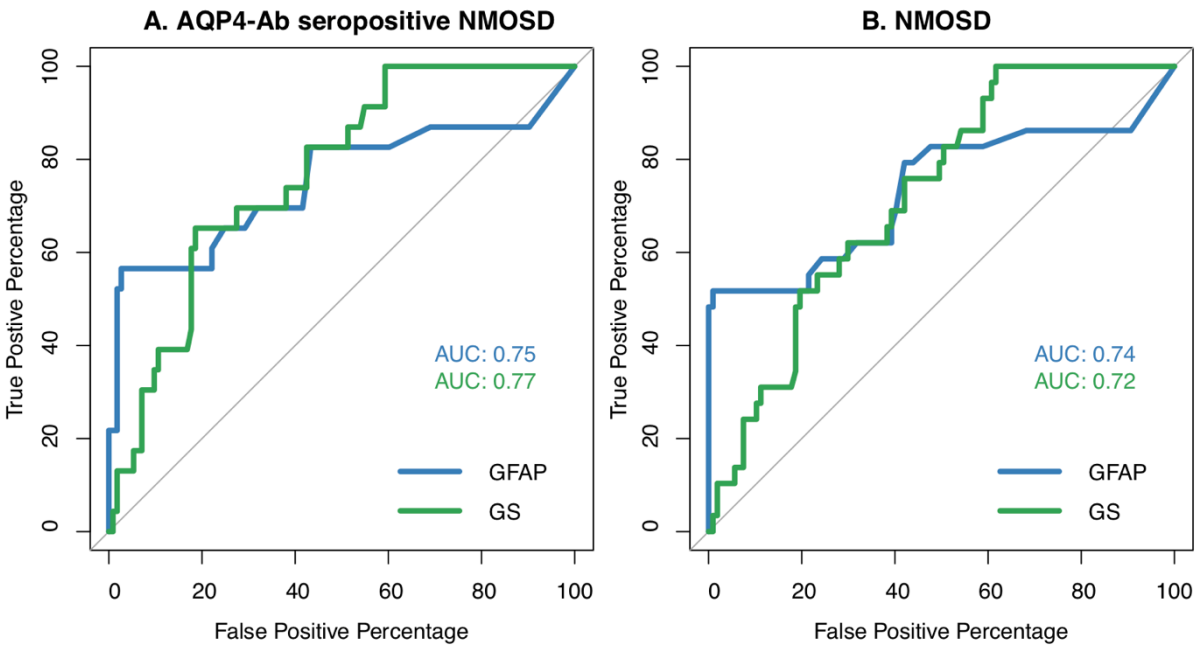

Figure 9.3 ROC curves GS and GFAP A. Receiver operating characteristic (ROC) curve of the discriminative performance for the astrocytopathy AQP4-Ab-seropositive NMOSD of GFAP (blue line) and GS (green line). B. ROC curve of the discriminative performance for NMOSD of GFAP (blue line) and GS (green line).

9.4.6. *Diagnostic performance for astrocytopathy*

The AUC of the ROC curves in discriminating for AQP4-Ab-seropositive NMOSD status was 0.75 (95% CI: 0.61-0.89) for GFAP and 0.77 (95% CI: 0.67-0.86) for GS. The AUC of the ROC curves for identifying all types of NMOSD were slightly lower for both GFAP (0.74; 95% CI: 0.61-0.86) and GS (0.72; 95% CI: 0.63-0.82) (Figure 9.3). The optimally effective cut-off of GFAP concentration to identify AQP4-Ab-seropositive NMOSD was 4.0 ng/mL, with an associated specificity of 97 % and sensitivity of 57 %. The optimally effective cut-off for GS was 268.4 µg/L, with an associated sensitivity of 89 % and specificity of 41 %. The negative predictive value of a GS level lower than 268.4 µg/L was 94 %. So, GS can achieve a substantially higher

sensitivity but a lower specificity for AQP4-Ab-seropositivity compared with GFAP. This is in line with the observation that all of the 10 AQP4-Ab-seropositive NMOSD patients that had GFAP levels below the identified threshold of 4.0 ng/mL, did have GS levels higher than the threshold of 268.4 µg/L.

9.5. Discussion

Here, CSF levels of astrocytic biomarkers GS and GFAP in NMOSD, MS, ON and non-neurological controls were reported. Levels of both biomarkers were highest in AQP4-Ab-seropositive NMOSD. The strong correlation between GS and GFAP in AQP4-Ab-seropositive NMOSD suggests that GS is released as a result of astrocytic injury in these patients. GS has a higher sensitivity, but a lower specificity, to astrocytopathy compared with GFAP. Additionally, a subset of double-Ab-seronegative NMOSD cases had substantially increased GFAP levels. This observation suggests astrocytic damage in some double-Ab-seronegative NMOSD patients and hints at the existence of a yet unidentified astrocytic autoimmune target in this group.

These data replicate prior reports showing that CSF GFAP is increased in AQP4-Ab-seropositive NMOSD but not in MOG-Ab-seropositive NMOSD (Misu *et al.*, 2009; Petzold *et al.*, 2010, 2019; Takano *et al.*, 2010; Ikeda *et al.*, 2015; Kaneko *et al.*, 2016, Wei *et al.*, 2018*b*, *a*). These results are in line with current understanding of NMOSD pathophysiology, as AQP4-Ab-seropositive NMOSD is an autoimmune astrocytopathy, while MOG-Ab-mediated disease results in oligodendrocytic injury but no astrocytopathy (Papadopoulos and Verkman, 2012; Fujihara, 2019). Interestingly, the very substantial increases of GFAP were not exclusive to AQP4-Ab-seropositive NMOSD, but also occurred in double-Ab-seronegative NMOSD. This observation appears robust as it has been described before (Wei *et al.*, 2018*a*) and hints at the existence of one or more yet unidentified auto-antibodies targeting astrocytes in a subset of double-Ab-seronegative NMOSD patients. A high CSF GFAP concentration may be used to identify those double-Ab-seronegative NMOSD patients with evidence of astrocytopathy that are suitable for in-depth autoimmune screening using labour intensive clonal expansion techniques. Furthermore, double Ab-seronegative NMOSD patients pose a substantial diagnostic challenge, given the lack of a reassuring immunological marker (Wingerchuk *et al.*, 2015). Diagnosis is based solely on clinical and radiological features, resulting in uncertainty when making treatment decisions. A substantially elevated GFAP in these double-Ab negative patients might reinforce diagnosis of NMO and help guide clinical decision making in some patients.

This is the first study to report on GS levels in NMOSD and related disorders. It was shown that CSF levels of this astrocytic enzyme correlate with GFAP levels, especially in AQP4-Ab-seropositive NMOSD, indicating CSF GS may rise as a result of astrocytic damage, as has been suggested previously (Marignier *et al.*, 2010). Furthermore, GS and GFAP levels showed a similar pattern of elevation in AQP4-Ab-seropositive NMOSD, while levels in MOG-Ab-seropositive disease appeared to be generally low. However, in contrast to GFAP, GS levels were elevated in MS compared with control subjects as well. This might be because GS, although primarily an astrocytic enzyme, is expressed by oligodendrocytes to some degree as well (D'Amelio *et al.*, 1990). Oligodendrocytes are severely damaged in MS and GS immunoreactivity is reduced in MS brain lesions compared with unaffected and control tissues (Werner *et al.*, 2001). Additionally, the observed increases of GS in MS and NMOSD patients could partly arise due to leakage of systemic GS across the blood-brain barrier into the CSF, as the blood-brain-barrier is compromised in both disorders. ROC curves of GS and GFAP levels had similar AUCs when testing discriminative performance for AQP4-Ab-seropositive NMOSD. GS provides higher sensitivity compared with GFAP, although specificity for astrocytopathy is relatively low. As GS is elevated more generally in neuroinflammatory disease, it is not a more advantageous diagnostic test for NMOSD compared with GFAP. However, GS appears to be a more sensitive marker of astrocytopathy that could be useful to identify astrocytic injury in seronegative NMOSD patients that fulfil the stringent diagnostic criteria. The high negative predictive value of 94 % associated with GS, suggests that a level below the threshold predicts the absence of astrocytopathy with high accuracy.

The recently described disease entity GFAP autoimmune astrocytopathy may represent the underlying pathophysiologic mechanism in some of the double-Ab-seronegative NMOSD with signs of astrocytopathy (Fang *et al.*, 2016). However, currently there is still some uncertainty if GFAP autoimmunity is a primary disease process or a downstream effect of some forms of astrocytic injury (Zekeridou *et al.*, 2018). In the future measuring GFAP in the serum may be a less invasive alternative to CSF measurements, as serum GFAP levels have been shown to be increased in NMOSD as well (Watanabe *et al.*, 2019). An important consideration when talking about double-Ab-seronegative NMOSD diagnosis is the possibility of false-negative AQP4- or MOG-Ab results. In this study all antibody assessments were based on highly sensitive cell-based assays, minimising risk of false-negatives (Jiao *et al.*, 2013).

A limitation of this study was the limited available clinical data, especially regarding details on timing of symptom onset relative to CSF acquisition and disability severity, which influences GFAP levels (Petzold, 2015). Furthermore, because CSF volume was limited not all GFAP measurements could be repeated for all patients with the same immunoassay resulting in missing data. Future immunohistochemical analysis of GS and GFAP in NMOSD patients is needed to confirm the potential role of GS as a CSF biomarker for astrocyte injury

9.6. Conclusion

These results indicate there may be one or more yet unidentified astrocytic autoimmune targets in double-Ab-seronegative NMOSD patients. Screening of double-Ab-seronegative NMOSD patients for GFAP and GS may identify a subgroup of patients with evidence of astrocytopathy that are suitable for in-depth autoimmune screening to identify a possible new astrocytic immune target. GS has suitable properties for screening purposes, while GFAP can be used as a confirmatory test.

9.6.1. *Supplementary data*

Recruitment site	Controls	MS	Optic Neuritis	AQP+ NMOSD	MOG+ disease	Double-Ab neg NMOSD	Unknown MOG NMOSD
	Non-neurological controls	2005 criteria[23] + typical follow-up	2014 review[24]	2015 criteria[1]	2015 criteria[1]	2015 criteria[1]	2015 criteria[1]
Hôpital Neurologique Pierre Wertheimer, Lyon, France (n)	-	-	-	6	3	1	2
Clinic of Neurology Dietenbronn, Ulm, Germany (n)	-	1	-	3	-	1	2
Radboud Medical Centre, Nijmegen, Netherlands (n)	37	59	4	-	-	-	-
Hospital das Clinicas da Faculdade de Medicina, Sao Paolo, Brazil (n)	-	9	1	13	1	0	-
IDIBAPS, Barcelona, Spain (n)	-	-	-	6	-	1	2

Supplementary Table 9.1 Overview of number of cases included from the participating centres.

10. Summary, Discussion & Future Outlook

10.1. Summary

This thesis aimed to investigate neuroinflammatory disease through retinal imaging and biomarkers. Part 1 explored macular dysfunction in acute neuroinflammatory disease, presented two novel analysis techniques to investigate outer retinal function and metabolic health with optical coherence tomography (OCT) and included pilot OCT-angiography (OCTA) data. First, in chapter 2 a study that investigated the structure-function correlations of retinal dysfunction in acute optic neuritis was discussed. This study identified evidence for macular dysfunction in the acute stages of optic neuritis, and revealed that this might contribute to visual loss in these patients. Identified structure-function correlations with the inner nuclear layer (INL) seem to suggest that pathologic processes within this layer are important contributors to optic neuritis pathophysiology. Subsequently, chapter 3 discussed the development of a novel dark-adaptation optical coherence tomography (OCT) protocol and showed that dynamic light-associated compression of the outer retinal layers occurs consistently in healthy controls. Data from a pilot cohort seemed to suggest that this dynamic thickness change was reduced or absent in patients with acute optic neuritis, which was hypothesised to potentially be due to metabolic failure in these patients, given the known high energy demands of the retina during dark adaptation. In chapter 4 the development and performance of a novel analysis tool that extracts ellipsoid zone (EZ) reflectivity from OCT scans were discussed. EZ reflectivity may be an in-vivo non-invasive measure of mitochondrial health, as the high reflectivity of the EZ is likely due to local accumulation of mitochondria and the light scattering properties of mitochondria are known to be influenced by their metabolic status and health. Relative EZ reflectivity was shown to be reduced in neuroinflammatory disease, both in its acute stages, as evidenced in patients with acute optic neuritis, as well as in its chronic stages, as evidenced in multiple sclerosis (MS) patients with primary progressive optic neuropathy. Further consolidating the association of EZ reflectivity with mitochondrial health, patients with mitochondrial disease (chronic progressive external ophthalmoplegia and dominant optic atrophy) were shown to have a lower EZ reflectivity. Finally, chapter 5 presented limited pilot OCT-angiography (OCTA) data in acute optic neuritis patients. These data hinted that retinal vascular density may be reduced in both the affected and fellow eyes of acute optic neuritis patients.

Part 2 of this thesis had a more clinical focus. First the clinical and imaging characteristics of a cohort of MS patients with the rare clinical phenotype of primary progressive optic neuropathy (PPON) were described in chapter 6. It was shown that these patients have particularly severe retinal atrophy and are more likely to be male, similar to the demographics of primary progressive MS. Treatment with corticosteroids was (transiently) beneficial in some of these patients. Chapter 7 presented the findings of a study investigating the associations of modifiable risk factors (smoking and alcohol consumption) with disease risk and neurodegeneration in MS, by analysing of a large cohort of participants in the UK Biobank. This study replicated well-known associations with smoking and increased odds of MS diagnosis, but also identified a potential protective effect of moderate alcohol consumption. Furthermore, high alcohol consumption was associated with thinner retinal thickness measures, possibly reflecting an increased rate of brain atrophy given the known associations between retinal thickness and brain volume. The subsequent two chapters focused on describing and elucidating the pathophysiology of rare phenotypes of neuromyelitis optica spectrum disorder (NMOSD) and related diseases. In chapter 8 a myelin oligodendrocyte glycoprotein (MOG) seropositive case with an exceptionally long history of approximately 50 years of relapsing episodes with often simultaneously occurring steroid responsive epilepsy and optic neuritis. Finally, a study exploring astrocytopathy in NMOSD by measuring levels of biomarkers in the cerebrospinal fluid was presented in chapter 9. Results revealed that levels of these biomarkers were significantly elevated in patients with seronegative NMOSD, indicating that astrocytopathy may be an important pathophysiological process in these patients.

10.2. Discussion

The studies described in the first section of this thesis shared a focus on outer retinal changes and energy failure in neuroinflammatory disease, particularly in acute optic neuritis. There were some striking consistencies across the studies in section 1. Chapter 2 identified evidence for macular dysfunction in the affected eyes of acute optic neuritis patients, which could be related to the reduction in dynamic outer retinal thickness changes in these eyes described in chapter 3. Furthermore, the loss of EZ reflectivity in these patients described in chapter 4 and the OCTA data presented in chapter 5 hinted that mitochondrial function and vascular perfusion may be reduced in patients with acute optic neuritis compared with healthy

controls. All these findings consistently indicate that outer retinal changes, different from the well-established atrophy of inner retinal layers, occur within the context of neuroinflammatory disease. In contrast, there were also inconsistencies across the work presented in these chapters, particularly related to abnormal findings being restricted to affected eyes or findings being similar across both eyes of patients. Chapter 2 identified evidence for more severe macular dysfunction in the affected eye compared with the fellow eye, which partly recovered during follow-up. This suggests that macular dysfunction is increased in the context of acute inflammatory insult. Similarly, there was some suggestion that dark-adaptation deficits were more severe for affected compared with fellow eyes, although this is difficult to establish given the very limited sample size. In contrast, EZ reflectivity and vascular density appeared to be reduced to a similar degree in both eyes of patients with acute optic neuritis compared with healthy controls. These findings indicate that a background level of mitochondrial dysfunction and hypoperfusion occur in patients with MS or clinically isolated syndrome (CIS), independently from acute inflammatory activity. This would be in line with previous work finding evidence for increased mitochondrial DNA levels in CIS (Fissolo *et al.*, 2019), or in MS independent from disease duration (Varhaug *et al.*, 2017). Preliminary work investigating mitochondrial complex activity in serum monocytes has also identified reductions in mitochondrial function for MS patients (Hargreaves *et al.*, 2018; Gonzalo *et al.*, 2019). These differences between healthy controls and patients with acute optic neuritis could either represent established damage due to subclinical previous inflammatory damage, or may represent a background level of metabolic dysfunction that increases susceptibility to inflammatory events. In conclusion, the data presented in section 1 provide interesting new insights into the possibilities of investigating metabolic function non-invasively and also seem to consolidate the existence of metabolic failure in MS, both in its acute stages (such as in CIS) and in chronic disease (such as in PPON). The EZ reflectivity measure in particular may contribute a metric of metabolic failure or chronic progressive features in MS. EZ reflectivity likely visualises disease mechanisms other than inflammation, as chapter 4 of this thesis found no evidence for an association with optic neuritis, acutely or during follow-up. However, when interpreting the findings of section 1 it is important to consider the limitations of these studies. These are discussed in detail in each chapter separately, but most importantly relate to small sample sizes and retrospective data analysis.

The second section of this thesis had a more clinical focus and illustrates the utility of OCT in investigating neurodegeneration in neuroinflammatory disease. Chapter 6 showed that OCT scanning can identify differences in retinal features of patients with primary progressive optic neuropathy, with subjects showing severe retinal atrophy and a strikingly high prevalence of microcystic macular oedema (MMO) at 50 %. Chapter 7 illustrated the value that OCT has to investigate neurodegeneration through retinal imaging, as a surrogate marker for brain atrophy. These data showed that neurodegeneration in MS is likely increased in patients that have a high alcohol consumption, while smoking in MS patients trended towards being associated more neurodegeneration compared with control subjects. Data in chapter 6 and chapter 7 relate back to section 1, as energy failure may partly drive the retinal atrophy that is observed. Changes in mitochondrial function or morphology may play a role in primary progressive optic neuropathy, as EZ reflectivity was markedly reduced in these patients. More tangentially, metabolic failure could accelerate neurodegeneration in MS patients that smoke or have a high alcohol consumption, as both alcohol and smoking are related to microvascular dysfunction and oxidative stress (Ambrose and Barua, 2004; Das and Vasudevan, 2007). Chapter 8 describes a novel phenotype within the ever-expanding spectrum of MOG associated disease, and uses OCT to objectively measure the treatment success of hyperacute steroid treatment in this patient. Finally, chapter 9 uses cerebrospinal fluid (CSF) biomarkers to explore pathophysiology, relating to astrocytopathy, in the rare subtype of seronegative NMOSD. This chapter illustrates the utility of laboratory-based biomarkers in classifying neuroinflammatory disease. Combining CSF or serum biomarkers with retinal imaging, as suggested in 10.3 below, may improve understanding of pathophysiology in the various phenotypes of MS and NMOSD.

10.3. Future outlook

The work described in this thesis leaves several open-ended questions that serve as inspiration for future research. The findings presented in chapter 2, identifying evidence for outer retinal dysfunction in acute optic neuritis, require further clarification with regard to its underlying pathophysiology and its clinical relevance. Although the finding of macular dysfunction in acute optic neuritis seems robust, as it now has been consistently identified in three independent cohorts (Berninger and Heider, 1990; Holder, 1991), future larger studies including repeated measures are necessary to improve understanding of the evolution over

time. By combining electrophysiological data with clinically relevant measures such as visual acuity, the prognostic value of macular dysfunction in optic neuritis could be elucidated. Further follow-up data might also elucidate the evolution of the function and structure of the inner nuclear layer after optic neuritis and establish associations of macular dysfunction with the occurrence of MMO. In addition, adding measurements of retinal metabolic function (through OCTA and/or oximetry) or systemic metabolic function (through lactate or other biomarkers) might inform if the macular dysfunction observed in acute optic neuritis is associated with energy failure.

Furthermore, the presented dark-adaptation method in chapter 3 and the EZ reflectivity tool in chapter 4 open up tremendous possibilities for future research in neuroinflammatory disorders. Specifically, these techniques may help to establish the nature of outer retinal involvement and energy failure in neuroinflammatory disease. Given the known high energy demands associated with dark-adaptation and the accumulation of mitochondria in the EZ, these novel OCT analysis metrics may provide in-vivo non-invasive measures of mitochondrial health. Future studies are needed to confirm this association with metabolic function, by exploring associations with other in-vivo measures of mitochondrial function such as serum levels of mitochondrial DNA (Varhaug *et al.*, 2017; Fissolo *et al.*, 2019), ATP metabolites (Lazzarino *et al.*, 2017), lactate (Petzold *et al.*, 2015) or monocyte mitochondrial complex activity (Hargreaves *et al.*, 2018; Gonzalo *et al.*, 2019). Performing these analyses was initially planned to be explored more fully within this thesis, but as the COVID-19 pandemic curtailed clinical recruitment this remains a future goal. If the validity of these techniques as mitochondrial biomarkers can be confirmed, these analysis methods could have an important impact in research disentangling the role of metabolic function in the pathophysiology of neuroinflammatory disease. This is important clinically, as there is currently a lack of non-invasive measurement techniques for metabolic function which hampers research in this subject. By acquiring follow-up data with regard to patients with MS or NMOSD, and exploring the temporal associations of structural atrophy and metabolic failure, the role of energy failure in neurodegeneration may be better understood. A better understanding of the role of metabolic failure in neuroinflammatory disease may lead to the development of novel treatment methods focused on improving mitochondrial function, which may be particularly relevant in the progressive forms of multiple sclerosis. Developing effective treatments for

these neurodegenerative components of secondary progressive MS and primary progressive MS currently represents an important unmet need. Although siponimod and ocreluzimab have been approved as treatments in progressive MS (Montalban *et al.*, 2017; Kappos *et al.*, 2018; Derfuss *et al.*, 2020), these medications are targeted to disrupt the relatively minor inflammatory disease components in these patients. Currently, no effective drugs are approved to disrupt neurodegenerative pathogenic processes in MS, while these are related to a huge burden of disability. If their associations with metabolic function are confirmed in future work, the novel OCT analysis methods presented in this thesis may provide outcome measures in current or future clinical trials that explore the effects of metabolically targeted treatments in multiple sclerosis (Negrotto *et al.*, 2016; Chataway *et al.*, 2020).

The OCTA data presented in chapter 5 of this thesis are limited to pilot data. The findings need to be explored in larger cohorts, as was initially intended in this thesis but was hampered by COVID-19. Larger cohorts might still identify microvascular abnormalities specific to the affected eye associated with acute optic neuritis or could identify a clinically relevant prognostic value of OCTA. Importantly, by acquiring combined structural and microvascular measurements acutely and during follow-up could elucidate if microvascular changes precede or follow structural atrophy of retinal layers. This would help in establishing if microvascular abnormalities in neuroinflammatory disease drive neurodegeneration or are a result of reduced demand in atrophied tissue.

Finally, the description of the rare phenotype of primary progressive optic neuropathy in multiple sclerosis in chapter 6 may improve timely diagnosis in these patients, the analysis of associations of smoking and alcohol consumption with neurodegeneration in multiple sclerosis in chapter 7 could help guide clinical counselling regarding safe health behaviours in neuroinflammatory disease and, the study identifying evidence for astrocytopathy in seronegative neuromyelitis optica spectrum disease in chapter 9 helps to improve understanding of the pathophysiology in these patients.

Taken together, the work presented in this thesis shows that the potential of OCT imaging in neuroinflammatory disease extends beyond structural measurements of retinal layer thicknesses, for which is it is now primarily used. Analysis of dynamic thickness changes during

dark-adaptation, EZ reflectivity and vascular densities has the potential to provide valuable information on retinal function. In the future, harbouring the exciting potential of artificial intelligence and big data analysis may enable the development of a comprehensive analysis method for raw OCT data. This tool could theoretically provide a summary report on both qualitative scan features, such as presence of MMO, and quantitative scan features, such as layer thickness, vascular density and reflectivity. The holistic analysis of functional and structural OCT data together may facilitate diagnosis and inform on prognosis in neurological disease. Importantly, this comprehensive approach could provide insight into the role of metabolic failure in the pathophysiology of neuroinflammatory disease, as it combines measures that potentially reflect metabolic function and measures of structural atrophy.

Acknowledgements

Firstly, I would like to give special thanks to the optic neuritis patients that have participated in this research. This is the same for the group of friends and co-workers that have agreed to invest time and effort into helping me acquire the pilot dark-adaptation and reflectivity data. Their efforts are very much appreciated.

My sincere appreciation and thanks go out to my three PhD supervisors, Dr S Anand Trip, Dr Axel Petzold and Dr Gordon T Plant, who have been extremely supportive and encouraging throughout my PhD. I am very lucky to have three supervisors who are dedicated and genuinely care about my work. Their guidance, always prompt replies to any queries and support for open debate have been instrumental to the successful completion of my projects. Their knowledge and clinical skills are great sources of education and inspiration for me. I feel lucky also to have been one of the very last fellows who has been able to observe and learn from Dr Gordon Plant before his retirement. Every clinic seeing him at work has been a valuable learning experience.

Furthermore, I would like to thank professor Kenneth Smith for our discussions on energy failure and the potential use of nimodipine in multiple sclerosis, which have been extremely educational. For her expert and helpful guidance in the initial exploratory analyses of the UK Biobank data I would like to thank Fiona Ingleby of the London School of Hygiene and Tropical Medicine.

I would like to express my gratitude to the ECTRIMS for awarding me their postdoctoral research fellowship in 2018, which has allowed me to be able to finance my PhD. Furthermore, I would like to thank Fight for Sight for awarding me and co-applicants a grant for a pilot study investigating the use of nimodipine in acute optic neuritis.

My special thanks goes out to Sarah Houston, who helped me find my way around the Institute of Ophthalmology and has been great company there and outside of work. I am very happy to

have gotten to know Siegfried Wagner, and have very much enjoyed studying epidemiology together and collaborating on projects.

I would like to thank Shaun Leo at Moorfields for being very helpful at teaching me electrophysiology and always making time to fit in study patients in his busy schedule. I am extremely indebted to Vincent Rocco, for patiently and competently teaching me how to make high quality OCT scans.

Furthermore, I would like to express my gratitude to Charlotte Burt for figuring out all administrative complexities of UCL PhD registration and grant approval. All support staff at Moorfields has been hugely important for me to identify and schedule acute optic neuritis on such notice.

For the massive amount work that has been going into the preparations of RECOVER trial my sincere appreciation goes to Hayley Boston, Shivany Condor Montes, Tracy Tran and Ari Green. I look forward to getting this trial started and hopefully recruiting many patients.

I would like to thank my friends from the Netherlands for coming over to London often during non-covid times and making these weekends of exploring this city so much fun. I want to thank my family for their support throughout the years. My special thanks goes to Daniel, who is always an unwavering believer in my capabilities, academic or otherwise, even when I am not sure myself. He has always encouraged me to aim high academically which was one of the reasons I applied for a PhD at UCL. He has been a great cheerleader throughout, and it has been fun to collaborate on some of my projects.

Statement of author contributions

Chapter 2: Macular Dysfunction in Acute ON

Iris Kleerekooper, Lana Del Porto, Laura Dell'Arti, José Guajardo, Shaun Leo, Anthony G. Robson, S Anand Trip, Axel Petzold, Gordon T Plant, Graham E Holder

AP, GTP, AGR and GEH conceived and planned the experiments. IK, LDP, LDA, JG and SL recruited subjects and carried out the experiments. IK, AP, GTP and GEH analysed and interpreted the data. IK took the lead in writing up the findings. All authors contributed to the final interpretation of the results and provided guidance with the writing up stage.

Chapter 3: Dark Adaptation

Iris Kleerekooper, Gordon T Plant, S Anand Trip, Axel Petzold.

IK and AP conceived and planned the experiments. IK recruited subjects and carried out experiments. IK analysed the data, initially interpreted the data and took the lead in writing up the findings. AP, GTP and SAT all contributed to the interpretation of the findings and revised the writing for intellectual content

Chapter 4: EZ Reflectivity

Iris Kleerekooper, Daniel Vincent Verschueren, Gordon T Plant, . Anand Trip, Axel Petzold.

IK and AP conceived and planned the experiments. IK recruited subjects and carried out experiments. DVV developed the Python analysis tool together with IK. IK analysed the data, initially interpreted the data and took the lead in writing up the findings. AP, GTP and SAT all contributed to the interpretation of the findings and revised the writing for intellectual content

Chapter 5: Primary progressive optic neuropathy in multiple sclerosis

Iris Kleerekooper, Ghislaine L Traber, Laura Dell'Arti, Anne Catherine Chapelle, Lucas J Maillette de Buy Wenniger, Declan Chard, Axel Petzold, S Anand Trip, Gordon T Plant

GTP and AP conceived and planned the experiments. IK , GLT, LDA, ACC, LJMBW, DC, AP, SAT and GTP recruited subjects and carried out experiments. IK analysed the data, initially interpreted the data and took the lead in writing up the findings. AP, GTP, LJMBW, DC and SAT all contributed to the interpretation of the findings and revised the writing for intellectual content

Chapter 6: Smoking and Alcohol in multiple sclerosis (UKBB)

Iris Kleerekooper, Sharon Chua, Paul J Foster, S Anand Trip, Gordon T Plant, Axel Petzold, Praveen J Patel, The UK Biobank Eye and Vision Consortium.

IK, AP and PJP conceived and planned the design of this study. IK and SC performed the data collection. IK analysed the data, initially interpreted the data and took the lead in writing up the findings. All authors reviewed the results, read and critically revised the manuscript. A separate analysis on the data presented in this chapter (specifically a linear regression analysis of the association of modifiable risk factors and mGCIPL thickness) has previously been submitted in a project report for the MSc Epidemiology at the London School of Hygiene and Tropical Medicine).

Chapter 7: Expanding the phenotype of MOGAD: case-report

Iris Kleerekooper, S Anand Trip, Gordon T Plant, Axel Petzold

AP conceived the study and performed laboratory work. Data was collected by IK and AP. Data anlysis and interpretation was performed by IK, SAT, GTP and AP. IK and AP took the lead in writing up the findings.

Chapter 8: CSF levels of GS and GFAP in NMOSD

Iris Kleerekooper, Meghan K Herbert, H Bea Kuiperij, Douglas K Sato, Kazuo Fujihara, Dagoberto Callegaro, Romain Marignier, Albert Saiz, Makbule Senel, Hayrettin Tumani, Birgit De Jong, S Anand Trip, Ichiro Nakashima, Marcel M Verbeek, Axel Petzold

MKH, IK and AP were responsible for data collection and statistical analysis, interpretation of the data, the drafting and revision of the manuscript, HBK assisted with the revision of the manuscript and reading the manuscript for intellectual content. DKS, KF, DC, RM, AS, HT, BAJ, SAT and IN were responsible for data collection, assisting with interpretation of the data and reading the manuscript for intellectual content. MMV and AP were responsible for the design and conceptualisation of the study and reading the manuscript for intellectual content and revision of the manuscript.

Chapter 9: OCTA in neuroinflammatory disease

Iris Kleerekooper, Sarah Houston, Adam Dubis, S Anand Trip, Axel Petzold

IK and SH performed literature review and took the lead in writing the text. IK acquired the data and created the OCTA figures. AD, SAT and AP revised the manuscript for intellectual content.

References

Abdollahpour I, Nedjat S, Mansournia MA, Sahraian MA, van der Mei I. Lifestyle factors and multiple sclerosis: A population-based incident case-control study. Mult Scler Relat Disord 2018; 22: 128–133.
Abegg M, Dysli M, Wolf S, Kowal J, Dufour P, Zinkernagel M. Microcystic macular edema: Retrograde maculopathy caused by optic neuropathy. Ophthalmology 2014; 121: 142–149.
Abràmoff MD, Mullins RF, Lee K, Hoffmann JM, Sonka M, Critser DB, et al. Human photoreceptor outer segments shorten during light adaptation. Invest Ophthalmol Vis Sci 2013; 54: 3721–3728.
Absinta M, Maric D, Gharagozloo M, Garton T, Smith MD, Jin J, et al. A lymphocyte–microglia–astrocyte axis in chronic active multiple sclerosis [Internet]. Nature 2021Available from: http://dx.doi.org/10.1038/s41586-021-03892-7
Al-Nosairy KO, Horbrügger M, Schippling S, Wagner M, Haghikia A, Pawlitzki M, et al. Structure-Function Relationship of Retinal Ganglion Cells in Multiple Sclerosis. Int J Mol Sci 2021; 22: 1–14.
Albanese M, Zagaglia S, Landi D, Boffa L, Nicoletti CG, Marciani MG, et al. Cerebrospinal fluid lactate is associated with multiple sclerosis disease progression. J Neuroinflammation 2016; 13: 36.
Ambrose JA, Barua RS. The pathophysiology of cigarette smoking and cardiovascular disease: An update. J Am Coll Cardiol 2004; 43: 1731–1737.
Amorini AM, Nociti V, Petzold A, Gasperini C, Quartuccio E, Lazzarino G, et al. Serum lactate as a novel potential biomarker in multiple sclerosis. Biochim Biophys Acta - Mol Basis Dis 2014; 1842: 1137–1143.
Anstey K, Jorm A, Réglade-Meslin C, Maller J, Kumar R, Von Sanden C, et al. Weekly Alcohol Consumption, Brain Atrophy, and White Matter Hyperintensities in a Community-Based Sample Aged 60 to 64 Years. Psychosom Med 2006; 785: 778–785.
Arendt T, Allen Y, Sinden J, Schugens M, Marchbanks R, Lantos P, et al. Cholinergic-rich brain transplants reverse alcohol-induced memory deficits. Nature 1988; 332: 448–450.
Ashworth B. Chronic retrobulbar and chiasmal neuritis. Br J Ophthalmol 1967; 51: 698–702.
Aytulun A, Cruz-Herranz A, Aktas O, Balcer LJ, Balk L, Barboni P, et al. The APOSTEL 2.0 Recommendations for Reporting Quantitative Optical Coherence Tomography Studies. 2021
Balcer LJ, Raynowska J, Nolan R, Galetta SL, Kapoor R, Benedict R, et al. Validity of low-contrast letter acuity as a visual performance outcome measure for multiple sclerosis. Mult Scler J 2017; 23: 734–747.
Balk LJ, Coric D, Knier B, Zimmermann HG, Behbehani R, Alroughani R, et al. Retinal inner nuclear layer volume reflects inflammatory disease activity in multiple sclerosis; a longitudinal OCT study. Mult Scler J - Exp Transl Clin 2019; 5: 205521731987158.
Balk LJ, Cruz-Herranz A, Albrecht P, Arnow S, Gelfand JM, Tewarie P, et al. Timing of retinal neuronal and axonal loss in MS: a longitudinal OCT study. J Neurol 2016; 263: 1323–1331.
Balk LJ, Killestein J, Polman CH, Uitdehaag BMJ, Petzold A. Microcystic macular oedema confirmed, but not specific for multiple sclerosis. Brain 2012; 135: 10–11.
Balk LJ, Twisk JWR, Steenwijk MD, Daams M, Tewarie P, Killestein J, et al. A dam for retrograde axonal degeneration in multiple sclerosis? J Neurol Neurosurg Psychiatry 2014; 85: 782–789.
Beard E, West R, Michie S, Brown J. Association between smoking and alcohol-related

behaviours: a time–series analysis of population trends in England. Addiction 2017; 112: 1832–1841.
Beauvoit B, Evans S, Jenkins T, Miller E, B C. Correlation between the Light Scattering and Mitochondrial Content of normal Tissues and Transplantable Rodent Tumors. Anal Biochem 1995; 226: 167–174.
Beck R, Gal R, Bhatti M, Brodsky M, Buckley E, Chrousos G. Visual function more than 10 years after optic neuritis: Experience of the optic neuritis treatment trial. Am J Ophthalmol 2004; 137: 77–83.
Beck RW, Trobe JD, Moke PS, Gal RL, Xing D. High- and Low-Risk Profiles for the Development of Multiple Sclerosis Within 10 Years After Optic Neuritis: Experience of the Optic Neuritis Treatment Trial. Arch Ophtalmol 2003; 121: 944–949.
Bell S, Daskalopoulou M, Rapsomaniki E, George J, Britton A, Bobak M, et al. Association between clinically recorded alcohol consumption and initial presentation of 12 cardiovascular diseases: Population based cohort study using linked health records. BMJ 2017; 356: 1–7.
Berninger TA, Heider W. Pattern electroretinograms in optic neuritis during the acute stage and after remission. Graefe's Arch Clin Exp Ophthalmol 1990; 228: 410–414.
Bernstein H, Bannier J, Meyer-Lotz G, Steiner J, Keilhoff G, Dobrowolny H, et al. Distribution of immunoreactive glutamine synthetase in the adult human and mouse brain. Qualitative and quantitative observations with special emphasis on extra-astroglial protein localization. J Chem Neuroanat 2014; 61–62: 33–50.
Biousse V, Newman NJ. Diagnosis and clinical features of common optic neuropathies. Lancet Neurol 2016; 15: 1355–1367.
Birkeldh U, Manouchehrinia A, Hietala MA, Hillert J, Olsson T, Piehl F, et al. Retinal nerve fiber layer thickness associates with cognitive impairment and physical disability in multiple sclerosis. Mult Scler Relat Disord 2019; 36: 101414.
Bradl M, Reindl M, Lassmann H. Mechanisms for lesion localization in neuromyelitis optica spectrum disorders. Curr Opin Neurol 2018; 31: 325–333.
Braithwaite T, Subramanian A, Petzold A, Galloway J, Adderley NJ, Mollan SP, et al. Trends in Optic Neuritis Incidence and Prevalence in the UK and Association with Systemic and Neurologic Disease. JAMA Neurol 2020; 77: 1514–1523.
Brownlee WJ, Miller DH. Clinically isolated syndromes and the relationship to multiple sclerosis. J Clin Neurosci 2014; 21: 2065–71.
Burton JM, Eliasziw M, Trufyn J, Tung C, Carter G, Costello F. A prospective cohort study of vitamin D in optic neuritis recovery. Mult Scler 2017; 23: 82–93.
Campbell GR, Worrall JT, Mahad DJ. The central role of mitochondria in axonal degeneration in multiple sclerosis. Mult Scler J 2014; 20: 1806–1813.
Campbell GR, Ziabreva I, Reeve AK, Krishnan KJ, Reynolds R, Howell O, et al. Mitochondrial DNA deletions and neurodegeneration in multiple sclerosis. Ann Neurol 2011; 69: 481–492.
Campbell JP, Zhang M, Hwang TS, Bailey ST, Wilson DJ, Jia Y, et al. Detailed Vascular Anatomy of the Human Retina by Projection-Resolved Optical Coherence Tomography Angiography. Sci Rep 2017; 7: 1–11.
Carelli V, Ross-Cisneros FN, Sadun AA. Mitochondrial dysfunction as a cause of optic neuropathies. Prog Retin Eye Res 2004; 23: 53–89.
Çetinkaya E, Duman R, Duman R, Sabaner MC. Repeatability and reproducibility of automatic segmentation of retinal layers in healthy subjects using Spectralis optical coherence tomography. Arq Bras Oftalmol 2017; 80: 378–381.

Chataway J, De Angelis F, Connick P, Parker RA, Plantone D, Doshi A, et al. Efficacy of three neuroprotective drugs in secondary progressive multiple sclerosis (MS-SMART): a phase 2b, multiarm, double-blind, randomised placebo-controlled trial. Lancet Neurol 2020; 19: 214–225.
Chen X, Hou P, Jin C, Zhu W, Luo X, Shi F, et al. Quantitative analysis of retinal layer optical intensities on three-dimensional optical coherence tomography. Invest Ophthalmol Vis Sci 2013; 54: 6846–6851.
Chen Y, Shi C, Zhou L, Huang S, Shen M, He Z. The Detection of Retina Microvascular Density in Subclinical Aquaporin-4 Antibody Seropositive Neuromyelitis Optica Spectrum Disorders. Front Neurol 2020; 11: 1–9.
Cheng CS, Natividad MG, Earnest A, Yong V, Lim BA, Wong HT, et al. Comparison of the influence of cataract and pupil size on retinal nerve fibre layer thickness measurements with time-domain and spectral-domain optical coherence tomography. Clin Exp Ophthalmol 2011; 39: 215–221.
Chua SYL, Lascaratos G, Atan D, Zhang B, Reisman C, Khaw PT, et al. Relationships between retinal layer thickness and brain volumes in the UK Biobank cohort. Eur J Neurol 2021; 28: 1490–1498.
Chua SYL, Luben RN, Hayat S, Broadway DC, Khaw KT, Warwick A, et al. Alcohol Consumption and Incident Cataract Surgery in Two Large UK Cohorts. Ophthalmology 2021; 128: 837–847.
Chua SYL, Thomas D, Allen N, Lotery A, Desai P, Patel P, et al. Cohort profile: Design and methods in the eye and vision consortium of UK Biobank. BMJ Open 2019; 9: 1–13.
Cicchetti D V. Interreliability standards in psychological evaluations. Psychol Assess 1994; 6: 284–290.
Coric D, Bijvank JAN, Rijn LJ Van, Petzold A, Lisanne J. The role of optical coherence tomography and infrared oculography in assessing the visual pathway and CNS in multiple sclerosis. Neurodegener Dis Manag 2018; 8: 323–335.
Costello F, Coupland S, Hodge W, Lorello GR, Koroluk J, Pan YI, et al. Quantifying axonal loss after optic neuritis with optical coherence tomography. Ann Neurol 2006; 59: 963–969.
Costello F, Hodge W, Pan YI, Burton JM, Freedman MS, Stys PK, et al. Sex-specific differences in retinal nerve fiber layer thinning after acute optic neuritis. Neurology 2012; 79: 1866–1872.
Cottrell DA, Kremenchutzky M, Rice GPA, Koopman WJ, Hader W, Baskerville J, et al. The natural history of multiple sclerosis: A geographically based study. 5. The clinical features and natural history of primary progressive multiple sclerosis. Brain 1999; 122: 625–639.
Coupland SG, Kirkham TH. Flash Electroretinogram Abnormalities in Patients with Clinically Definite Multiple Sclerosis. Can J Neurol Sci / J Can des Sci Neurol 1982; 9: 325–330.
Cruz-Herranz A, Balk LJ, Oberwahrenbrock T, Saidha S, Martinez-Lapiscina EH, Lagreze WA, et al. The APOSTEL recommendations for reporting quantitative optical coherence tomography studies. Neurology 2016; 86: 2303–2309.
Cuenca N, Ortuño-Lizarán I, Pinilla I. Cellular Characterization of OCT and Outer Retinal Bands Using Specific Immunohistochemistry Markers and Clinical Implications. Ophthalmology 2018; 125: 407–422.
Curcio CA, Sparrow JR, Bonilha VL, Pollreisz A, Lujan BJ. Re: Cuenca et al.: Cellular characterization of OCT and outer retinal bands using specific immunohistochemistry markers and clinical implications (Ophthalmology. 2018;125;407-422). Ophthalmology 2018; 125: e47–e48.
D'Amelio F, Eng LF, Gibbs MA. Glutamine Sgnthetase Immunoreactivity is Present in

Oligodendroglia of Various Regions of the Central Nervous System. Glia 1990; 3: 335–341.
D'Haeseleer M, Hostenbach S, Peeters I, El Sankari S, Nagels G, De Keyser J, et al. Cerebral hypoperfusion: A new pathophysiologic concept in multiple sclerosis? J Cereb Blood Flow Metab 2015; 35: 1406–1410.
Das SK, Vasudevan DM. Alcohol-induced oxidative stress. Life Sci 2007; 81: 177–187.
Davies AL, Desai RA, Bloomfield PS, McIntosh PR, Chapple KJ, Linington C, et al. Neurological deficits caused by tissue hypoxia in neuroinflammatory disease. Ann Neurol 2013; 74: 815–825.
Davis BJK, Vidal JS, Garcia M, Aspelund T, Van Buchem MA, Jonsdottir MK, et al. The alcohol paradox: Light-to-moderate alcohol consumption, cognitive function, and brain volume. Journals Gerontol - Ser A Biol Sci Med Sci 2014; 69: 1528–1535.
Derfuss T, Mehling M, Papadopoulou A, Bar-Or A, Cohen JA, Kappos L. Advances in oral immunomodulating therapies in relapsing multiple sclerosis. Lancet Neurol 2020; 19: 336–347.
Desai RA, Davies AL, Del Rossi N, Tachrount M, Dyson A, Gustavson B, et al. Nimodipine Reduces Dysfunction and Demyelination in Models of Multiple Sclerosis. Ann Neurol 2020; 88: 123–136.
Desai RA, Davies AL, Tachrount M, Kasti M, Laulund F, Golay X, et al. Cause and Prevention of Demyelination in a Model Multiple Sclerosis Lesion. Ann Neurol 2016; 79: 591–604.
Desai RA, Smith KJ. Experimental autoimmune encephalomyelitis from a tissue energy perspective. F1000Research 2017; 6: 1973.
Diaz-Cruz C, Chua AS, Malik MT, Kaplan T, Glanz BI, Egorova S, et al. The effect of alcohol and red wine consumption on clinical and MRI outcomes in multiple sclerosis. Mult Scler Relat Disord 2017; 17: 47–53.
Dobson R, Ramagopalan S, Davis A, Giovannoni G. Cerebrospinal fluid oligoclonal bands in multiple sclerosis and clinically isolated syndromes: A meta-analysis of prevalence, prognosis and effect of latitude. J Neurol Neurosurg Psychiatry 2013; 84: 909–914.
Dougherty RJ, Moonen J, Yaffe K, Sidney S, Davatzikos C, Habes M, et al. Smoking mediates the relationship between SES and brain volume: The CARDIA study. PLoS One 2020; 15: 1–11.
Eikelenboom M, Killestein J, Uitdehaag B, Polman C. Opticospinal Multiple Sclerosis: a Pathogenetically distinct form? Mult Scler 2004; 10: 334–335.
Falsini B, Bardocci A, Porciatti V, Bolzani R, Piccardi M. Macular dysfunction in multiple sclerosis revealed by steady-state flicker and pattern ERGs. Electroencephalogr Clin Neurophysiol 1992; 82: 53–59.
Fang B, McKeon A, Hinson S, Kryzer T, Pittock S, Aksamit A, et al. Autoimmune Glial Fibrillary Acidic Protein Astrocytopathy: A Novel Meningoencephalomyelitis. JAMA Neurol 2016; 73: 1297–1307.
Farhat G, Mariampillai A, Yang VXD, Czarnota GJ, Kolios MC. Detecting apoptosis using dynamic light scattering with optical coherence tomography. J Biomed Opt 2011; 16: 070505.
Feucht N, Maier M, Lepennetier G, Pettenkofer M, Wetzlmair C, Daltrozzo T, et al. Optical coherence tomography angiography indicates associations of the retinal vascular network and disease activity in multiple sclerosis. Mult Scler J 2019; 25: 224–234.
Filgueiras TG, Oyamada MK, Preti RC, Apóstolos-Pereira SL, Callegaro D, Monteiro MLR. Outer retinal dysfunction on multifocal electroretinography may help differentiating multiple sclerosis from neuromyelitis optica spectrum disorder. Front Neurol 2019; 10: 1–10.

Filippi M, Preziosa P, Banwell BL, Barkhof F, Ciccarelli O, De Stefano N, et al. Assessment of lesions on magnetic resonance imaging in multiple sclerosis: practical guidelines. Brain 2019; 142: 1858–1875.
Fischer MT, Sharma R, Lim JL, Haider L, Frischer JM, Drexhage J, et al. NADPH oxidase expression in active multiple sclerosis lesions in relation to oxidative tissue damage and mitochondrial injury. Brain 2012; 135: 886–899.
Fissolo N, Cervera-Carles L, Villar Guimerans LM, Lleó A, Clarimón J, Drulovic J, et al. Cerebrospinal fluid mitochondrial DNA levels in patients with multiple sclerosis. Mult Scler J 2019; 25: 1535–1538.
Fleischer V, Gröger A, Koirala N, Droby A, Muthuraman M. Increased structural white and grey matter network connectivity compensates for functional decline in early multiple sclerosis. 2016: 1–10.
Foiadelli T, Matteo G, Silvia S, Diego F, Salvatore S. Seizures and myelin oligodendrocyte glycoprotein (MOG) antibodies: Two paradigmatic cases and a review of the literature. Mult Scler Relat Disord 2020; 41: 102011.
Forooghian F, Sproule M, Westall C, Gordon L, Jirawuthiworavong G, Shimazaki K, et al. Electroretinographic abnormalities in multiple sclerosis: Possible role for retinal autoantibodies. Doc Ophthalmol 2006; 113: 123–132.
Frohman EM, Fujimoto JG, Frohman TC, Calabresi PA, Cutter G, Balcer LJ. Optical coherence tomography: A window into the mechanisms of multiple sclerosis. Nat Clin Pract Neurol 2008; 4: 664–675.
Frohman EM, Racke MK, Raine CS. Medical progress: Multiple sclerosis - The plaque and its pathogenesis. N Engl J Med 2006; 354: 942–955.
Frohman TC, Davis SL, Beh S, Greenberg BM, Remington G, Frohman EM. Uhthoff's phenomena in MS - Clinical features and pathophysiology. Nat Rev Neurol 2013; 9: 535–540.
Fujihara K. Neuromyelitis optica spectrum disorders: Still evolving and broadening. Curr Opin Neurol 2019; 32: 385–394.
Gasperini C, Pozzilli C, Bernardi S. Irreversible total blindness in multiple sclerosis. Ital J Neurol Sci 1991; 12: 329.
Geel WJA Van, Reus HPM De, Nijzing H, Verbeek MM, Vos PE, Lamers KJB. Measurement of glial fibrillary acidic protein in blood: an analytical method. Clin Chim Acta 2002; 326: 151–154.
Gelfand JM, Cree BA, Nolan R, Arnow S, Green AJ. Microcystic inner nuclear layer abnormalities and neuromyelitis optica. JAMA Neurol 2013; 70: 629–633.
Gelfand JM, Nolan R, Schwartz DM, Graves J, Green AJ. Microcystic macular oedema in multiple sclerosis is associated with disease severity. Brain 2012; 135: 1786–1793.
Ghafaryasl B, Vermeer KA, Kalkman J, Callewaert T, de Boer JF, Van Vliet LJ. Analysis of attenuation coefficient estimation in Fourier-domain OCT of semi-infinite media. Biomed Opt Express 2020; 11: 6093.
Giordano A, Colombo B, Spinelli E, Gelibter S, Guerrieri S, Leocani L, et al. Progressive visual function impairment as the predominant symptom of the transition phase to secondary progressive multiple sclerosis: a case report. Mult Scler Relat Disord 2018; 24: 69–71.
Giorgi C, Marchi S, Pinton P. The machineries, regulation and cellular functions of mitochondrial calcium. Nat Rev Mol Cell Biol 2018; 19: 713–730.
Gong Y, Chen LJ, Pang CP, Chen H. Ellipsoid zone optical intensity reduction as an early biomarker for retinitis pigmentosa. Acta Ophthalmol 2021; 99: e215–e221.
Gonzalo H, Nogueras L, Gil-Sánchez A, Hervás JV, Valcheva P, González-Mingot C, et al.

Impairment of Mitochondrial Redox Status in Peripheral Lymphocytes of Multiple Sclerosis Patients. Front Neurosci 2019; 13: 1–10.
Gorman GS, Chinnery PF, DiMauro S, Hirano M, Koga Y, McFarland R, et al. Mitochondrial diseases. Nat Rev Dis Prim 2016; 2: 16080.
Gourraud PA, Harbo HF, Hauser SL, Baranzini SE. The genetics of multiple sclerosis: An up-to-date review. Immunol Rev 2012; 248: 87–103.
Granqvist M, Boremalm M, Poorghobad A, Svenningsson A, Salzer J, Frisell T, et al. Comparative effectiveness of rituximab and other initial treatment choices for multiple sclerosis. JAMA Neurol 2018; 75: 320–327.
Green AJ, Cree BAC. Distinctive retinal nerve fibre layer and vascular changes in neuromyelitis optica following optic neuritis. J Neurol Neurosurg Psychiatry 2009; 80: 1002–1005.
Green AJ, McQuaid S, Hauser SL, Allen I V., Lyness R. Ocular pathology in multiple sclerosis: Retinal atrophy and inflammation irrespective of disease duration. Brain 2010; 133: 1591–1601.
Ha A, Kim YK, Jeoung JW, Park KH. Ellipsoid Zone Change According to Glaucoma Stage Advancement. Am J Ophthalmol 2018; 192: 1–9.
Haider L, Zrzavy T, Hametner S, Höftberger R, Bagnato F, Grabner G, et al. The topograpy of demyelination and neurodegeneration in the multiple sclerosis brain. Brain 2016; 139: 807–815.
Halliday AM, Mcdonald WI, Mushin J. Delayed Visual Evoked Response in Optic Neuritis. Lancet 1972; 299: 982–985.
Hanson JVM, Hediger M, Manogaran P, Landau K, Hagenbuch N, Schippling S, et al. Outer retinal dysfunction in the absence of structural abnormalities in multiple sclerosis. Investig Ophthalmol Vis Sci 2018; 59: 549–560.
Harding A, Sweeney M, Miller D, Mumford C, Kellar-Wood H, Menard D, et al. Occurrence of a multiple sclerosis-like illness in women who have a Leber's hereditary optic neuropathy mitochondrial DNA mutation. Brain 1992; 115: 979–989.
Hargreaves I, Mody N, Land J, Heales S. Blood Mononuclear Cell Mitochondrial Respiratory Chain Complex IV Activity Is Decreased in Multiple Sclerosis Patients: Effects of β-Interferon Treatment. J Clin Med 2018; 7: E36.
Haufschild T, Shaw SG, Kaiser HJ, Flammer J. Transient raise of endothelin-1 plasma level and reduction of ocular blood flow in a patient with optic neuritis. Ophthalmologica 2003; 217: 451–453.
Hedström A, Hillert J, Olsson T, Alfredsson L. Alcohol as a Modifiable Lifestyle Factor Affecting Multiple Sclerosis Risk. JAMA Neurol 2014; 71: 300–305.
Hedström AK, Hillert J, Olsson T, Alfredsson L. Factors affecting the risk of relapsing-onset and progressive-onset multiple sclerosis. J Neurol Neurosurg Psychiatry 2021: 1–7.
Henderson APD, Trip SA, Schlottmann PG, Altmann DR, Garway-Heath DF, Plant GT, et al. A preliminary longitudinal study of the retinal nerve fiber layer in progressive multiple sclerosis. J Neurol 2010; 257: 1083–1091.
Herbert MK, Kuiperij HB, Verbeek MM. Optimisation of the quantification of glutamine synthetase and myelin basic protein in cerebrospinal fluid by a combined acidification and neutralisation protocol. J Immunol Methods 2012; 381: 1–8.
Higashiyama T, Nishida Y, Ohji M. Optical coherence tomography angiography in eyes with good visual acuity recovery after treatment for optic neuritis. PLoS One 2017; 12: 1–10.
Höftberger R, Guo Y, Flanagan EP, Lopez-Chiriboga AS, Endmayr V, Hochmeister S, et al. The

pathology of central nervous system inflammatory demyelinating disease accompanying myelin oligodendrocyte glycoprotein autoantibody. Acta Neuropathol 2020; 139: 875–892.
Höftberger R, Sabater L, Marignier R, Aboul-enein F, Bernard-valnet R, Rauschka H, et al. An Optimized Immunohistochemistry Technique Improves NMO-IgG Detection: Study Comparison with Cell-Based Assays. PLoS One 2013; 8: 6–11.
Höftberger R, Sepulveda M, Armangue T, Blanco Y, Rostásy K, Calvo AC, et al. Antibodies to MOG and AQP4 in adults with neuromyelitis optica and suspected limited forms of the disease. Mult Scler 2015; 21: 866–874.
Hokari M, Yokoseki A, Arakawa M, Saji E, Yanagawa K, Yanagimura F, et al. Clinicopathological features in anterior visual pathway in neuromyelitis optica. Ann Neurol 2016; 79: 605–624.
Hokazono K, Raza AS, Oyamada MK, Hood DC, Monteiro MLR. Pattern electroretinogram in neuromyelitis optica and multiple sclerosis with or without optic neuritis and its correlation with FD-OCT and perimetry. Doc Ophthalmol 2013; 127: 201–215.
Holder G, Votruba M, Carter A, Bhattacharya S, Fitzke F, Moore A. Electrophysiological findings in dominant optic atrophy (DOA) linking to the OPA1 locus on chromosome 3q 28-qter. Doc Ophthalmol 1999; 95: 217–228.
Holder GE. The effects of chiasmal compression on the pattern visual evoked potential. Electroencephalogr Clin Neurophysiol 1978; 45: 278–280.
Holder GE. Significance of abnormal pattern electroretinography in anterior visual pathway dysfunction. Br J Ophthalmol 1987; 71: 166–171.
Holder GE. The incidence of abnormal pattern electroretinography in optic nerve demyelination. Electroencephalogr Clin Neurophysiol 1991; 78: 18–26.
Holder GE. The pattern electroretinogram in anterior visual pathway dysfunction and its relationship to the pattern visual evoked potential: A personal clinical review of 743 eyes. Eye 1997; 11: 924–934.
Holder GE. Pattern electroretinography (PERG) and an integrated approach to visual pathway diagnosis. Prog Retin Eye Res 2001; 20: 531–561.
Holder GE. Electrophysiological assessment of optic nerve disease. Eye 2004; 18: 1133–1143.
Van Horssen J, Witte ME, Ciccarelli O. The role of mitochondria in axonal degeneration and tissue repair in MS. Mult Scler J 2012; 18: 1058–1067.
Huang D, Swanson E a, Lin CP, Schuman JS, Stinson WG, Chang W, et al. Optical Coherence Tomography. Science (80-) 1991; 254: 1178–1181.
Huang Y, Zhou L, ZhangBao J, Cai T, Wang B, Li X, et al. Peripapillary and parafoveal vascular network assessment by optical coherence tomography angiography in aquaporin-4 antibody-positive neuromyelitis optica spectrum disorders. Br J Ophthalmol 2019; 103: 789–796.
Ikeda K, Kiyota N, Kuroda H, Sato DK, Nishiyama S. Severe demyelination but no astrocytopathy in clinically definite neuromyelitis optica with anti-myelin-oligodendrocyte glycoprotein antibody. Mult Scler J 2015; 21: 656–659.
Ivashynka A, Copetti M, Naldi P, D'alfonso S, Leone MA. The impact of lifetime alcohol and cigarette smoking loads on multiple sclerosis severity. Front Neurol 2019; 10: 1–8.
Jacobs BM, Noyce AJ, Bestwick J, Belete D, Giovannoni G, Dobson R. Gene-Environment Interactions in Multiple Sclerosis. Neurol - Neuroimmunol Neuroinflammation 2021; 8: e1007.
Jadidi E, Mohammadi M, Moradi T. High risk of cardiovascular diseases after diagnosis of multiple sclerosis. Mult Scler J 2013; 19: 1336–1340.

Janáky M, Jánossy, Horváth G, Benedek G, Braunitzer G. VEP and PERG in patients with multiple sclerosis, with and without a history of optic neuritis. Doc Ophthalmol 2017; 134: 185–193.
Jasse L, Vukusic S, Durand-Dubief F, Vartin C, Piras C, Bernard M, et al. Persistent visual impairment in multiple sclerosis: Prevalence, mechanisms and resulting disability. Mult Scler J 2013; 19: 1618–1626.
Jiang H, Delgado S, Tan J, Liu C, Rammohan KW, DeBuc DC, et al. Impaired Retinal Microcirculation in Multiple Sclerosis. Mult Scler 2016; 22: 1812–1820.
Jiang H, Gameiro GR, Liu Y, Lin Y, Hernandez J, Deng Y, et al. Visual Function and Disability Are Associated with Increased Retinal Volumetric Vessel Density in Patients with Multiple Sclerosis. Am J Ophthalmol 2020; 213: 34–45.
Jiang N, Lee YO, Ling PM. Association between tobacco and alcohol use among young adult bar patrons: A cross-sectional study in three cities. BMC Public Health 2014; 14: 1–9.
Jiao Y, Fryer JP, Lennon VA, Jenkins SM, Quek AML, Smith CY, et al. Updated estimate of AQP4-IgG serostatus and disability outcome in neuromyelitis optica. Neurology 2013; 81: 1197–1204.
Jindahra P, Hedges TR, Mendoza-Santiesteban CE, Plant GT. Optical coherence tomography of the retina: Applications in neurology. Curr Opin Neurol 2010; 23: 16–23.
Jindahra P, Petrie A, Plant GT. Retrograde trans-synaptic retinal ganglion cell loss identified by optical coherence tomography. Brain 2009; 132: 628–634.
Joyal J, Gantner ML, Smith LEH. Retinal energy demands control vascular supply of the retina in development and disease: The role of neuronal lipid and glucose metabolism. Prog Retin Eye Res 2018; 64: 131–156.
Juurlink BHJ. The Evidence for Hypoperfusion as a Factor in Multiple Sclerosis Lesion Development. Mult Scler Int 2013; 2013: 1–6.
Kahana E, Leibowitz U, Fishback N, Alter M. Slowly progressive and acute visual impairment in multiple sclerosis. Neurology 1973; 23: 729–733.
Kalkers N, Ameziane N, Bot J, Minneboo A, Polman C, Barkhof F. Longitudinal brain volume measurement in multiple sclerosis: rate of brain atrophy is independent of the disease subtype. Arch Neurol 2002; 59: 1572–6.
Kaneko K, Sato D, Nakashima I, Nishiyama S, Tanaka S, Marignier R, et al. Myelin injury without astrocytopathy in neuroinflammatory disorders with MOG antibodies. J Neurol Neurosurg Psychiatry 2016; 87: 1257–1259.
Kappos L, Bar-Or A, Cree BAC, Fox RJ, Giovannoni G, Gold R, et al. Siponimod versus placebo in secondary progressive multiple sclerosis (EXPAND): a double-blind, randomised, phase 3 study. Lancet 2018; 391: 1263–1273.
Kappos L, Stefano N De, Freedman MS, Cree BAC, Radue E, Sprenger T, et al. Inclusion of brain volume loss in a revised measure of ' no evidence of disease activity ' (NEDA-4) in relapsing – remitting multiple sclerosis. Mult Scler J 2016; 22: 1297–1305.
Karbowski M, Youle RJ. Dynamics of mitochondrial morphology in healthy cells and during apoptosis. Cell Death Differ 2003; 10: 870–880.
Kaufhold F, Zimmermann H, Schneider E, Ruprecht K, Paul F, Oberwahrenbrock T, et al. Optic Neuritis Is Associated with Inner Nuclear Layer Thickening and Microcystic Macular Edema Independently of Multiple Sclerosis. PLoS One 2013; 8
Kaushik M, Wang CY, Barnett MH, Garrick R, Parratt J, Graham SL, et al. Inner Nuclear Layer Thickening Is Inversley Proportional to Retinal Ganglion Cell Loss in Optic Neuritis. PLoS One 2013; 8: 4–11.

Kawachi I, Lassmann H. Neurodegeneration in multiple sclerosis and neuromyelitis optica. J Neurol Neurosurg Psychiatry 2017; 88: 137–145.
Keegan BM, Kaufmann TJ, Weinshenker BG, Kantarci OH, Schmalstieg WF, Paz Soldan MM, et al. Progressive solitary sclerosis: Gradual motor impairment from a singleCNSdemyelinating lesion. Neurology 2016; 87: 1713–1719.
Khawaja AP, Chua S, Hysi PG, Georgoulas S, Currant H, Fitzgerald TW, et al. Comparison of Associations with Different Macular Inner Retinal Thickness Parameters in a Large Cohort: The UK Biobank. Ophthalmology 2020; 127: 62–71.
Kidd D, Burton B, Plant G, Graham E. Chronic relapsing inflammatory optic neuropathy (CRION). Brain 2003; 126: 276–284.
Kim DY, Fingler J, Werner JS, Schwartz DM, Fraser SE, Zawadzki RJ. In vivo volumetric imaging of human retinal circulation with phase-variance optical coherence tomography. Biomed Opt Express 2011; 2: 1504.
Kleerekooper I, Houston S, Dubis AM, Trip SA, Petzold A. Optical Coherence Tomography Angiography (OCTA) in Multiple Sclerosis and Neuromyelitis Optica Spectrum Disorder. Front Neurol 2020; 11: 1–17.
Knier B, Schmidt P, Aly L, Buck D, Berthele A, Mühlau M, et al. Retinal inner nuclear layer volume reflects response to immunotherapy in multiple sclerosis. Brain 2016; 139: 2855–2863.
Kong GYX, Van Bergen NJ, Trounce IA, Crowston JG. Mitochondrial dysfunction and glaucoma. J Glaucoma 2009; 18: 93–100.
Koo TK, Li MY. A Guideline of Selecting and Reporting Intraclass Correlation Coefficients for Reliability Research. J Chiropr Med 2016; 15: 155–163.
Kubota M, Nakazaki S, Hirai S, Saeki N, Yamaura A, Kusaka T. Alcohol consumption and frontal lobe shrinkage: Study of 1432 non-alcoholic subjects. J Neurol Neurosurg Psychiatry 2001; 71: 104–106.
Kvistad S, Myhr KM, Holmøy T, Benth JŠ, Løken-Amsrud KI, Wergeland S, et al. No association of tobacco use and disease activity in multiple sclerosis. Neurol Neuroimmunol NeuroInflammation 2016; 3: 1–6.
Kwapong WR, Peng C, He Z, Zhuang X, Shen M, Lu F. Altered Macular Microvasculature in Neuromyelitis Optica Spectrum Disorders. Am J Ophthalmol 2018; 192: 47–55.
Lanzillo R, Cennamo G, Criscuolo C, Carotenuto A, Velotti N, Sparnelli F, et al. Optical coherence tomography angiography retinal vascular network assessment in multiple sclerosis. Mult Scler J 2017; 24: 1–9.
Lassmann H. Pathology and disease mechanisms in different stages of multiple sclerosis. J Neurol Sci 2013; 333: 1–4.
Lassmann H. Mechanisms of white matter damage in multiple sclerosis. Glia 2014; 62: 1816–1830.
Lassmann H, Van Horssen J, Mahad D. Progressive multiple sclerosis: Pathology and pathogenesis. Nat Rev Neurol 2012; 8: 647–656.
Lazzarino G, Amorini AM, Petzold A, Gasperini C, Ruggieri S, Quartuccio ME, et al. Serum Compounds of Energy Metabolism Impairment Are Related to Disability, Disease Course and Neuroimaging in Multiple Sclerosis. Mol Neurobiol 2017; 54: 7520–7533.
Lennon VA, Wingerchuk DM, Kryzer TJ, Pittock SJ, Lucchinetti CF, Fujihara K, et al. A serum autoantibody marker of neuromyelitis optica: distinction from multiple sclerosis. Lancet 2004; 364: 2106–2112.
Levin M, Bennett J, Verkman A. Optic Neuritis in Neuromyelitis Optica. Prog Retin Eye Res

2013; 36: 159–171.
Li Y, Fariss RN, Qian JW, Cohen ED, Qian H. Light-induced thickening of photoreceptor outer segment layer detected by ultra-high resolution OCT imaging. Investig Ophthalmol Vis Sci 2016; 57: OCT105–OCT111.
Lightman S, Mcdonald WI, Bird AC, Francis DA, Hoskins A, Batcholer JR, et al. Retinal venous sheathing in optic neuritis: Its significance for the pathogenesis of multiple sclerosis. Brain 1987; 110: 405–414.
Litts KM, Zhang Y, Freund KB, Curcio CA. Optical Coherence Tomography and Histology of Age-Related Macular Degeneration Support Mitochondria As Reflectivity Sources. Retina 2018; 38: 445–461.
London A, Benhar I, Schwartz M. The retina as a window to the brain - from eye research to CNS disorders. Nat Rev Neurol 2013; 9: 44–53.
Lu CD, Lee B, Schottenhamml J, Maier A, Jr ENP, Fujimoto JG. Photoreceptor Layer Thickness Changes During Dark Adaptation Observed With Ultrahigh-Resolution Optical Coherence Tomography. Investig Ophthalmol Vis Sci 2017; 1: 4632–4643.
Lucchinetti C, Bruck W. The pathology of primary progressive multiple sclerosis. Mult Scler 2004; 10: 93–97.
Lucchinetti CF, Mandler RN, McGaver D, Bruck W, Gleich G, Ransohoff R, et al. A role for humoral mechanisms in the pathogenesis of Devic's neuromyelitis optica. Brain 2002; 125: 1450–1461.
Lujan BJ, Roorda A, Knighton RW, Carroll J. Revealing Henle's fiber layer using spectral domain optical coherence tomography. Investig Ophthalmol Vis Sci 2011; 52: 1486–1492.
Mackenzie IS, Morant S V., Bloomfield GA, MacDonald TM, O'Riordan J. Incidence and prevalence of multiple sclerosis in the UK 1990-2010: a descriptive study in the General Practice Research Database. J Neurol Neurosurg Psychiatry 2014; 85: 76–84.
Mahad DH, Trapp BD, Lassmann H. Pathological mechanisms in progressive multiple sclerosis. Lancet Neurol 2015; 14: 183–193.
Manouchehrinia A, Tench CR, Maxted J, Bibani RH, Britton J, Constantinescu CS. Tobacco smoking and disability progression in multiple sclerosis: United Kingdom cohort study. Brain 2013; 136: 2298–2304.
Mao P, Reddy PH. Is multiple sclerosis a mitochondrial disease? Biochim Biophys Acta - Mol Basis Dis 2010; 1802: 66–79.
Marignier R, Berard-Valnet R, Giraudon P, Collongues N, Casey R, Confavreux C. Aquaporin-4 antibody–negative neuromyelitis optica. Distinct assay sensitivity–dependent entity. Neurology 2013; 80: 2194–2200.
Marignier R, Nicolle A, Watrin C, Touret M, Confavreux C. Oligodendrocytes are damaged by neuromyelitis optica immunoglobulin G via astrocyte injury. Brain 2010; 133: 2578–2591.
Marrie RA, Horwitz R, Cutter G, Tyry T, Campagnolo D, Vollmer T. High frequency of adverse health behaviors in multiple sclerosis. Mult Scler 2009; 15: 105–113.
Martinez-Lapiscina EH, Arnow S, Wilson JA, Saidha S, Preiningerova JL, Oberwahrenbrock T, et al. Retinal thickness measured with optical coherence tomography and risk of disability worsening in multiple sclerosis: A cohort study. Lancet Neurol 2016; 15: 574–584.
Martinez Sosa S, Smith KJ. Understanding a role for hypoxia in lesion formation and location in the deep and periventricular white matter in small vessel disease and multiple sclerosis. Clin Sci 2017; 131: 2503–2524.
Mauguiere F, Holder G, Luxon L, Pottinger R. Abnormal waveforms and diagnostic yield of evoked potentials. In: Osselton J, Binnie C, Cooper R, Fowler C, Mauguiere F, Prior P,

editor(s). Clinical neurophysiology: EMG; nerve conduction and evoked potentials. Oxford: Butterworth-Heinemann; 1995. p. 431–481
McDonald WI, Compston A, Edan G, Goodkin D, Hartung H, Lublin F, et al. Recommended diagnostic criteria for multiple sclerosis: Guidelines from the international panel on the diagnosis of Multiple Sclerosis. Ann Neurol 2001; 50: 121–127.
McIntosh C, Chick J. Alcohol and the nervous system. J neurol Neurosurg Psychiatry 2004; Suppl III: iii16–iii21.
Mealy MA, Kim S, Schmidt F, López R, Arango JAJ, Paul F, et al. Aquaporin-4 serostatus does not predict response to immunotherapy in neuromyelitis optica spectrum disorders. Mult Scler J 2018; 24: 1737–1742.
Mejia-Vergara AJ, Karanjia R, Sadun AA. Journal of the Neurological Sciences OCT parameters of the optic nerve head and the retina as surrogate markers of brain volume in a normal population , a pilot study. J Neurol Sci 2021; 420: 117213.
Messenger W, Hildebrandt L, Mackensen F, Suhler E, Becker M, Rosenbaum JT. Characterisation of uveitis in association with multiple sclerosis. Br J Ophthalmol 2015; 99: 205–209.
Miller DH, Leary SM. Primary-progressive multiple sclerosis. Lancet Neurol 2007; 6: 903–912.
Miller DH, Newton FMR, Van Der Poel JC, Boulay EPGH, Halliday AM, Kendall BE, et al. Magnetic resonance imaging of the optic nerve in optic neuritis. Neurology 1988; 38: 175–179.
Misu T, Takano R, Fujihara K, Takahashi T, Sato S, Itoyama Y. Marked increase in cerebrospinal fluid glial fibrillar acidic protein in neuromyelitis optica: an astrocytic damage marker. J Neurol Neurosurg Psychiatry 2009; 80: 575–577.
Modrzejewska M, Karczewicz D, Wilk G. Assessment of Blood Flow Velocity in Eyeball Arteries in Multiple Sclerosis Patients With Past Retrobulbar Optic Neuritis in Color Doppler Ultrasonography. Klin Ocz 2007; 109: 183–186.
Monsalve P, Ren S, Jiang H, Wang J, Kostic M, Gordon P, et al. Retinal ganglion cell function in recovered optic neuritis: Faster is not better. Clin Neurophysiol 2018; 129: 1813–1818.
Montalban X, Hauser S, Kappos L, Arnold D, Bar-Or A, Comi G, et al. Ocrelizumab versus placebo in primary progressive multiple sclerosis. N Engl J Med 2017; 376: 209–220.
Monti L, Donati D, Menci E, Cioni S, Bellini M, Grazzini I, et al. Cerebral circulation time is prolonged and not correlated with EDSS in multiple sclerosis patients: A study using digital subtracted angiography. PLoS One 2015; 10: 1–12.
Mühlemann F, Grabe H, Fok A, Wagner F, Brügger D, Sheldon CA, et al. Homonymous hemiatrophy of ganglion cell layer from retrochiasmal lesions in the visual pathway. Neurology 2020; 94: e323–e329.
Mukamal KJ, Longstreth WT, Mittleman MA, Crum RM, Siscovick DS. Alcohol consumption and subclinical findings on magnetic resonance imaging of the brain in older adults the cardiovascular health study. Stroke 2001; 32: 1939–1945.
Murphy OC, Kwakyi O, Iftikhar M, Zafar S, Lambe J, Pellegrini N, et al. Alterations in the retinal vasculature occur in multiple sclerosis and exhibit novel correlations with disability and visual function measures. Mult Scler J 2019: 1–14.
Nag TC, Wadhwa S. Immunolocalisation pattern of complex I–V in ageing human retina: Correlation with mitochondrial ultrastructure. Mitochondrion 2016; 31: 20–32.
Nathoo N, Rogers JA, Yong VW, Dunn JF. Detecting deoxyhemoglobin in spinal cord vasculature of the experimental autoimmune encephalomyelitis mouse model of multiple sclerosis using susceptibility MRI and hyperoxygenation. PLoS One 2015; 10: 1–11.

Nave KA. Myelination and support of axonal integrity by glia. Nature 2010; 468: 244–252.
Negrotto L, Farez MF, Correale J. Immunologic effects of metformin and pioglitazone treatment on metabolic syndrome and multiple sclerosis. JAMA Neurol 2016; 73: 520–528.
Nijland PG, Witte ME, van het Hof B, van der Pol S, Bauer J, Lassmann H, et al. Astroglial PGC-1alpha increases mitochondrial antioxidant capacity and suppresses inflammation: Implications for multiple sclerosis. Acta Neuropathol Commun 2014; 2: 1–13.
Nikić I, Merkler D, Sorbara C, Brinkoetter M, Kreutzfeldt M, Bareyre FM, et al. A reversible form of axon damage in experimental autoimmune encephalomyelitis and multiple sclerosis. Nat Med 2011; 17: 495–499.
Ning K, Zhao L, Mat W, Sun F, Toga AW. Association of relative brain age with tobacco smoking , alcohol consumption , and genetic variants. Sci Rep 2020; 30: 1–10.
Odom JV, Bach M, Brigell M, Holder GE, McCulloch DL, Mizota A, et al. ISCEV standard for clinical visual evoked potentials: (2016 update). Doc Ophthalmol 2016; 133
Okawa H, Sampath AP, Laughlin SB, Fain GL. ATP Consumption by Mammalian Rod Photoreceptors in Darkness and in Light. Curr Biol 2008; 18: 1917–1921.
Olsson T, Barcellos LF, Alfredsson L. Interactions between genetic, lifestyle and environmental risk factors for multiple sclerosis. Nat Rev Neurol 2016; 13: 26–36.
Ormerod IEC, McDonald WI. Multiple sclerosis presenting with progressive visual failure. J Neurol Neurosurg Psychiatry 1984; 47: 943–946.
Pache F, Zimmermann H, Mikolajczak J, Schumacher S, Lacheta A, Oertel FC, et al. MOG-IgG in NMO and related disorders: A multicenter study of 50 patients. Part 4: Afferent visual system damage after optic neuritis in MOG-IgG-seropositive versus AQP4-IgG-seropositive patients. J Neuroinflammation 2016; 13: 1–10.
Pakpoor J, Goldacre R, Disanto G, Giovannoni G, Goldacre MJ. Alcohol misuse disorders and multiple sclerosis risk. JAMA Neurol 2014; 71: 1188–1189.
Palace J. Multiple sclerosis associated with Leber's Hereditary Optic Neuropathy. J Neurol Sci 2009; 286: 24–27.
Papadopoulos M, Verkman A. Aquaporin 4 and neuromyelitis optica. Lancet Neurol 2012; 11: 535–544.
Papp V, Magyari M, Aktas O, Berger T, Broadley SA, Cabre P, et al. Worldwide Incidence and Prevalence of Neuromyelitis Optica: A Systematic Review. Neurology 2021; 96: 59–77.
Parisi V. Correlation between morphological and functional retinal impairment in patients affected by ocular hypertension, glaucoma, demyelinating optic neuritis and Alzheimer's disease. Semin Ophthalmol 2003; 18: 50–57.
Pasternack RM, Zheng J-Y, Boustany NN. Optical scatter changes at the onset of apoptosis are spatially associated with mitochondria. J Biomed Opt 2010; 15: 040504.
Pasternack RM, Zheng JY, Boustany NN. Detection of mitochondrial fission with orientation-dependent optical Fourier filters. Cytom Part A 2011; 79 A: 137–148.
Patel PJ, Foster PJ, Grossi CM, Keane PA, Ko F, Lotery A, et al. Spectral-domain optical coherence tomography imaging in 67 321 adults: Associations with macular thickness in the UK biobank study. Ophthalmology 2016; 123: 829–840.
Pau D, Al Zubidi N, Yalamanchili S, Plant GT, Lee AG. Optic neuritis. Eye 2011; 25: 833–842.
Paul CA, Au R, Fredman L, Massaro JM, Seshadri S, DeCarli C, et al. Association of alcohol consumption with brain volume in the Framingham study. Arch Neurol 2008; 65: 1363–1367.
Petzold A. Glial fibrillary acidic protein is a body fluid biomarker for glial pathology in human disease. Brain Res 2015; 1600: 17–31.
Petzold A, Balcer LJ, Calabresi PA, Costello F, Frohman TC, Frohman EM, et al. Retinal layer

segmentation in multiple sclerosis: a systematic review and meta-analysis. Lancet Neurol 2017; 16: 797–812.
Petzold A, Chua SYL, Khawaja AP, Keane PA, Khaw PT, Reisman C, et al. Retinal asymmetry in multiple sclerosis. Brain 2020: 1–12.
Petzold A, Marignier R, Verbeek M, Confavreux C. Glial but not axonal protein biomarkers as a new supportive diagnostic criteria for Devic neuromyelitis optica? Preliminary results on 188 patients with different neurological diseases. J Neurol Neurosurg Psychiatry 2011; 82: 467–469.
Petzold A, Nijland PG, Balk LJ, Amorini AM, Lazzarino G, Wattjes MP, et al. Visual pathway neurodegeneration winged by mitochondrial dysfunction. Ann Clin Transl Neurol 2015; 2: 140–150.
Petzold A, Pittock S, Lennon V, Maggiore C, Weinshenker BG, Plant GT. Neuromyelitis optica-IgG (aquaporin-4) autoantibodies in immune mediated optic neuritis. J Neurol 2010; 81: 109–111.
Petzold A, Wattjes MP, Costello F, Flores-Rivera J, Fraser CL, Fujihara K, et al. The investigation of acute optic neuritis: A review and proposed protocol. Nat Rev Neurol 2014; 10: 447–458.
Petzold A, Wong S, Plant GT. Autoimmunity in visual loss. In: Pittock S, Vincent A, editor(s). Handbook of Clinical Neurology. Elsevier B.V.; 2016. p. 353–376
Petzold A, Woodhall M, Khaleeli Z, Tobin WO, Pittock SJ, Weinshenker BG, et al. Aquaporin-4 and myelin oligodendrocyte glycoprotein antibodies in immune-mediated optic neuritis at long-term follow-up. J Neurol Neurosurg Psychiatry 2019; 90: 1021–1026.
Pfeffer G, Burke A, Yu-Wai-Man P, Compston DAS, Chinnery PF. Clinical features of MS associated with Leber hereditary optic neuropathy mtDNA mutations. Neurology. 2013 Nov 6 (epub ahead of print). Neurology 2013; 81: 2073–2081.
Pietroboni A, Dell'Arti L, Caprioli M, Scarioni M, Carandini T, Arighi A, et al. The loss of macular ganglion cells begins in the early stages of disease and correlates with brain atrophy in multiple sclerosis patients. Mult Scler J 2017; 25: 31–38.
Pittock S, Verthele K, Fujihara K, Kim H, Levy M, Palace J, et al. Eculizumab in Aquaporin-4–Positive Neuromyelitis Optica Spectrum Disorder. N Engl J Med 2019; [Epub ahea
Plant GT, Hess RF, Thomas SJ. The pattern evoked electroretinogram in optic neuritis: A combined psychophysical and electrophysiological study. Brain 1986; 109: 469–489.
Plant GT, Sibtain NA, Thomas D. Hyperacute Corticosteroid Treatment of Optic Neuritis at the Onset of Pain May Prevent Visual Loss: A Case Series. Mult Scler Int 2011; 815068: 1–8.
Polman CH, Reingold SC, Edan G, Filippi M, Hartung H, Kappos L, et al. Diagnostic Criteria for Multiple Sclerosis: 2005 Revisions to the " McDonald Criteria ". Ann Neurol 2005; 58: 840–846.
Read SJ, Harrison JD, Pender MP. Progressive visual loss: An unusual presentation of multiple sclerosis. J Clin Neurosci 1996; 3: 264–267.
Reich DS, Lucchinetti CF, Calabresi PA. Multiple Sclerosis. N Engl J Med 2018; 378: 169–180.
Revesz T, Kidd D, Thompson AJ, Barnard RO, Mcdonald WI. A comparison of the pathology of primary and secondary progressive multiple sclerosis. Brain 1994; 117: 759–765.
Rimm EB, Giovannucci EL, Willett WC, Colditz GA, Ascherio A, Rosner B, et al. Prospective study of alcohol consumption and risk of coronary disease in men. Lancet 1991; 338: 464–468.
Risseeuw S, Bennink E, Poirot MG, de Jong PA, Spiering W, Imhof SM, et al. A reflectivity measure to quantify bruch's membrane calcification in patients with pseudoxanthoma

elasticum using optical coherence tomography. Transl Vis Sci Technol 2020; 9: 1–12.
Robson AG, Nilsson J, Li S, Jalali S, Fulton AB, Tormene AP, et al. ISCEV guide to visual electrodiagnostic procedures. Doc Ophthalmol 2018; 136: 1–26.
Roemer SF, Parisi JE, Lennon VA, Benarroch EE, Lassmann H, Bruck W, et al. Pattern-specific loss of aquaporin-4 immunoreactivity distinguishes neuromyelitis optica from multiple sclerosis. Brain 2007; 130: 1194–1205.
Rohowetz LJ, Vu Q, Ablabutyan L, Gratton SM, Kunjukunju N, Wallace BS, et al. Microperimetry as a diagnostic tool for the detection of early , subclinical retinal damage and visual impairment in multiple sclerosis. BMC Ophthalmol 2020; 20: 367.
Romano F, Arrigo A, Leone PP, Saladino A, Bandello F, Battaglia Parodi M. Altered ellipsoid zone reflectivity and deep capillary plexus rarefaction correlate with progression in Best disease. Br J Ophthalmol 2020; 104: 461–465.
Rosso M, Chitnis T. Association between Cigarette Smoking and Multiple Sclerosis: A Review. JAMA Neurol 2020; 77: 245–253.
Rosso M, Kimbrough DJ, Gonzalez CT, Glanz BI, Healy BC, Rocca MA, et al. Cross-sectional study of smoking exposure: no differential effect on OCT metrics in a cohort of MS patients. Mult Scler J - Exp Transl Clin 2019; 5: 205521731982840.
Rucker C. Sheathing of the retinal veins in Multiple Sclerosis. JAMA 1945; 127: 970–973.
Saab AS, Nave KA. Myelin dynamics: protecting and shaping neuronal functions. Curr Opin Neurobiol 2017; 47: 104–112.
Sadeghian M, Mastrolia V, Rezaei Haddad A, Mosley A, Mullali G, Schiza D, et al. Mitochondrial dysfunction is an important cause of neurological deficits in an inflammatory model of multiple sclerosis. Sci Rep 2016; 6: 33249.
Saidha S, Al-Louzi O, Ratchford J, Bhargava P, Oh J, Newsome S, et al. Optical coherence tomography reflects brain atrophy in multiple sclerosis: a four-year study. Ann Neurol 2015; 75: 801–813.
Saidha S, Al-Louzi O, Ratchford JN, Bhargava P, Oh J, Newsome SD, et al. Optical coherence tomography reflects brain atrophy in multiple sclerosis: A four-year study. Ann Neurol 2015; 78: 801–813.
Saidha S, Syc SSB, Ibrahim MMA, Eckstein C, Warner CVC, Farrell SSK, et al. Primary retinal pathology in multiple sclerosis as detected by optical coherence tomography. Brain 2011; 134: 518–533.
Saleh M, Flores M, Gauthier AS, Elphege E, Delbosc B. Quantitative analysis of photoreceptor layer reflectivity on en-face optical coherence tomography as an estimator of cone density. Graefe's Arch Clin Exp Ophthalmol 2017; 255: 2119–2126.
Salter AR, Tyry T, Vollmer T, Cutter GR, Marrie RA. "Seeing" in NARCOMS : a look at vision-related quality of life in the NARCOMS registry. Mult Scler J 2012; 19: 953–960.
Sati P, Oh J, Todd Constable R, Evangelou N, Guttmann CRG, Henry RG, et al. The central vein sign and its clinical evaluation for the diagnosis of multiple sclerosis: A consensus statement from the North American Imaging in Multiple Sclerosis Cooperative. Nat Rev Neurol 2016; 12: 714–722.
Sato DK, Callegaro D, Aurelio Lana-Peixoto M, Waters PJ, Haidar FM De, Takahashi T, et al. Distinction between MOG antibody- positive and AQP4 antibody-positive NMO spectrum disorders. Neurology 2014; 82: 474–481.
Sato DK, Callegaro D, Jorge FMDH, Nakashima I, Nishiyama S, Takahashi T, et al. Cerebrospinal Fluid Aquaporin-4 Antibody Levels in Neuromyelitis Optica Attacks. Ann Neurol 2014; 76: 305–309.

Schuman J, Puliafito C, Fujimoto J. Optical coherence tomography of ocular diseases. New Jersey: Slack, Inc.; 2004
Schwartz DM, Fingler J, Kim DY, Zawadzki RJ, Morse LS, Park SS, et al. Phase-variance optical coherence tomography: A technique for noninvasive angiography. Ophthalmology 2014; 121: 180–187.
Seitz CB, Droby A, Zaubitzer L, Krämer J, Paradis M, Klotz L, et al. Discriminative power of intra-retinal layers in early multiple sclerosis using 3D OCT imaging. J Neurol 2018; 0: 0.
Shams P, Plant G. Optic Neuritis: a review. Int MS J 2009; 16: 82–89.
Smith KJ, Kapoor R, Felts P. Demyelination: the role of reactive oxygen and nitrogen species. Brain Pathol 1999; 9: 69–92.
Snyder AW, Pask C. The Stiles-Crawford effect-explanation and consequences. Vision Res 1973; 13: 1115–1137.
Sotirchos ES, Gonzalez Caldito N, Filippatou A, Fitzgerald KC, Murphy OC, Lambe J, et al. Progressive Multiple Sclerosis Is Associated with Faster and Specific Retinal Layer Atrophy. Ann Neurol 2020; 87: 885–896.
Spain RI, Liu L, Zhang X, Jia Y, Tan O, Bourdette D, et al. Optical coherence tomography angiography enhances the detection of optic nerve damage in multiple sclerosis. Br J Ophthalmol 2018; 102: 520–524.
Sriram P, Wang C, Yiannikas C, Garrick R, Barnett M, Parratt J, et al. Relationship between optical coherence tomography and electrophysiology of the visual pathway in non-optic neuritis eyes of multiple sclerosis patients. PLoS One 2014; 9: 1–10.
Stellmann JP, Krumbholz M, Friede T, Gahlen A, Borisow N, Fischer K, et al. Immunotherapies in neuromyelitis optica spectrum disorder: Efficacy and predictors of response. J Neurol Neurosurg Psychiatry 2017; 88: 639–647.
Strouthidis NG, Grimm J, Williams GA, Cull GA, Wilson DJ, Burgoyne CF. A comparison of optic nerve head morphology viewed by spectral domain optical coherence tomography and by serial histology. Investig Ophthalmol Vis Sci 2010; 51: 1464–1474.
Su K, Bourdette D, Forte M. Mitochondrial dysfunction and neurodegeneration in multiple sclerosis. Front Physiol 2013; 4 JUL: 1–10.
Suomalainen A, Battersby BJ. Mitochondrial diseases: The contribution of organelle stress responses to pathology. Nat Rev Mol Cell Biol 2018; 19: 77–92.
Takano R, Misu T, Takahashi T, Sato S, Fujihara K, Itoyama Y. Astrocytic damage is far more severe than demyelination in NMO: a clinical CSF biomarker study. Neurology 2010; 75: 208–216.
Taki Y, Goto R, Evans A, Zijdenbos A, Neelin P, Lerch J. Voxel-based morphometry of human brain with age and cerebrovascular risk factors. 2004; c: 455–463.
Tallantyre EC, Bø L, Al-Rawashdeh O, Owens T, Polman CH, Lowe JS, et al. Clinico-pathological evidence that axonal loss underlies disability in progressive multiple sclerosis. Mult Scler 2010; 16: 406–411.
Tanga L, Roberti G, Oddone F, Quaranta L, Ferrazza M, Berardo F, et al. Evaluating the effect of pupil dilation on spectral-domain optical coherence tomography measurements and their quality score. BMC Ophthalmol 2015; 15: 1–6.
Tao LW, Wu Z, Guymer RH, Luu CD. Ellipsoid zone on optical coherence tomography: a review. Clin Exp Ophthalmol 2016; 44: 422–430.
Tettey P, Siejka D, Simpson S, Taylor B, Blizzard L, Ponsonby AL, et al. Frequency of comorbidities and their association with clinical disability and relapse in multiple sclerosis. Neuroepidemiology 2016; 46: 106–113.

Teunissen CE, Petzold A, Bennett J, Berven F, Brundin L, Comabella M, et al. A consensus protocol for the standardization of cerebrospinal fluid collection and biobanking. Neurology 2009; 73: 1914–1922.
Tewarie P, Balk L, Costello F, Green A, Martin R, Schippling S, et al. The OSCAR-IB consensus criteria for retinal OCT quality assessment. PLoS One 2012; 7: 1–7.
Thiele S, Isselmann B, Pfau M, Holz FG, Schmitz-Valckenberg S, Wu Z, et al. Validation of an automated quantification of relative ellipsoid zone reflectivity on spectral domain-optical coherence tomography images. Transl Vis Sci Technol 2020; 9: 1–10.
Thompson AJ. Challenge of progressive multiple sclerosis therapy. Curr Opin Neurol 2017; 30: 237–240.
Thompson AJ, Banwell BL, Barkhof F, Carroll WM, Coetzee T, Comi G, et al. Diagnosis of multiple sclerosis: 2017 revisions of the McDonald criteria. Lancet Neurol 2018; 17: 162–173.
Thompson AJ, Baranzini SE, Geurts J, Hemmer B, Ciccarelli O. Multiple sclerosis. Lancet 2018; 391: 1622–1636.
Toosy AT, Mason DF, Miller DH. Optic neuritis. Lancet Neurol 2014; 13: 83–99.
Topiwala A, Allan CL, Valkanova V, Zsoldos E, Filippini N, Sexton C, et al. Moderate alcohol consumption as risk factor for adverse brain outcomes and cognitive decline : BMJ 2017; 357: j2353.
Topiwala A, Ebmeier K, Maullin-Sapey T, Nichols T. No safe level of alcohol consumption for brain health: observational cohort study of 25,378 UK Biobank participants. medRxiv Prepr 2021
Toprak I, Yaylalı V, Yildirim C. Early deterioration in ellipsoid zone in eyes with non-neovascular age-related macular degeneration. Int Ophthalmol 2017; 37: 801–806.
Toussaint D, Périer O, Verstappen A, Bervoets S. Clinicopathological study of the visual pathways, eyes, and cerebral hemispheres in 32 cases of disseminated sclerosis. J Clin Neuroophthalmol 1983; 3: 211–220.
Trapp BD, Stys PK. Virtual hypoxia and chronic necrosis of demyelinated axons in multiple sclerosis. Lancet Neurol 2009; 8: 280–291.
Trip SA, Schlottmann PG, Jones SJ, Altmann DR, Garway-Heath DF, Thompson AJ, et al. Retinal nerve fiber layer axonal loss and visual dysfunction in optic neuritis. Ann Neurol 2005; 58: 383–391.
Trip SA, Schlottmann PG, Jones SJ, Li WY, Garway-Heath DF, Thompson AJ, et al. Optic nerve atrophy and retinal nerve fibre layer thinning following optic neuritis: Evidence that axonal loss is a substrate of MRI-detected atrophy. Neuroimage 2006; 31: 286–293.
Trobe JD, Beck RW, Moke PS, Cleary PA. Contrast sensitivity and other vision tests in the optic neuritis treatment trial. Am J Ophthalmol 1996; 121: 547–553.
Tumani H, Shen GQ, Peter JB. Purification and immunocharacterization of human brain glutamine synthetase and its detection in cerebrospinal fluid and serum by a sandwich enzyme immunoassay. J Immunol Methods 1995; 188: 155–163.
Tychinsky V. The metabolic component of cellular refractivity and its importance for optical cytometry. J Biophotonics 2009; 2: 494–504.
Ulrich J, Groebke-Lorenz W. The optic nerve in multiple sclerosis: A morphological study with retrospective clinico-pathological correlations. Neuro-Ophthalmology 1983; 3: 149–159.
Ulusoy MO, Horasanlı B, Işık-Ulusoy S. Optical coherence tomography angiography findings of multiple sclerosis with or without optic neuritis. Neurol Res 2020; 42: 319–326.
Varga AW, Johnson G, Babb JS, Herbert J, Grossman RI, Inglese M. White matter hemodynamic abnormalities precede sub-cortical gray matter changes in multiple sclerosis. J

Neurol Sci 2009; 282: 28–33.
Varhaug KN, Vedeler CA, Myhr KM, Aarseth JH, Tzoulis C, Bindoff LA. Increased levels of cell-free mitochondrial DNA in the cerebrospinal fluid of patients with multiple sclerosis. Mitochondrion 2017; 34: 32–35.
Vermeer KA, Mo J, Weda JJA, Lemij HG, de Boer JF. Depth-resolved model-based reconstruction of attenuation coefficients in optical coherence tomography. Biomed Opt Express 2014; 5: 322.
Viswanathan S, Frishman LJ, Robson JG. The uniform field and pattern ERG in macaques with experimental glaucoma: Removal of spiking activity. Investig Ophthalmol Vis Sci 2000; 41: 2797–2810.
Vladimirova O, Connor JO, Cahill A, Alder H, Butunoi C, Kalman B. Oxidative damage to DNA in plaques of MS brains. Mult Scler 1998; 4: 413–418.
Wang JJ, Jaunmuktane Z, Mummery C, Brandner S, Leary S, Trip S. Inflammatory demyelination without astrocyte loss in MOG antibody-positive NMOSD. Neurology 2016; 87: 229–231.
Wang M, Guo H, Li S, Wang G, Long Y, Meng X, et al. Electrophysiological and Structural Changes in Chinese Patients with LHON. J Ophthalmol 2020; eCollectio: 4734276.
Wang X, Jia Y, Spain R, Potsaid B, Liu JJ, Baumann B, et al. Optical coherence tomography angiography of optic nerve head and parafovea in multiple sclerosis. Br J Ophtalmol 2014; 98: 1368–1373.
Warrant E. Mammalian Vision: Rods Are a Bargain. Curr Biol 2009; 19: R69-71.
Watanabe M, Nakamura Y, Michalak Z, Isobe N, Barro C, Leppert D, et al. Serum GFAP and neuro fi lament light as biomarkers of disease activity and disability in NMOSD. Neurology 2019; [Epub ahea
Waters P, Reindl M, Saiz A, Schanda K, Tuller F, Kral V, et al. Multicentre comparison of a diagnostic assay: Aquaporin-4 antibodies in neuromyelitis optica. J Neurol Neurosurg Psychiatry 2016; 87: 1005–1015.
Wei Y, Chang H, Li X, Du L, Xu W, Cong H, et al. CSF-S100B Is a Potential Candidate Biomarker for Neuromyelitis Optica Spectrum Disorders. Biomed Res Int 2018; 2018: 5381239.
Wei Y, Chang H, Li X, Wang H, Du L, Zhou H. Cytokines and Tissue Damage Biomarkers in First-Onset Neuromyelitis Optica Spectrum Disorders: Significance of Interleukin-6. Neuroimmunomodulation 2018; 25: 215–224.
Weiland TJ, Hadgkiss EJ, Jelinek GA, Pereira NG, Marck CH, Van Der Meer DM. The association of alcohol consumption and smoking with quality of life, disability and disease activity in an international sample of people with multiple sclerosis. J Neurol Sci 2014; 336: 211–219.
Wentling M, Lopez-Gomez C, Park H-J, Amatruda M, Ntranos A, Aramini J, et al. A metabolic perspective on CSF-mediated neurodegeneration in multiple sclerosis. Brain 2019; 142: 2756–2774.
Werner P, Pitt D, Raine CS. Multiple Sclerosis: Altered Glutamate Homeostasis in Lesions Correlates with Oligodendrocyte and Axonal Damage. Ann Neurol 2001; 50: 169–180.
Wilson JD, Bigelow CE, Calkins DJ, Foster TH. Light scattering from intact cells reports oxidative-stress-induced mitochondrial swelling. Biophys J 2005; 88: 2929–2938.
Wilson JD, Cottrell WJ, Foster TH. Index-of-refraction-dependent subcellular light scattering observed with organelle-specific dyes. J Biomed Opt 2007; 12: 014010.
Wingerchuk D, Banwell B, Bennett JL, Cabre P, Carroll W, Jacob A, et al. International consensus diagnostic criteria for neuromyelitis optica spectrum disorders. Neurology 2015;

85: 177–189.
Witte M, Bø L, Rodenburg R, Belien J, Musters R, Hazes T, et al. Enhanced number and activity of mitochondria in multiple sclerosis lesions. J Pathol 2009; 219: 193–204.
Witte ME, Nijland PG, Drexhage JAR, Gerritsen W, Geerts D, Van Het Hof B, et al. Reduced expression of PGC-1α partly underlies mitochondrial changes and correlates with neuronal loss in multiple sclerosis cortex. Acta Neuropathol 2013; 125: 231–243.
Wong-Riley M. Energy metabolism of the visual system. Eye Brain 2010; 2: 99–116.
Wood AM, Kaptoge S, Butterworth A, Nietert PJ, Warnakula S, Bolton T, et al. Risk thresholds for alcohol consumption: combined analysis of individual-participant data for 599 912 current drinkers in 83 prospective studies. Lancet 2018; 391: 1513–1523.
Wu Z, Ayton LN, Guymer RH, Luu CD. Relationship between the second reflective band on optical coherence tomography and multifocal electroretinography in age-related macular degeneration. Investig Ophthalmol Vis Sci 2013; 54: 2800–2806.
Yang R, Dunn JF. Reduced cortical microvascular oxygenation in multiple sclerosis: A blinded, case-controlled study using a novel quantitative near-infrared spectroscopy method. Sci Rep 2015; 5: 16477.
Yang R, Dunn JF. Multiple sclerosis disease progression: Contributions from a hypoxia–inflammation cycle. Mult Scler J 2018; Jul 27: 1352458518791683.
Yilmaz H, Ersoy A, Icel E. Assessments of vessel density and foveal avascular zone metrics in multiple sclerosis: an optical coherence tomography angiography study. Eye 2020; 34: 771–778.
You Y, Graham EC, Shen T, Yiannikas C, Parratt J, Gupta V, et al. Progressive inner nuclear layer dysfunction in non-optic neuritis eyes in MS. Neurol Neuroimmunol NeuroInflammation 2018; 5: 1–9.
You Y, Gupta VK, Graham SL, Klistorner A. Anterograde Degeneration along the Visual Pathway after Optic Nerve Injury. PLoS One 2012; 7
Yu-Wai-Man P, Griffiths PG, Gorman GS, Lourenco CM, Wright AF, Auer-Grumbac M, et al. Multi-system neurological disease is common in patients with OPA1 mutations. Brain 2010; 133: 771–786.
Yu D, Cringle SJ, Yu PK, Balaratnasingam C, Mehnert A, Sarunic M V, et al. Retinal capillary perfusion: Spatial and temporal heterogeneity. Prog Retin Eye Res 2019; S1350-9462: 30072–30077.
Yu J, Huang Y, Quan C, Zhou L, ZhangBao J, Wu K, et al. Alterations in the Retinal Vascular Network and Structure in MOG Antibody-Associated Disease. J Neuro-Ophthalmology 2020; Publish Ah: 1–9.
Zekeridou A, McKeon A, Flanagan E. A path to understanding autoimmune GFAP astrocytopathy. Eur J Neurol 2018; 25: 421–422.
Zhang J, Xiao Y, Meng L, Yang X, Shi S. Alemtuzumab versus interferon beta 1a for relapsing-remitting multiple sclerosis. Cochrane Database Syst Rev 2014; 2014
Zipp F, Gold R, Wiendl H. Identification of inflammatory neuronal injury and prevention of neuronal damage in multiple sclerosis: Hope for novel therapies? JAMA Neurol 2013; 70: 1569–1574.
Zipp F, Wendling U, Beyer M, Grieger U, Waiczies S, Wagenknecht B, et al. Dual effect of glucocorticoids on apoptosis of human autoreactive and foreign antigen-specific T cells. J Neuroimmunol 2000; 110: 214–222.